INVESTIGATING THE ARCHAEOLOGICAL IMPLICATIONS OF ENVIRONMENTAL CHANGE DURING THE MIDDLE STONE AGE: A CONTRIBUTION FROM THE GEOCHEMICAL ANALYSIS OF SPELEOTHEMS IN THE SOUTHERN CAPE, SOUTH AFRICA

Jane Sabina Adigun

A thesis submitted to the Faculty of Science, University of the Witwatersrand, Johannesburg, in fulfilment of the requirements for the degree of Doctor of Philosophy

Johannesburg, 2016

DECLARATION

I declare that this thesis is my own, unaided work. It is being submitted for the Degree of Doctor of Philosophy in the University of the Witwatersrand, Johannesburg. It has not been submitted before for any degree of examination in any other University.

_____

(Jane Sabina Adigun)

24th day of May 2016

ABSTRACT

In current Middle Stone Age research there is interest in understanding whether climatic and environmental factors played a role in behaviours related to subsistence, mobility patterns and material culture production. From a palaeoenvironmental perspective, the southern Cape is recognized as an important study region for exploring the link, if any, between past environmental conditions and key MSA occurrences. The research presented in this thesis aimed to contribute to the existing database of past environments in the southern Cape through the geochemical analysis of speleothems from a previously uninvestigated locality in the De Hoop Nature Reserve. Together, the De Hoop speleothems provide a discontinuous record of environmental change from marine oxygen isotope stage MIS 5a to MIS 3 (and the Holocene). Results from the De Hoop records indicate warm summer rain and C4 vegetation in early MIS 5a (c. 85 ka to 80 ka) but more variability by late MIS 5a (c. 79 ka to 74 ka). At Klasies River main site, also on the southern Cape coast, the upper MSA II is associated with the warm early MIS 5a conditions. At Blombos Cave, another important coastal MSA site, the Still Bay occurring within terminal MIS 5a was linked to warm but more variable late MIS 5a conditions. While early MIS 4 (c. 73 ka to 68 ka) was comparatively cooler, conditions were similar to those in early MIS 5a. From this research, the earlier phase of the Howiesons Poort at Klasies River main site and the Howiesons Poort at Klipdrift Shelter were correlated with the early MIS 4 conditions in De Hoop. By late MIS 4 (c. 67 ka to 60 ka), conditions remained cool, but were seemingly more variable than during the earlier part of this

stage. Highly variable and possibly unstable conditions were indicated for early MIS 3 (c. 59 ka to 50 ka) although warm summer rain and C4 vegetation occurred during part of early MIS 3. The occurrence of the MSA III or post-Howiesons Poort at Klasies River main site was associated with these warmer early MIS 3 conditions. Overall, it was found that MIS 3 is the most regionally variable period in the southern Cape.

ACKNOWLEDGEMENTS

I have spent five years of my life on this thesis and it has been a long journey; from the early days of proposal writing to the final stages of fitting together the puzzle pieces of the story I present in this thesis. I would not have been able to finish this work without the guidance, support and extreme patience of my supervisors, Dr. Sarah Wurz, Prof. Christopher Henshilwood and Prof. Stein-Erik Lauritzen. You have collectively made an effort to encourage and push me to complete this thesis, often at times when I didn't inspire confidence. As we have come to the end of this journey together, I thank you for always trying to help me at various stages of my project. A special thanks to Dr. Sarah Wurz for a consistent stream of e-mails with new literature, for organising discussion groups, making time to read incoherent and scruffy drafts that were often few and far between. I appreciate all the personal sacrifices you made in helping me throughout the duration of my PhD studies and I apologise for all the times I was slow in meeting deadlines.

I also thank Prof. Henshilwood, Magnus Haaland, Dr. Riaan Rifkin and Dr. Karen van Niekerk, who took turns changing the condoms I used for collecting dripwater in the caves. This was an important part of the research and I really appreciate your assistance in the field at times when I was occupied in the lab.

Thanks to Prof. Stein-Erik Lauritzen for introducing me to the world of speleothems, isotopes and uranium-series dating. You have been a wonderful teacher and a generous host on each occasion when I have been in Bergen.

I also thank Siv Dundas at the ICP lab (University of Bergen) for introducing me to the ICP instrument and allowing me to run my samples after hours. I thank Rune Søraas and Pål Tore Mørkved at the Bjerknes Centre for helping me with the stable isotope analyses and dripwater analysis respectively. I also thank the staff at the Dept. of Archaeolgy, History Cultural and Religious Studies (AHKR, Univeristy of Bergen) - particularly, Arne Mykkeltveit and Åshild Anderssen Tetler for practical arrangements related to my study visit. Dr. Brian Chase is thanked for thoughtful discussions on the data and for helping to clarify my understanding of climate change and the complexity that it entails.

I received financial support from the University of Witwatersrand Study Abroad Fund and the Palaeoanthropological Scientific Trust (PAST) and its Scatterlings of Africa programmes. Additional funding was received from the Norwegian Research Council under the Yggdrasil Mobility Programme (Project No. 219716/F11). Funding for the degree was provided by a National Research Foundation (NRF) SARChI chair grant in “The origins of modern human behaviour” held by Prof. Henshilwood at the Institute for Human Evolution, University of the Witwatersrand. Laboratory and field-related costs were covered with funds from a European Research Council (ERC) Advanced Grant (FP7 programme) awarded jointly to Prof. Henshilwood and Prof. d'Errico for the TRACSYMBOLS project. A permit to collect the speleothem samples was issued by Cape Nature to Prof. Henshilwood (Permit No. 0052-AAA004-00011). Permission to export the material from South Africa and analyse it at the University of Bergen was granted to Prof. Henshilwood with permits issued by the South African Heritage Resources Agency (SAHRA) (Permit No. 80/11/05/019/52) and

Heritage Western Cape (HWC) (Permit No. 2011/03/001), respectively. I also acknowledge the South African Weather Service for providing comparative historical rainfall and temperature data. Dr. Siep Talma kindly provided access to the Cango Cave data.

I am especially grateful to my mommy, Sybil Josephs for unwavering support and words of encouragement over the many years I spent studying. Words cannot express my gratitude to everyone that encouraged and motivated me to persevere at times when I was experiencing short, infrequent bursts of writing and feeling completely overwhelmed. Thanks to my brother Dominic Noah for making me laugh on days when I was missing everything familiar and comforting back home. A special thanks to my wonderful husband, Celebrity Tunji Adigun for helping to preserve my sanity. I am truly blessed to have you in my life. Finally, I thank God for seeing me through.

TABLE OF CONTENTS

`

LIST OF FIGURES

LIST OF TABLES

Chapter 1 – INTRODUCTION

1.1 General introduction

The South African Middle Stone Age (MSA) refers to the period from *c.* 300 ka to between 35 ka and 20 ka (McBrearty & Brooks 2000; Wadley 2015). Interest in the MSA comes from its rich material culture record which includes lithic tools, worked bone, engraved ochres, decorated ostrich eggshell and perforated marine shell beads. In addition, the MSA also contains the earliest fossil evidence for anatomically modern humans with skeletal elements dating to between *c.* 195 ka and 160 ka and between *c.* 105 ka and 79 ka coming from the sites of Omo and Herto in Ethiopia (Dusseldorp *et al.* 2013). In the South African context, cranial fragments dating to between 110 ka and 40 ka come from Klasies River on the southern Cape coast and these have also been linked to extant humans (Dusseldorp *et al.* 2013).

On the South African southern Cape coast, well-known MSA sites occurring within this 320 km stretch of coast include Die Kelders Cave, Blombos Cave, Nelson Bay Cave, Pinnacle Point and Klasies River. Evidence emerging from Blombos Cave and Pinnacle Point, in particular, is providing unique insights into our understanding of aspects of MSA life including subsistence behaviours, mobility patterns, intra-site spatial patterning and material culture production. These sites therefore play an important role in the generation of knowledge pertinent to the MSA (Henshilwood & Dubreuil 2011; Wadley 2013; Wurz 2013). Pinnacle Point for example has the earliest MSA occupation record on the southern Cape coast that dates to between *c.* 167 ka and 157 ka (Marean *et al.* 2007; Marean 2010; Jacobs 2010). Here there are also a number of coastal caves dating to marine oxygen isotope (MIS) stage 5 (*c.* 128 ka – 85 ka, Carto *et al.* 2009). Other southern Cape sites with occupations or MSA deposits associated with MIS 5 include Blombos Cave and Klasies River main site.

With regards to MIS 4 (*c.* 73 ka – 57 ka, Martinson *et al.* 1987; *c.* 72 ka – 62 ka, Carto *et al.* 2009), this period is generally associated with the Still Bay and Howiesons Poort. These are of the most intensively investigated MSA occurrences, not only in the southern Cape, but also in a wider South African context. The interest in the Still Bay and Howiesons Poort comes from proxy evidence for complex cognition. In the archaeological record, complex cognitive abilities (comparable with those of modern humans, Wadley 2013) are recognised from engraved ostrich eggshell, the use of ochre, shell beads and hafted lithics and bone artefacts (Wadley *et al.* 2009; Wadley 2013). While the Still Bay and Howiesons Poort are associated with the development of cognitive skills necessary for 'modern' culture and language these abilities are also inferred from archaeological findings in the southern Cape, at sites such as Blombos Cave, Klasies River main site, Klipdrift Shelter, Pinnacle Point during the earlier MSA (Wurz 1999; Henshilwood *et al.* 2009; Henshilwood & Dubreuil 2011; Henshilwood 2012).

For MIS 3 (*c.* 59 ka – 24 ka, Martinson *et al.* 1987) there are very few sites along the southern Cape coast correlated with MIS 3 and the key sites with occupations dating to this stage are Boomplaas Cave, part of the Klasies River main site sequence and Klipdrift Shelter (see discussion in Chapter 2 section 2.3). Some have for example suggested that the paucity of sites dating to MIS 3 reflect occupational hiatuses that are linked to cool and dry climatic conditions (Deacon & Thackeray 1984).

Within contemporary MSA research, interest has been focused on exploring the relationship between the environment and key behavioural changes. This includes for example, those behaviours linked to the emergence of the Still Bay and Howiesons Poort. The extent to which climatic change may have influenced human behavioural development during the MSA is however complex. While some researchers argue for links between extreme climate change and social change (Deacon 1989: 560; Ambrose 2002; Henshilwood & Marean 2003; McCall 2007), there is some debate (Chase 2010; Henshilwood 2008; Jacobs *et al.* 2008). There

are also further differing interpretations on the palaeoenvironmental conditions that occurred during the MSA. For example, the Howiesons Poort is thought to have occurred during relatively humid climatic conditions (Chase 2010), while others have linked it to an interval of mostly warm conditions (Thackeray & Avery 1990; Thackeray 1992, 2009). However, based on the widespread occurrence of Howiesons Poort assemblages across South Africa, some suggest that climatic influences were negligible at this time (Jacobs *et al.* 2008; Jacobs & Roberts 2009). Similarly, for MIS 3 there are varying opinions on whether sites in the southern Cape reflect adaptation to arid conditions (Deacon & Thackeray 1984; Klein *et al.* 2004) or whether humid conditions in fact existed as suggested by for example Mitchell (2008).

The differing views regarding the past environmental conditions that Middle Stone Age people adapted to is further complicated by the wide range of climate proxies which can be interpreted at varying spatial and temporal resolutions. Some of these proxies include amongst others, micromammal and large mammal fauna, pollen, shellfish, geochemical sediments and ostrich eggshell. Developing high resolution chronologies for archaeological sites is therefore central to the debate regarding the influence of environmental change on human biogeography during the MSA.

1.2 Rationale

Establishing high-resolution climate proxies plays an essential role in helping to refine our understanding of the relationship between changing environments and Middle Stone Age occurrences. Evidence from archaeological and geomorphological contexts for environmental change in the southern Cape region has been discussed in a number of papers (Meadows & Baxter 1999; Butzer 2004; Carr *et al.* 2006, 2007, 2010; Chase & Meadows 2007; Henshilwood 2008; Bar-Matthews *et al.* 2010; Chase 2010; Compton 2011; Hillestad-Nel 2013; Quick 2013; Braun 2014). The environmental proxies associated with the Middle Stone Age

come primarily from the archaeological record with interpretations derived from analyses on micromammal (Avery *et al.* 1987, 2005; Hillestad-Nel 2013), large mammal fauna (Klein 1976; van Pletzen 2000; Henshilwood *et al.* 2001) and shellfish (Galimberti 2010; Langejans *et al.* 2012), and more recently from ostrich eggshell fragments (Roberts 2013).

There is a growing body of work on speleothems from the southern Cape aimed at refining understanding of the environment in the Middle and Late Pleistocene. In the southern Cape, speleothem studies were undertaken on a stalagmite from the Cango Cave in Oudtshoorn (Talma & Vogel 1992) and from Crevice Cave at Pinnacle Point (Bar-Matthews *et al.* 2010). Speleothem samples from Staircase Cave at Pinnacle Point were also recently analysed and these date between *c.* 510 ka and 120 ka (Braun 2014). Speleothem data are also available from Herold's Bay Cave and Sandkraal Cave in George (Braun 2014). In this thesis the study of speleothems from an area not previously investigated add to this body of data.

The current study investigates the speleothem record from Bloukrantz Cave and Klipdrift Sea Cave in the De Hoop Nature Reserve. At the De Hoop Nature Reserve a new HP occurrence dating to *c*. 65.5 ka and 59.4 ka was recently identified at Klipdrift Shelter (Henshilwood *et al*. 2014). The site is also very close to Blombos Cave, which has an occupation sequence that has recently been refined to between 73 ka and 101 ka (Henshilwood *et al*. 2011; Jacobs *et al.* 2013). This provides an ideal opportunity to investigate the environment of the period immediately preceding the Still Bay, MIS 5a, the Still Bay, Howiesons Poort and post Howiesons Poort palaeoenvironment at the end of MIS 3. Some information on a Holocene aged stalagmite from Klipdrift Sea Cave is also provided, although it does not form part of the Middle Stone Age focus of this thesis.

1.3 Research Aims

In the context of this study, the intention is to reconstruct past environmental, and by extension climatic conditions, along the southern Cape coast of South Africa during the Middle Stone Age.

With that in mind, the objectives of this study are to:

- Date and extract stable carbon and oxygen isotopes from speleothems sampled at Klipdrift Sea Cave and Bloukrantz Cave in the De Hoop Nature Reserve;
- Reconstruct past environmental conditions in the southern Cape by using the isotope data (from the speleothems) as a proxy for vegetation, rainfall and to a lesser extent temperature;
- Interpret the results from the current study within the broader framework created by other southern Cape speleothem studies (Talma & Vogel 1992; Bar-Matthews *et al.* 2010; Braun 2014).

1.4 Hypotheses

- The BL1 stalagmite from Bloukrantz Cave in De Hoop indicates that MIS 5a (*c.* 85 ka - 74 ka) was characterised by warmer temperatures and increased summer rainfall that favoured C_4 vegetation;
- The KDS stalagmite from Klipdrift Shelter links MIS 4 (*c.* 72 ka - 62 ka) with cooler temperatures and wetter conditions due to stronger winter rains as suggested by Chase (2010). Under these cooler MIS 4 conditions, C_3 vegetation cover was favoured.
- In MIS 3 (*c.* 59 ka – 24 ka), the De Hoop stalagmites from Bloukrantz Cave (BL1 ,BL3 & BL4) indicate generally cooler and seasonally drier conditions due to a decrease in winter rainfall (Chase 2010) with variable vegetation.

1.5 Thesis Structure

This thesis contains seven chapters. The first is this introductory chapter that provides a brief overview of the research. The second chapter focuses on the southern Cape and a background to the environmental and archaeological context of the study region is presented here. Chapter 3 provides a background to the methodology and its application in this study. The results obtained using the selected methods are presented and discussed in Chapter 4. In Chapter 5, the results are summarised and evaluated against other speleothem proxy evidence from the southern Cape. Chapter 6 summarises the palaeoenvironmental interpretations derived from the speleothem record in the context of archaeological proxies (*viz.* shellfish, micromammals, large mammal fauna & ostrich eggshell). The final chapter presents a summary of the research findings and here the hypotheses outlined in section 1.4 are evaluated.

Chapter 2 – BACKGROUND TO THE ENVIRONMENTAL & ARCHAEOLOGICAL CONTEXT OF THE SOUTHERN CAPE

2.1 Introduction

South Africa's southern Cape[1] is increasingly identified as a region of archaeological and climatic importance. From an archaeological perspective, a number of significant Middle Stone Age finds have emerged from this region. These include, amongst others, fragmentary human skeletal remains from Klasies River main site (Rightmire & Deacon 1991; Deacon 2008) and evidence for pigment use, coastal occupation, and utilisation of marine resources at Pinnacle Point (Marean *et al.* 2007). There is also evidence for artistic ability and personal adornment during the Middle Stone Age. This has been interpreted respectively from cross-hatched designs on pieces of ochre (Henshilwood *et al.* 2002, 2009) and perforated marine shells from Blombos Cave (Henshilwood *et al.* 2004; d'Errico *et al.* 2005). Further, within a broader context of human evolution, the southern Cape is thought to have served as a migratory and dispersal corridor for people and animals (Marean 2010; Compton 2011; Armitage *et al.* 2012).

From a climatic perspective, the southern Cape is recognised as an important region for understanding southern African climate and vegetation dynamics. This is because the region is the confluence for the Indian and Atlantic Oceans and falls within South Africa's year-round rainfall zone (Meadows & Baxter 1999; Chase & Meadows 2007). Since climatic changes in this region are known to have occurred in response to variations in global oceanic and atmospheric circulation, it is also important

[1] Here it is defined as the region between Cape Town and Cape Recife and includes De Hoop Nature Reserve and the areas of Plettenberg and Tsitsikamma

within a broader southern hemisphere context (Tyson 1986; Cockcroft *et al.* 1987; Chase & Meadows 2007; Chase 2010).

The current chapter consists of four main sections. The first provides an overview of the chapter and the second section (section 2.2) focuses on the present-day environments in the southern Cape. In section three (section 2.3), the discussion is directed towards the Middle Stone Age context of the southern Cape. This section also includes an overview of the current hypotheses and interpretations of Middle Stone Age environments from MIS 5a to MIS 3 (section 2.3.2). In section 2.4 of this chapter, the study site of De Hoop Nature Reserve is introduced and each of the caves where stalagmites were sampled are described individually.

2.2 Present-day environments in the southern Cape

2.2.1 Geology & topography

The geology of the southern Cape and by extension De Hoop traces back to the break-up of Gondwana *c*. 135 Ma. The underlying geology comprises Cape Supergroup rocks with quartz arenites of Table Mountain sandstone (TMS), with overlying Bokkeveld mudstones and shales (Tankard *et al.* 2012). The Bokkeveld shales are in turn found below the Uitenhage shale conglomerates (Partridge & Maud 1987; Holmes *et al*. 2007). These shale deposits are capped by younger Tertiary mostly limestone deposits belonging to the Bredasdorp Group (Marker & Holmes 1999, 2005). The Bredasdorp Group is further subdivided into five different formations which are all of marine origin (Malan 1989). The oldest of these is the De Hoop Vlei Formation which is primarily composed of calcarenites and overlain by the consolidated aeolian sands of the Wankoe Formation. The Wankoe deposits are in turn covered by unconsolidated sands belonging to the Klein Brak Formation, which is found beneath the calcretes of the younger Waenhuiskrans and Strandveld dune sands deposits. The latter is of Holocene age (Malan 1989; Marker & Holmes

2005). As a whole, aeolian sands of the Bredasdorp Group are a prominent feature of the region and include barrier dunes, lunette dunes and aeolianites (Marker & Holmes 2010; Quick 2013).

The southern Cape coastal platform which is a prominent off-shore feature of the area is believed to have formed during the Gondwana split (Holmes & Meadows 2012). This coastal platform can be traced from Bot River (34º14'S, 19º12'E) east of Cape Town to Grahamstown (33º18'S, 26º52'E) (Marker 2003: 33). The coastal platform contains the Riversdale and Agulhas Plains with the Riversdale Plain, surrounded in the north by the Langeberg Mountains, stretching for 40 km inland and elevated close to 300 m amsl (Henshilwood 1995). Blombos Cave lies along the Riversdale Plain while De Hoop Nature Reserve is situated on the eastern side of the Agulhas Plain. This includes the sites of Bloukrantz Cave, West Cave, Klipdrift Sea Cave and the archaeological sites forming the Klipdrift Complex (*i.e.* Klipdrift Shelter & Klipdrift Cave). The local Potberg Mountain, which is a remnant of the older Cape Fold Belt (CFB) range (Henshilwood *et al.* 2014), is an isolated mountain that rises some 311 m from the Agulhas Plain. Although the coastal platform is relatively flat, in places it drops abruptly to form steep cliffs. This dramatic change in topography is most evident at Tsitsikamma where there are deep gorges cut into incised into the mountain by the local rivers and the coastal platform drops steeply to the sea (Moffett & Deacon 1977; Talma & Vogel 1992). Between Knysna, Mossel Bay and Plettenberg steep cliffs are also exposed on the coastal platform.

Another prominent feature of the southern Cape is the two parallel mountain ranges that form part of the greater Cape Fold Belt system. The formation of the CFB is linked to the orogeny of the Cape Supergroup rocks which were lithified and deformed *c.* 260 Ma (Compton 2004, 2011). The first range is the coastal mountains of the Langeberg and Tsitsikamma with the latter forming a continuous range with the Outeniqua Mountains in the east (Paterson-Jones 2006). The second mountain

range, known as the Swartberg is located beyond the Langeberg Mountains. The Little Karoo lies between the western end of the Outeniqua-Tsitsikamma range and on the southern side of the Swartberg while the Great Karoo is north of the Swartberg (Paterson-Jones 2006). The Cango Caves and the archaeological site of Boomplaas Cave are located in the foothills of the Swartberg (Moffet & Deacon 1977; Talma & Vogel 1992). The Little Karoo speleothems that were recently analysed by Kirsten Braun also come from a cave system that lies within the Swartberg (Braun 2014 also see discussion in Chapter 5 & 6).

With regards to the karst topography of the southern Cape, and specifically De Hoop, the limestones in the region are formed primarily of calcified sands belonging to the Wankoe Formation (Holmes *et al.* 2007; Marker & Holmes 2012). At De Hoop, the limestones have an east-west orientation and include dolines (circular hollows), uvalas, poljes (circular & oval shaped depressions) and caves (Holmes & Meadows 2012: 30). The De Hoop caves are primarily marine abrasion cavities (sea caves) that formed from weathering of the basal Table Mountain sandstone. Many of the sea cliffs in the region also formed because of wave action. The weathered quartzite sea cliffs alternate with sandy bays such as Mossel Bay, Walker Bay and Still Bay. The alternation between sea cliffs and sandy bays is evident throughout the southern Cape and is also present at De Hoop. At some localities such as the Knysna-Wilderness area limestone is typically replaced by barrier dunes and coversands (Holmes *et al*. 2007: 131).

As a whole, the geology of the southern Cape has had an important influence on landscape topography which in turn, has influenced the distribution of vegetation types through its effect on soil properties (*e.g.,* texture & structure) and rainfall distribution. This is discussed further below.

2.2.2 Rainfall, vegetation & major climate drivers of the southern Cape (temperature, atmospheric circulation & ocean currents)

Rainfall

In South Africa, seasonal rainfall is currently distributed across three zones; the winter rainfall zone (WRZ), summer rainfall zone (SRZ) and year-round rainfall zone (YRZ) (Chase & Meadows 2007) (Fig. 2.1). The extent of each of these rainfall zones is thought to have shifted throughout the Quaternary and a number of different conceptual models have been proposed to further explain the dynamics of the shifts in the position of the WRZ in particular (Van Zinderen-Bakker 1976; Cockcroft *et al.* 1987; Chase 2010; Stager *et al.* 2012; Weldeab *et al.* 2013). The present-day WRZ is estimated to receive more than 66% of its rain during the austral winter months whereas in the SRZ rainfall is mainly distributed during the summer months (Chase & Meadows 2007). In contrast to the WRZ and SRZ, where rainfall is highly seasonal, the YRZ receives rainfall throughout the year with between 33% and 66% of rain derived from winter rainfall sources (Chase & Meadows 2007: 109). As a whole, the present-day southern Cape receives year-round rainfall derived from both summer and winter precipitation.

However, due to the combined effects of topography and atmosphere and ocean circulation patterns, local rainfall distribution is highly variable across the area. For example, the orographic effect of the Outeniqua-Tsitsikamma range is associated with higher (annual average) precipitation over Knysna (*c.* 716 mm pa) and George (*c.* 662 mm p.a) including Klasies River (*c.* 1200 mm p.a.) and Plettenberg Bay (912 mm p.a). In contrast, on the relatively flat Riversdale and Agulhas Plains, where Blombos Cave and De Hoop Nature Reserve are located, average annual precipitation is lower at 384 mm p.a. and 380 mm p.a., respectively. Synoptic scale systems related to the westerly wind

disturbances also influence rainfall dynamics in the southern Cape with cut-off lows bringing heavy rain to the area in winter while coastal lows are associated with relatively drier conditions (see discussion below).

Vegetation

With regards to vegetation, the southern Cape is located within the Fynbos Biome of the Cape Floristic Region (CFR) which is recognised as a one of the world's most botanically diverse regions (Cowling 1990; Goldblatt & Manning 2002; Linder 2007). As a whole, the CFR is dominated by fynbos, renosterveld and strandveld vegetation (Mucina & Rutherford 2006). The majority of the fynbos taxa occuring in the Fynbos Biome belong to the Restionaceae, Proteaceae and Ericaceae (Thwaites & Cowling 1988; Meadows & Baxter 1999; Goldblatt & Manning 2002). Fynbos vegetation as a whole is characterised by sclerophyllous shrubs and typically occurs on the nutrient-poor, oligotrophic soils produced from the sandstone rocks belonging to the Cape Supergroup (Linder 2007).

The distribution of the plants within the biome is strongly influenced by the underlying geology, which in turn determines the soil that can support specific vegetation types (Cowling 1990). Mountain fynbos (also sandstone fynbos) for example, typically occurs on oligotrophic soils derived from granites and sandstones of the Cape Supergroup rocks. It is primarily associated with mountain ranges and with the exception of the western section of the Agulhas Plain, mountain fynbos is atypical of the coastal parts of the southern Cape (Thwaites & Cowling 1988; Lombard *et al.* 1997; Mucina & Rutherford 2006). Limestone fynbos, which is dominated by asteraceous, restiods and proteoid type fynbos, favours alkaline soils belonging to the Bredasdorp Group (Mucina & Rutherford 2006). On the coastal lowlands sand fynbos is more widespread and tends to grow in deep, acidic soils (Mucina & Rutherford 2006). Strandveld is recognised as a non-fynbos variant and occurs on calcareous dunes along the coast (Quick 2013). Renosterveld on the other hand occurs in soils derived from underlying Bokkeveld Shales and is typically found in incised

river valleys (Meadows & Baxter 1999) and in fragmented patches on the Agulhas Plain (Lombard *et al.* 1997). Another important vegetation type found in the southern Cape is the Afrotemperate forest which forms the Wilderness-Tsitsikamma forest complex that extends from Knysna to Port Elizabeth (Mucina & Rutherford 2006). This vast expanse of indigenous forest also includes the areas of George, Mossel Bay and Klasies River. The different vegetation types identified across South Africa, including the fynbos variants associated with the southern Cape and discussed above are illustrated in Fig. 2.2.

In addition to soil conditions, vegetation structure is also influenced by rainfall. Across South Africa as a whole, vegetation composition is closely correlated with annual and seasonal rainfall. Based on this link between rainfall and vegetation, C_4 photosynthesising grasses and plants typically occur in the interior summer rainfall parts of South Africa while C_3 trees and shrubs are widespread in the present-day winter rainfall areas. Fluctuating atmospheric carbon dioxide levels are also recognised as an important control on vegetation composition particularly over longer time scales such as a glacial-interglacial periods (Vogel *et al.* 1978; Cerling *et al.* 1997; Ehleringer *et al.* 1997; 2002; Bond *et al.* 2003). The general prediction is that C_4 plants and grasses typically expand their distribution under warm growing season conditions with low CO_2 levels (Cerling *et al.* 1997; Ehleringer *et al.* 1997, 2002). In contrast, C_3 expansion is favoured as atmospheric carbon dioxide levels increase and associated growing season temperatures are cooler. From a palaeoenvironmental perspective, glacial periods associated with low atmospheric CO_2 levels are thought to provide conditions suitable for C_4 expansion relative to C_3 plants. Under present-day conditions of negligible atmospheric CO_2, C_4 plants are more widespread in warmer conditions while C_3 plants typically occur under cooler conditions. In the context of this study, the potential influence of changes in atmospheric CO_2 levels on the southern Cape vegetation from MIS 5a to MIS 3 is discussed further in Chapter 6.

In addition to geology, soil conditions and atmospheric CO_2 levels, vegetation composition and distribution, at least within the CFR, is also influenced by local climate, rainfall seasonality and fire regime (Cowling 1983; Goldblatt & Manning 2002; Mucina & Rutherford 2006; Linder 2007). For example, as a whole, fynbos expansion is associated with higher summer temperatures, more seasonal winter rainfall and frequent, intense fires (Cowling *et al.* 1992; Mucina & Rutherford 2006). In contrast, the southern Cape Afrotemperate forests of the Wilderness-Tsitsikamma region tend to favour conditions with less seasonal rainfall, low fire frequency and equable temperatures (Linder 2007; Quick 2013).

Temperature

Temperatures along the southern Cape coast are largely regulated by the combined effects of the ocean currents and local rainfall dynamics with very little variation around the average annual temperature of 18^{o}C at the coast. As a whole, temperatures along the coast are fairly mild but generally much cooler during the austral winter months (June, July & Aug.) when cut-off lows bring heavy rain to many parts of the southern Cape (see discussion below). During the warmer summer months (Nov., Dec. & Jan.) maximum temperatures reach up to 27^{o}C when Berg wind conditions associated with coastal lows are more pervasive (See discussion below).

Atmospheric circulation

In the Southern Hemisphere the easterlies are located at 0^{o}S and 30^{o}S and are embedded within the tropical easterly flow and converge at the Intertropical Convergence Zone (ITCZ) (Fig. 2.3). The winds are a rain bearing system, which brings warm moisture from the Indian Ocean (Tyson & Preston-Whyte 2000). In the South African context, the tropical easterlies are responsible for rainfall in the SRZ (between Nov. & Mar.) when the strength of the tropical easterly winds is greatest (Tyson & Lindsey 1992; Tyson & Preston-Whyte 2000). In addition to the easterly flow, seasonal shifts in the South Atlantic Anticyclone also play a role in bringing rain to South Africa. The South Atlantic Anticyclone is linked to

reduced rainfall and overall drier conditions in the interior. This is because of its role in blocking easterly flows that bring summer rain to SRZ and the southern Cape coast, where it is also linked to the formation of cut-off lows (Tyson & Preston-Whyte 2000; Chase 2015).

Summer rainfall variability is also linked to the formation of temperate tropical troughs (TTTs). Temperate tropical troughs are produced through the interaction between tropical convection (*e.g.* easterly flows) and mid-latitude westerly perturbations (Macron *et al.* 2014: 1634). The occurrence of TTTs is largely associated with the formation of cloud bands and these are responsible for large amounts of rain over the South African interior during the austral summer (Tyson & Preston-Whyte 2000; Macron *et al.* 2014). In the context of the southern Cape, TTTs also bring increased amounts of rainfall to the coast.

Ocean currents

The southern Cape, located at the confluence of the Indian and Atlantic Oceans, is influenced by the Agulhas and Benguela currents. The latter occurs on the west coast of South Africa and is a major upwelling region while the southern Cape is more strongly influenced by the warm Agulhas current (Quick 2013). Variations in ocean sea surface temperatures (SSTs) have previously been recognised as having an important influence on rainfall variability in South Africa, which is for example due to its effect on moisture and heat fluxes (Cohen & Tyson 1995; Washington & Todd 1999; Lutjeharms *et al.* 2001; Chase 2010; Macron *et al.* 2014). While the southern Cape is not a major upwelling system, it has recently been suggested that weaker Benguela upwelling along the west coast could enhance upwelling along the southern Cape coast (Chase 2015). This would seemingly allow for increased tropical easterly flow that brings rain to the interior and southern Cape coast during summer.

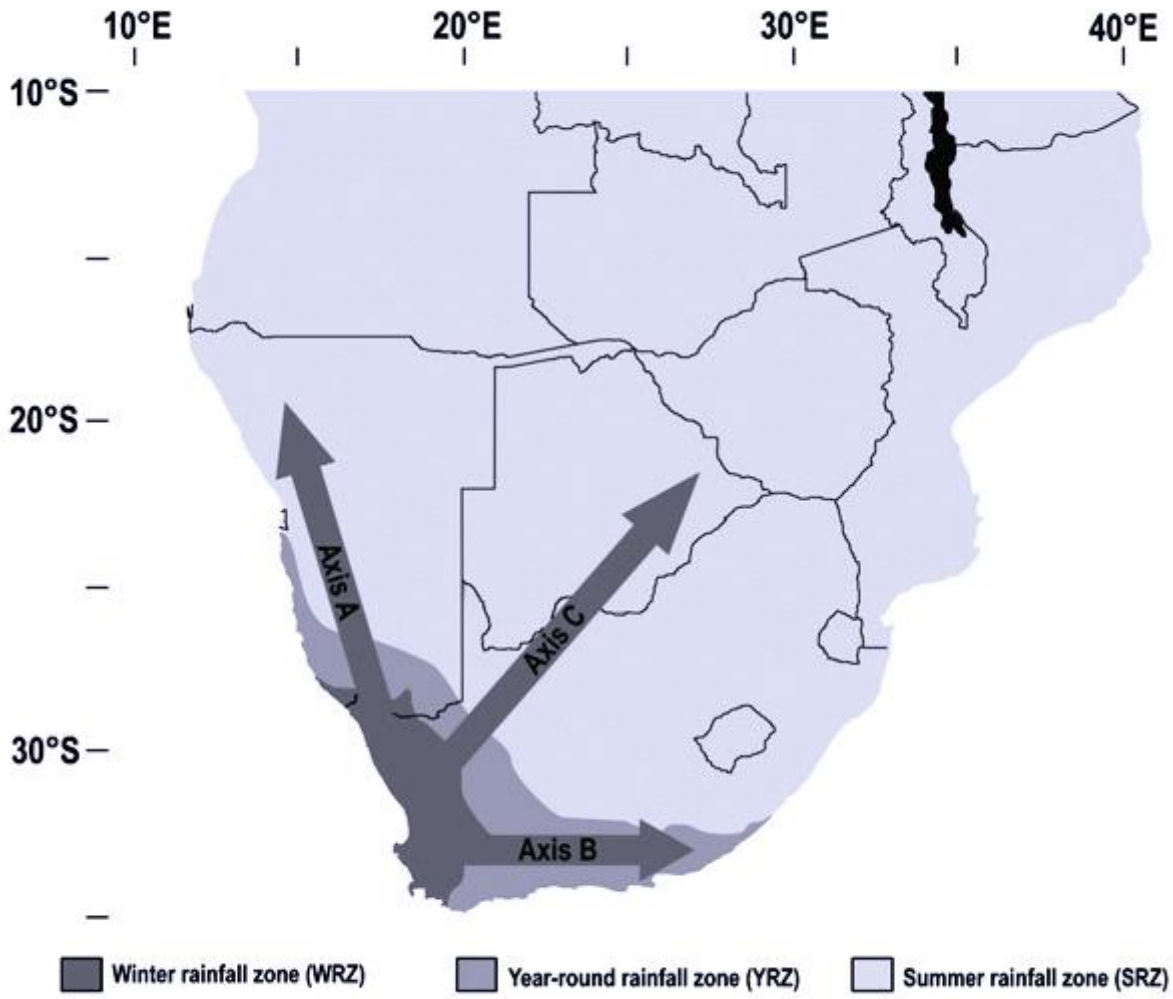

Fig. 2.1 Extent of South Africa's rainfall zones (after Chase & Meadows 2007)

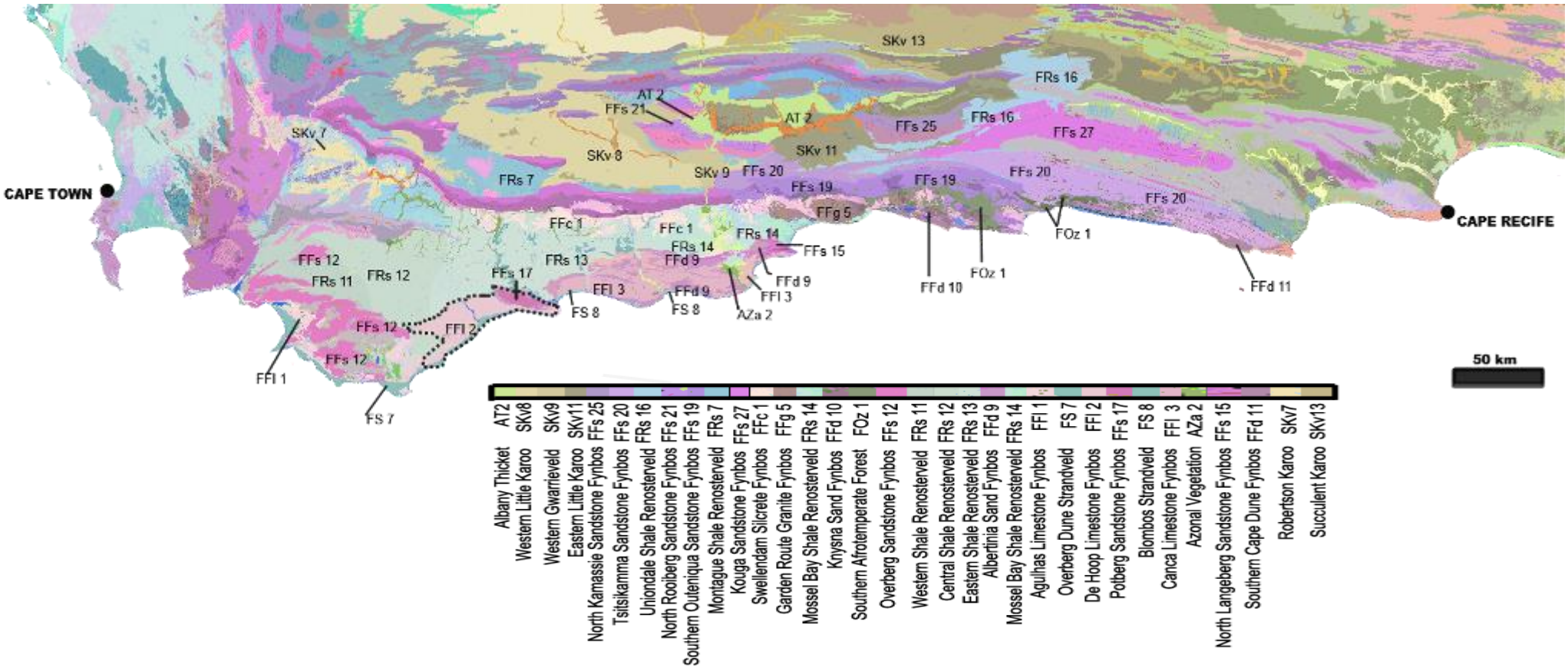

Fig. 2.2 Vegetation map for the southern Cape which is defined here as the area between Cape Town and Cape Recife. The extent of the De Hoop Nature Reserve (.....) is also shown along with the distribution of different vegetation types found in the Fynbos Biome of the Floristic Region (after Mucina & Rutherford 2006; http://bgisviewer.sanbi.org/BGISLUDS-SL-Viewer/Viewer.html?Viewer=National%20vegetation%20map%202006&layerTheme=National%20Vegetation%20Map%202006)

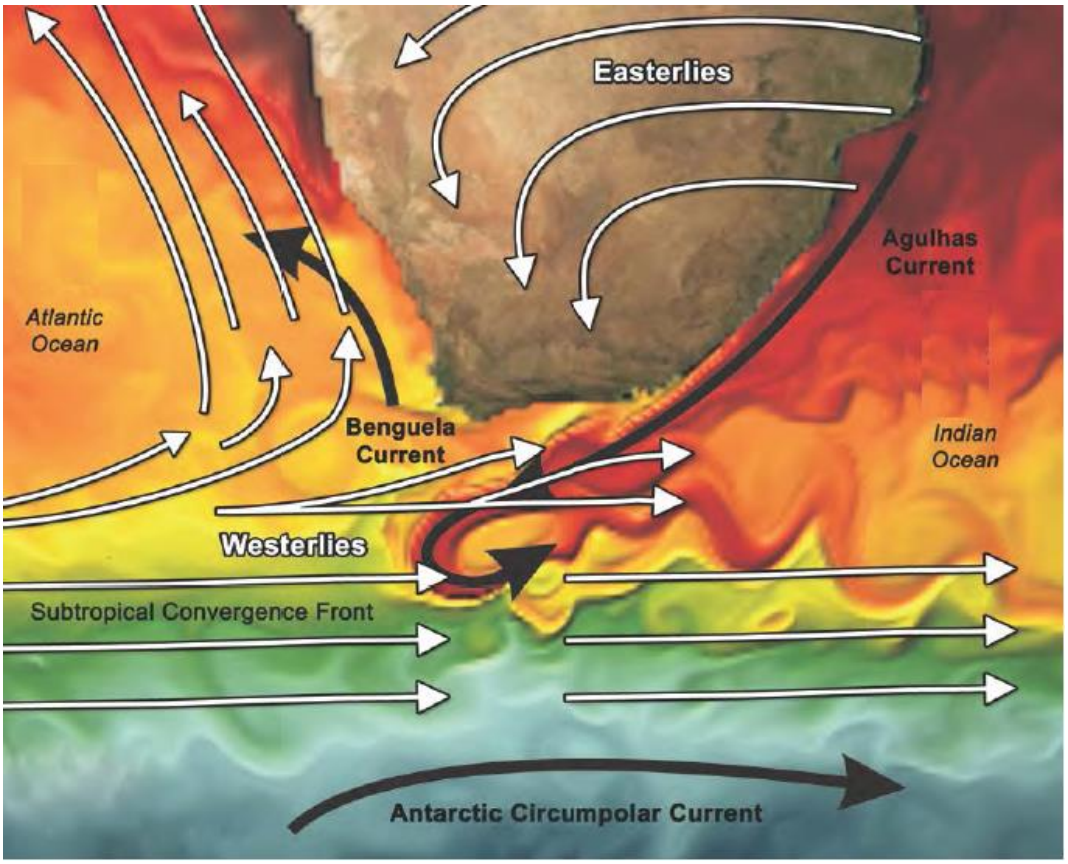

Fig. 2.3 Key atmospheric-ocean interactions around the southern Cape (from Quick 2013: 25)

Fig. 2.4 Key southern Cape archaeological sites mentioned in the text (Die Kelders Cave, Klipdrift, Blombos Cave, Pinnacle Point, Boomplaas Cave & Klasies River). (After Henshilwood *et al.* 2014)

2.3 The Middle Stone Age of the southern Cape

The South African Middle Stone Age (hereafter MSA) was first described in 1929 and identified as a flake industry (Goodwin & van Riet Lowe 1929). Different periods within the MSA have historically been named according to the diagnostic lithic assemblages that characterise it. Based on the extensive MSA lithics from Klasies River, four techno-complexes are identified within the MSA for the Southern Cape and these have previously been described by Singer and Wymer (1982), Volman (1984) and Wurz (2002, 2013). The Late Pleistocene MSA in the southern Cape is subdivided into four main phases (Lombard et al. 2012; Wurz 2013; Wadley 2015). Klasies River main site has the most extensive sequence in the southern cape, and here the MIS 5 lithics consist of two phases, the MSA I (also known as Klasies River techno-complex, and MSA 2a) and MSA II (also known as Mossel Bay techno-complex, or MSA 2b) (Wurz 2002, 2013; Volman 1984). The two other main MIS 5 assemblages from the southern Cape are from Pinnacle Point (Thompson *et al.* 2010) and Blombos Cave (Douze et al. 2015). Technologically they are broadly similar to the Klasies River assemblages, in that they are characterised by local raw material utilisation, and unretouched blades and points produced with prepared core techniques, but unique elements occur (Thompson et al 2010; Douze et al 2015).

The second phase is the Still Bay that dates to the last part of MIS 5 (*c.* 75.5 ka – 67.8 ka) (Jacobs *et al.* 2008, 2013; Henshilwood 2012). Currently the only stratified Still Bay site in the southern Cape isBlombos Cave and is associated with retouched bifacial points that have a foliated appearance (Henshilwood 2008, 2012). These particular tools were mostly produced from silcrete although quartz and quartzite were also used.

The Howiesons Poort is the third phase (*c.* 64.8 ka – 59.5 ka) (Jacobs *et al.* 2008). It is regarded as a microlithic industry characterised by small blades, backed pieces (or segments) and notched artefacts and fine grained raw mateirals (Lombard 2009) although regional variability occurs (Wurz 2013; Mackay et al 2014). In the southern Cape this industry occurs at Klasies River, Pinnacle Point, Klipdrift Cave, Boomplaas Cave and Nelson Bay Cave (Wurz 2013).

The post-Howiesons Poort (*c.* 58 ka – 45 ka) (also known as MSA III & MSA IV or late MSA) makes up the fourth phase. It is described as a unifacial point dominated assemblage that also contains scrapers and blades (Wadley 2015). The post-Howiesons Poort industry is not as extensive in the southern Cape as the Howiesons Poort techno-complexes, and assemblages from Klasies River, Boomplaas, Pinnacle Point 5/6 and Klipdrift Shelter are known. In a recent review on the Middle Stone Age, it has however been noted that at some sites (*viz.* Diepkloof Rockshelter & Sibudu) the MSA sequence contains assemblages that do not fall neatly within the current sequence from South Africa (Lombard et al 2012; Wadley 2015). In the context of the southern Cape, there is a rich MSA record that includes key finds such as fossil human remains, shell beads, hafted lithics and bone tools, incised ochres and decorated ostrich eggshell. These and other artefacts have been used as proxy indicators of cognitive ability in the MSA and also helped to refine our understanding of various aspects of MSA life. This includes for example, subsistence behaviours, lithic production strategies and social organization.

In the context of this study, the stalagmite data analysed and interpreted overlap with the MSA techno-complexes mentioned above. For this reason, a background to the southern Cape sites associated with the MSA II, Still Bay, Howiesons Poort and to a lesser extent post-Howiesons Poort is provided below.

2.3.1 Background to the sites, MSA periods covered and dating

Blombos Cave

Blombos Cave (34.4ºS, 21.2ºE) is situated in a wave cut cliff of formed of calcarenites belonging to the Wankoe Formation. The site is elevated at 34.5 m above modern sea level (amsl) and located *c.* 320 km east of Cape Town, *c.* 100 km west of De Hoop Nature Reserve and 400 km northeast of Klasies River main site. Blombos contains Later Stone Age (LSA) and Middle Stone Age deposits.

The latter MSA deposits have been extensively dated using luminescence (OSL & TL), electron spin resonance and uranium-series techniques (Vogel 2001; Feathers 2002; Eggins *et al*. 2005; Tribolo *et al*. 2005; Jacobs *et al*. 2008). The MSA layers are divided from the top to the base into the M1, M2 (upper & lower) and M3 phases. Stratigraphically, the M1 consists of layers CA, CB, CC, CCC, CD and CDA and CDB (Fig. 2.5). The most recent OSL dates for the M1 (at 1σ) are: 73 ± 4 ka, 75 ± 4 ka and 73 ± 5 ka, which collectively place the M1 between *c*. 69 ka and 79 ka (Jacobs *et al.* 2013). Near the end of the M1 occupation, the cave was sealed by a dune infill dating to *c.* 70 ka (Jacobs *et al.* 2003, 2006). This represents a hiatus layer and seperates the MSA and LSA deposits at the site.

The M2 is subdivided into the upper and lower M2 with the upper M2 represented by layers CFA, CFB/CFC and CFD while the lower M2 contains layers CGAA, CGAB, CGABh1 and CGAC. The most recent OSL dates (1σ) for the upper M2 phase are: 70 ± 4 ka, 76 ± 5 ka, 69 ± 5 ka and 77 ± 5 ka and places the upper M2 to between 69 ka and 77 ka. The lower M2 has recently been dated to 79 ± 6 ka (Jacobs *et al.* 2013). The M1 and upper M2 contain the Still Bay techno-complex and based on the current OSL age determinations, these levels fall primarily within MIS 5a.

The key finds from the Blombos Still Bay levels are the diagnostic Still Bay points, evidence for heat treatment and subsequent pressure flaking of the

points, marine shell beads of *Nassarius krausianus*, engraved ochres and bone tools (Henshilwood *et al.* 2001, 2002; Henshilwood 2007, 2008, 2009, 2012, Mourre *et al*. 2010). The oldest phase in the Blombos stratigraphy is the M3 which consists of layers CH, CI, CJ and CJh1, CK, CL and CM down to CR. This phase is dated between 97 ka and 101 ka (Jacobs *et al.* 2013).

With regards to the environmental proxies from the site, shellfish, micromammals, large mammal fauna and ostrich eggshell from the Still Bay levels are pertinent to this study. A number of different names and groupings have previously been used when describing the Blombos proxy data. The shellfish data for example is reported for each of the M1, M2 and M3 phases as a whole whereas the micromammal data for the M2 is subdivided into upper and lower levels. This particular proxy record contains a very detailed analysis of the Blombos MSA micromammals and as a result the lower M2 is represented by units CGAC, CGABh1 and CG-CGAA and CGAB of which CG-CGAA contains a grouping of layers (CG, CGA and CGAA). The upper M2 is represented by units CFD, CFB/CFC and CF-CFA (containing layers CFH, CFh1 & CFA) (Hillestad-Nel 2013). In the M1, micromammal data comes from the CD and CA-CCC units (containing layers CCC, CC, CB & CA) which represent the "…*transition of MIS 5a/4 and possibly the beginning of MIS 4…"* (Hillestad-Nel 2013: 217).

Unlike the micromammal data from the M2 levels, the large fauna was not initially separated into the upper and lower M2 (Henshilwood *et al.* 2001). More recent taphonomic analyses of the Blombos fauna have however sub-divided the M2 levels into the upper and lower M2 (Reynard 2011; Reynard *et al.* 2014; Thompson & Henshilwood 2011, 2014a, b). In terms of the ostrich eggshell (OES) proxy data from the Still Bay levels at Blombos, those samples representing the M1 come from layers CC and CD, those for the upper M2 are from CFB/CFC and the M3 is represented by samples from layers CIB, CJ, CK, CL and CN/CO (Roberts 2013).

Based on the OES data, the M1 and M2 (upper) are combined into a single group named Blombos 1 (Roberts 2013).

Each of these proxies are discussed further in Chapter 6 in relation to the De Hoop speleothems and other records of environmental change in the southern Cape.

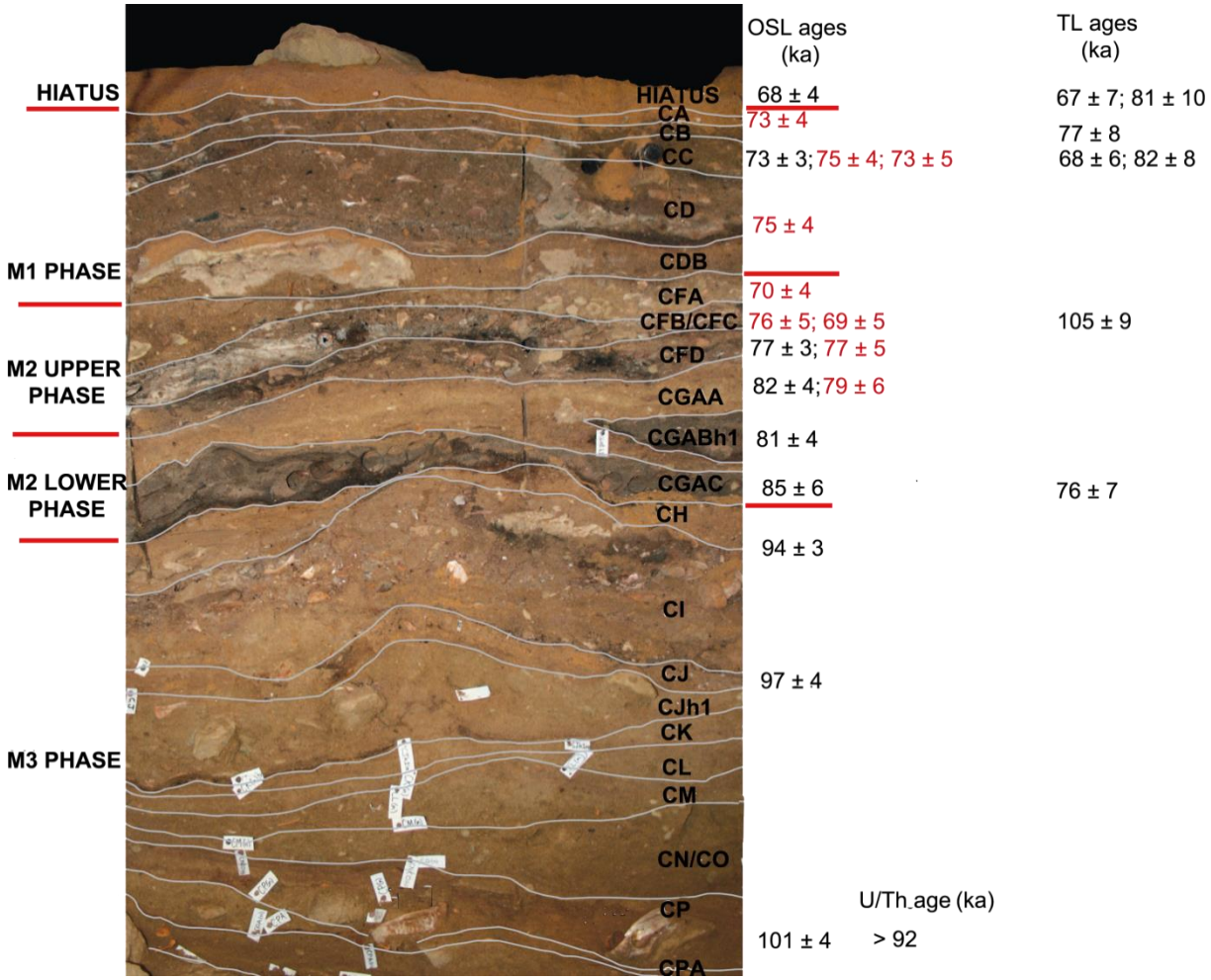

Fig. 2.5 Stratigraphic units of the Middle Stone Age phases (M1, M2 & M3) at Blombos Cave. The recently reported OSL ages for the M1 and M2 (upper & lower) phases reported by Jacobs *et al.* (2013) are shown in red. For comparative purposes the OSL and TL ages previously determined for the site are presented in black (Modified from Henshilwood *et al.* 2011: 220).

Klasies River main site

Klasies River Mouth (34°06'S, 24°24'E) is located *c.* 530 km east of De Hoop, *c.* 290 km east of Pinnacle Point and *c.* 130 km west of Port Elizabeth. The main site consists of a series of caves and shelters denoted as cave 1, 1A-C and 2 (Deacon & Geleijnse 1988; Wurz 2002: 1002) and is often referred to as Klasies River Mouth or Klasies River main site. At Klasies the caves were formed in quartz arenites of the Cape Supergroup rocks that form the Tsitsikamma Mountain. The main site consists of Caves 1 and 2, and shelters 1A and 1B, (Singer & Wymer 1982; Deacon & Deacon 1999). The MSA deposit in the main site is roughly 21 m thick (Deacon & Geleijnse 1988) and the stratigraphy consists from the base to the top of the LBS Member, the SAS Member and the Upper Member (Singer & Wymer 1982; Deacon & Geleijnse 1988; Wurz 2000).

Within the stratigraphy of the main site, the LBS Member is dated to *c.* 115 ka while the MSA II in the SAS Member is dated to between 108 ka and 77 ka. The upper part of the SAS Member is pertinent to this study because it dates to part of early MIS 5a with dates of *c.* 85 ka and *c.* 77 ka (Vogel 2001; Feathers 2002; Wurz 2002). The latter date of *c.* 77 ka comes from a carbonate crust in layer 14 near the top of the SAS member (Vogel 2001). The SAS member found beneath the Rockfall Member (or RF & also Layer 22, Singer & Wymer 1982) is 0.5 m thick and situated between the SAS and Upper Member. OSL age determinations place the RF Member between *c.* 72.3 ka and 70.8 ka (Feathers 2002; Jacobs *et al.* 2008).

The RF Member is in turn overlain by the Upper Member which has been dated to between 65 ka and 52 ka (Jacobs *et al.* 2008). This member contains the Howiesons Poort and MSA III (post-Howiesons Poort) (Singer & Wymer 1982; Deacon & Geleijnse 1988; Wurz 2002). These phases in the Upper Member correlate respectively with MIS 4 (*c*. 64.8 ka – 59.5 ka; Jacobs *et al.* 2008) and part of MIS 3 (*c.* 60.2 ka – 55.6 ka; Jacobs *et al.* 2008). At Klasies, a weighted mean age of *c*. 56 ka obtained by TL

methods has also been reported for the Howiesons Poort deposits (Tribolo 2003). A single uranium series age of *c.* 65.5 ka obtained on carbonate crust also places the Howiesons Poort deposits at the Klasies River main site within MIS 4 (Vogel 2001). This age determination is however considered contentious because of thorium contamination issues which are suspected of comprising the accuracy of the age estimate.

With regards to the MSA III, this phase falls within early MIS 3 and these deposits have been dated by luminescence techniques (TL & OSL) with age determinations between 57.9 ka (Jacobs *et al*. 2008) and *c*. 50 ka (Feathers 2002). The transition from the Howiesons Poort to the MSA III has similarly been dated to early MIS 3 with electron-spin resonance techniques dating this occurence to between 56 ka and 53 ka (Eggins *et al.* 2005). The key finds from the Howiesons Poort layers are the characteristic microlithics of small blades and backed geometrics as well as bone tools and an ochre crayon (Watts 1999; Wurz 2000, 2013). In the SAS Member there are dense shellfish layers in the upper part of the member as well as bone tools and fossil human teeth.

In terms of the environmental indicators from the site, the main proxies pertinent to this study come from the shellfish assemblage in the SAS Member of MSA II, and the micromammals from the MSA II, Howiesons Poort and MSA III as well as the large mammal fauna associated with each of these periods. The data are discussed further within a broader environmental context of the southern Cape in Chapter 6.

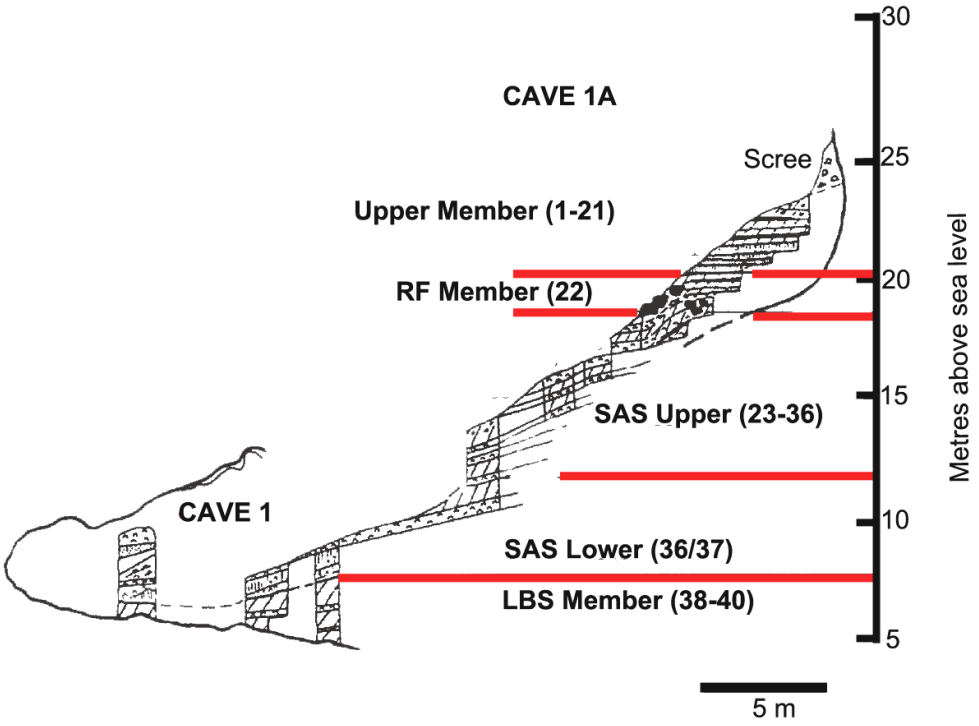

Fig. 2.6 Stratigraphic members of the Klasies River main site sequence (Modified after Wurz 2002)

Klipdrift Shelter

Klipdrift Shelter forms part of the Klipdrift Complex (34º27.0963' S, 20º43.4582'E) and is located within a coastal cliff in the eastern side of the De Hoop Nature Reserve. The site is a *c*. 7 m deep shelter that is elevated *c.* 19 m amsl and 45 km south-west of Blombos Cave (Henshilwood *et al.* 2014). The archaeological deposits are truncated and extend for 7 m^2 on a slope of 29º behind the dripline (Henshilwood *et al.* 2014: 286). Excavations were started in 2011 and twenty layers have been excavated at the site. The Howiesons Poort assemblage is however mostly within layers PCA, PBE, PBD, PBC, PBA/PBB, PAZ and PAY (Fig. 2.7). These layers are collectively dated by single grain OSL techniques to between *c*. 65.5 ka and 59.4 ka which places the Howiesons Poort at Klipdrift Shelter within MIS 4 (Henshilwood *et al*. 2014).

The Howiesons Poort lithics excavated from the site include backed and notched tools, blades, points and borers (Henshilwood *et al.* 2014). These

tools are characteristic of the Howiesons Poort and at Klipdrift Shelter these are composed on a variety of local raw materials such as quartzite, quartz, silcrete, calcrete and cryptocrystalline silicate. Other finds include processed ochre pieces occurring in ground and scraped forms as well as crayon-like pieces found in layers PCA, PBC and PBE and ninety-five engraved ostrich eggshell pieces in layers PAX and PAY to PAC (Henshilwood *et al.* 2014).

Based on the preliminary data from the site, the environmental indicators presently available comes from shellfish, small mammal and large mammal fauna and ostrich eggshell. With the exception of the ostrich eggshell, interpretations of the Klipdrift Shelter data has focused on the stratigraphic layers PAY to PCA. This was primarily because of the highly fragmented assemblage and the resultant small sample sizes (Henshilwood *et al.* 2014). The Klipdrift Shelter archaeo-proxy data are discussed further in Chapter 6.

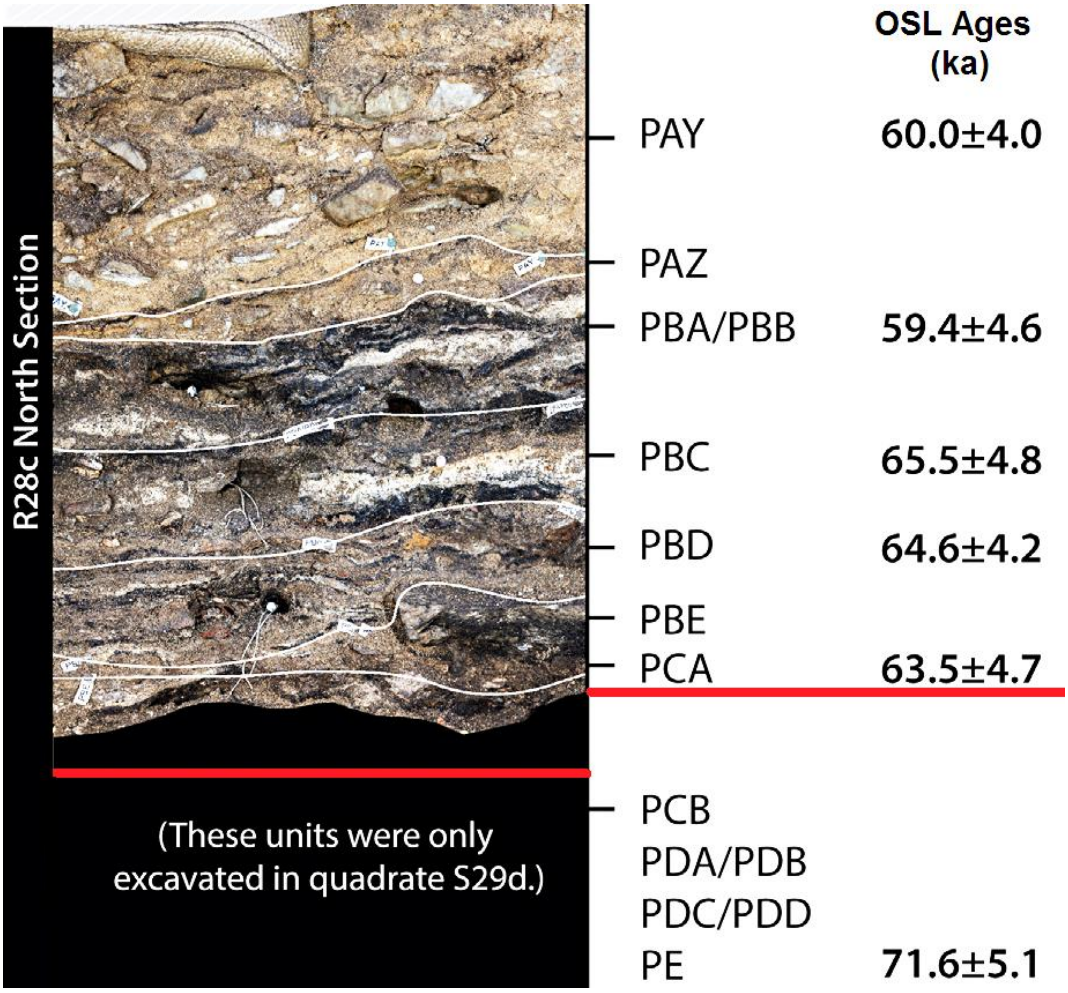

Fig. 2.7 Stratigraphy of the Klipdrift Shelter showing the layers containing the majority of the Howiesons Poort assemblage (after Henshilwood *et al.* 2014)

Boomplaas Cave

Boomplaas Cave (33.23'S, 22.01'E) is located *c.* 302 km north-east from De Hoop Nature Reserve and 4 km east of the Cango Caves. It forms part of the Cango Valley in the foothills of the Swartberg Mountains (Deacon 1979; Klein 1978). The archaeological site, which is formed in a limestone outcrop, is *c.* 75 km inland from the coast and contains Middle and Later Stone Age deposits. The Middle Stone Age deposit of Boomplaas contains clearly defined stratigraphic units with the MSA units, knowns as members, subdivided into the upper and lower MSA. Of these the upper MSA is correlated with MIS 3 and the lower MSA to MIS 4. The part of the MSA associated with MIS 3 is represented by the OLP, BP, YOL and LPC

members and of these YOL is undated (Deacon 1979, 1995; Faith 2013). The OLP member dates from 48 kcal BP to 40 kcal BP (Deacon 1979) while the overlying BP member dates to between 38.6 kcal BP and 36.0 kcal BP and the LPC member to *c.* 25.8 kcal BP (Deacon 1979; Mller *et al.* 1999; Faith 2013). Amino-acid racemization (AAR) estimates have also dated the OLP member to between 48 ka and 44 ka. For the lower MSA units, which are represented by the OCH and LOH members, only the OCH member has been dated (Faith 2013). Uranium-series age determinations place the accumulation of OCH between 66 ka and 55 ka with a corresponding AAR estimate of 71 ka to 59 ka also from OCH (Miller *et al.* 1999). The stratigraphic units from the Boomplaas Cave sequence which are pertinent to this study are shown in Fig. 2.8.

With regards to the environmental proxies derived from the archaeological deposit at the site, the key indicators come from the large mammal fauna (Klein 1978; Faith 2013) and a limited micromammal assemblage (Avery 1982) and also from an analysis of fossil charcoal (Scholtz 1986). Each of these will be discussed in detail in comparison with other proxies pertinent to the southern Cape in Chapter 6.

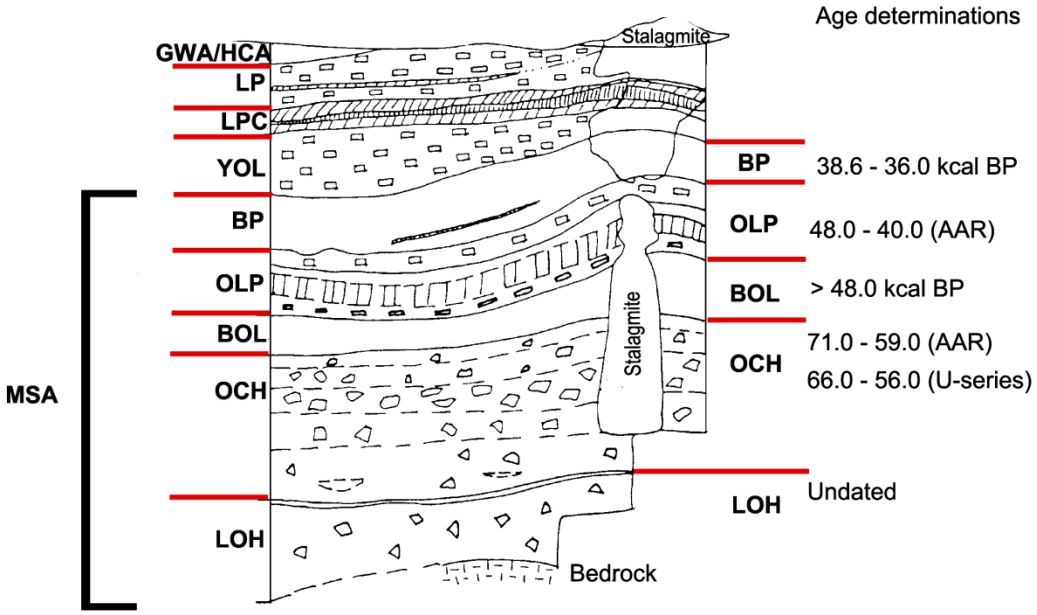

Fig. 2.8 Stratigraphy of the MSA members in the Boomplaas Cave sequence (Modified after Deacon 1979 & Faith 2013)

Die Kelders Cave

The Die Kelders Cave (34º32'S; 19º22'E) is located 120 km south-east of Cape Town. It consists of two coastal caves with the larger one denoted as DK1 and a smaller chamber called DK2 (Grine *et al.* 1991; Marean *et al.* 2000). The site is elevated at 8 m amsl and formed on an unconformity between TMG quartz arenites and overlying limestones of the Bredasdorp Group sediments (Schweitzer 1970; Grine *et al.* 1991; Marean *et al.* 2000). There are also limestone roof spall fragments found within the MSA deposits contained in stratigraphic layers 15 to 4 (Schwarcz & Rink 1999; Marean *et al.* 2000) (Fig. 2.9). At DK1, which is referred to as Die Kelders Cave in this thesis, the MSA deposits are found in stratigraphic layers 15 to 4 (Schwarcz & Rink 1999; Marean *et al.* 2000) (Fig. 2.9). The MSA layers at Die Kelders have been variously dated using luminescence and electron-spin resonance techniques. Luminescence (TL, OSL & IRSL) age determinations (from layers 4/5, 7, 9, 11 and 13) give a mean age for the MSA at Die Kelders of between 60 ka and 70 ka (Feathers & Bush 2000)

which is comparable with a mean ESR age (obtained from layers 4-6, 10 & 12) of 66 ka to 74 ka (Schwarcz & Rink 1999).

From a palaeoenvironmental perspective, the MSA at Die Kelders contains large mammal fauna, tortoise and micromammals as well as birds, reptiles and poorly preserved shellfish (Klein & Cruz-Uribe 1999).

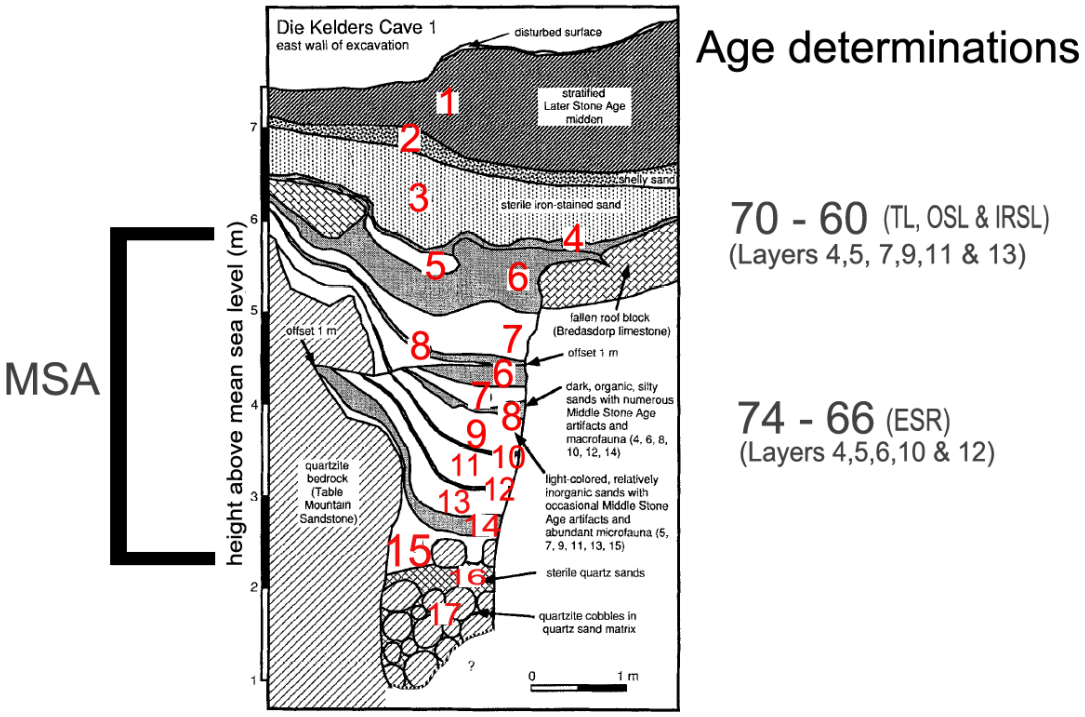

Fig. 2.9 Stratigraphy of the MSA layers at Die Kelders Cave (From Grine *et al.* 2001)

2.3.2 Middle Stone Age environments: an overview of current palaeoenvironmental interpretations and major hypotheses from MIS 5a to MIS 3

In this section I discuss the palaeoenvironment in the southern Cape between MIS 5a and 3, as the data discussed in Chapter 4 cover these periods the most reliably.

MIS 5a (85-74 ka, Martinson et al. 1987)

In terms of MIS 5a environments, current evidence suggests relatively warm and wet conditions at this time (Runge 2010; Blome *et al.* 2012). Sea surface temperatures (SSTs) obtained from alkenones in the TN057-21 sediment core (41^{o}8'S, 7^{o}49'E) north of the Agulhas Ridge in the southern Cape basin also indicate warm conditions. Here temperatures between 17.5^{o}C and 22^{o}C are reported during MIS 5a (Sachs & Anderson 2003). Equable or stable climatic conditions in the southern Cape are inferred from high species diversity values for micromammals in stratigraphic levels correlated with MIS 5a at Blombos Cave and Klasies River (Avery 1987; Avery *et al.* 2005; Hillestad-Nel 2013) (see Chapter 6 section 6.2). Similar to the sediment core TN057-21, the micromammals at Blombos Cave mainly imply warm, wet conditions with evenly distributed rainfall and grassy vegetation with some fynbos. Similar inferences also come from Klasies River. Here warm, wet conditions, but with irregular (seasonal or unequable) rainfall characterised by habitats with dense grassy vegetation is inferred from the micromammals in the upper MSA II (Hillestad-Nel 2013) (Also see discussion in Chapter 6). The associated large mammal fauna from both sites, which contains relatively more browsers than grazers (Klein 1976; van Pletzen 2000; Henshilwood *et al.* 2001), further imply closed habitats supporting an inference of dense vegetation in parts of the southern Cape during MIS 5a.

With regards to MIS 5a sea levels, global estimates indicate seas between 44 m and 19 m lower relative to modern levels (van Andel 1989;

Langejans *et al.* 2012). While global sea levels were comparatively lower in MIS 5a, in the southern Cape, high stands of up to +1.5 m relative to modern sea levels are reported between Cape Hangklip and Plettenberg Bay (Compton 2011). This inference is further supported by palaeoscape model estimates for the Pinnacle Point area and Klasies River which places both sites within close proximity of *c.* 2 km of the coast in MIS 5 (van Andel 1989; Fisher *et al.* 2010). This includes the beginning of MIS 5a. Relatively high shellfish densities from Blombos (upper & lower M2 combined) and Klasies River (MSA ll in the SAS member) similarly imply that sites were close to the sea during MIS 5a (Thackeray 1988; Henshilwood *et al.* 2001; Langejans *et al.* 2012) (see Chapter 6 section 6.2).

In the southern Cape, the formation of aeolianites, which are lithified calcareous dune sand, have been linked to sea level transgressions (*e.g.*, Bateman *et al.* 2004, Carr *et al.* 2007, 2010). Bateman *et al.* (2004: 1694) identified three phases of aeolianite deposition in the Cape Agulhas area that are correlated to MIS 5e, MIS 5b and MIS 5a, the latter dated to *c*. 73 ka-80 ka. Aeolianites are associated with transgressive seas because they contain carbonate minerals which are typically derived from marine organisms such as molluscs (James & Jones 2015). As a result, aeolianites are regarded as highstand deposits because they require a constant supply of marine carbonate to form. Based on this, the formation of the Cape Agulhas aeolianites has been linked to an increase in carbonate-rich sediment supplied to region's beaches (Bateman *et al.* 2004, Carr *et al.* 2007). Other factors that have been associated with episodes of dune building and sandy beach development in MIS 5, including MIS 5a, is onshore wind activity and wave action which redistribute sediments (Carr *et al.* 2010).

In the context of MIS 5a, it appears that aeolianites, at least in the southern Cape, were formed during sea level highstands. While there does appear to be a link between sea level highstands and the formation

of aeolianites this relationship is rather complex. This is because other variables also contribute to the formation of such features. Key amongst these factors is sediment supply, vegetation cover, wind activity and precipitation (Bateman *et al.* 2004; Chase 2009; Thomas & Burrough 2012). From a palaeoenvironmental perspective, episodes of dune development are generally used to infer that environmental conditions were dry and possibly windy (Stokes *et al.* 1997; Stuut *et al.* 2002). However, within the last decade this interpretation has been challenged since current evidence from a broader southern African context does not support a clear link between episodes of dune formation and aridity (review in Chase 2009).

In relation to environmental reconstruction, there is at present not much data pertinent to MIS 5a in particular as researchers previously focused on MIS 5 as a whole (Mackay *et al.* 2014; Kandel *et al.* 2015). One exception is Compton (2011), who links sea level changes in the southern Cape during glacial-interglacial cycles with the archaeological record. He suggests that the southern coastal platform was open during glacial periods and closed (or leaky) during interglacials which includes MIS 5a. According to his model, in MIS 5a sea level was sufficiently high (-45 to +1.5 m) for closure of the southern coastal portal (SCP) situated between Cape Hangklip and Plettenberg Bay. Based on this model, Compton (2011) predicts that closure of the SCP caused habitat loss and restricted movement of both large migratory herds and people. This is thought to have contributed to competition for resources and may have consequently played a role in driving cultural change in the southern Cape at this time. Archaeological sites containing vegetation, rainfall and temperature proxies pertinent to MIS 5a are discussed in Chapter 6 section 6.2.

MIS 4 (73-59 ka, Martinson et al. 1987)

Globally, MIS 4 is characterised as a glacial period with temperatures of *c.* 2ºC to 5ºC lower relative to the present (Lambeck *et al.* 2002). These palaeotemperature estimates come primarily from coral reefs, benthic

foraminifera in ice cores and alkenones (Nürnberg 2000). Similarly low temperatures are reported for the southern Cape where results from the TN057-21 sediment core indicate temperatures between 15^{o}C and 18.5^{o}C during MIS 4 (Sachs & Anderson 2003). In the southern Cape context, MIS 4 is associated with cooler and wetter conditions related to the expansion of the westerly wind driven winter rainfall belt across South Africa (Chase 2010; Blome *et al.* 2012; Ziegler *et al.* 2013). The relatively large sized Cape dune mole rats (*Bathyergus suillus*) and Cape grey mongoose (*Galerella pulverulenta*) at Die Kelders Cave also imply cool and wet conditions in MIS 4 (See Chapter 6 section 6.4). Wet conditions, at least in Die Kelders during MIS 4, is further interpreted from the presence of water dependent large mammal fauna that include southern reedbuck (*Redunca arudinum*), blue antelope (*Hippotragus leucophaeus*), black wildebeest (*Connochaetus gnou*) and hartebeest (*Alcelaphus bucelaphus*) (Discussed further in Chapter 6 section 6.4). Wet conditions are similarly implied by the relative abundance of vlei rats (*Otomys irroratus*) in the part of the Klasies sequence correlated with MIS 4. While MIS 4 is generally associated with cooler conditions, warmer conditions have also been suggested for part of MIS 4 (Thackeray & Avery 1990; Jacobs *et al.* 2008; Thackeray 2009). It should, however, be kept in mind that local climates in South Africa, and by extension in the southern Cape, respond asynchronously to changes recorded in global records (Chase 2010; Blome *et al.* 2012).

Marine oxygen isotope stage 4 represents a period during which northern hemisphere ice sheets expanded and sea levels were *c.* 75 m below msl (Lambeck *et al.* 2002). In the southern Cape context, similarly low sea levels of between 75 m and 103 m below msl are reported between Cape Hangklip and Plettenberg Bay in MIS 4 (Compton 2011). Regressive MIS 4 seas have been linked to the occurrence of lower shellfish densities at Klasies River in the Upper Member (Thackeray 1988; Galimberti 2010; Langejans *et al.* 2012). In the southern Cape, episodes of coastal aeolian deposition have similarly been linked to sea level regression in MIS 4.

Evidence for this comes from lunette and barrier dune formation on the Agulhas Plain that broadly falls within MIS 4. During these phases, sediments exposed on the continental shelf by lowered seas are thought to have been transported and reworked by wind activity (Carr *et al.* 2006). Further evidence for sandy conditions during part of MIS 4 also come from the Klasies sequence where molluscs that favour sand substrates are relatively more abundant in stratigraphic members correlated with MIS 4. In Chapter 6 section 6.4 vegetation, rainfall and temperature proxies from the above-mentioned archaeological sites are further discussed in the context of MIS 4.

In terms of the archaeology and palaeoenvironment, there are two MSA occurrences known as the Still Bay and Howiesons Poort which are correlated with MIS 4. Unlike MIS 5a, for which there is at present very little debate on cultural change, MIS 4 is associated with a number of interesting and conflicting debates on the relationship between cultural change and the environment. Some researchers have for example suggested that "…*deteriorating environments at the beginning of OIS 4*…" played a role in the development of the Still Bay and the Howiesons Poort (McCall 2007: 1750). McCall (2007: 1749) suggests that due to colder and drier MIS 4 conditions, people developed lithic technologies, such as the bifacial Still Bay points and became increasingly mobile, in order to procure scarce and widely distributed resources.

Evidence for cold and dry MIS 4 conditions may come from Klasies River. Here open, grassland habitats are interpreted from the abundance of grazing fauna that imply cool and dry conditions in MIS 4 (Klein 1976; van Pletzen 2000) (Discussed further in Chapter 6 section 6.4). Chase (2010: 1361) has however cautioned that inferences of cold and dry conditions based on the occurrence of grassy, open vegetation might not be entirely accurate. This is because vegetation of the southern Cape is thought to follow a pattern of succession where (succulent) karroid shrubland occurs when conditions are cold and dry. This pattern of vegetation change also

links the occurrence of grassland/thicket with increasing rainfall (Cowling 1983). Furthermore, while phases of lunette construction imply colder and drier conditions in MIS 4 than present (Carr *et al.* 2006: 259) these deposits are not regarded as reliable aridity proxies (Chase & Meadows 2007 also see Chase 2009).

An inference of generally cold, dry and deteriorating environments in MIS 4 is however not widely accepted. Mostly warm conditions with temperatures between 13ºC and 14ºC have for example been associated with the Howiesons Poort in the Upper Member at Klasies River main site (Thackeray 1987; Thackeray & Avery 1990). Warm temperatures are similarly associated with the SAS Member in the MSA II (Thackeray 1992). This interpretation comes from temperature indices that were constructed by applying multivariate statistical techniques to the microfauna, in addition to analyses of marine molluscs in the Howiesons Poort assemblage at Klasies River main site (Thackeray 1992). There are also arguments for wetter conditions in MIS 4 (Chase 2010). This interpretation is echoed by Ziegler *et al.* (2013) who analysed a marine sediment core CD154-17-17K (33º16.1'S, 29º7.3'E) sampled off South Africa's Eastern Cape coast. Like Chase (2010), Ziegler *et al.* (2013) correlated humid phases identified in the sediment core record with MIS 4. Further support for humid conditions in MIS 4 comes from a meta-analysis of published environmental data, pertinent to the African continent, for the period between *c.* 150 ka and 30 ka (Blome *et al.* 2012).

While recent evidence suggests that MIS 4 was cool and wet, the extent to which climatic factors influenced MSA behaviours during the Still Bay and Howiesons Poort remains unclear. Ziegler *et al.* (2013: 4), for example, correlates these MSA occurrences with rapid, short-term humid phases. However, Blome *et al.*'s (2012) meta-analysis provides little support for interpretations linking MSA occurrences in MIS 4 with climate change events. Compton (2011) on the other hand proposes that in MIS 4 lower glacial sea levels contributed to cultural change. He links the occurrence of

the Still Bay, and to a lesser extent, the Howiesons Poort to the expansion or opening of the SCP between Cape Hangklip and Plettenberg Bay. His model suggests that the SCP expanded as previously submerged habitats become exposed and opened up new biomes for plants and animals. These MIS 4 habitats are thought to have contained a heterogeneous mosaic of C_3 and C_4 vegetation. According to Compton (2011: 511) the SCP may have acted as a glacial refuge for migratory herds and people wanting to escape the unfavourable, drier conditions in the interior.

Still, others see no relationship between cultural changes, particularly in MIS 4, and climate (Jacobs *et al.* 2008; Jacobs & Roberts 2009; Chase 2010; Mackay *et al.* 2014; Kandel *et al.* 2015). For example, Jacobs *et al.* (2008) suggest a weak climate influence based on their regional chronology for the Still Bay and Howiesons Poort. While Mackay *et al.* (2014) associate MIS 4 with cool and wet conditions they comment on similarities in Still Bay and Howiesons Poort lithic production systems (see also Jacobs & Roberts 2009; Wurz 2013; Wadley 2015). They interpret this as indicating population interaction or coalescence, and argue that social factors contributed to the similarities in lithic systems in MIS 4.

Results from a related, independent study, that investigated a possible link between MSA lithic technologies in different environments, similarly found climate influence to be weakly related to MSA occurrences (Kandel *et al.* 2015). Here it was suggested that landscape features influenced MSA site selection in the Still Bay, Howiesons Poort and post-Howiesons Poort (Kandel *et al.* 2015). Kandel *et al.* (2015: 36), for example, suggest that Still Bay people preferred sites at low elevation and with high aspect. This is presumably so that they could be close to water sources such as rivers or the sea while also having a scenic and strategic view of the landscape. However, only negligible differences in site selection were identified between these MSA occurrences. Based on this, the palaeoenvironmental inference is that climate did not influence site selection in MSA times. Instead, Kandel *et al.* (2015: 37) identify behavioural flexibility as a key

driver in the development of MSA technologies. Taken together, recent evidence is complementary in suggesting that MIS 4 was a period of cool and wet conditions. Based on this, it seems unlikely that unequable, and more specifically deteriorating climatic conditions, played a role in the emergence of either the Still Bay or Howiesons Poort.

MIS 3 (59-24, Martinson et al. 1987)

Globally, MIS 3 is recognised as a glacial period but it is also characterised by short-term cycles of *c.* 1 kyr periodicity comprising warm interstadial and cool stadial events (Rabassa & Ponce 2013). These are referred to as Dansgaard-Oeschger (DO) and Heinrich events, respectively (van Meerbeeck*et al.* 2009). Temperature estimates from $\delta^{18}O$ in Antarctic ice cores and from coral terraces in the SW Pacific Ocean place MIS 3 between 3ºC and 15ºC warmer than during the Last Glacial Maximum (Lambeck *et al.* 2002; Siddall *et al.* 2008; van Meerbeeck*et al.* 2009). As a whole, MIS 3 is thought to have been only marginally cooler (0.5ºC to 2.0ºC) relative to present-day conditions (Rabassa & Ponce 2013: 98). In the southern Cape, SST from the TN057-21 sediment core is between 12ºC and 17.5ºC indicating similarly warm temperatures in MIS 3 (Sachs & Anderson 2003).

In terms of MIS 3 sea levels, early MIS 3 (*c.* 60 ka to 50 ka) is associated with a relatively higher sea level of *c.* 40 m below msl compared to MIS 4 (Siddall *et al.* 2008). In contrast, a relatively lower sea level of 100 m below msl is linked to late MIS 3 (*c.* 48 ka to *c.* 24 ka). Similar MIS 3 sea levels are estimated for the southern Cape. Here early MIS 3 seas were between 45 m and 80 m below msl between Cape Hangklip and Plettenberg Bay. In late MIS 3 sea levels were 60 m to 110 m below msl (Compton 2011).

In a broader South African context, generally cold, dry conditions with low rainfall and humidity are inferred during MIS 3 times (Hall &Woodborne 2011) with some referring to this stage as a period of hyperaridity (Deacon

& Thackeray 1984; Klein *et al.* 2004). These interpretations come primarily from archaeo-proxies such as pollen, charcoal, faunal remains and sedimentary deposits from the South African interior and east coast (Partridge 1997; Partridge *et al.* 1997; Scott 1999; Herries 2006). On the other hand, a period of climate amelioration is thought to have followed the MIS 4 glacial (Deacon & Lancaster 1988) and for this reason it is proposed that MIS 3 environments were generally more productive relative to those in MIS 4 (Deacon & Lancaster 1988; Mitchell 2002, 2008; McCall 2007).

In his review of the archaeological and environmental evidence for MIS 3, Mitchell (2008) suggests fluctuating environmental conditions with brief humid periods that might have been wetter than present. He also identified between twenty-five and thirty-three MSA sites dating to the post-Howiesons Poort and comments that …"*claims of hyperaridity and site invisibility are overstated*…" (Mitchell 2008: 54). More recent environmental evidence does not however support this inference. Chase (2010), for example suggests drier conditions at the transition from MIS 4 to MIS 3 which presumably lasted throughout early MIS 3. According to him, this drying trend is characterised by cooler SSTs in the SW Indian Ocean (van Campo *et al.* 1990) and contraction of the winter rainfall belt associated with a southward shift in the STC (see also Mackay *et al* (2014). These contradictory interpretations also reflect in the proxies from some archaeological sites and are discussed further in Chapter 6 section 6.6.

In the southern Cape, these cooler/colder and drier conditions have been linked to the occurrence of occupational hiatuses during the period between *c.* 50 ka and *c.* 30 ka (Deacon & Thackeray 1984; Klein *et al.* 2004). More recently, Mackay *et al*. (2014) also commented on the occurrence of occupational hiatuses in MIS 3. They distinguish between coastal and interior populations based on the heterogeneity and localised lithic production systems between the WRZ/YRZ and SRZ. They interpret this in terms of population fragmentation, which they link to a break down

in social interactions between groups living across the southern Cape. This fragmented pattern, which is not evident in the interior, is correlated to the occurrence of occupational hiatuses at southern Cape MSA sites. According to Mackay *et al.* (2014), the onset of these hiatuses started in early MIS 3 and accelerated from mid-to-late MIS 3. This confirms the earlier observation by Deacon *et al*. (1984) (see also Klein *et al*. 2004).

In the context of the southern Cape, there is evidence for cooler and drier, as well as cooler and wetter conditions. In the post-Howiesons Poort at Klasies River, that dates to between *c.* 57 ka and 43 ka, there is micromammal evidence for cool and wet conditions in early MIS 3 (Wurz 2002; Wadley 2015). Cool, wet conditions are for example implied from the abundance of Saunder's vlei rat (*Otomys saundersiae*) (Avery 1987; see also Hillestad-Nel 2013 for the relationship between this species and cool, wet conditions). Temperature indices obtained by applying factor analysis to the micromammal abundances measures for the Klasies River assemblage, including MSA III, has been equated to a temperature of *c.* 14^{o}C (Thackeray 1987; Thackeray & Avery 1990). This value was also correlated with a corresponding warming interval in the Vostok ice core record (Thackeray 1992, 2009). These earlier interpretations by Thackeray (1987, 1992) and Thackeray and Avery (1990) are consistent with SST from the TN057-21 and comparable with the main trends in the Vostok ice core.

On the other hand, evidence for cool/colder and dry/drier MIS 3 conditions comes from Boomplaas Cave. At this site, cool and dry conditions are implied by the low species diversity values coupled with the large sized shrews (*M. varius*) from the older than 48 kcal BP BOL. Similar inferences also come from the spindly growth habit of fossil wood (Scholtz 1986) and from grassland fauna at the site (Faith 2013). Comparable evidence for open habitats with grassland vegetation, implying cool, dry conditions also comes from the post-Howiesons Poort levels at Klasies where grazers and equids are abundant throughout MIS 3 (Klein 1976; Faith 2013). However,

see Chase (2010:1361) who equates grassland with increased rainfall and karroid vegetation with drier conditions (Cowling 1983).

For the period between *c.* 48 kcal BP to 36 kcal BP, in the OLP and BP members at Boomplaas Cave, cool and wet conditions are also recorded. Here this interpretation is based on the abundance of browsers, forest shrews (*Myosorex varius*) and woody taxa that occurs in OLP (*c.* 48 kcal BP – 40 kcal BP) and BP (38.6 kcal BP – 36 kcal BP) members (see Chapter 6 section 6.6 for details). Evidence for relatively wetter conditions in late MIS 3 further comes from the Agulhas Plain where humid phases are identified in sediment records post-dating lunette accretion dating to between *c.* 60 ka and 45 ka (Carr *et al.* 2006).

As a whole, MIS 3 is a fairly long stage and, as discussed above, it is sometimes referred to as a period of cooler/colder and drier conditions. There is however some evidence for cooler/colder and wetter conditions occurring in parts of this stage. Contradictions may arise, as some researchers do not differentiate between different periods of MIS 3.

Archaeologically, marine isotope stage 3 is poorly investigated relative to MIS 4 (Mitchell 2008). This is in part because MIS 4 coincides with the Still Bay and Howiesons Poort which are generally well-dated and intensively investigated. However, current research focuses on addressing the paucity of the archaeological and environmental interpretations associated with MIS 3 (Mitchell 2008; Blome *et al.* 2012; Wurz 2013). As a whole, MIS 3 coincides with the occurrence of the post-Howiesons Poort (also MSA III or Late MSA) (Wurz 2013) or Sibudu techno-complex (Lombard *et al* 2012). Based on this, the suggestion is that in MIS 4, MSA people experienced ecological stress and social pressure to produce complex lithics and symbolic artefacts (Mitchell 2002). This includes those associated with the Still Bay and Howiesons Poort. In contrast, by the onset of MIS 3, it was suggested that conditions became more equable and as a result, people presumably reverted to using earlier forms of lithic technology (Mitchell 2002; McCall 2007). Compton (2011) also suggests

that the reversion back to pre-Howiesons Poort technology is linked to habitat productivity in MIS 3 environments. He proposes that throughout early MIS 3 (*c.* 61 ka - 50 ka), the SCP was closed as sea levels remained relatively high. At this time large grazing herds were unable to penetrate the SCP as previously exposed MIS 4 habitats were re-submerged. As a result, people reverted to earlier forms of lithic production as an adaptive response to these MIS 3 conditions (but see Lombard & Parsons 2012 & Wurz 2013 who argue against notions of a simplistic reversion to pre-Howiesons Poort technology).

In the context of the southern Cape, it appears that there is indeed evidence for cooler and drier conditions in part of MIS 3. However, the suggestion that conditions were generally hyperarid is not widely accepted. Taken together, it seems that early MIS 3 was colder and drier than MIS 4 and that conditions in the southern Cape differed from the interior and the eastern part of the country. This discussion shows that early MIS 3 in the southern Cape was probably colder and drier in some areas (*e.g.*, in the early part of the Boomplaas sequence & in parts of the Agulhas Plain). In other areas, for example Klasies River, conditions seem to have been comparatively wetter with a more humid signal in late MIS 3 also recorded at Boomplaas Cave. Regarding the archaeology, there seems to be a discontinuation of occupation in the WRZ and YRZ after MIS 4 but these hiatuses are not evident in the SRZ.

2.4 Introduction to the study site

2.4.1 Location and environmental setting of the De Hoop Caves and Klipdrift Sea Cave

Location

The De Hoop Nature reserve is *c.* 260 km east from Cape Town and is located along the southern cape coast of South Africa (Fig. 2.10). The terrestrial section of the reserve covers an area of *c.* 340 km^2 and extends for approximately 5 km towards the sea.

Modern environmental setting: rainfall, temperature & vegetation

The De Hoop area receives precipitation throughout the year (*viz.* as mist, hail & fog) but because the reserve lies within the eastern boundary of southern Africa's winter rainfall zone it has a predominant Mediterranean-type climate. During the summer months (Dec. – Feb.) mean annual precipitation is around 380 mm and occurs primarily as occasional cloudbursts whereas storms are more frequent during the austral winter months (Jun.-Aug.). Rainfall also varies orographically between the mountains and the lower lying dune areas. For example, on the limestone hills and the Potberg Mountains, which are respectively at 611 m amsl and 311 m amsl rainfall of 700 mm/pa has been recorded. By contrast, along the coast at Koppie Alleen rainfall is comparatively lower at 400 mm/p.a.

The temperatures are relatively stable throughout the year, with a maximum temperature of *c.* 22^{o}C recorded in summer with winter temperatures reaching a minimum of 11^{o}C. The lack of variation in seasonal temperatures in the area is in part because De Hoop is centrally located at the confluence between the Indian and Atlantic oceans (as discussed in section 2.2). The meterological data for the sampling period, including the dripwater collections, is shown in Fig.

The terrestrial vegetation is dominated by sclerophyllous fynbos which grows primarily on the acidic, nutrient-poor soils derived from the underlying sandstone rocks. Fynbos is endemic to the Western Cape region of South Africa and is a mosaic vegetation comprising species in the Proteaceae, Ericaceae, Restionaceae and Asteraceae families. Variations do occur in the relative distribution and dominance of these floral species and depends on factors such as elevation, rainfall seasonality and soil conditions (as discussed in section 2.2). Within the De Hoop area, for example, Ericaceae *spp*. are ubiquitous within the limestone hills at an altitude of 224 m amsl (Willis *et al.* 1996) whereas within the coastal dunes Proteaceae *spp*. are absent while Asteraceae types occur more frequently (Cowling & Pierce 1988). In addition to fynbos, many succulent plants species (*viz.* Mesembs & Crassula) also occur within the region.

Fig 2.10a Location map of the De Hoop Nature Reserve (study area) containing Bloukrantz Cave (BLOU), West Cave (WC) and Klipdrift Sea Cave (KDC). The extent of the reserve is shown (- - - -) and the location of the other speleothem bearing caves in the southern Cape. These sites are the Cango Cave, Pinnacle Point (containing PP29 & Crevice Cave), the Little Karoo, Sandkraal Cave and Herold's Bay Cave

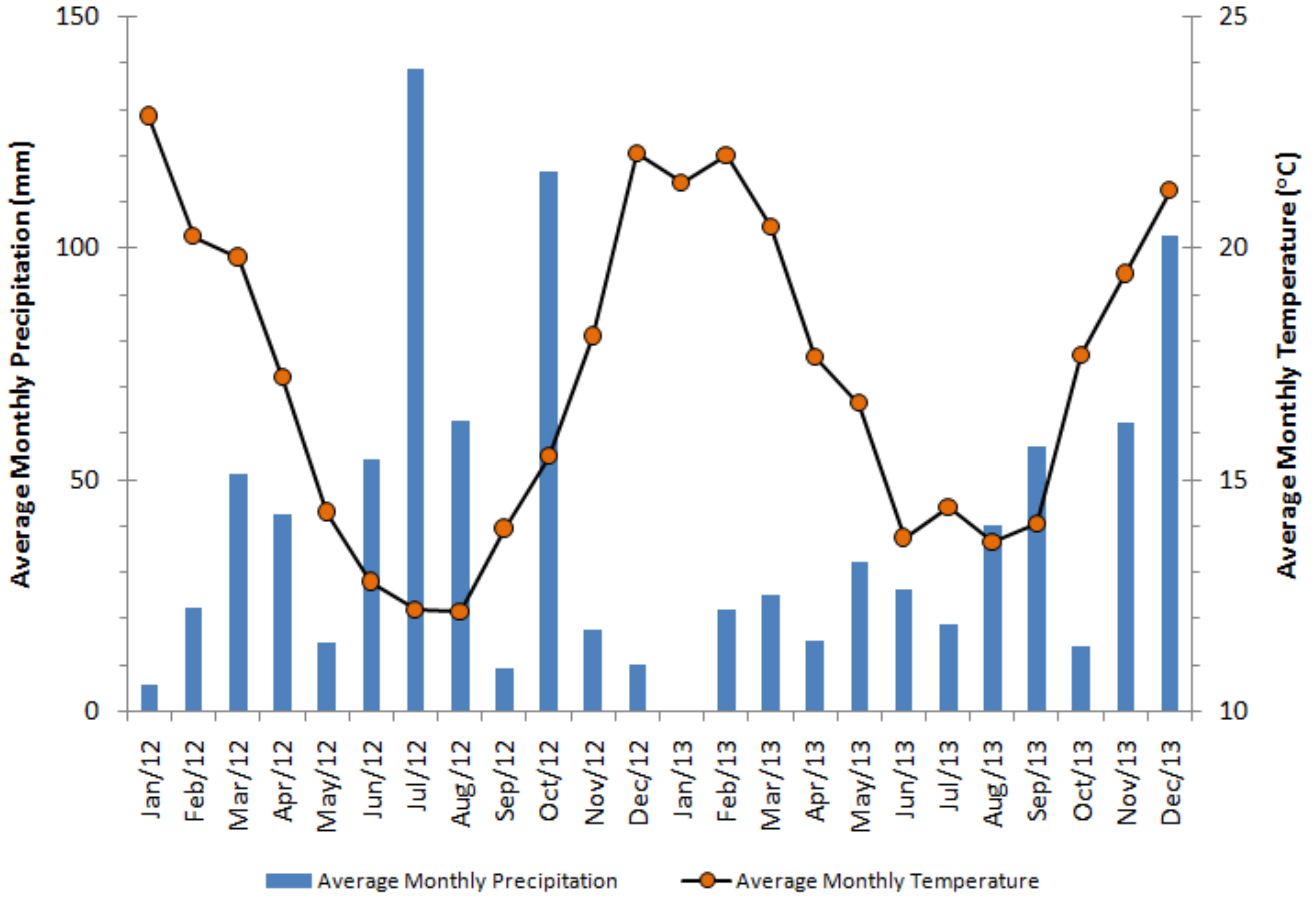

Fig 2.10b Meterological data from Still Bay, the nearest weather station to De Hoop Nature Reserve, showing monthly variations in rainfanll and temperature during a 12-month period from January 2012 to December 2013.

2.4.2 Site selection and speleothem sampling

There are approximately twenty-one documented limestone caves found throughout the reserve (Butcher 2010) and many of these caves contain speleothem deposits at different stages of development (Noah 2011). These limestone caves are formed primarily in calcium carbonate and dissolution occurs in the presence of carbonic acid (H_2CO_3). During the acid digestion of the limestone, calcite is typically incorporated into the speleothem fabric. To a lesser extent, other minerals such as aragonite may also be incorporated.

In April 2008, a preliminary study was undertaken to try to identify caves within the reserve that contained suitable speleothem deposits for uranium-series dating and environmental analysis. This formed the basis for the author's master's dissertation (Noah 2011). The current study builds on this initial work and includes more intensive sampling of Bloukrantz Cave and West Cave which form part of the Stilgat sea caves complex. Additional samples are taken from the Klipdrift Sea Cave and Klipdrift Shelter that collectively form part of the Klipdrift Complex.

The sampling strategy used in this study focused on collecting stalagmites of varying length and thickness. Samples were typically collected between *c.* 15 and 50m from the cave entrance although this distance varied depending on the depth of the cave. Preference was given to those speleothems of variable length and diameter with the assumption that these samples might cover different time periods. Between February and March 2011, six stalagmites were collected from the De Hoop caves including the Klipdrift Complex. These were analysed and are described individually in Chapter 3. The stalagmite samples are collectively from the western and eastern sections of the reserve and were inactive at the time of collection.

Cave dripwater was collected in order to obtain a modern $\delta^{18}O$ reference sample for evaluating if the speleothem calcite formed in isotopic equilibrium with the dripwater from which it precipitated (discussed in detail in Chapter 3 section 3.4.5). This is an important consideration when making environmental inferences based on variations in $^{18}O/^{16}O$ ratios derived from speleothem calcite. West Cave and Klipdrift Sea Cave were selected for this purpose of calibrating the dripwaters because they are more accessible than the other caves (*e.g.*, Bloukrantz Cave, Morris' Cave & Box Cave) where speleothem samples were previously collected by Noah (2011). In other words, dripwater was not collected from Bloukrantz Cave. However, West Cave and Klipdrift Sea Cave were selected because these caves have multiple localities with actively dripping soda straw stalactites and are in close proximity to Bloukrantz Cave where speleothems were also sampled. Based on these features, the dripwater $\delta^{18}O$ data from West Cave and Klipdrift Sea Cave was expected to provide comparable data for interpreting the ^{18}O signal of the speleothem calcite. Collectively, twenty-three dripwater collectors were setup in West Cave and Klipdrift Sea Cave (see Chapter 3 section 3.4.5. for details). It is worth mentioning that due to time constraints, additional variables such as a temperature and relative humidity were not measured in the caves.

With regards to each of the sampled caves, Bloukrantz Cave is formed in sandstone and has limestone cap from which sandy stalactites can be seen hanging down from the lip of the cave. The cave has a small visible entrance at the base which leads down an unstable slope to the main cavern (Fig. 2.11). West Cave is *c.* 5 km from Bloukrantz Cave and has two entrances; there is tall, narrow northern entrance (*c.* 2 m high) and a wider main entrance (*c.* 4 m across) thats leads down an unstable scree slope to the main chamber (Fig. 2.12). The walls inside the main chamber are covered in mottled green flowstones and the cave floor is littered with fossil stalagmites many of which are broken. Three dripwater collectors were set up approximately 40 m from the main entrance inside the main chamber. Branching off from the main entrance are two side passages and

the southern tunnel is partially concealed by weathered, fossil stalagmites while its walls are covered in flowstone. This passage also contains small actively dripping stalactites. The northern side passage contains both fossil and actively forming stalactites and stalagmites and there are also many deposits with false floors. For the dripwater analysis an additional five samples were collected from each of the side passages inside West Cave (see Chapter 3 section 3.4.5 for details)

Klipdrift Sea Cave (Figs. 2.13, 2.14 & 2.15) is located *c.* 15 km from the Stilgat sea caves and is directly adjacent to the archaeological sites of Klipdrift Cave (upper & lower) and Klipdrift Shelter (Fig. 2.16) which form the Klipdrift Complex. Klipdrift Sea Cave (previously known as Noetsie sea cave by the Cape Peninsula Spelaeological Society) is elevated at -27 m amsl and extends for 192 m from the 6m wide main entrance to the back of the cave. A fossil, hollowed out stalagmite was found on the beach cobbles and rocks directly in front of main entrance to the cave. From the main entrance there is a slight slope covered with compact, elevated sediment deposits with green-coloured speleothems on the floor. Leading off from the main entrance there is a short, partially concealed side passage. Here there are fossil columns and very low hanging stalactites that are growing downwards from a flowstone covered rock face. Inside this passage, there is a mosaic of fossil and active stalagmites scattered throughout as well as actively dripping stalactites.

Branching off on the right side of the main entrance there is an extension leading to another cave denoted as Klipdrift Sea Cave East (Fig. 2.14). At this entrance there appears to be an Early Middle Stone Age deposit containing shellfish debris and lithics in a cemented matrix. Two dripwater samples were collected in a side passage closer to the back section of the cave (see Chapter 3 section 3.4.5). Five dripwater samples were collected about 56 m from the entrance. On the left side of Klipdrift Sea Cave East there is a side passage approximately 65m from the entrance with soft sand, wet walls and very few speleothem deposits (*viz.* small stalagmites).

Thirteen dripwater samples were collected from Klipdrift Sea Cave and the extension of Klipdrift Sea Cave East (see Chapter 3 section 3.4.5).

Fig. 2.11 (a-e) Bloukrantz Cave (a) sandy stalactites hanging from the lip of the cave (b) fossil stalagmites and broken columns at the main (c) view to the back of the cave (d) light coming into the cave from a narrow entrance above the roof the of cave (e) tall fossil columns

Fig. 2.12 (a-e) West Cave (a) main entrance (b) scree slope and green-coloured speleothems on the cave floor leading to the main chamber (c) speleothem formations inside the northern passage (d) broken fossil stalagmites and false floors in the southern tunnel of West Cave (e) large fossil stalagmites inside the main chamber of West Cave

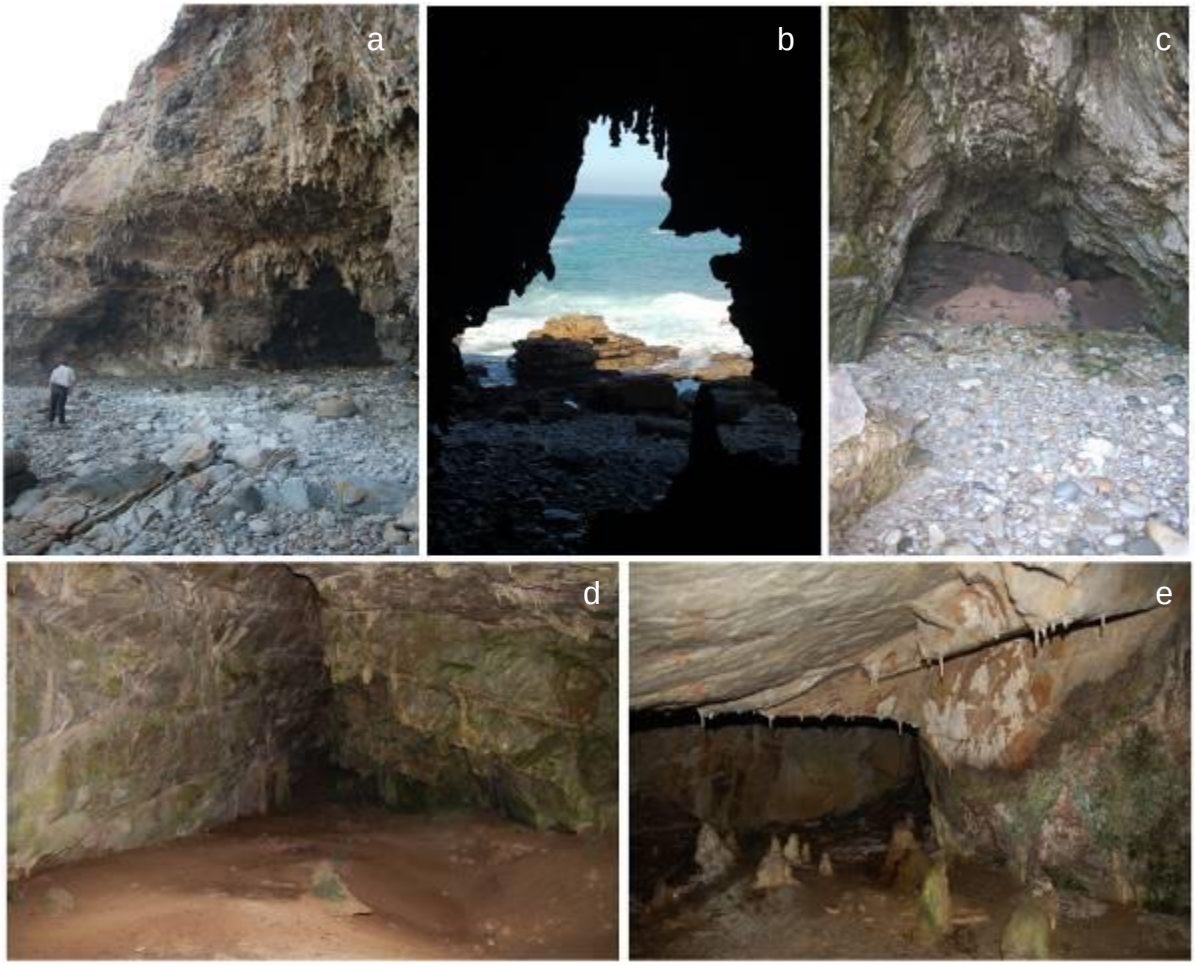

Fig. 2.13 (a-e) Klipdrift Sea Cave (a) main entrance to Klipdrift Sea Cave (b) view from the entrance to Klipdrift Sea Cave (c) Sediment slope leading to the main chamber of Klipdrift Sea Cave (d) inside the main chamber of Klipdrift Sea Cave (e) Speleothem formations in the main chamber and a flowstone covered rockface partially concealing the entrance to the side passage in Klipdrift Sea Cave

Fig. 2.14 (f-j) Klipdrift Sea Cave East (f) cemented deposit close to side entrance of Klipdrift Sea Cave leading to Klipdrift Sea Cave East (g) main entrance to Klipdrift Sea Cave East (h) view from the main entrance to Klipdrift Sea Cave East (i) inactive fossil stalagmites and low hanging stalactites inside Klipdrift Sea Cave East (j) view from the side tunnel in Klipdrift Sea Cave East showing wet flowstone deposits on the cave walls

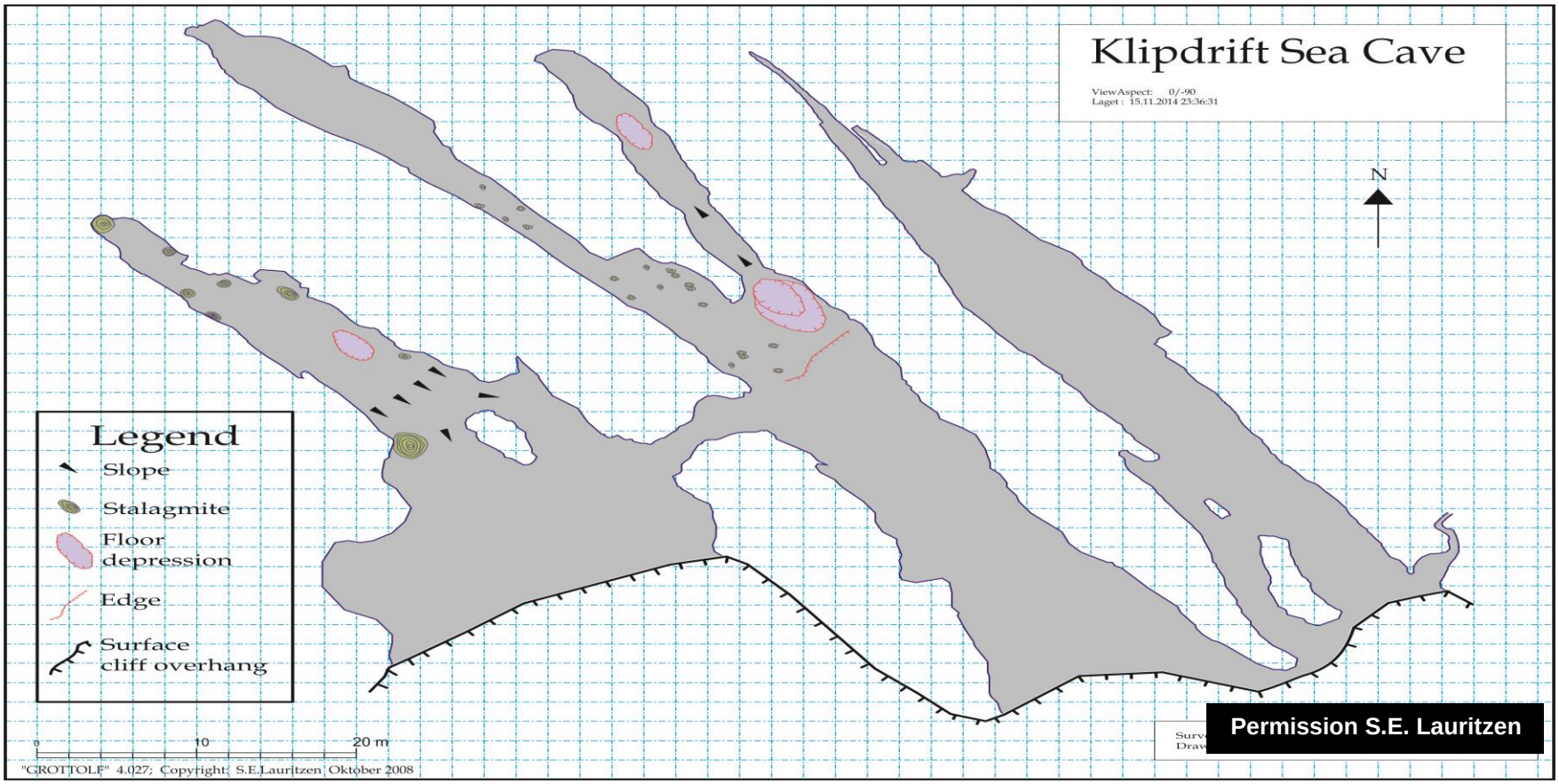

Fig. 2.15 Survey map of Klipdrift Sea Cave showing the passages and location of stalagmite deposits inside the cave and its extension of Klipdrift Sea Cave East

Fig. 2.16 The archaeological sites of Klipdrift Shelter and Klipdrift Cave (upper & lower)

2.5 Summary

This chapter introduced the southern Cape by focusing on its geological history (section 2.2.1) and present-day environmental setting (section 2.2.2). A broad overview of the stratigraphy and dating of the Middle Stone Age sites pertinent to this study was also presented (section 2.3.1). A current synthesis of the proxy evidence available for the area from MIS 5a to MIS 3 was also discussed (section 2.3.2). Against this background narrative the study site of De Hoop Nature Reserve and the selected caves where the speleothems were sampled was also discussed (section 2.4). In the next chapter (Chapter 3) there is a review of the methodological approach applied to each of the speleothems that form the core of this thesis.

Chapter 3 – THEORETICAL BACKGROUND TO THE METHODS

3.1 Introduction

Secondary cave carbonates are collectively called speleothems and the most recognised forms are flowstones, stalagmites and stalactites. Stalagmites are the most commonly used forms in environmental analysis and they grow in such a way that younger layers are almost always deposited above older ones. Speleothems are formed from calcite and to a lesser extent from aragonite and gypsum. During the precipitation of the carbonate minerals from a supersaturated solution, a wide range of environmental information may be preserved in individual growth layers. This proxy environmental and by extension climate data can determined by analysing various speleothem attributes. These include amongst others, fluid inclusions, stable isotopes, variations in growth laminae thickness and fluorescence and trace element composition. The intervals during which speleothems were formed can be stratigraphically constrained using high resolution uranium-series dating methods which are based on the ^{238}U decay chain. For speleothems, the $^{230}Th/^{234}U$ method is commonly used and has a practical range up to 500 ka. These attributes make speleothems particularly useful terrestrial archives of Quaternary environmental change.

The current chapter provides an overview of the theoretical basis for the method used in this study. The specific procedure used for selecting sub-samples for dating and stable isotope analyses are discussed. Here the discussion focuses on the principles, applications, and constraints of the $^{230}Th/^{234}U$ dating methods applied to each of the samples. In the final section of the chapter, the discussion focuses on the sampling approach used for extracting stable isotopes of carbon and oxygen and the age

models used to constrain the isotopic data. An overview of the dripwater and temperature reconstruction analyses are also presented.

3.2 U-series dating of speleothems

3.2.1 Principles and applications

Uranium series dating techniques are widely used in Quaternary research because they are applicable to a broad range of terrestrial deposits (*e.g*. speleothems, shell, bone, lacustrine sediments, corals, peat) that are often beyond the *c*. 50 ka range of radiocarbon. U-series methods are based on the radioactive decay of parent isotopes to daughter isotopes and this technique provides chronological constraint for a variety of materials at relatively high resolution. Uranium has two and Th has one naturally occurring radioactive decay chain, each of which starts with an actinide nuclide (^{238}U, ^{235}U & ^{232}Th) and ends with a stable isotope of lead (^{206}Pb, ^{207}Pb & ^{208}Pb, respectively) (Bourdon *et al.* 2003) (Fig. 3.1).

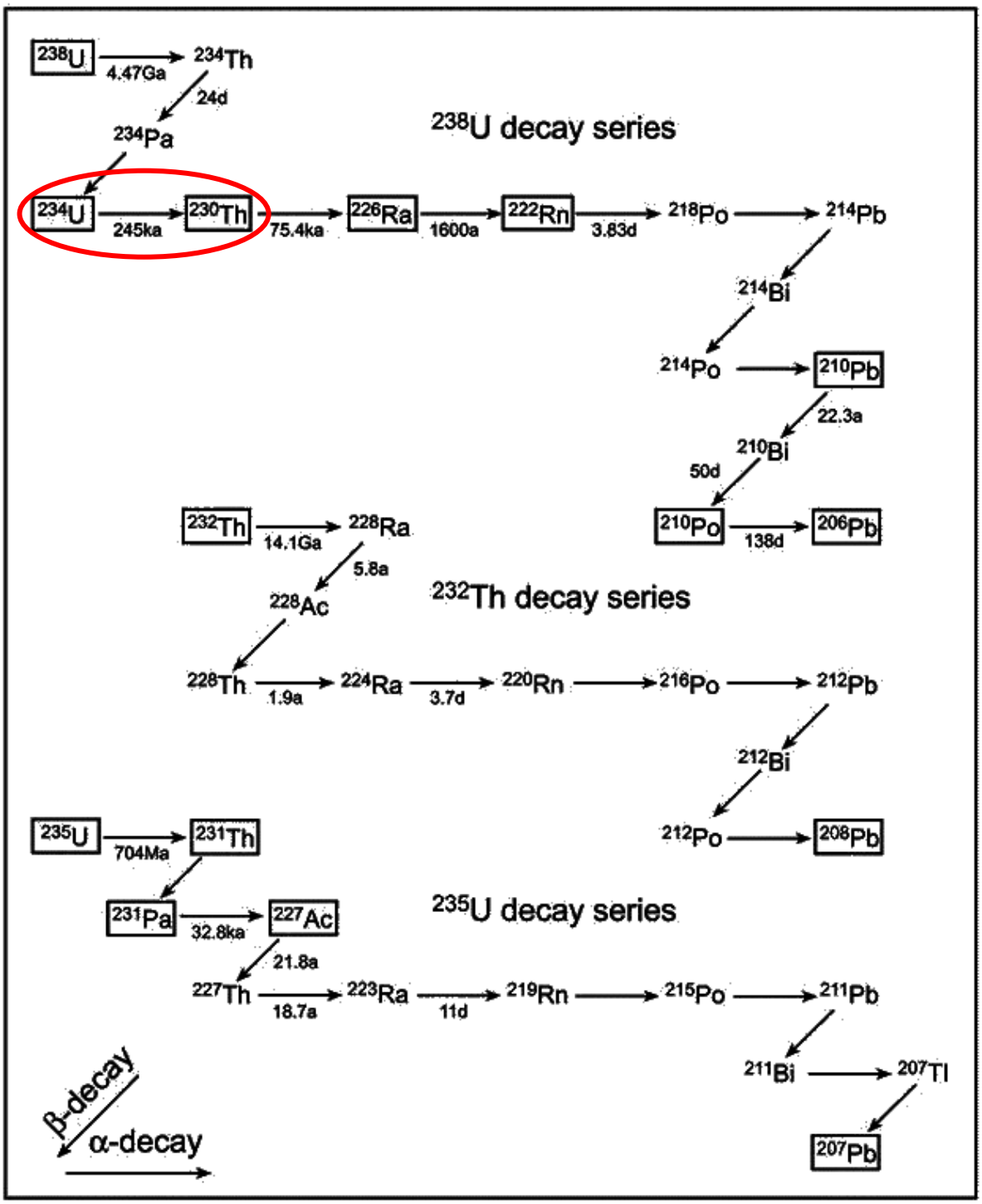

Fig. 3.1 Radioactive decay series of ^{238}U, ^{232}Th and ^{235}U showing the $^{230}Th/^{234}U$ daughter-disequilibrium isotope pair in the ^{238}U decay chain which is used for dating speleothem deposits in this study. β-decay changes are denoted by diagonal arrows and α-decay by horizontal ones (From Fairchild & Baker 2012: 292)

This study uses U-series dating of the activity of the $^{230}Th/^{234}U$ daughter/parent isotope pair which has an effective age range of *c*. 500ka. The method is based on the disequilibrium that exists between the concentrations of parent (^{238}U) and daughter (^{234}U) isotopes with ^{230}Th being mostly absent in the sample. In the ^{238}U decay chain, ^{234}U is produced as ^{238}U decays over time and in turn, ^{230}Th progressively increases as ^{234}U decays (Smart & Frances 1991). This relationship is defined statistically by (Bourdon *et al.* 2003):

$dN_1 / dt = -\lambda_1 N_1$

Where *N* is the number of atoms and *λ* represents the decay constant

The rate at which a parent decays to its daughter nuclide is given by the exponential law of radioactive decay (Smart & Frances 1991):

$N_2\lambda_2 = N_1\lambda_1 (1-e^{-\lambda_2 t})$

N_1 = *number of parent atoms*

λ_1 = *decay constant of the parent isotope*

N_2 = *number of daughter atoms*

λ_2= *decay constant of daughter isotope*

t = time

And $\lambda = \ln 2 / T_{1/2}$

Where, $T_{1/2}$ = the half life

In speleothem carbonates, disequilibrium between U and Th isotopes occurs because of fractionation resulting from the initial dissolution of the limestone bedrock and subsequent precipitation of the carbonate inside the cave at the time the speleothem was forming (Richards & Dorale 2003). The extent to which each of these actinides is fractionated is determined primarily by their geochemical properties. The U-series nuclides for example can be fractionated, amongst others, during phase

changes, weathering, crystallisation, transportation, dissolution, degassing, adsorption and complexation (Ku 1976; Gascoyne 1992a; Bourdon *et al*. 2003). These processes, particularly the ability of U and Th to form complexes with other ions, are collectively influenced by the mobility of U and Th in natural waters (Gascoyne 1992a; Langmuir & Herman 1980; Choppin & Stout 1989; Bourdon *et al.* 2003). Thorium has a common oxidation state of Th^{4+} and is abundant in the Earth's crust, in granite rocks and to a lesser extent in soils. Uranium's most common oxidation states are U^{+4} (immobile) and U^{+6} (mobile), the latter of which can be readily oxidised to form a water soluble uranyl ion UO_2^{2+}. The reaction with water to form soluble ions is known as hydrolysis and is represented by the following equation (Bourdon *et al.* 2003):

$$M^{n+} + xH_2O \rightarrow MO_x^{(n-2x)+} + 2xH^+$$

In acidic solutions, the Th and U exist as M^{n+} ions and as the pH of the solution increases, the oxidised forms of Th and U form water soluble ions or hydroxides (*e.g.* $Th(OH)_4$ & $UO_2(OH)_2$) (Bourdon *et al.* 2003: 11). Unlike Th, uranium has an affinity for alkaline, carbonate-rich water and because of this, uranium is most abundant in ocean waters although natural deposits are also found in phosphate rocks and lignite mineral deposits. Both Th and U can be released during rock weathering although the mobility of the Th^{4+} and UO_2^{2+} in solution is also affected by the presence of organics (*e.g*. humic & fulvic acids) and clay minerals (Langmuir & Herman 1980; Gascoyne 1992b; Bourdon *et* al. 2003; Crançon & van der Lee 2003). Mobility may also increases at higher pH (≥ 7.5) due to increasing ionization of the carboxylate groups (Langmuir & Herman 1980; Choppin & Stout 1989). Thorium concentrations in limestone are however comparatively lower than uranium because thorium is typically adsorbed onto clay minerals and organics in its Th^{4+} state (Choppin & Stout 1989). However, Th carrier minerals (*i.e.* monazite, phosphate & silicate) can generally be resistant to weather and sorption processes regardless of changes in pH (Langmuir & Herman 1980).

The differential fractionation resulting in part from the solubility of U and Th species slows down once the carbonates are precipitated. As a result, the system eventually returns to a secular state with the ^{230}Th reaching equilibrium with its parent ^{234}U isotope (Smart & Frances 1991; Walker 2005). The age at which the speleothem carbonate was precipitated is then inferred from an increase in the activity of ^{230}Th/^{234}U (Walker 2005: 68). This ^{230}Th/^{234}U activity ratio can be measured by mass spectrometric techniques if the following conditions are met:

1. At the time of carbonate precipitation, there were no daughter isotopes in the system (*i.e.* ^{230}Th) however if Th was present it should be possible to correct for this (Ku 1976; Richards & Dorale 2003)
2. There was no gain or loss of either U or Th nuclides from the carbonates since its formation (*i.e.* post-deposition change is absent) (Smart & Frances 1991; Gascoyne 1992a,b).

Additional, less strictly enforced requirements are that:

3. A minimum U concentration of > 0.1 ppm is required to reduce the influence of instrument related analytical errors on the final age estimate (Gascoyne 1992b). This value is generally set as a baseline when measuring activity ratios using alpha spectrometry (Smart & Frances 1991). However, developments in instrumentation techniques, improvements in sampling protocols and interlaboratory comparisons have, in recent years, allowed for high precision dating even at relatively low concentrations (*e.g*. Shen *et al*. 2002; Eggins *et al.* 2005; Hoffmann *et al.* 2009)
4. The decay coefficients are known; at present, the most precise values are set to *c*. 245kyr for ^{234}U and at *c.* 76kyr for ^{230}Th (Cheng *et al.* 2000)
5. The activity ratios of the daughter/parent nuclides can be quantified to a high level of precision. This condition is usually met with little difficulty as mass spectrometry techniques by TIMS and ICPMS is

continually being refined with succinct reviews in Goldstein & Stirling 2003; Dorale *et al*. 2004 and Hoffmann *et al*. 2009.

Constraints of $^{230}Th/^{234}U$ dating

Based on these criteria, the age of a sample can be determined from the $^{230}Th/^{234}U$ activity ratio using a modified form of the basic equation described previously in 3.4.1. This equation is expressed mathematically as:

$$(^{230}Th/^{234}U) =$$

$$(^{238}U/^{234}U) \times [1 - \exp(-\lambda_0 t)] + [1- (^{238}U/^{234}U)] \times [\lambda_0/(\lambda_0-\lambda_4)] \times [1- \exp(\lambda_4 - \lambda_0)t]$$

(Ku 1976: 364)

Where,

λ_0 = Decay constant for ^{230}Th

λ_4 = Decay constant for ^{234}U and,

$^{230}Th/^{234}U$ and $^{238}U/^{234}U$ = (respective) measured activity ratios

An inherent assumption of the $^{230}Th/^{234}U$ dating method is that the concentration of ^{230}Th in the speleothem is almost zero at the time it formed and increases progressively over time from the decay of ^{234}U (Fig. 3.2).

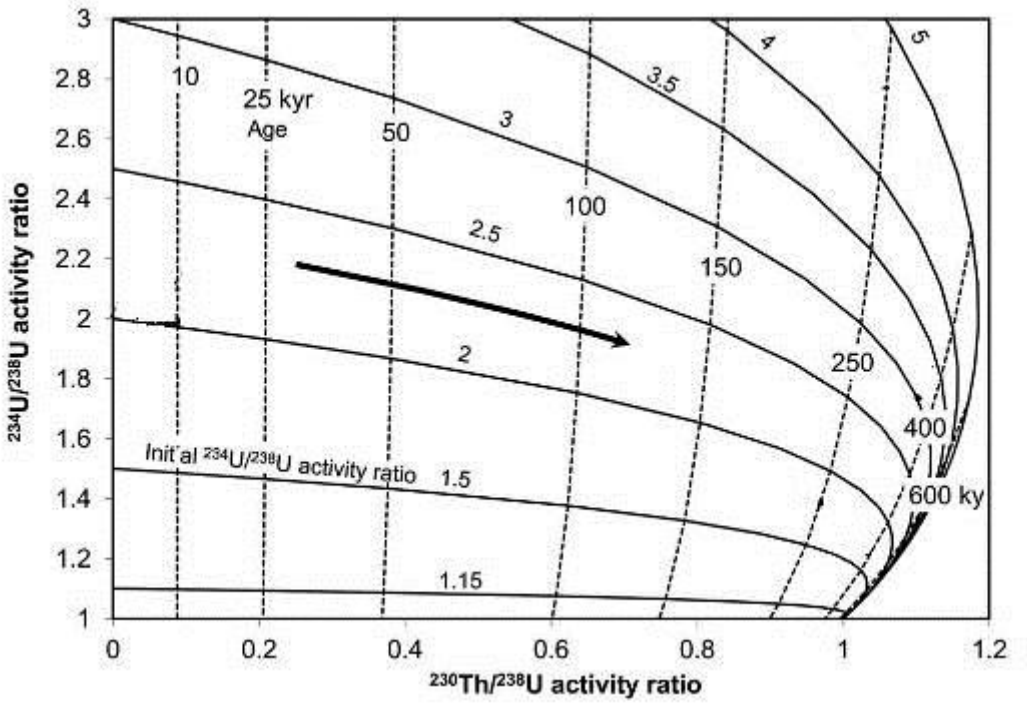

Fig. 3.2 An isochron diagram showing the decay activities for $^{234}U/^{238}U$ and $^{230}Th/^{238}U$ occurring at different initial $^{234}U/^{238}U$ values. The rate of radioactive decay is plotted on the y-axis and follows a trajectory indicated by sub-horizontal lines. The trajectory followed by the $^{234}U/^{238}U$ as it decays over time to $^{230}Th/^{238}U$ is the basis for the U-Th dating method used in this study (Modified from Fairchild & Baker 2012: 296)

In natural environments deviations from the hypothetical ideal occur quite regularly as carbonates formed in these settings usually have up to 20% Th (Alcaraz-Pelegrina & Martínez-Aguirre 2005). This is because allogenic Th is typically incorporated into the speleothem fabric through dust, or adsorbed onto allochtonous minerals and introduced during flooding events whereas authigenic U can be lost through post-depositional leaching (Ku 1976; Luo & Ku 1991; Smart & Frances 1991; Richards & Dorale 2003; Fairchild & Baker 2012). Other studies have demonstrated that U and Th concentrations can also vary in speleothems with mixed mineralogy and this can produce unusual ages (*e.g.,* Frisia *et al*. 2012; Lachniet *et al.* 2012).

3.2.2 Refining $^{230}Th/^{234}U$ age estimates

Corrections for initial ^{230}Th

Over the years, various approaches have emerged to help refine the age estimates derived from impure calcites and those deposited under open-system conditions. These different procedures fall broadly into two categories and they collectively focus on applying corrections for the presence of initial Th by tracing the activity of ^{232}Th in the sample. It is important to correct for any Th in the sample because uncorrected age determinations are often significantly older than the 'true' age. Corrections for detrital Th are typically applied when activity ratios for ($^{230}Th/^{232}Th$) are < 20 (Smart & Frances 1991) but for ICPMS this baseline value has been set to 300 (Hellstrom 2006).

The first approach attempts to quantify the initial Th by using leachate or residue analyses to evaluate differences between the isotopic composition of U and Th in multiple sample aliquots (*c*. 4-6) taken from the same or coeval speleothems (Schwarz & Lathan 1989; Luo & Ku 1991; Bischoff & Fitzpatrick 1991; Alcaraz-Pelegrina & Martínez-Aguirre 2005). These aliquots usually consist of separate fractions for pure and contaminated carbonates which are derived from an individual sample. The respective U and Th ratios of these sub-samples may then be plotted in isochron diagrams (Fig. 3.2) to obtain an age and error for each sample which is based on corrected values for the initial detrital component (Alcaraz-Pelegrina & Martínez-Aguirre 2005). The second approach by contrast, uses a global average (*e.g*., 0.8+/-0.8) for the initial ratio (Richards & Dorale 2003). This mean value is typically called the bulk Earth value and is thought to be constant over time. Several studies have however demonstrated that initial Th values are quite variable in carbonate samples and correcting for this variation will often change the resultant age estimates (*e.g*., Hellstrom 2006; Shen *et al*. 2008) (Fig. 3.3).

To account for the presence of detrital Th in carbonates, isochron techniques can be used to determine a mean value for initial ($^{230}Th/^{232}Th$)

in the sample. This technique is traditionally applied to activity ratios determined on *c.* four sample aliquots which are derived from either leachate or residue procedures. With this technique, activity ratios for ^{230}Th and ^{234}U for sub-samples of similar age are usually plotted with a common denominator such as ^{238}U or ^{232}Th (Ku 1976; Smart & Frances 1991; Ludwig 2003). A mean value for initial ^{230}Th/^{232}Th may then be determined from this plot and subtracted from the measured ^{230}Th before calculating the sample age (Ludwig 2003; Richards & Dorale 2003). The validity of isochron ages is usually checked using error weighted least squares regression.

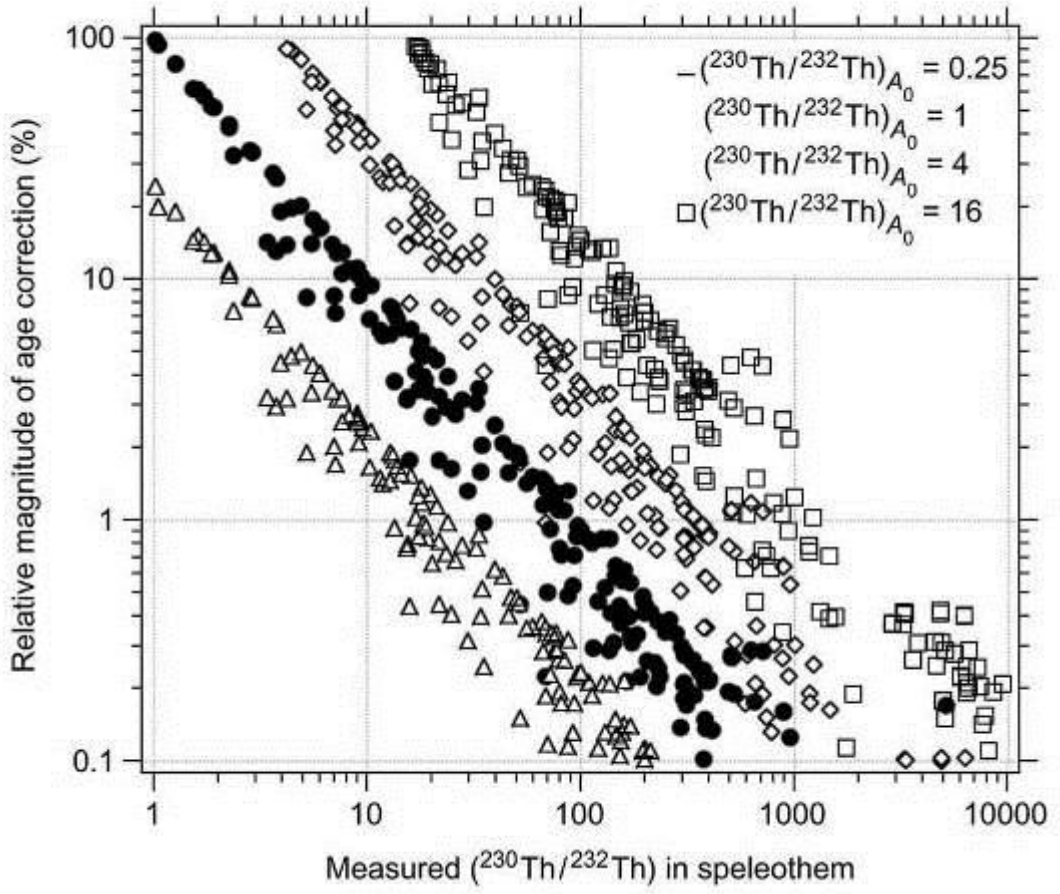

Fig. 3.3 An XY plot showing the effect of ^{230}Th corrections on age estimates calculated with different initial (^{230}Th/^{232}Th) ratios. The extent to which the calculated ages changed is expressed as a percentage on the Y-axis with the measured (^{230}Th/^{232}Th) on the X-axis (From Fairchild & Baker 2012: 297)

Uncorrected ratios for initial $^{230}Th/^{232}Th$ can also produce infinite ages and in these cases, the data are essentially useless. Infinite ages can occur in isochron plots when individual sub-horizontal lines move closer together (Fig. 3.2). As these lines converge, it generally indicates that the sample age is approaching the 500 ka limit of the dating method. Monte Carlo simulations are potentially useful in this context for quantifying initial Th values (Hellstrom 2006) and constraining the age estimates so that they fall within the range of the $^{230}Th/^{234}U$ method (Ludwig 2003). For isotope ratios measured using ICPMS techniques, corrections are typically applied on $^{230}Th/^{232}Th$ activity ratios which are less than the standard baseline value of 300. In this study however, corrections will be applied on Th activity ratios < 50 using the mean Earth value for $^{230}Th/^{232}Th$. This approach can potentially underestimate the detrital thorium-232 content in each of the samples but it was adopted for several reasons. Firstly, preliminary age determinations obtained for the samples had relatively large standard deviations and corrected age estimates did not change these values significantly. For this reason, Th contamination was regarded as negligible and it was considered acceptable to use a lower thorium activity threshold for applying corrections. Secondly, these preliminary age determinations did not exceed the upper limit of the U-Th dating method and therefore Monte Carlo simulations were not prerequisite. In addition, individual growth laminae with obvious signs of recrystallization and dirty calcite were intentionally avoided to reduce the incidence of sampling layers with detrital thorium.

Measurement uncertainty

In addition to detrital thorium, age determinations can also be affected by analytical uncertainties which occur independently of the sample geochemistry. These effects are generally considered negligible although variations do occur depending on the instrumentation and operator experience (*e.g.*, Ludwig & Titterington 1994; Goldberg & Stirling 2003). Instrument errors are often random and in this study the main concerns on

the Element 2 was matrix effects and plasma parameters which often vary with each run (see section 3.3.4). One strategy used in this study was to reduce matrix effects by diluting samples with 2% HNO_3 to minimise the possibility of the sample tubing being clogged by incompletely dissolved particles. Matrix effects and plasma conditions collectively reduce the signal intensity and this in turn affects the precision of the age estimates obtained from the measured isotope ratios.

Because of the inherent complexity associated with the geochemical history of an individual speleothem it is generally safer to avoid dating samples with physical characteristics attributed to open-system conditions. Recrystallization, high porosity, dirty speleothem fabrics and waxy, irregular shaped forms are usually the most obvious signs of deposition under less than ideal settings (Luo & Ku 1991; Smart & Frances 1991; Richards & Dorale 2003).

3.2.3 Method for preparing speleothem samples

Each of the samples were first cast and cut parallel to the central growth axis. The plaster-of-Paris cast was removed by soaking the sample in water and then cleaning the surface of the speleothem with 37% (technical grade) HCl. Once the samples were cleaned, subsamples of *c.* 0.5g weight and a thickness of 5-10mm each were drilled out from the individual stratigraphic layers. These samples were conditioned for heating inside a Binder drying oven and then ignited at high temperature (*c.* 600-850^{o}C) for *c.* 4-6hrs. After ignition, the samples were dissolved in 14M HNO_3, spiked with uranium and centrifuged to remove insoubles at 2,500 rpm for *c.* 5min. The samples were then evaporated to almost dryness and re-dissolved in 1M HNO_3 up to a volume of 10ml. Actinides in the samples were extracted via ion exchange chromatography using Eichrom TRU resin columns (100-150µg grain size). The resin is activated in 1M HNO_3 and is used to bind U and Th actinides which form complexes with the nitrates in the solution.

The resin columns were prepared from 3ml graduated dropping pipettes with a 4mm fritted filter disc placed into each of the columns (Fig. 3.4). Resin was added in water to each of the columns which were then washed with 0.1M HCl/0.2M HF (2 x 2 CV) and conditioned with 1M HNO_3 (1+2 CV). After conditioning, the sample was added to the column and any calcium salts in the sample washed out with 1M HNO_3 (1 + 1 CV). The column was changed from HNO_3 by adding (1+ 1) 4M HCl before the actinides were eluted from the resin with (1+ 2+ 2+ 2 CV) 0.1M HCl /0.2 M HF. The samples were finalised for running on the Element 2 mass spectrometer by evaporating to approximately 1 ml before adding one drop of 14M HNO_3 to the eluate.

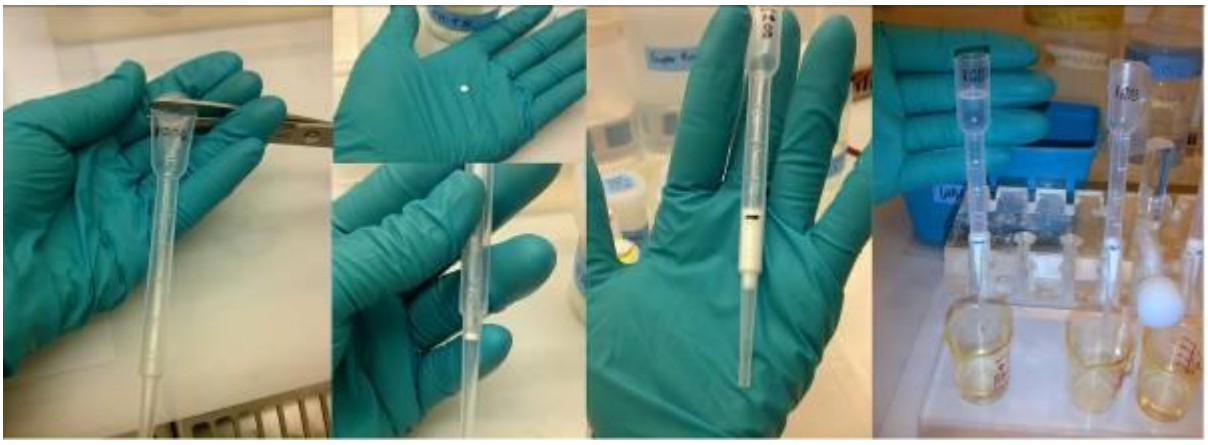

Fig. 3.4 Column preparation for U-Th elution

3.2.4 Measuring U-series isotope ratios using the Element 2

The Element 2 is a single collector inductively coupled plasma (ICP) mass spectrometer. It consists of a plasma torch, a sample introduction system, an ion transport system, an ion detector and a mass separation system (Fig. 3.5). The instrument runs on argon plasma which is generated from Ar gas that is passed inside a three-tube torch with a copper load coil. By charging the coil using a radiofrequency (RF) potential, energised electrons are produced within the torch and when these electrons collide with the atoms in the Ar gas, positively charged Ar+ ions are produced. As the frequency of the collisions between Ar atoms and electrons increases it produces a plasma which has a temperature between *c.* 6,000 and 10, 000 K. The plasma is fed by argon gas flowing through the outer tube of the torch at *c.* 18L/min as well as auxiliary gas flowing through one of the other tubes of the torch at *c.* 0.64 L/min. The latter controls the position of the plasma at the front end of the torch.

At the sample introduction system, a peristaltic pump operating is used to transport the liquid sample into the nebuliser where the sample is converted into an aerosol. The sample flow rate at the pump is supported by a spray chamber that is coupled to the nebuliser, and in this way, the sample aerosol is directed via the central torch tube into the plasma. For

the Element 2, the sample gas was pumped into the nebuliser and spray chamber at a rate of 1.170 L/min. As the sample aerosol travels through the high temperature environment of the plasma, it is dried, vapourised, converted to atoms and then ionised (Thomas 2001). Once the sample was ionised into it constituent parts, it was extracted from the plasma via a series of cones located in the interface region of the ion transport system. The interface region separates the high temperature (> 6000 K) and high pressure (*c.* 8-10 bar) plasma from the high vacuum environment of the mass spectrometer. As the sample ions pass through the mass spectrometer, the signal intensity of the ions are measured at the detector and these measurements are recorded in counts per second (cps) readings.

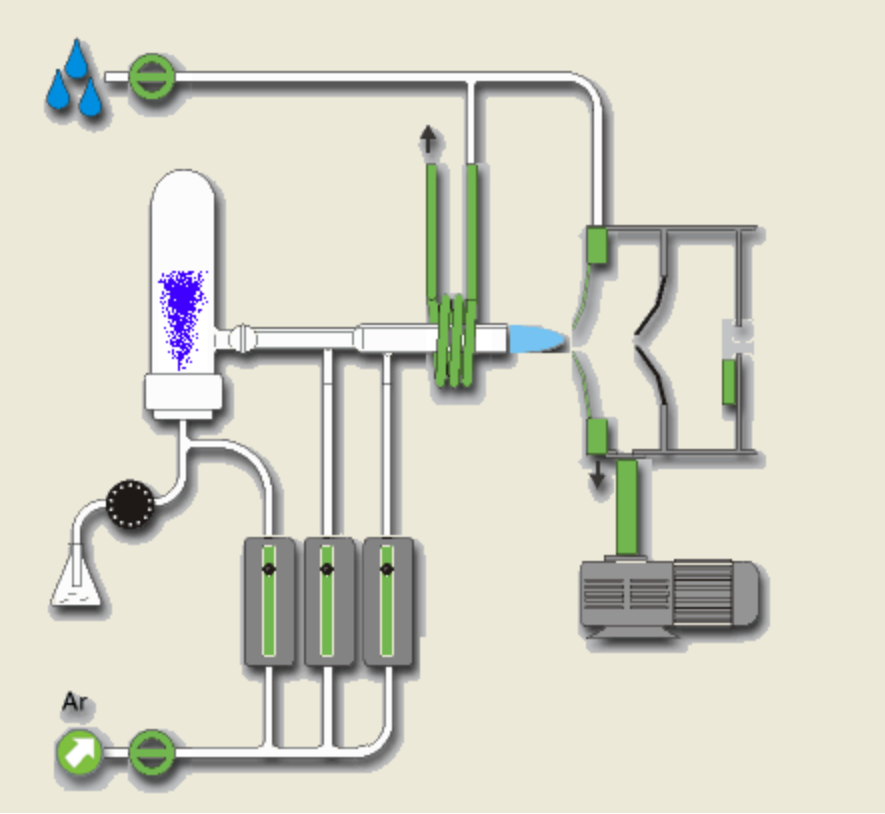

Fig. 3.5 Schematic of the main components of the Element 2 mass spectrometer

Before the sample sequence was initiated, the instrument was calibrated using an external blank containing 2% HNO_3 and an internal standard

solution containing indium (^{115}In) and bismuth (^{209}Bi). Signal intensity was maximised for each sample run by manually tuning parameters such as the nebuliser gas flow rate, RF power, torch position and signal intensity peak shapes. Instrument sensitivity was typically set to 1.6x10^{6} on ^{115}In. After manual tuning, there was generally a trade-off of *c.* 5-8% between oxides (which can interfere with signal intensity) and the instrument tune parameters. All isotope ratio measurements were performed using low resolution (R=300 parts per trillion - ppt) tune parameters, which is generally used for the analysis of non-interfered isotopes.

The Element 2 magnet has a mass range of 0-260u, and for this study, the magnet mass range was set to 208.980 with a mass window of +/- 10% used for detecting low abundance U isotopes as ^{233}U, ^{234}U, ^{235}U and ^{236}U and thorium as ^{229}Th, ^{230}Th and ^{232}Th simultaneously. The pump speed was set to 7.75 rpm with a sample take-up time of 10 seconds to run approximately 520 scans for each sample. The sample take-up time and pump speed often varied depending on the sample volume and the length of tubing used to pump the sample solution into the instrument. Each of the samples were prepared for running on the Element 2 by transferring the liquid contents into a labelled, acid-cleaned glass tube and then typically diluting it with 1-2ml of 2% HNO_3 to make up a 2-5ml volume of solution for analysis. This solution was then spun on a whirly mixer for 30 seconds before being pumped into the plasma via the sample introduction system. Although the instrument has an autosampler device, samples were loaded manually to reduce loss and maximise the precision of the isotope determinations. In addition, signal stability and overall analytical precision were also evaluated after each sample run by checking the %RSD (percentage relative standard deviation) on the ^{236}/^{233}U ratio of the uranium spike in each of the samples, which typically produced RDS values between 5 and 10% during a sequence run.

After each sample scan, the nebulizer capillary, spray chamber and tubing were cleaned for 4-5min with a weak solution containing 5% HNO_3 and 2

drops of HF. This step helped to flush out any residual Th from the instrument and prevents cross contamination between samples. After the wash solution, an in-house blank (2% HNO_3) was run to check the signal stability on the instrument. The blank was ideally low on ^{232}Th (< 100 cps) and ^{235}U (<20 cps) with 5% uranium oxides (UO). In instances where the ^{232}Th signal intensity on the blank solution was > 250, 000 cps (counts per second) the instrument was flushed with a stronger 10% HNO_3 solution for 8-10 min to ensure that the ThO (thorium oxides) were thoroughly removed. It was important to control for any ThO in the blank as many of the samples had very low Th concentrations, and therefore any anomalously high Th values could potentially skew the isotope determinations and thereby produce incorrect age estimates.

The onboard Element 2 software was used for tuning the instrument parameters and for evaluating the data after each sampling sequence.

3.3 Stable isotope analyses of speleothem carbonates

3.3.1 Principles and applications in speleothems

Over time and many drips later, speleothems will eventually form from the progressive build-up of precipitated carbonate. The main driver of this process is degassing of CO_2 from a supersaturated percolation solution until calcite precipitates (Baldini *et al.* 2006). Degassing occurs because of differences in the partial pressure of the carbon dioxide (pCO_2) which exists between hydrated CO_2 in the drip water and the gaseous CO_2 in the cave atmosphere (Baldini *et al.* 2006). The CO_2 levels in the dripwater are derived primarily from the soil zone and is typically much higher (between 0.1-3.5% vol.) than the CO_2 in the cave (0.06-0.6% vol.) (McDermott *et al.* 2006). Carbon isotopes in speleothems are therefore an admixture of soil and cave carbon and this forms the basis for using the isotopes as an

environmental proxy. The main carbon isotope pairs used in speleothem research are ^{12}C and ^{13}C. Variations in the $^{12}C/^{13}C$ ratio are expressed in delta notation (δ) relative to the marine carbonate standard Vienna Pee Dee Belemnite (V-PDB) in parts per mil (‰). Oxygen isotope signals are by contrast more intricate because of a suite of complex interactions that shift the isotopic composition of the carbonate rich dripwater (see section 3.2.2). The isotope changes can occur as the dripwater passes through the soil and meanders through fissures in the limestone on its way to the cave. Once the dripwater solution enters the cave and the carbonates suspended in solution eventually precipitate out further isotopic shifts can take place.

Oxygen isotopes in speleothems are however primarily derived from dripwater originating from precipitation above the cave. This relationship forms the basis for using the oxygen isotopes as an environmental proxy although interpreting the speleothem oxygen isotope signal in not quite as simple. Variations in the ^{16}O and ^{18}O isotope pairing are used to interpret the oxygen isotope composition of calcite. This $^{16}O/^{18}O$ ratio is similarly reported in δ notation relative to V-PDB with values expressed in ‰.

3.3.2 Constraints and fractionation effects

It is inherently complex trying to interpret variations in the composition of carbon and oxygen isotopes in speleothem calcite. This is because the isotopic signature of the calcite is influenced by events occurring both above and within the cave environment. The main events which occur on the surface of the cave are linked to the hydrological cycle (Fig. 3.6) and soil productivity (Fig. 3.7). With regards to the hydrological cycle, these variables include amongst others, altitude, evaporation from the ocean, rainfall amount and air temperature (McDermott 2004; Lachniet 2009; White 2004). Evapotranspiration, photosynthesis, microbial activity from organic matter decay, plant root respiration and residence times of the percolation solution in the epikarst zone are the most influential processes

occurring within the soil (White 2004). Within the cave environment, isotope signals are affected by fluctuating cave temperatures, variable dripping intervals and varying degassing rates (Mühlinghaus *et al*. 2009). This broad range of physical and chemical processes is collectively responsible for changing the isotopic composition of the calcite and is known as isotope fractionation. Fractionation is dependent on physical parameters such as temperature and humidity and there are two types of fractionation that can influence interpretations of environmental proxies derived from speleothems. These are kinetic fractionation and equilibrium fractionation and with both processes variations in the isotopic composition of ^{13}C and ^{18}O profiles occur between water and calcite. Identifying the main sources of fractionation and quantifying its effects is therefore essential when making inferences of climate from ^{13}C and ^{18}O signals in speleothems.

Fractionation of carbon isotopes

Carbon isotopes in speleothems come from the soil and dissolution of $CaCO_3$ in the host rock and to a lesser extent atmospheric ^{13}C (Schwarcz 1986). For carbon isotopes in speleothems, fractionation therefore occurs primarily during carbonate precipitation between HCO_3^- and $CaCO_3$ as follows:

$$Ca^{2+} + 2HCO_{3\text{-}(aq)} \rightarrow CO_{2(g)} + CaCO_3 + H_2O$$

This reaction produces gaseous CO_2 which contains lighter ^{12}C while the bicarbonate solution becomes enriched in the heavier ^{13}C isotope (Fairchild 2012). As degassing progresses, this enrichment of ^{13}C in the bicarbonate solution will produce higher $\delta^{13}C$ values (Fairchild 2012)**.** Carbon dioxide can however be degassed from solution before calcite precipitation takes place and this can happen in ventilated caves.

Fractionation of oxygen isotopes

The oxygen isotope composition of speleothem calcite is typically derived from the cave water which in turn comes from the meteoric water above the cave (Feng *et al.* 2012). Because of this relationship, variations in oxygen isotope values may be interpreted in terms of rainfall and temperature. These interpretations are not however quite so straightforward because speleothem ^{18}O values are the end result of complex interactions of environmental processes in the ocean, atmosphere, soil zone, epikarst and cave system (Feng *et al*. 2012). Factors operating above the cave that affect the distribution of ^{18}O in meteoric and cave waters are related to the various phase changes occurring in the hydrological cycle (Fig. 3.6). These factors are latitude, altitude, the oceanic effect, rainfall amount and the air temperature (McDermott 2004). Evaporation from the ocean at lower latitudes tends to increase the atmospheric concentration of ^{16}O in those regions due to the higher vaporization of $H_2{}^{16}O$. However as convections begin transporting the newly formed water vapour towards the poles, cooler temperatures and upper level divergences eventually cause condensation and precipitation to occur. During the process of condensation, the first water molecules to precipitate are those containing ^{18}O. Initial precipitation during a rain or snow even is therefore typically enriched in ^{18}O and will gradually become more depleted. This process is defined as the rain out effect.

In addition to the effects from the hydrological cycle, isotopic fractionation can also occur when water accumulates and then evaporates before entering the cave. Air movement and low humidity with the cave can also cause kinetic fractionation through the evaporation of cave drips (Wigley & Brown 1976; Mattey *et al.* 2008; Frisia *et al.* 2011),

As an environmental proxy, understanding the relationship between $^{18}O_{calcite}$ and $^{18}O_{dripwater}$ is essential when using ^{18}O values for climatic interpretations. The composition of precipitation is a primary component in

the isotopic signal found in calcite. Evaporation, degassing and short residence times of water in the soil may shift the isotopic compositions in the deposited speleothems (White 2007: 158). Temperature also plays an important role in fractionation of oxygen isotopes. The general trend is that an increase in temperature (^{o}C) will cause a concomitant increase in the ^{18}O composition of precipitation (Mickler *et al*. 2006: 66). This temperature dependent fractionation extends to the epikarst zone where Mickler and colleagues (2006: 66) demonstrated that the ^{18}O of cave dripwater could increase in response to both longer residence times of dripwater and with rapid evaporation from the soil zone. Under equilibrium conditions, deposition between the cave dripwater and the precipitated calcite the ^{18}O of the calcite will reflect the ^{18}O signal of the dripwater and the temperature-dependent fractionation between the drip waters and the deposited calcite. Ideally, the $^{18}O_{calcite}$ should record the weighted mean ^{18}O of meteoric water that falls on the surface above the cave. A conventional approach used for identifying and evaluating equilibrium deposition of calcite is defined by the Hendy Test (discussed in section 3.2.3). The basic tenet of the Hendy Test is that ^{18}O and ^{13}C should not covar, either laterally or axially along a single growth layer, and that ^{18}O remain constant.

As with interpretations of ^{13}C isotope signals, general trends also come from ^{18}O signals in cave dripwaters. The main traits are listed as follows:

1. $^{18}O_{dripwater}$ reflects $^{18}O_{precipitation}$
2. seasonal variations in ^{18}O may be linked to effects of isotope distribution in the hydrological cycle (see Fig. 3.6)
3. $^{18}O_{calcite}$ may reflect fluctuations in mean air temperature but this is not a simple relationship (*e.g*., Talma & Vogel 1992, Lauritzen & Lundberg 1999)
4. Variations in $^{18}O_{calcite}$ are independent of the drip interval and only depends on the temperature (Mühlinghaus *et al*. 2009: 7285)
5. Enrichment of $^{18}O_{calcite}$ typically occurs at higher temperatures

The strong temperature dependence associated with the extent of fractionation occurring at equilibrium for water is described by the Global Meteoric Water Line (GMWL) (Craig 1961). The GMWL describes the linear relationship that exists between ^{18}O and ^{2}H isotopes in natural meteoric waters.

Temperature dependent fractionation occurs during meteoric processes and also during carbonate precipitation. In secondary carbonates such as speleothems the $^{18}O_{calcite}$ signal is presumed to be sensitive to temperature and this sensitivity forms the basis for using $\delta^{18}O_{calcite}$ to estimate palaeotemperatures. This is discussed further in section 3.3.6.

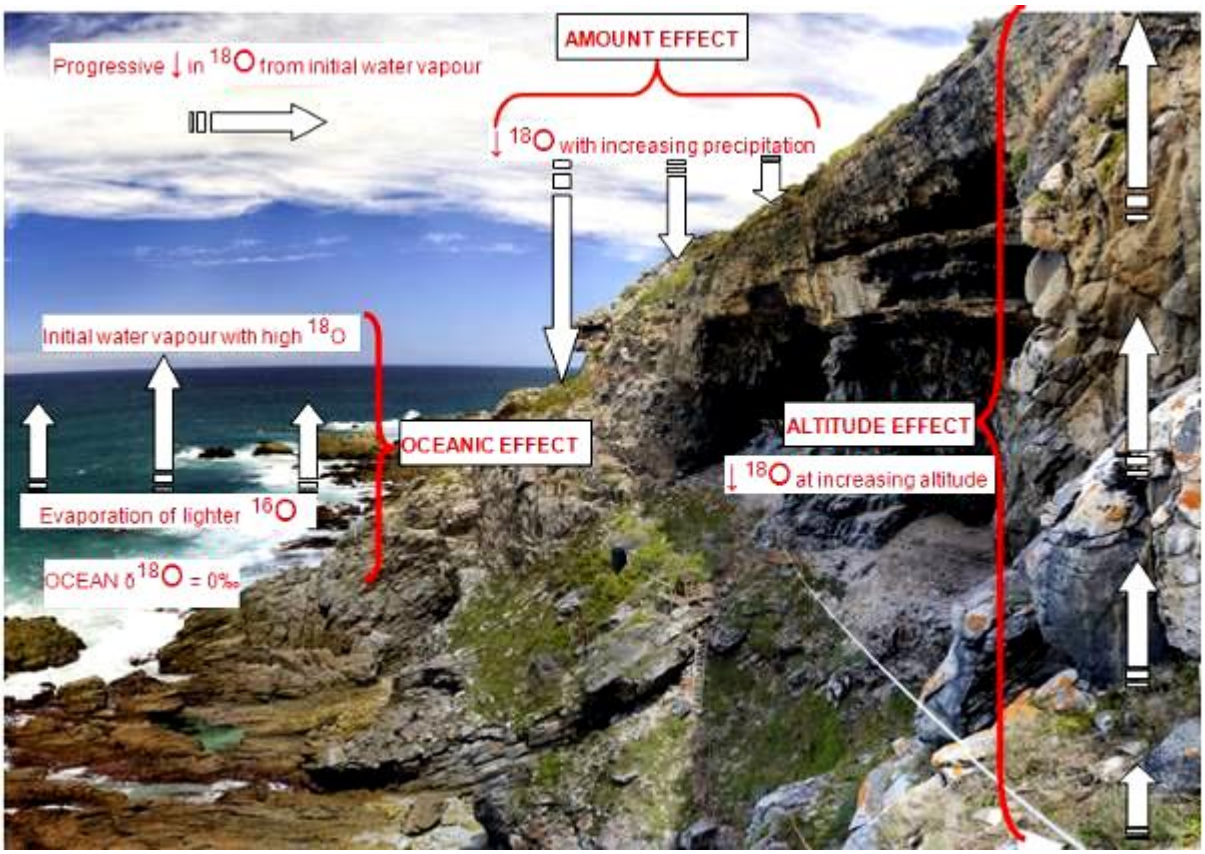

Fig. 3.6 Processes within the hydrological cycle responsible for fractionation of the^{18}O isotope. The influence of Rayleigh distillation on the distribution of ^{16}O and ^{18}O occurring with the condensation and evaporation of water vapour is also shown

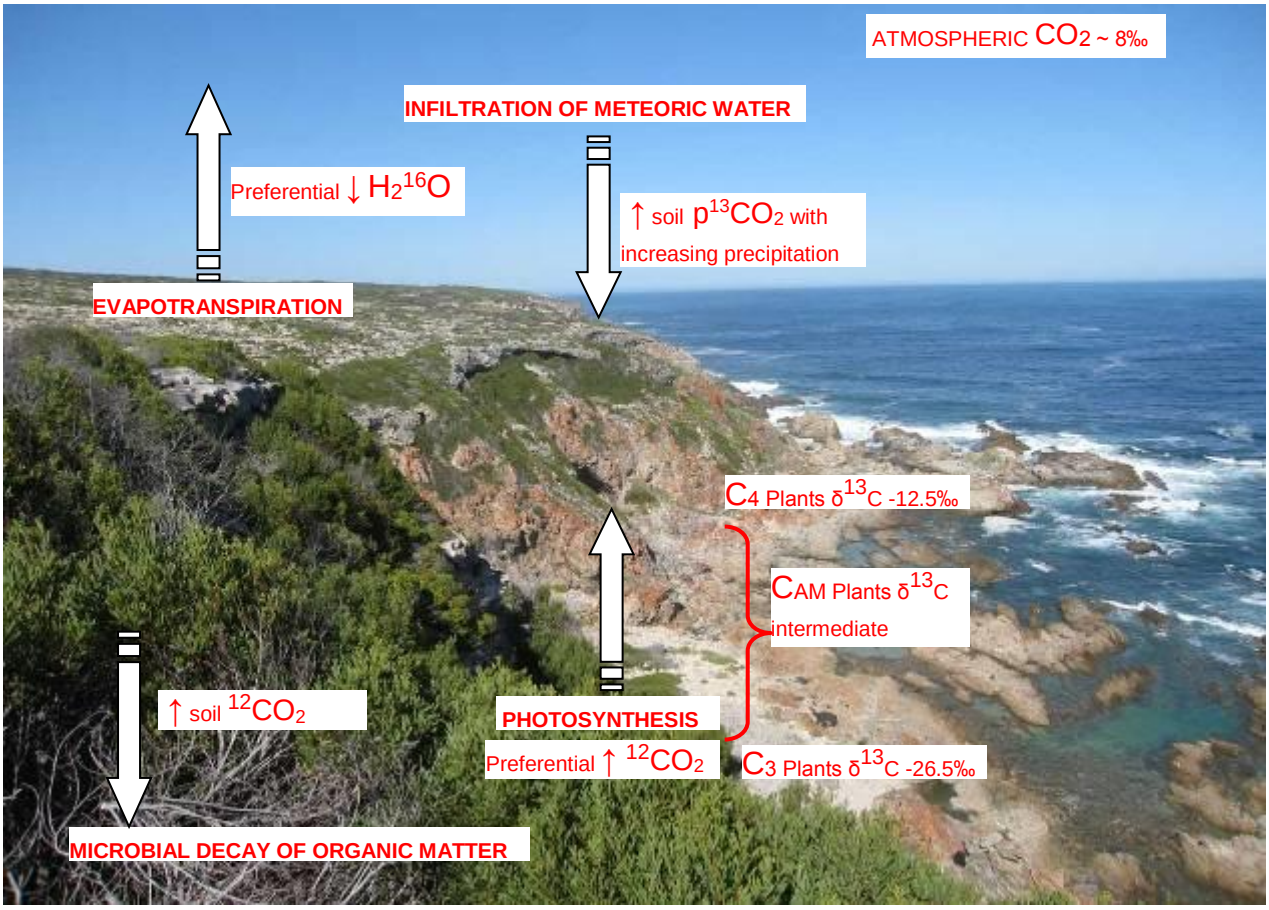

Fig. 3.7 Processes above the cave which affects the distribution of ^{12}C and ^{13}C isotopes

3.3.3 Sampling approach for stable carbon and oxygen isotopes

Collecting samples for stable isotope analysis

Samples for stable isotope analysis were collected using a micro-drill approach which is a commonly used low resolution technique (Spötl & Mattey 2006). Powdered samples, weighing between 50 and 80ug each, were collected manually using a dentist drill with a 0.5mm burr tip. These micro-drilled subsamples were taken along the vertical length of each of the samples at a sampling interval between 2 and 5mm which varied depending on the length of the individual stalagmites. After each subsample was drilled, the stalagmite was checked for any residual powder under an LED magnifying lamp with 10x magnification. This was

done to prevent possible cross-contamination between samples. As a precaution, the drill tip and workspace was cleaned with rubbing alcohol between successive samples. Subsamples for the Hendy Test were typically taken at regular intervals from the central axis along individual growth laminae. Samples were not drilled out in areas where multiple layers converged (*viz*. on the flanks of the stalagmite) and in instances where it was difficult to track the growth path of a particular layer.

Once the sample powders were collected, it was transferred individually into sterile glass autosampler vials and loaded into an autosampler carousel before being analysed on a Finnigan MAT252 mass spectrometer (see section 3.2.4).

Hendy Test

Evaluating the isotopic integrity of speleothems is an important consideration when using the isotope signals to make inferences about environmental and by extension climatic changes. The Hendy Test has conventionally been used for this purpose.

It is based on the principle that during calcite precipitation, CO_2 is removed from the supersaturated dripwater solution as it enters the cave because of a pressure gradient that exists between the CO_2 inside the cave and the CO_2 in the percolation water. Under ideal conditions, the rate of CO_2 removal will be sufficiently slow, so that isotopic equilibrium is be maintained between the CO_2 in the solution and the precipitated calcite.

This relationship is expressed as:

$$CO_{2(aq)} + H_2O \leftrightarrow HCO_3^- + H^+$$

$$CO_{2(aq)} + OH^- \leftrightarrow HCO_3^-$$

(Hendy 1971: 815)

The second reaction is typical for supersaturated solutions in limestone caves at pH 8 and it reasonable to assume that dissolution of the De Hoop

limestone occurred via a similar reaction. This is because the pH of the sampled dripwater that was obtained from the study sites also had a high pH between 7.5 and 8.

Aqueous CO_2 can also be lost through evaporation. Under evaporative conditions, CO_2 is removed quite rapidly and this disrupts the equilibrium between the bicarbonate in the calcite and the CO_2 in the dripwater. The disruption causes a concomitant change in the isotopic composition of the dripwater CO_2 and the bicarbonate (HCO_3^-) and can therefore result in non-equilibrium deposition of calcite (Hendy 1971). Under equilibrium conditions by contrast, the isotopic composition of the carbon is thought to exhibit little variation while the oxygen isotope signal will vary in response to changes in cave temperature or a change in the isotopic composition of the precipitation falling above the cave. The mechanism for equilibrium deposition is represented by the following reaction:

$$H^{12}C^{16}O_2{}^{18}O^- \leftrightarrow {}^{12}C^{16}O^{18}O_{(aq)} \rightarrow {}^{12}C^{16}O^{18}O_{(aq)}$$

$$H^{12}C^{16}O_2{}^{18}O^- \leftrightarrow {}^{12}C^{16}O_{2(aq)}$$

Based on this principle, the Hendy Test predicts that speleothem calcite formed under less than ideal conditions will become progressively enriched in $\delta^{13}C$ and $\delta^{18}O$. Non-equilibrium deposition can therefore be evaluated from the correlation between $\delta^{13}C$ and $\delta^{18}O$ sampled along or across a single growth layer. In contrast, under equilibrium conditions, there will be no relationship between $\delta^{13}C$ and $\delta^{18}O$.

However, in recent years the suitability of the Hendy Test in identifying speleothems for palaeoclimatic analysis has been questioned. There are important concerns on the limitations of using the Hendy Test. A number of studies have demonstrated that the controls on kinetic and equilibrium isotope effects are more complex than initially described by Hendy (1971). This includes for example, cave monitoring programs (*e.g.*, Mickler *et a*l. 2004, 2006), lab-based carbonate precipitation simulations (*e.g.*, Polag *et*

al. 2010; Day & Henderson 2011) and modelling experiments (*e.g*., Scholz *et al*. 2009; Mühlinghaus *et al.* 2009). Another limitation of the Hendy Test is that it is based on the sampling of a single growth layer but in reality, there are practical difficulties in sampling a single growth layer. This is because speleothems generally have very thin and sometimes closely banded layers that are almost impossible to sample individually with drill burr tips ranging in diameter from 0.3 mm up to 1 mm (Sasowsky & Mylroie 2004). In these instances, there is an increased risk of getting a false negative result (McDermott 2004; Mickler *et al*. 2006) and of "...*averaging out the isotopic values across the width of the sample...and [also] creates problems sampling the same or coeval bands at several locations within a single speleothem*..." (Sasowsky & Mylroie 2004: 8).

In a review on the limitations of the Hendy Test, Dorale and Liu (2009) stated that the Hendy Test was ..."*not reliably effective at screening stalagmites for palaeoclimatic suitability."* (Dorale & Liu 2009: 74). As mentioned previously the two main Hendy Test criteria used to indicate equilibrium deposition is that (1) $\delta^{18}O$ remains constant and (2) there is no relationship between $\delta^{13}C$ and $\delta^{18}O$ along or across a growth layer. In their criticism of the Hendy Test, Dorale and Liu (2009) argued that kinetic fractionation could occur along the sides of a speleothem while isotopic equilibriums occur in the centre. This has been demonstrated in several modelling studies (Polag 2010; Mühlinghaus *et al.* 2009). For Dorale and Liu (2009), the Hendy Test pre-requisite that there is no correlation between $\delta^{13}C$ and $\delta^{18}O$ is flawed because it assumes that $\delta^{13}C$ isotopic values are not affected by climatic variables. This is because factors influencing the $\delta^{13}C$ signal such as soil productivity and vegetation type are in turn linked to environmental and by extension climatic controls. A number of published studies have shown that correlations between $\delta^{13}C$ and $\delta^{18}O$ can in some instances be related to climatic influences (*e.g*., Dorale *et al*. 1998; Fleitmann *et al*. 2004; Dorale & Liu 2009; Zhou *et al*. 2011).

Based on the practical and theoretical drawbacks of using the Hendy Test Dorale and Liu (2009) propose that a Replication Test, which provides stronger evidence for judging speleothem suitability, be used as an alternative. The Replication Test is based on the idea that isotopic equilibrium can be evaluated from two or more speleothems exhibiting similar isotopic variability, that are coeval in age, and are located in close proximity to each other (*i.e.* from the same cave or nearby caves). The pre-requisite for using this approach is that kinetic processes should be absent or have affected spatially separated speleothems in the same way. The replication approach has been used in several studies (*e.g.*, Dorale *et al.* 1998; Constantin *et al.* 2007).

An advantage of this approach is that it allows one to use speleothem isotope proxies even when the $\delta^{13}C$ and $\delta^{18}O$ isotopic signatures are strongly correlated provided that the isotopic profile is replicated by similar aged speleothems within a given cave (Dorale & Liu 2009). This allows one to investigate more closely whether environmental factors such as rainfall or temperature changes are influencing the variability in isotopic records by comparing it with other independent climatic and environmental records.

In the context of this thesis, the replication approach is used along with the Hendy Test. The latter is included for the sake of completeness with the understanding that it may not be accurate. It is emphasised that stronger evidence in support of the isotopic integrity of the speleothem isotope records presented here may well come from using Dorale and Liu's (2009) Replication Test. Further support may also come from comparisons with independent palaeo-records from southern Cape proxies for vegetation, rainfall and temperature.

3.3.4 Measurement of ^{13}C and ^{18}O by mass spectrometry

Stable isotope ratios were measured using a Kiel carbonate device connected to a Finnigan MAT252 mass spectrometer. The Kiel carbonate device consists of a temperature controlled reaction region (*i.e.* acid tank & oven), a trapping system, an inlet system and gas cleaning system (Thermo Finnigan 2002). Carbonate sample powders are transferred to glass vials and are loaded into a numbered magazine tray along with a series of standards (*viz.* Carrara marble & NBS18) and two empty vials. This occurs inside the reaction region of the carbonate device. The empty vials are used respectively to check the vacuum on the instrument and for collecting waste. Once the magazine tray was loaded into the Kiel carbonate device CO_2 was evacuated from each of the samples vials under vacuum before a reacting with 100% H_3PO_4 at 70^{o}C. Carbon dioxide was liberated from the sample during this reaction as follows:

$$H_3PO_{4(aq)} + CaCO_{3(s)} = H_2O_{(l)} + CO_{2(g)}$$

The CO_2 was then separated from any additional (non-condensable) gases that were produced during the reaction by a series of traps which are housed in the trapping system. At trap #1, CO_2 and H_2O are removed from the reaction region by freezing at -170^{o}C with liquid nitrogen. The trap is then heated to -90^{o}C and while the water remains frozen, the CO_2 is transferred into the microvolume inlet system (Thermo Finnigan 2002). The frozen water on trap #1 is then heated to 150^{o}C and pumped out of the system. While the water is being removed from the system, the microvolume is heated up and the CO_2 sample gas is transported into the changeover valve of the MAT252 mass spectrometer. The $^{13}C/^{12}C$ ratios are calculated from measured mass ratios between $^{44}CO_2$ (as $^{16}O^{12}C^{16}O$) and $^{45}CO_2$ ($^{16}O^{13}C^{16}O$ & $^{17}O^{12}C^{16}O$). The $^{18}O/^{16}O$ ratio is determined from the mass ratio of $^{44}CO_2$ and $^{46}CO_2$. Each of these calculation steps is fully automated and isotope ratios are automatically corrected for isobaric interference (*viz.* from ^{17}O on mass 45) using the onboard Isodat 2.0 software. Each of the measured isotopic ratios is expressed in parts per mil (‰) relative to the V-PDB standard. Mean analytical precision of

standards (Carrara marble & NBS18) was 0.08‰ (1σ) for $\delta^{18}O$ and 0.04‰ (1σ) for $\delta^{13}C$**.**

3.3.5 Dripwater analysis of ^{18}O

It was necessary to collect a reference sample from modern precipitation and the cave dripwater to try and establish a link between the oxygen isotope signals in the speleothem calcite (denoted as $\delta^{18}O_{calcite}$). This is because the oxygen isotope composition of calcite is influenced by factors operating inside and above the cave environment. The latter is primarily linked to processes of the hydrological cycle (*i.e.* rainfall amount, type & duration of rainfall events) (Fig. 3.6, as discussed in section 3.3.2). On the other hand intra-cave influences on $\delta^{18}O_{calcite}$ may include evaporative effects, water storage in the epikarst zone and variable drip rates (Baldini *et al*. 2006; Fairchild & Baker 2012; Polk *et al*. 2011, 2012).

Precipitation should ideally be collected within close proximity (*c.* 30km) of the study area so that a local meteoric water line (LMWL) can be determined for the study area (using the approach described by Polk *et al.* 2011, 2012). The De Hoop Nature Reserve is however prone to storm events and flooding during the austral winter months (June-August). Therefore for practical and safety reasons it was not possible to setup a weather station here. The resources for setting up a dedicated weather station to record and collect the modern data was also lacking. As an alternative historical meteorological data (*viz*. rainfall & temperature) were obtained from nearby weather stations in Still Bay and Potberg. This data was used to provide a robust view of the rainfall patterns in the region. By extension when combined with the cave dripwater data, the meteorological data could possibly help to constrain interpretations of the $\delta^{18}O_{calcite}$ signal.

With regards to the De Hoop dripwater collections there are no water samples from Bloukrantz Cave where stalagmites BL1 to BL4 come from. This is because the cave has no actively dripping stalactites. West Cave

was used as a proxy for Bloukrantz Cave because along with Bloukrantz Cave and Double Barrel Cave it forms part of the Stilgat Sea Caves complex. These caves have a shared geomorphology and are in close proximity of about 6km to each other.

At Klipdrift Shelter where the KDS stalagmite was collected there are also no dripwater-calcite pairs because this sample grew elsewhere and was recovered within an archaeological deposit. For the Holocene age sample KDC5 dripwater samples were obtained from Klipdrift Sea Cave and its extension which is referred to as Klipdrift Sea Cave East. Klipdrift Sea Cave is only a few hundred meters from Klipdrift Shelter and the Klipdrift Complex is located *c.* 25 km from the Stilgat caves. The entire Klipdrift Complex has a shared geology and similar geomorphological features and because of this Klipdrift Sea Cave was used as a proxy for KDS.
Eight drip sites were selected for collection inside West Cave (denoted as WCD1 through to WCD8) and after the collection period eighteen water samples were obtained from four of the initial eight localities (WCD1, WCD2, WCD8 & WCD6). Seventeen dripwater samples were obtained from six drip sites inside Klipdrift Sea Cave (KDCD1 to KDCD6) and also from two drips inside its extension Klipdrift Sea Cave East (KDCED1 & KDCED2). The strategy for sampling from different locations within a single cave was to account for localised variations in drip rates and infiltration. In each instance drip water locations inside the caves were determined on site with a preference for active stalactites with varying flows (*i.e.* fast & slow drips). The stalactites feeding each of the drip sites at West Cave and Klipdrift Sea Cave were also collected for analysis of its calcite $\delta^{18}O$ content using the method described below.

Dripwater was collected directly from actively dripping stalactites using a simple but effective condom-cable tie setup (Fig. 3.8). Eight condom collectors were setup inside West Cave (denoted as WCD1 to WCD8). Six dripwater sampling sites were setup throughout Klipdrift Sea Cave (denoted as KDCD1 to KDCD6) between 20 and 30m from the main

entrance. Seven sampling sites were setup inside an extension of Klipdrift Sea Cave and dripwater obtained from this section was labelled as Klipdrift Sea Cave East (KDCE). The dripwater samples KDCED1 and D2 were located between 26 and 30m from the main entrance near a crevice in the rock face on the ceiling of the cave. The remaining four samples KDCED3 to KDCED6 were collected in a relatively sheltered part of the cave at *c.* 56m from the entrance.

Fig. 3.8 Dripwater collection setup used at West Cave and Klipdrift Sea Cave in the De Hoop Nature Reserve. Latex condoms were attached to actively dripping stalactites and secured in place using cable ties. Sample labels were printed on a Brother label printer. The sample ID consisted of an abbreviated cave name and the drip point location. For example, WCD3 refers to West Cave (WC) and D3 denotes dripwater location #3. This system was used because multiple drip sites were identified within a single cave

The condoms were typically changed quarterly (*i.e.*, every three months) with the water being transferred into sterile medical-grade urine sample

containers and sealed with leak-proof caps. In total, thirty-six samples were collected over a 14-month period from February 2012 to March 2013. These samples were kept refrigerated at 4°C until analysed at the Bjerknes Centre on a Delta V Plus equipped with a Gas Bench II.

The main components of the GasBench II is the autosampler, gas sampling system, water removal system, a loop injection system, a gas chromatograph (GC) column, the active open split interface and a reference gas injection system (Hilkert & Avak 2004) (Fig. 3.9).

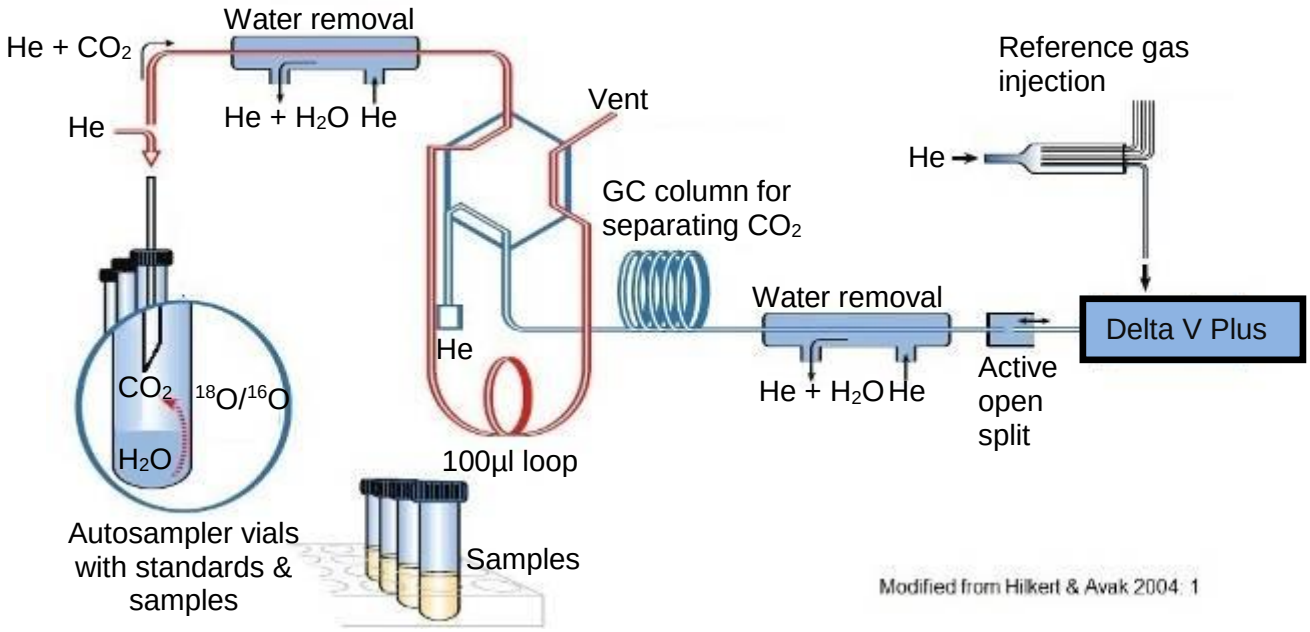

Fig. 3.9 Schematic of the main components of the GasBench II

For the measurement of ^{18}O in water by GasBench II mass spectrometry, each of the dripwater samples were prepared for analysis by pipetting 0.5ml (500µl) of sample into a clean 10ml exetainer vial. The individual vials were closed with standard septa tops, placed into an autosampler tray and then flushed with 0.3% CO_2 in He for 3-4 min at a flow rate of *c.* 30-40 ml/min. Helium is used as a carrier gas because it is inert. Flushing removes any air inside the sample vial and afterwards each of the vials was equilibrated at 24°C for 18-24hrs (Fig. 3.10).

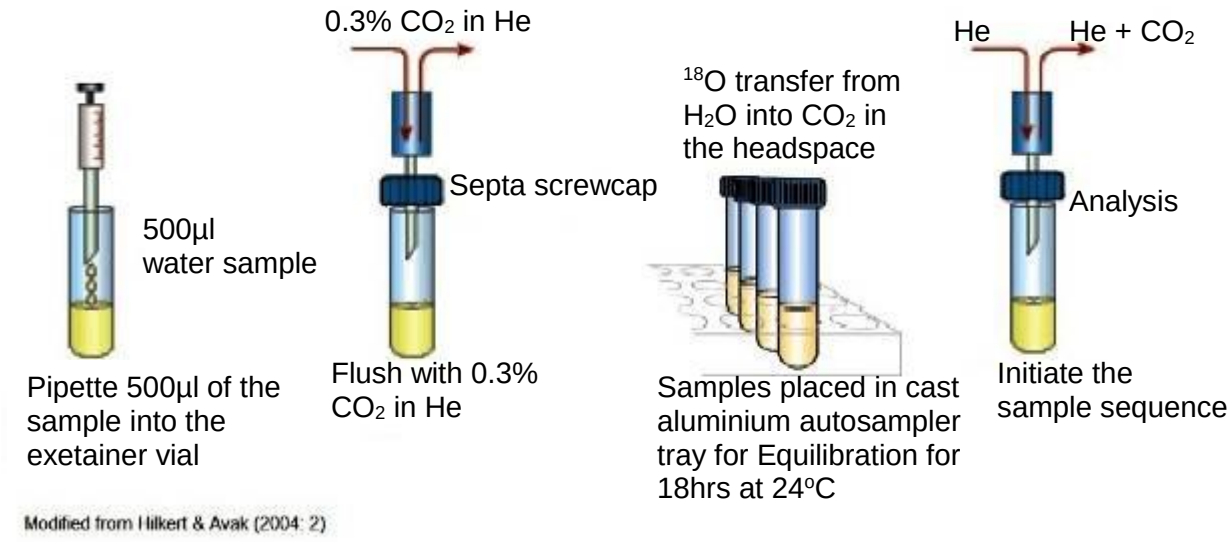

Fig. 3.10 Sample preparation for ^{18}O analysis on the GasBench II

After equilibration, the sample was injected into the injection port with a specialised hypodermic needle that is contained inside a rubber septum (Fig. 3.10). The sample is moved by He through water trap #1 where water vapour is removed from the sample gas. The sample then fills the loop injection system where 100µl sample aliquots are extracted from the sample headspace and transferred to the GC column. It is on the isothermal GC column where CO_2 is seperated from other gases in the sample. Water vapour is removed from the GC column at water trap #2. At the reference gas injection system, international standard gases are introduced for comparing with each of the sample aliquots (Hilkert & Avak 2004). This process is repeated for each sample in the run sequence.

The condition of the instrument was checked prior to the sample run by measuring the CO_2/He activity on two blanks (empty exetainer vials) that were slowly flushed with 0.3% CO_2 in He. After the blanks, quartets of internal "housewater" standards were run. The housewater is tested seawater from a nearby fjord in Bergen. A series of international water standards comprising GISP, SLAP and VSMOW were also run prior to the samples. To maximise the sample output on the instrument, several dripwater samples were run in triplicate. The replicated samples from West Cave were WCD3-08/12, WCD2.1- 11/12, WCD2-03/13 and WCD6-03/13 and those from KDC were KDCD6-11/2 and KDCED2-05/12. The single sample obtained during the collection from KDCE only contained 0.1ml (100µl) of water and because of this small volume; it was possible that fractionation could have occurred between the sample water and the CO_2 in the headspace of the container. This was taken into consideration during the run by pipetting equivalent volumes of housewater and measuring these in sequence, followed by triplicate measurements taken on standard volumes (0.5ml) of housewater at the end of the run.

The onboard Isodat 3.0 software was used for analysing and processing the dripwater data. Isotopic ratios for dripwater $\delta^{18}O$ are expressed in parts per mil (‰) relative to the V-SMOW standard. Mean analytical precision of

V-SMOW and SLAP standards was 0.05‰ and 0.03‰, respectively. Dripwater sample replicates are reproducible at an average precision of 0.03‰ (1σ).

After the dripwater analysis the $\delta^{18}O$ content of the calcite corresponding to the dripwater was also measured. The $\delta^{18}O$ analysis of the carbonate material was conducted using the sample procedure described in section 3.3.4. The $\delta^{18}O_{calcite}$ and $\delta^{18}O_{dripwater}$ content was evaluated by comparing the measured values with published $\delta^{18}O$ data determined for calcite that precipitated in isotopic equilibrium with its parent dripwater. The comparative data comes from Demény *et al.* (2010: 3525).

The $\delta^{18}O$ measurements for recently precipitated calcite along with the corresponding dripwater were also used as a temperature proxy. This is discussed further in section 3.3.6 below.

3.3.6 Temperature reconstructions using the speleothem $\delta^{18}O$

As mentioned in section 3.3.2 the temperature dependent fractionation of ^{18}O isotopes forms the basis for using measured $\delta^{18}O$ values as a palaeothermometer. Current research on temperature reconstructions derived from speleothem data are focused on new techniques such as clumped isotopes (Affek *et al.* 2008; Daëron *et al.* 2011), the analysis of $\delta^{18}O$ in fluid inclusions (Talma & Vogel 1992; Genty *et al.* 2002; McGarry *et al.* 2004) and the measurement of noble gases in fluid inclusions (Kluge *et al.* 2008). Clumped isotope thermometry compares the abundance of $^{13}C^{18}O$ bonds (denoted as Δ_{47}) in CO_2 which is extracted from carbonate material (*e.g.*, speleothems) during acid digestion (Affek *et al.* 2008). This technique does not require prior knowledge or estimates of the palaeodripwate which should ideally be obtained from fluid inclusions. Temperatures are instead determined directly from the measured Δ_{47} values (Daëron *et al.* 2011). There are however ongoing issues with calibrating Δ_{47} and temperature which preclude its widespread use as an

independent temperature proxy (Affek *et al.* 2008; Guo *et al.* 2009). For this reason clumped isotope thermometry was not applied to the De Hoop and Klipdrift Sea Cave stalagmites.

The analysis of $\delta^{18}O$ in fluid inclusions contained in speleothems is another technique that can be used as a temperature proxy. Fluid inclusions are basically trapped bubbles of water that contain the isotopic signal of the dripwater at the time of calcite precipitation (White 2004). By analysing the $\delta^{18}O$ content of fluid inclusions it is possible to calibrate the constants of Lauritzen and Lundberg's (1999) speleothem delta function (SDF). The SDF can theoretically be used to convert $\delta^{18}O_{calcite}$ to absolute temperatures (see below). Because none of the stalagmite samples discussed here contained fluid inclusions this technique could not be used. Here palaeotemperature estimates were instead determined using the conventional approach that uses variations in the $\delta^{18}O$ as a palaeothermometer.

In speleothems temperature inferences are made on the basis of the temperature dependent fractionation that occurs in $\delta^{18}O$ between calcite and its corresponding dripwater during precipitation (Friedman & O'Neil 1977; Lauritzen & Lundberg 1999; Beck *et al.* 2005; Coplen 2007; Chacko & Deines 2008). This relationship is well documented in the literature and the temperature at which calcite is formed is then calculated using known fractionation factors (Friedman & O'Neil 1977; Kim & O'Neil 1997; Coplen 2007; Demény *et al.* 2010). A general assumption of this fractionation factor approach is that isotopic equilibrium is maintained between $\delta^{18}O_{calcite}$ and its dripwater through time (Harmon *et al.* 2004). This is probably not entirely correct as dripwater $\delta^{18}O$ are sensitive to site-specific factors, that include amongst others, cave ventilation and temperature, water storage in the epikarst zone, degassing rates and soil pH (as discussed in section 3.3.2).

In speleothem calcite temperature dependent fractionation comes from two sources; the dripwater and the cave. Friedman and O'Neil (1977) were

the first to develop a mathematical equation to describe the fractionation relationship that exists between dripwater and its calcite. This equation only considers the influence of temperature to explain variations in $\delta^{18}O_{calcite}$ and has since been modified by Lauritzen and Lundberg (1999) to include additional variables. They developed an equation known as the speleothem delta function (SDF) that incorporates two terms; (1) the temperature dependent fractionation between dripwater and its calcite and (2) a thermodynamic fractionation factor. The SDF is expressed mathematically as:

$$\delta^{18}_{calcite}O = \epsilon \left[\left(T1^{\frac{a}{+273.15}}\right) - b\right] x \left[F(T2,t,g) + 10^3\right] - 10^3$$

The first term of the SDF relates to the temperature dependent fractionation that occurs between calcite and water inside the cave (T1). This term is known as the thermodynamic fractionation (*TFr*) (Lauritzen & Lundberg 1999).

The second term of the SDF is called the dripwater function *F(T2, t, g)* and contains site specific variables that describe the temperature dependence of precipitation (*T2*) and its dripwater. The variables *t* and *g* are related to the difference sources of ^{18}O variation in the dripwater before it precipitates calcite (Lauritzen & Lundberg 1999: 660). Some of the main variables that can influence the ^{18}O content of the dripwater are the residence time of the water in the epikarst (soil) zone, mixing of waters of different oxygen isotope compositions and the history of rainfall (*i.e.*, rainfall source, type & amount) (Lauritzen & Lundberg 1999). The expression for the dripwater function is shown below:

$$F(T2,t,g) = \delta O^{18}_{precipitation} = cT + d + \Delta_{SMOW}$$

The empirical coefficients *a* and *b* of the SDF can be calibrated by using independent temperature estimates. Proxy temperatures can for example be obtained by comparing $\delta^{18}O$ in fossil aquifers, fluid inclusions and measured $\delta^{18}O_{calcite}$ from modern samples (Lauritzen & Lundberg 1999:

660). Once these constants are calibrated the SDF can be used to convert the $\delta^{18}O_{calcite}$ values to actual temperatures (Lauritzen & Lundberg 1999; White 2004). Proxy palaeotemperature data pertinent to the southern Cape comes from the Cango Cave stalagmite (Talma & Vogel 1992) and from rodent micromammal indices at Klasies River (Thackeray 1990). These temperature estimates could potentially be used to calibrate the second term of the SDF but in reality it is problematic to apply. This is because the Cango Cave and Klasies Cave temperatures cover very different periods of time. It is also not clear how these temperature estimates link to the $\delta^{18}O_{calcite}$ data obtained here.

More recent studies on $\delta^{18}O_{calcite}$ based temperature reconstructions have proposed that previously reported fractionation factors may not be applicable to all carbonates (Demény *et al.* 2010). This is because it was previously assumed that carbonates such as corals and speleothems had the same temperature dependent fractionation factor. A recent approximation by Demény et al. (2010) cast doubt on this. It also raises concerns about the influence that the choice of fractionation factor can have on the accuracy of temperature reconstructions. Demény *et al.* (2010) analysed different carbonates (*e.g.*, warm water tufas, freshwater travertines & cave deposits) from a range of cave environments and temperatures (from 10 ^{o}C up to70^{o}C) in western and north-eastern Hungary. The cave environments they sampled included well and low ventilated caves, caves with strongly degassing drips and those with calcites formed close to equilibrium (Demény *et al*. 2010: 3522). They calculated fractionation values (denoted as 1000-lnα) for warm water tufas, freshwater travertines and cave deposits on the basis of the definition

$$\alpha = [\frac{(1 + \delta^{18}\text{Ocalcite}/1000)}{(1 + \delta^{18}\text{Owater}/1000)}]$$

In the formula above α is calculated using $\delta^{18}O_{calcite}$ and $\delta^{18}O_{water}$ values that are reported relative to V-PDB. Dripwater $\delta^{18}O$ is however conventionally reported relative to V-SMOW whereas $\delta^{18}O$ for carbonate

minerals (*i.e.*, calcite) is reported relative to V-PDB. In order to make the $\delta^{18}O$ data from the water samples comparable to its corresponding calcite $\delta^{18}O$ the dripwater $\delta^{18}O$ values were converted to the V-PDB scale using the following formula:

$$\delta O^{18}{}_{V-PDB} = 0.97002\,x \cdot \delta O^{18}{}_{V-SMOW} - 29.98\ ‰$$ (Coplen 1988)

With this conversion the dripwater $\delta^{18}O$ values are reported relative to the same V-PDB standard as the stalactite calcite it precipitates.

From the α values obtained for their cave deposit samples Demény *et al*. (2010: 3525) developed the following empirical equation which describes the $\delta^{18}O$ fractionation between calcite and water at 10-25^{o}C

$$1000 \times ln\alpha = \left(\frac{17500}{T}\right) - 29.89$$

The revised temperature fractionation equation above is applicable to stalagmites including those from De Hoop and Klipdrift Sea Cave. From this mathematical expression temperature is calculated as follows:

$$T = \left(\frac{17500}{1000\ x\ ln\alpha}\right) + 29.89$$

In the formula shown above *T* refers to temperature and is reported in ^{o}Kelvin. Temperature is obtained in ^{o}C using the following standard conversion:

$$T\ (°C) = K - 273.15$$

Where K refers to temperature in ^{o}Kelvin.

Demény *et al*.'s (2010) updated fractionation equation describes the first term of Lauritzen and Lundberg's (1999) SDF which is referred to as the thermodynamic term. As discussed previously there are difficulties in calibrating the second term of the SDF. This is a pre-requisite which has to be met in order to reconstruct temperature from the $\delta^{18}O_{calcite}$ data. As a result the SDF cannot be applied to the stalagmite samples used here.

For the De Hoop samples temperature reconstructions were instead estimated on the basis of the temperature dependent relationship that exists between $\delta^{18}O$ in dripwater and its corresponding calcite. Here temperatures are calculated using the empirical equation of Demény *et al.* (2010) (outlined above). This equation was applied to the $\delta^{18}O$ data obtained from recently precipitated calcite and its parent dripwater. These samples were collected inside West Cave and the Klipdrift Sea Cave (see section 3.2.5). Temperature estimates were then calculated using the approached described above and a summary of the steps involved is presented below:

1. Convert the $\delta^{18}O_{dripwater}$ values for each of the West Cave and Klipdrfit Sea Cave samples to V-PDB scale

$$\delta O^{18}{}_{V-PDB} = 0.97002\, x \cdot \delta O^{18}{}_{V-SMOW} - 29.98\ ‰$$

2. Calculate values for α using the expression

$$\alpha = \left[\frac{(1 + \delta^{18}\text{Ocalcite}\ /1000)}{(1 + \delta^{18}\text{Owater}\ /1000)}\right]$$

3. Use the fractionation values of α to calculate temperature using the empirical equation of Demény *et al.* (2010)

$$T = \left(\frac{17500}{1000\ x\ ln\alpha}\right) + 29.89$$

4. Convert the calculated temperatures into ^{o}C using

$$T\ (°C) = K - 273.15$$

The above mentioned steps were applied to each of the dripwater and stalactite tip samples from West Cave and Klipdrift Sea Cave.The resultant temperature values are presented in Table 5.6 and 5.7 of Chapter 5.

3.3.7 Constructing age models for the stable ^{13}C and ^{18}O data

In this study the StalAge algorithm developed by Denis Scholz and Dirk Hoffmann (2011) is used to construct the age models for each of the stalagmite samples (*i.e.*, BL1 – BL4, KDS & KDC5). The algorithm is written using the R statistical software and each of the age models are constructed using the following inputs:

1. The raw U-series ages and associated errors for each of the subsamples. Average uncertainty values were however used in the current study since the upper and lower error values are often different for each of the samples.
2. The centre position (in mm) for each of the dated subsamples referred to in point 1, and
3. Distance measurements (in mm) for each of the stable isotope points taken along the vertical growth axis of the stalagmite

The StalAge algorithm was chosen over more widely used approaches such as Bayesian statistics and smoothing spline functions. Bayesian statistics for example are useful in archaeological contexts for calibrating ^{14}C based chronologies (Buck *et al.* 1996; Turney & Bird 2002; Millard 2006, 2008). This statistical approach is also typically applied to Holocene aged speleothems and corals dated either by radiocarbon techniques (Hua *et al.* 2012) or uranium-series methods (Kaplan *et al.* 2005). Spline functions are constructed from joined sections of polynomials and can be used to obtain speleothem growth models by wiggle-matching either smoothing or cubic splines to the data (Richards & Dorale 2003; Spötl *et al.* 2006).

The StalAge algorithm differs from the two approaches outlined above in the following ways:

1. The algorithm is specifically designed for modelling stalagmite growth
2. There are no adjustable parameters and this greatly reduces the inherent risk with overinterpreting the data

3. StalAge is robust and is able to generate reproducible age models with 95% confidence limits that are comparable with speleothem records obtained in other studies (Scholz & Hoffmann 2011: 377)
4. The StalAge interface does not require any prior knowledge of stalagmite growth and geochemical history and is therefore user-friendly

Additionally, a major criterion underlying the application of the StalAge model is the absence of age inversions whereas this condition is not a prerequisite when using spline functions. Based on this assumption of monotonic growth, a stalagmite should show increasing age with increasing distance from the top of the sample (Scholz & Hoffmann 2011: 372). Once this basic condition is met in StalAge, a straight line representing the average growth for the modelled section of the stalagmite is fitted through the age data points along with the corresponding errors bars.

The StalAge algorithm uses a three step process to simulate stalagmite growth for the sample in question. First, the raw U series age data are screened for major outliers. This category of outliers refers to any data points in the age sequence that is significantly different (2σ) than at least two other data points (Scholz &Hoffmann 2011). After the screening process, the data are scanned for minor outliers and age inversions, with Monte Carlo simulations being used to identify the latter. During the third and final step the age model and associated 95% confidence limits are calculated for the sample. Using this three-step modelling process an age model was simulated for the growth of each of the De Hoop stalagmite samples (BL1, BL3, BL4) and the sample from Klipdrift Shelter (KDS) and Klipdrift Sea Cave (KDC5). Each of the age models are presented later in Chapter 5.

3.3 Summary

The inactive, fossil stalagmites used in this study come from selected caves in the De Hoop nature reserve on the southern Cape coast of South Africa. These speleothems were stratigraphically constrained using the $^{230}Th/^{234}U$ disequilibrium method which is conventionally used to date carbonate deposits up to a range of 500 ka (section 3.2). Proxy data in the form of stable carbon and oxygen isotopes were extracted along the vertical length of each of the stalagmites using a manual microdrill (section 3.3.3). These sample powders were analysed under vacuum with CO_2 by reacting with 100% phosphoric acid inside a Kiel carbonate device coupled to a MAT252 mass spectrometer (section 3.3.4). Variations in the distribution of the ^{13}C and ^{18}O signals were interpreted respectively in terms of vegetation, precipitation and temperature. There are inherent challenges when trying to link shifts in ^{13}C and ^{18}O signals with specific environmental conditions and these problems were addressed in this chapter (section 3.3.2). In the chapter that follows, Chapter 4, the methods and materials used in this study are discussed.

Chapter 4 – METHODS AND MATERIALS

4.1 Introduction

The current chapter focuses on the stalagmite samples that form the core of this thesis. These samples come from the De Hoop Nature Reserve on South Africa's southern Cape coast and were taken from Bloukrantz Cave, Klipdrift Sea Cave and Klipdrift Shelter located in the eastern section of the Reserve. As discussed in the previous chapter, there are import pre-requisites that have to be met when uusing speleothems for palaeoenvironemntal interpretations. One of which relates to the geochemical history of an individual speleothem. This can be quite complex and is nearly impossible to determine in the field. However, it is generally safer to avoid dating samples with physical characteristics attributed to open-system conditions (discussed in Chapter 3 section 3.3). The most obvious physical attributes that are thought to reflect deposition under less than ideal conditions are recrystallization, high porosity, dirty speleothem fabrics and waxy, irregular shaped forms (Luo & Ku 1991; Smart & Frances 1991; Richards & Dorale 2003). The formation of so-called entrance facies speleothems are dominated by evaporation rather than degassing, and results in a chalky, porous texture and irregular shape. The above-mentioned features can often be identified during visual inspection of the sample and provides important insight into the likely conditions under which the carbonate may have been deposited. Here six stalagmites were identified for analysis (BL1, BL3, BL4, KDS & KDC5) and are described individually below. In addition, to describing the physical appearance and other morphological attributes of the samples, the methods used to prepare each of the samples for uranium-series dating are also discussed. In addition, the procedure used to prepare the samples for isotopic analyses are also presented here.

4.2 Sample descriptions

4.2.1 BL1 (Fig. 4.1)

Sample macromorphology

BL1 is one of four samples collected inside Bloukrantz Cave which is located on the eastern edge of the De Hoop Nature Reserve. This particular speleothem is an inactive columnar shaped stalagmite with a height of 550 mm from the top to the base. It has a diameter of 58 mm at the top, 120 mm at its widest part and 100 mm at the base. There are visible growth layers throughout sample and these vary according to thickness, colour and degree of crystallization (Fig. 4.1).

The top 10 mm are closely banded and these layers alternate in colour between very pale (10YR 8/2) and almost white (10YR 8/1). A noticeable morphological change is represented by suspected aragonite deposition as light grey (5Y 6/1) crystals in the growth layer at 12 mm from the top. There are also visible remnants of this crystalline layer extending on either side of the sample towards the base. Mixed mineralogy speleothems have been reported previously in Bloukrantz Cave (Noah 2010) but the possible reasons for the depositional change between calcite and aragonite minerals has not been explored. The deposition of aragonite may be explained by any number of factors, for example, reduced cave drip rates, a shift in the percolation path of the dripwater through the host rock, or insufficient water availability (*e.g.* reduced rainfall above the cave environment) (Railsback *et al*. 1994; Asrat *et al.* 2007; Frisia *et al.* 2002; Lachniet *et al*. 2012). At this stage, it is not clear what may have caused the mineralogical change observed in the sample. The presence of aragonite in the speleothem fabric could however reflect a growth change. A layer at 23-33 mm from the top has alternating swirls of

pale brown (5YR 5/2) and light grey (5Y 6/1) that may indicate the presence of humic substances.

There appears to be a shift in the drip position between 32 and 37 mm and in this section the calcite is also finely laminated. An opaque white, porous pocket of potentially recrystallized calcite was observed at 43 mm from the top. Recrystallisation often causes a change in the trace element composition of calcite and this may cause a loss of uranium from the geochemical system. For this reason recrystallisation sites are best avoided when using U-Th dating methods because of the risk of producing spurious age estimates (Ortega *et al.* 2005). As a necessary precaution no dating samples were taken in this section of BL1.

The laminae at 51 mm is characterised by a crusty, honeycomb coloured band. This could represent the boundary for a growth break (hiatus) which is followed by the deposition of a 8mm thick band of compact calcite. From 61-260mm there appears to be continuous deposition of visible laminations although these appear as thin white striations from 131-260mm.

There are five instances where shifts from the central growth axis were noted. These changes in the growth axis were only observed in growth layers located in the lower half of the sample. The lateral shift in the growth axis occurs in stratigraphic layers at 265 mm, 295 mm and between 350-364 mm from the top. There are additional shifts between 485-495 mm from the top and also from 545 mm towards the base. These sideways shifts from the central axis are mainly related to changes in the landing position of water drops (Fairchild & Baker 2012: 4). In BL1 dense, sandy brown (5YR 5/2) coloured layers are found in four of the five stratigraphic sections where the aforementioned growth re-directions occur. In this stalagmite, the laminae associated with a lateral shift in the growth axis, are frequently deposited closer towards the outer edge of the sample. A similar feature was recognised

in a stalagmite from south- eastern Ethiopia. In the Ethiopian stalagmites researchers suggested that deposition towards the outer edges of the sample could indicate seasonally or continuously faster drip rates (Asrat *et al*. 2007: 56). In the context of the BL1 sample this is also quite plausible.

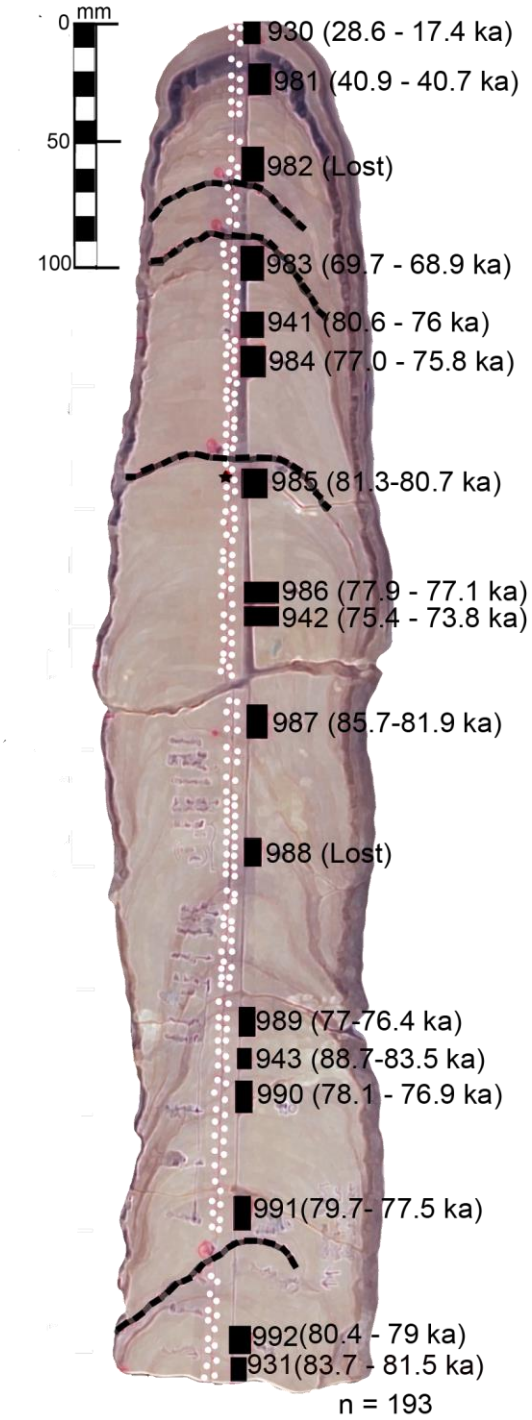

Fig. 4.1 A polished section of BL1 with the U-Th dating sample locations denoted by open boxes symbols (□). The Hendy Test sampled laminae represented by solid lines (-). The isotope samples which are taken from the vertical length of the stalagmite are indicated by solid circles (•)

There is cutting damage from the rock saw on the sample between 275 and 285 mm and no dating or isotopic samples were taken here. The widest part of BL1 is between 295 and 340 mm from the top and here there are white bands of varying thickness. Between 386 and 451 mm there are light brown (5YR 5/2) bands and from 460-480 mm the growth layers alternate between very pale and white. The stratigraphic section at 481 mm was glued due to cutting damage.

An interval of slow growth is inferred from the stratigraphic layers between 497 mm and 521 mm (from the top). A thin sandy brown layer was deposited at 522 mm (from the top) and between 530 and 540 mm there is a thick white layer. The change in growth direction at 545 mm mentioned previously also occurs with heavy banding of compact, white growth layers.

Sample preparation for U-series dating by $^{234}U/^{230}Th$

The samples were pre-treated for U-series dating by inductively coupled plasma mass spectrometry (ICPMS) at the Earth Science Department in the University of Bergen using an approach adopted from Hellstrom (2003) and described in Noah (2010). The stalagmite was cast in plaster-of-Paris before cutting a 10mm thick longitudinal section through the sample. This slice was then cut in two equal halves down the main growth axis. One half was used for U-series dating subsamples and the other for coring isotope subsamples. Seventeen subsamples with an average thickness of 7mm and a mean weight of 0.5g were extracted from the top to the base using a micro-drill with a 3mm diamond coated disc burr. After extraction, the samples were conditioned for heating at 100^{o}C for 30min and ignited at 600 ^{o}C for 4 hours. The ignition aims at removing organics, which otherwise would hamper chromatographic seperation of actinides in the column step. After ignition, each of the samples was dissolved in a minimum amount (*c.* 1-2 ml) of 14M HNO_3. Following the methods of Noah (2010), five of the 17 subsamples (U-Th lab no. 930-931 & 940-943) were spiked with 50 µl of the in-house JL369

spike. This spike contains a cocktail of 14M HNO_3, super pure water and a known ratio of ^{236}U, ^{233}U and ^{229}Th isotopes. A departure from the methodology followed in Noah (2010) is the use of an Element 2 instrument instead of a Nu Plasma MC-ICPMS. The advantage of using the Element 2 is that it requires smaller samples (*c.* 2-5ml of sample in solution) and has a fast output (running 520 scans per sample in 5min). The disadvantage is that this instrument has relatively weaker sensitivity with regards to signal detection compared to the MC-ICPMS. Therefore, in order to refine the signal detected by the Element 2, and consequently improve the precision of the age estimates obtained on the instrument, the remaining BL1 subsamples were spiked with 100µl of JL369. Problems with signal detection and ionisation efficiency are the main drawbacks of measuring U and Th isotopes by ICP mass spectrometry on the Element 2 instrument. ICPMS is however preferred when dating low uranium speleothems because the sample preparation is relatively straightforward and the analytical precision is comparatively better than that obtained on AMS and TIMS techniques (McDermott 2004).

After the spike addition, each of the subsamples was prepared for ion exchange chromatography using TRU resin (100-150µg grain size) columns. To prepare the columns, the bulb tip was cut off from a 3ml graduated Pasteur pipette, a 4mm fritted filter disc was inserted into the neck of the pipette and 1 CV (CV = column volume = 1ml) of TRU resin added in water to the column (see section 3.4.2). The column was then washed with 2CV water to check for normal dripping (*i.e.* slow and steady drips) and then cleaned with (2x2 CV) 0.1M HCl/0.2M HF. After cleaning, the column was conditioned for the sample to be added with (1+2 CV) 1M HNO_3. During the sample separation step (1+2 CV) 1M HNO_3 was added to the column followed by (1+1 CV) 1M HCl to wash out any NO_3^- ions remaining in the column from the sample addition step (Noah 2010: 28). This step is important because any trace of HNO_3 in the column at this stage would interfere with the elution of

the U and Th actinides. The column was changed from HNO_3 to HCl by adding (1+1 CV) 4M HCl. The intention with using a stronger concentration of HCl acid was to reduce the chances of losing any actinides, as this is a possibility when the acid is too dilute. For the final stage of eluting the U and Th from the sample, (1+2+2+2 CV) 0.1M HCl/0.2M HF was added to the column and the eluate collected in a labelled, clean Teflon container. The eluate was evaporated with 1-2ml remaining and then 1 drop of 14M HNO_3 was added. This adjustment was made to ensure that there would be 2ml of sample solution available to run at least 500 scans on the Element 2. Overall, for BL1 the 17 subsamples analysed on the Element 2 had an average ^{238}U content of 0.78 ppm.

Sample preparation for stable C and O isotope analysis

The primary proxy data obtained from BL1 is stable isotopes of carbon and oxygen derived from subsamples of the stalagmite carbonate. The subsamples weighed between 50 and 80µg each and were collected in powdered form and analysed in the Bjerknes Centre for Climate Research (BCCR) at University of Bergen. The powders were drilled along the central growth axis using a dentist drill with a 0.5mm diamond coated burr tip. In total, one-hundred and twenty-three subsamples were taken along both sides of the line at an average interval of 2.5mm (Fig. 4.1). This is the standard procedure that is used when collecting samples for stable isotope analysis on speleothems (*e.g.,* Asrat *et al.* 2007; Couchoud *et al.* 2009; Linge *et al.* 2009). The conventional technique of sampling growth layers on either side of a line drawn down the vertical length of the stalagmite is typically used to obtain a general isotopic signature for the sample (Constantin *et al.* 2007). In short, this strategy helps to reduce the chances of obtaining spurious values which could in turn contribute to an over interpretation of the isotopic signal when the variation may not be ‘real’.

An additional 65 subsamples were taken for the Hendy Test which is widely used to evaluate the suitability of a speleothem sample for palaeoenvironmental analysis (Hendy 1971; Fig. 4.1; see Chapter 3 section 3.2 for details). The test essentially checks if the speleothem calcite was deposited in isotopic equilibrium with the dripwater from which it was formed. If this is the case, then the oxygen isotope signal of the dripwater can be related to the precipitation above the cave while the carbon isotope signal in the calcite may be related to the soil and vegetation from which it was derived. This inference is rather complex and is discussed in more detail in later in this chapter. In BL1, Hendy Test samples were taken along single growth layers from the central axis moving towards the flanks of the sample. These layers are located at 65mm from the top of the sample, at 87mm, 175mm and 513mm from the top. The strategy was to sample laminae with relatively clean calcite and clearly defined bands to help reduce the chances of unintentionally sampling combined layers.

4.2.2 BL2 (Fig. 4.2)

Sample macromorphology

BL2 is the second stalagmite collected inside Bloukrantz Cave. It has a long, narrow broomstick-shaped shaft and is 550mm long from top to base with a diameter of 2mm at the top. The sample has fine, closely banded growth layers and these alternate in colour between pale (10YR 8/2), very pale greyish-orange (10YR 7/4), pale brown (5YR 5/2) and light brown (5YR 6/4). No visible hiatuses or lateral shifts in the growth axis were identified in the sample. This may suggest continuous, possibly rapid growth from a single drip location.

The width increases incrementally along the length from 3.5 to 6mm thickness between 20 mm and 220 mm from the top. At 240 mm, there is some cutting damage on the sample. The shaft width narrows to 5mm between 245 and 320 mm from the top and at 270 mm there is a physical break. The sample thickens to 6mm between 320 and 355 mm from the top. An irregular wedge-shaped extension occurs on the left side of the sample between 365 and 445 mm from the top and this is the widest part of the sample with a width of 111 mm. BL2 has laminations growing towards the sides of the stalagmite and these layers only occur on the left side of the sample. Similar types of wavy layers forming on the sides of speleothem were also observed in the BL1 sample and also in a stalagmite sample 32206 from Crevice Cave (Braun 2014). The latter sample is strikingly similar to BL2 and shares the same colouration, wavy laminations and displays similar signs of pitting near the base. In BL2 there is a relatively large section of pitted calcite in the speleothem fabric from 465 mm towards the base. It is not clear what could have caused the pitting although the most likely possibilities include dissolution, recrystallization, and the influence of microbial activity or rapid deposition.


mm
0
50
100
925
139.2-134.8 ka
964
142-130.3 ka
965
129.7-116.7 ka
966
139-119.8 ka
926
146.8-143.2 ka
967
158.8-151.3 ka
968
120.6-115.5 ka
927
153.6-146.5 ka
969
137-133.1 ka
970
114.9-111.1 ka
928
126.3-112.4 ka
971
117.4-114.6 ka
972
118.5-115.5 ka
973
114.8-109.3 ka
929
128.2-123.9 ka
POROUS!
NOT DATED
n = 134

Fig. 4.2 A polished section of BL2 showing the U-Th dating sample locations (□), Hendy Test sampled laminae (-) and the positions of drilled subsamples taken for stable isotope analyses (•)

Sample preparation for U-series dating by $^{234}U/^{230}Th$

For BL2, subsamples with an average weight of 0.5g and an average thickness of 9 mm each were typically removed along the vertical length of the stalagmite. The pitted section of the sample at 465mm from the top seemed problematic because it did not have the smooth, clean, dense calcite which is the preferred material for U-Th dating and therefore no samples for dating were taken here. Additionally, in the stratigraphic section between 160 and 220 mm from the top there is heavy banding with multiple laminae merging and this made it difficult to identify individual layers. As a result, no dating subsamples were taken in this region of the sample either. The same protocol detailed for BL1 was used to prepare the U-Th samples from BL2. Overall, fifteen subsamples with an average U content of 0.41ppm was prepared for dating by ICP mass spectrometry on the Element 2.

Sample preparation for stable C and O isotope analysis

The same protocol used for BL1 was used here with subsamples weighing between 50 and 70µg each extracted along the central growth axis A total of one-hundred and ninety-two subsamples were taken along both sides of the line at an average interval of 3mm (Fig. 4.2). Sixteen additional samples were taken for the Hendy Test and these come respectively from individual layers at 94mm and 350mm from the top. However, because of the merged growth layers observed on the left side of the sample, sampling individual layers on this side of the growth axis was problematic. Consequently, the Hendy Test points that were sampled for BL2 only come from the sections of the growth traverse with clearly defined and traceable laminations.

4.2.3 BL3 (Fig. 4.3)

Sample macromorphology

BL3 is the third sample collected inside Bloukrantz Cave and this stalagmite fragment has a height of 425mm from the top to the base and a diameter of 35 mm at the top (Fig. 4.3). The thickest part of the sample occurs at 170 mm with a width of 105 mm. This sample has a rounded top with a wavy outline and slightly resembles cactus in shape. The stalagmite has multiple bands of visible growth layers and a distinct hiatus. Sub-vertical laminae are also present and these reflect a lateral shift in the growth direction.

In the stratigraphic layers between 0 and 95 mm from the top, the finely laminated calcite occurs as opaque layers of cream (10YR 8/2), pale brown (5YR 5/2) and white (10YR 8/1). A boundary layer at 95mm from the top indicates the transition from opaque calcite in the uppermost part of the sample to more semi-translucent calcite in the central zones of the sample. On the central axis of BL3, the translucent calcite has horizontal striations. Closer towards the flanks, these laminations grow downwards in a wavy pattern. The extent of this morphological change is prominent between 100 and 160 mm from the top with some remnants of semi-translucent calcite remaining on the flanks of the sample although this thins out visibly towards to the base.

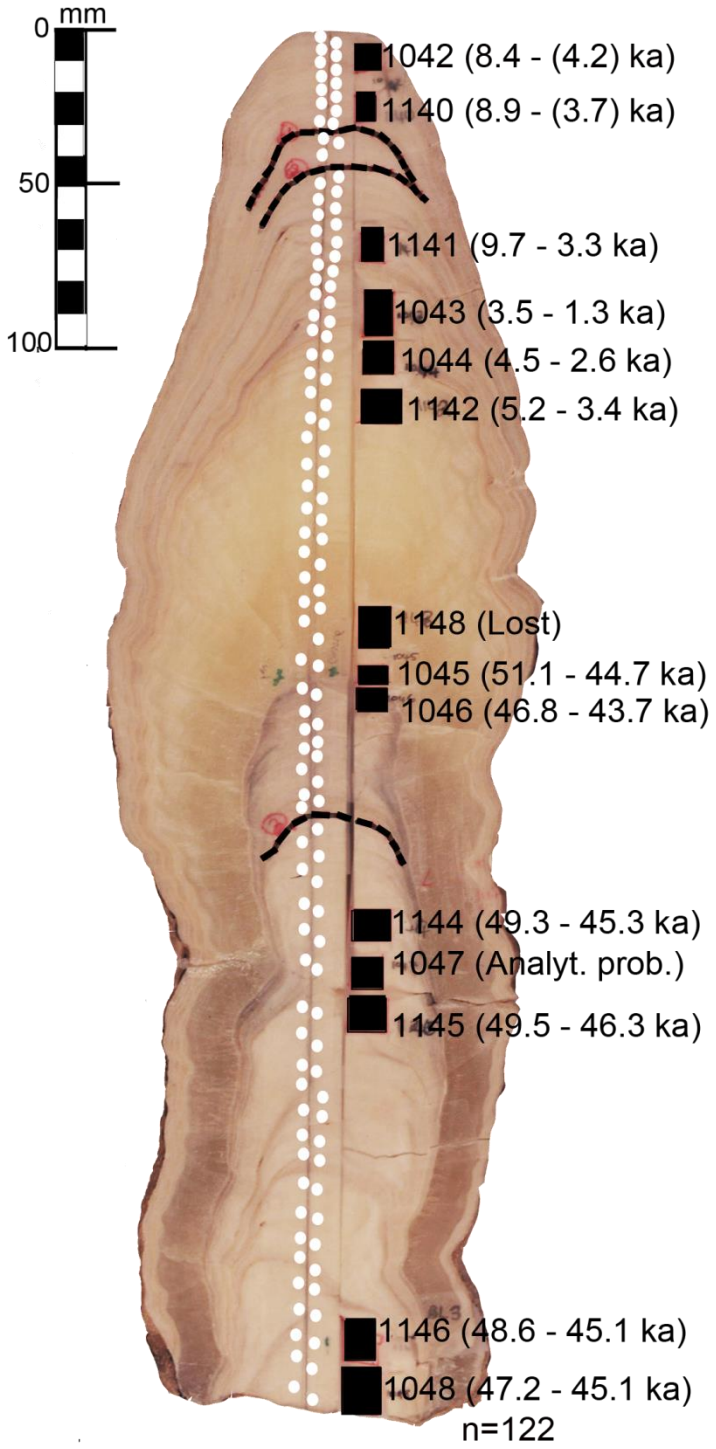

Fig. 4.3 A polished section of BL3 showing the boundary for the growth hiatus, U-Th dating sample locations and Hendy Test sampled laminae. The positions of drilled subsamples taken for stable isotope analyses are also shown

The section of the stratigraphy between 0 and 200mm also has also multiple layers merging and growing down the sides of the sample from the top. These merged layers form in soft ripples and are thickest at the widest part of the sample around 107 mm and taper off from 280 mm towards the base. BL3 is the third stalagmite the quartet of samples from Bloukrantz Cave with laminae growing towards the sides of the sample. This may imply, at least superficially, that these samples could be responding to similar thresholds operating either within or above the cave environment. The layer at 200mm from the top marks the boundary for a hiatus in the sample. In this stalagmite, the hiatus is recognised as a distinctively different shaped stalagmite occurring within the larger form of the sample. This section of BL3 also has growth bands with variations in the position of the growth axis occurring between 210 and 239 mm, between 317 and 348 mm, and at 380 mm from the top.

Sample preparation for U-series dating by $^{234}U/^{230}Th$

The general procedure described previously for BL1 and BL2 was also used for this stalagmite. One exception is that for BL3, additional subsamples were often taken in duplicate in those sections of the stratigraphy with macroscopic changes in the speleothem fabric. Duplicate subsamples were taken between 5 and 28 mm from the top and at the bases while triplicate subsamples were collected at the hiatus section. This was primarily because of instrument signal stability issues experienced during the sample run for some of the subsamples. In these cases, precision was quite weak (> 7kyr) and this contributed to poor chronological control. Additional samples were then taken either in duplicate or triplicate to help refine the age estimates. Overall, fourteen subsamples with an average U concentration of 0.29ppm were prepared for analysis on the Element 2.

Sample preparation for stable C and O isotope analysis

For BL3 the same protocol decscribed for BL1 and BL2 was used here with a total of one-hundred subsamples' weighing between 45 and 80µg each extracted along the central growth axis of BL3 (Fig. 4.3). Thirty-eight additional samples were taken for the Hendy Test and these come respectively from individual layers at 31mm, 44mm and 245mm from the top.

4.2.4 BL4 (Fig. 4.4)

Sample macromorphology

BL4 is the fourth sample from Bloukrantz Cave and is a columnar shaped stalagmite fragment that is broken at both ends. It is *c*. 450 mm long and has a relatively uniform thickness from the top to the base with a diameter of 75 mm at the top. Growth laminae are visible throughout and these vary in colour between creamy white (10YR 8/2) and light brown (5YR 6/4). No visible hiatus (es) were identified in this stalagmite.

This sample was fractured during the sawing process at three sections; between 50 and 60 mm from the top, at 258 mm and at 325 mm. In the stratigraphic section between 0 and 230 mm there are thick ripples of stacked growth bands growing on either side of the sample. These ripples grow inwards towards the central axis and this made it difficult to identify single laminae. At 235 mm, there is a change from the comparatively 'messy' stratigraphy in the upper half of the sample to a more clearly banded calcite layers. This change occurs from 235mm to the base. No changes were identified in the position of the vertical growth axis in BL4. When compared to the other samples from Bloukrantz Cave, BL4 does not display any of the mineralogical changes observed in BL1 and it is composed exclusively of calcite. Additionally, this sample does not have any of the porous inclusions that were observed in the speleothem fabric of BL2.

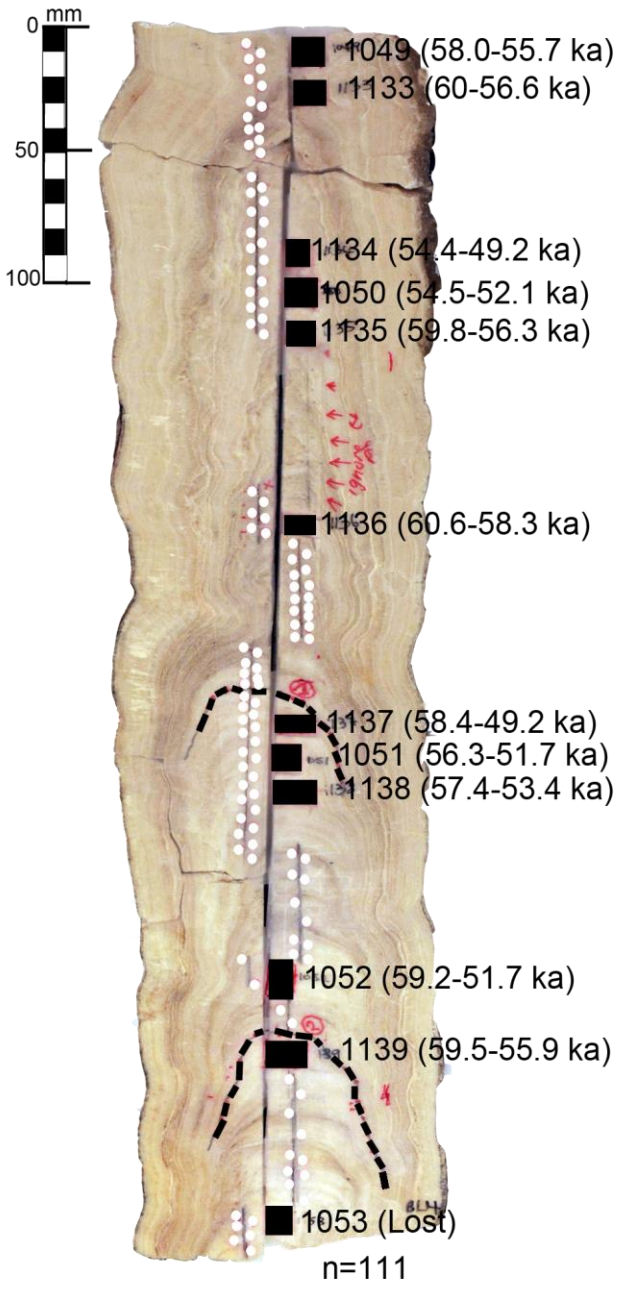

Fig. 4.4 A polished section of BL4 showing the visible growth laminae, the position of U-Th dating sample locations and Hendy Test sampled laminae. The positions of drilled subsamples taken for stable isotope analyses are also shown

Sample preparation for U-series dating by $^{234}U/^{230}Th$

This stalagmite fragment was cast in plaster-of-Paris before cutting a 10mm thick slab parallel to the growth axis. This slice was divided into two equal halves along the growth axis with one section for U-Th dating and the other for stable isotope analysis. The same procedure described previously for the other Bloukrantz Cave samples was used for the BL4 sample. Overall, twelve subsamples with an average ^{238}U concentration of 0.31ppm were analysed on the Element 2 mass spectrometer.

Sample preparation for stable C and O isotope analysis

Using the same procedure described previously for the other Bloukrantz Cave samples, sixty-one isotope points, weighing between 45 and 80µg were drilled out and collected from BL4. An additional fifty-two samples were taken for the Hendy Test from the growth layers located at 244mm and 370mm from the top.

As mentioned previously, the upper 235mm of this sample is characterised by multiple merged layers converging at the centre of the sample. This messy stratigraphy is also observed in the BL2 stalagmite. These merging layers are problematic because of the difficulty in tracing individual laminae for sampling. The fine laminations observed in the upper part of the sample may have formed quite rapidly and perhaps within a short period. If this is true, then sampling these layers may be less important when trying to assess the stable isotope signal within a palaeoenvironmental context. Further investigation is therefore necessary to determine this. For these reasons, fewer isotope samples were taken from BL4 compared to the other stalagmites collected from Bloukrantz Cave.

4.2.5 KDS (Fig. 4.5 a & b)

Sample macromorphology

The KDS sample is a small, stalagmite that was found in an archaeological context during the 2012 excavation season at Klipdrift Shelter. The sample comes from quadrate R29c in the PBA/PBB stratigraphic unit which also contained poorly preserved bone, shellfish, burnt pieces of ostrich eggshell and lithic artefacts. An interesting feature of the KDS stalagmite is that it is covered in micro-cracks with the top cap coverd in tiny pock-marks. The stalagmite was also not find in a growing position in the Middle Stone Age archaeological deposit. Together, this is suggestive of anthropogenic use of the stalagmite by Middle Stone Age tool makers and should potentially be investiaged further.

The stalagmite sample is conical shaped and has a rounded top with a broad, slightly angular base that resembles a thick cut of T-bone steak. There was a cross-sectional break in the stalagmite that separated the top from the bottom half when it was recovered from the deposit. It is quite small with a height of 90 mm, a diameter of 50 mm at the top and a width of 110 mm at its widest part. There are visible growth laminae of varying thickness, alternating in colour between warm brown (5YR 5/6), taupe (5YR 2/2) and light brown (5YR 6/4). The rich brown hues of these growth bands may reflect the presence of humic substances in the dripwater. No hiatuses were observed. Visible signs of recrystallisation are also absent. Although there are stalactites on an exposed overhang that forms part of the Klipdrift Shelter, it is not plausible that the KDS stalagmite formed within the deposit where it was found. This is because there were no signs to indicate that it formed within the archaeological deposit. It is unclear how it ended up buried in the archaeological deposit. One plausible scenario is that the stalagmite was

removed anthropogenically, perhaps from a cave in the vicinity of the site, and subsequently incorporated into the deposit.

Because of its small size, this sample was not cast in plaster before cutting. A transverse slab of *c.* 10 mm thick was removed parallel to the growth axis and this slice was used for dating and stable isotope analyses. The stalagmite was surprisingly fragile and significant damage occurred during cutting when it split into multiple pieces, most likely due to the impact of the rock saw cutting blade. These individual pieces were subsequently glued and the sample pieced back together by using the intact stratigraphic layers as a guide. Sub-vertical shifts in the central growth axis were recorded closer towards the base at 52mm and *c.* 63mm from the top. This may either suggest changes in the position of the water drops falling from the stalactite feeding the KDS stalagmite, or that tha sample grew on unconsolidated sediments that might have moved. No lateral shifts in the position of the growth axis were observed in the upper sections of the stratigraphy. Bands growing towards the sides of the sample, which was frequently observed in samples from Bloukrantz Cave, are not present in the KDS stalagmite. The absence of these features, suggests that at least prior to the KDS sample most likely forming from slow, possibly continuous drips of humic-rich water. A view of the KDS stalagmite is provided from two different angles (Fig. 4.5a). However, due to the extensive cutting damage on the sample a sketch is provided that shows where the U-Th dating subsamples, Hendy Test laminae and stable isotopes subsamples were taken (Fig. 4.5b).

Fig. 4.5 (a) A overview of the KDS stalagmite from Klipdrift Shelter

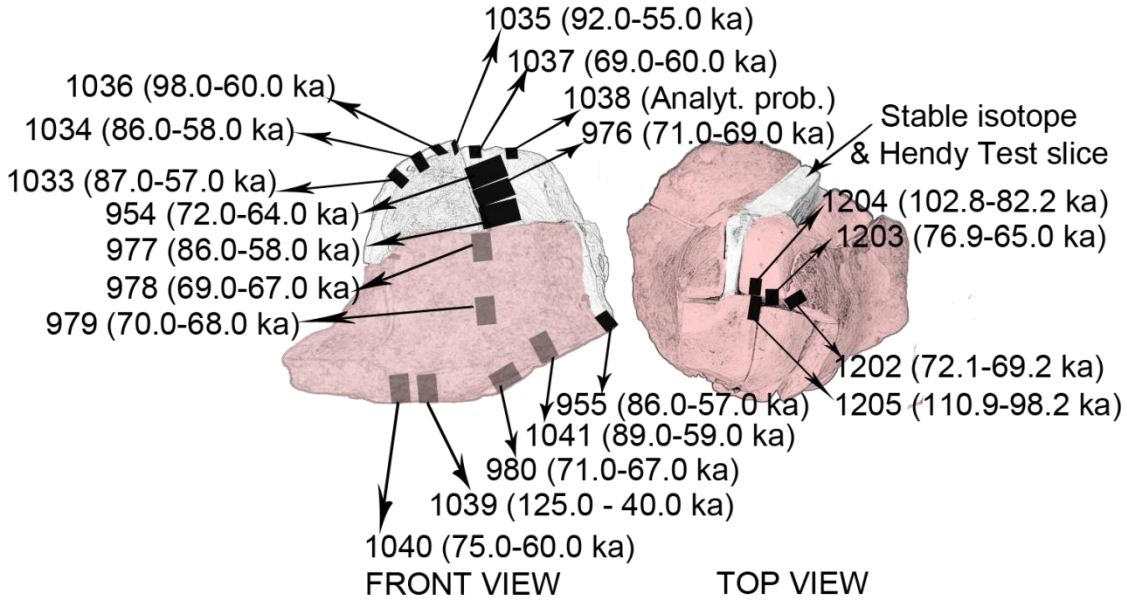

Fig. 4.5 (b) A sketch of the KDS sample showing the positions of U-Th dating sample locations and the section of the stalagmite from where Hendy test laminae and stable isotope subsamples were taken. The light pink colour overlay on selected parts of the illustration represents the outside of the stalagmite. Those parts of the sample that are not in shadow represent the inside parts of the sample. (Not to scale)

Sample preparation for U-series dating by $^{234}U/^{230}Th$

For U-Th dating, the same procedure described for the Bloukrantz Cave samples was used here. Because this particular sample was excavated from dark (5YR 2/1), sticky layers a heat-intensive treatment was use to remove organics from KDS before chemical preparation. For this reason, the twenty subsamples collected from KDS were conditioned for heating at 100^{o}C for 1hr and ignited at 850^{o}C for 5hrs to remove any organics. Overall, the twenty subsamples had an average ^{238}U concentration of 0.91ppm.

Since the stalagmite was found within an archaeological context, it was decided to explore the possibility that it was removed anthropogenically. For this reason, multiple subsamples were taken from the very top of the stalagmite which corresponds to the terminal growth phase. The suggestion was that refining the ages for the last growth phase might have provided some insight into the interval when the stalagmite could have been removed by MSA people.

Sample preparation for stable C and O isotope analysis

For KDS, the same protocol described previously for the Bloukrantz Cave samples was used. In KDS thirty subsamples, weighing between 30 and 80µg each, were drilled and collected with an additional 29 points sampled for the Hendy Test at stratigraphic layers at 23 and 36mm from the top.

4.2.6 KDC5 (Fig. 4.6)

Sample macromorphology

The KDC 5 samples has a typical stalagmite shape with a rounded top, wide

diameter and stacked growth layers which are clearly defined. It has a height of 230 mm and a width of 98.5 mm at its widest part. In KDC 5 there is a sharp colour contrast in the growth layers along the vertical length of the sample which could suggest deposition under changing environmental conditions as there appears to be varying inputs of humics and organics presumably from plant organic material (Ford & Williams 2007). These growth layers alternate between white (10YR 8/1), cream (10YR 8/3), medium brown (7.5YR 5/6) and dark brown (7.5YR 3/4) with the darker coloured layers occurring more frequently in the bottom half of KDC 5 where they dominate in the bottom right section at the base (Fig. 3.6). The stalagmite appears to be composed exclusively of calcite and no visible hiatuses or signs of recrystallisation were observed. In addition, no changes were identified in the position of the vertical growth axis which is suggestive of deposition from a fairly stable dripwater source.

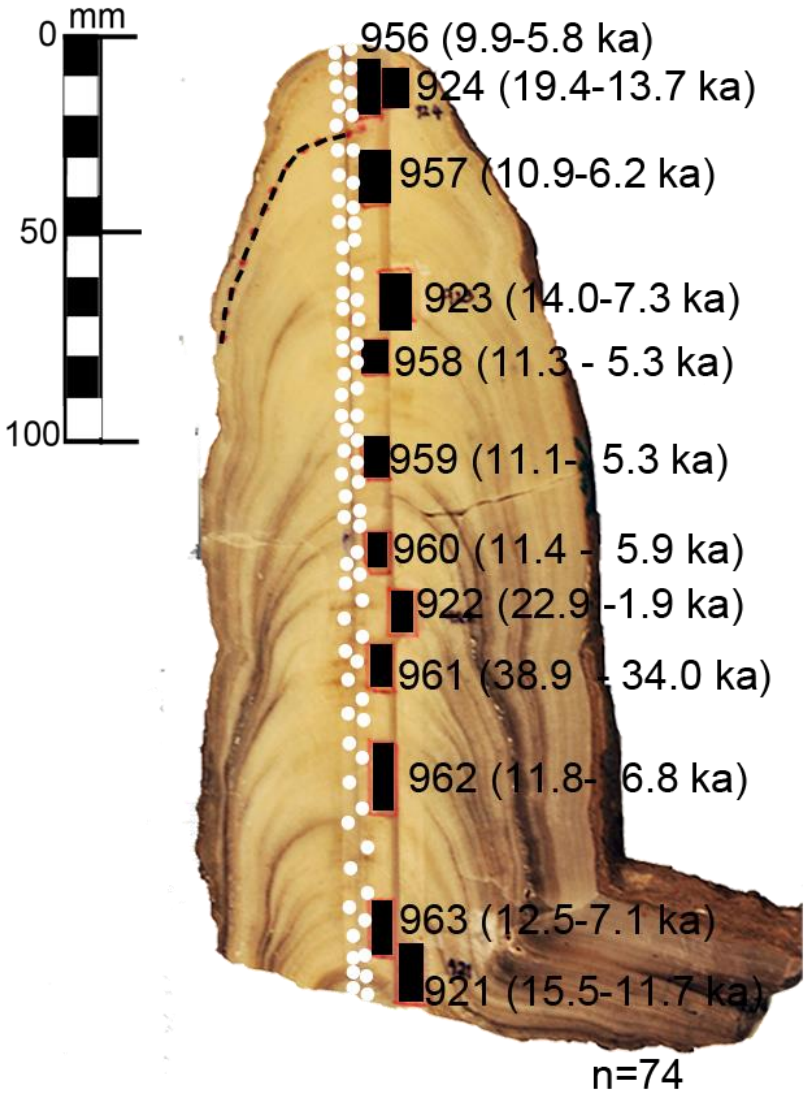

Fig. 4.6 A polished section of KDC5 showing the visible growth laminae, the position of U-Th dating sample locations and Hendy Test sampled laminae. The positions of micromilled subsamples taken for stable isotope analyses are also shown

Sample preparation for U-series dating by $^{234}U/^{230}Th$

Here the same protocol described previously for the samples from Bloukrantz Cave and Klipdrift Shelter was used with four subsamples with a mean weight of 0.23g and an average thickness of 13.0mm initially removed fromthe vertical lengthof KDC5. Eight additional subsamples were

subsequently taken to improve the precision of the age determinations obtained during the initial run on the Element 2. These sample aliquots, with an average weight of *c.* 0.60g and a mean thickness of 14.1mm were sampled along the length of the stalagmite. Overall, twelve subsamples with an average ^{238}U concentration of 1.29ppm were obtained and analysed on the Element 2.

Sample preparation for stable C and O isotope analysis

Using the same protocol described previously for the Bloukrantz Cave samples (BL1, BL2, BL3 & BL4) and Klipdrift Shelter sample (KDS), seventy-three subsamplesweighingbetween 40 and 75µg each, were drilled out. An additional 10 points were sampled for the Hendy Test and these were taken from a single stratigraphic layer at 22 mm from the top.

Chapter 5 – RESULTS

5.1 Introduction

This chapter focuses on the individual results obtained for each of the stalagmites analysed in this study, BL1, BL3, BL4, KDS and KDC5. One exception is the BL2 stalagmite sample from Bloukrantz Cave. There were inherent problems in establishing a sound chronology for BL2 and for this particular sample the individual results are instead presented in an Appendix at the end of this thesis. In the current chapter the data are presented across three main sections for each sample. The first section presents the ICPMS dating results of which the analytical methods were discussed in the previous chapter (Chapter 4). Here the ICPMS results are presented in section 5.2 where the individual uranium and thorium activity ratios and corresponding age determinations are discussed. The data are presented in sections 5.2.1, 5.2.2, 5.2.3, 5.2.4 and 5.2.5 for BL1, BL3, BL4, KDS and KDC 5, respectively. In section 5.2 the age models that were applied to each of the isotope measurements is also discussed. The basis for the modelling approach is two-fold. The intention is firstly to stratigraphically constrain the isotope proxy data and secondly to establish an absolute chronology for each of the stalagmite isotope records. This chronological framework helps to ensure that the proxy data obtained from the speleothem samples is directly comparable with other terrestrial proxy records.

The corresponding stable carbon and oxygen isotope proxy data are detailed in the second section of this chapter across sections 5.3.1, 5.3.2, 5.3.3, 5.3.4 and 5.3.5. Thirdly, the discussion shifts to the dripwater data (section 5.4.1) and resultant temperature reconstructions (section 5.4.2) derived from modern dripwaters sampled from West Cave and Klipdrift Sea Cave (section 5.4). The Holocene samples, part of BL3, and KDC5, were included as it provides an opportunity to compare the Holocene vegetation and rainfall conditions with interstadial conditions as reflected in

the speleothems that cover MIS 3 (part of BL1, and BL3 and BL4). Furthermore, modern drip water from West Cave and Klipdrift Sea Cave are analysed to reconstruct temperatures. This is compared to actual temperatures from the nearby weather station. A summary of the data are provided at the end of the chapter (section 5.5).

5.2 ICPMS U-Th Ages

As discussed in the previous chapter sandstone and calcrete limestone deposits are ubiquitous within the De Hoop study site. In these types of deposits dissolved uranium can be precipitated by adsorption onto sediments and precipitated under reducing conditions. Under reducing conditions oxidised U(VI) is precipitated from solution to insoluble U(IV)) by reducing agents such as detrital plant debris and marine algae (Langmuir 1978; Cuney 2009).

Under closed system conditions $^{234}U/^{238}U$ activity ratios are invariant. In natural settings however this is not always the case. This is because rock-water interactions (weathering) frequently produce variable activity ratio values (Osmond & Cowart, 1976; Ivanovich & Harmon, 1982). During the process of weathering ^{234}U is preferentially lost from the parent rock and mobilised in groundwaters (Kronfield & Adams 1974; Lundberg 1990; Whitehead *et al.* 1999). As a result excess 234U is introduced into groundwaters while the ^{238}U radionuclide is retained in the host rock (Cherdyntsev 1971; Osmond & Cowart 1976). Although weathering is a major source of uranium nuclide variability other processes have also been identified. Key amongst these are alpha (α) recoil (Rosholt *et al*. 1963; Kigoshi 1971; Bonotto & Andrews 2000), low temperature redox changes (Brennecka *et al*. 2010; Petersen 2013), adsorption and desorption (Osmond *et al*. 1983) and soil properties such as pH and redox potential (Osmond & Cowart 1976).

Weathering and leaching effects are widely recognised as the major sources of fractionation in carbonate rocks. Moreover, because fractionation processes alter the distribution and relative abundance of radionuclides it is important to assess their influence on the precision of the $^{230}Th/^{234}U$ ages. For this reason potential leaching effects were determined by comparing the initial $(^{234}U/^{238}U)_0$ and measured activity ratios. This is because the initial activity ratio is thought to reflect the isotopic composition of the groundwater feeding the cave drips at the time each of the speleothems was formed.

In stalagmites uranium leaching can be recognised by a decreasing trend in both the uranium concentrations and the $^{238}U/^{234}U$ activity ratios along the vertical length of a sample. This trend is thought to show the preferential leaching of soluble ^{234}U as it is lost from the source rock over time. On the other hand changes in the percolation path of the water flowing through fissures in the host rock can also produce spurious uranium concentrations (Lundberg 1990; Linge *et al.* 2001, 2009).

5.2.1 BL1 Sample

Uranium concentration and activity ratios

Fifteen U-Th ages were obtained for the BL1 stalagmite and the data are summarised in Table 4.1. Values are given for the uranium concentration and each of the activity ratios of uranium ($^{234}U/^{238}U$, $(^{234}U/^{238}U)_0$), thorium ($^{230}Th/^{232}Th$) and the activity ratio of $^{230}Th/^{234}U$. Changes in the latter ratio form the basis for the dating method used in this study. The stratigraphic position of each of the subsamples is denoted either by T (top), M (middle) or B (base). Errors are 1σ and ages are reported as kyr (thousand years).

In the BL1 stalagmite the uranium concentration is fairly stable with very few deviations (Fig. 4.1). A peak in the uranium concentration of 2.1328 ppm coincides with post-hiatus growth in humic rich layers at 23-33 mm (from the top), corresponding to section dating to 40.8 ± 0.1 ka (Table 5.1). The presence of organic-rich depositional layers coupled with the

relatively high uranium content suggests that the uranium was possibly mobilised by organic matter in the soil above the cave.

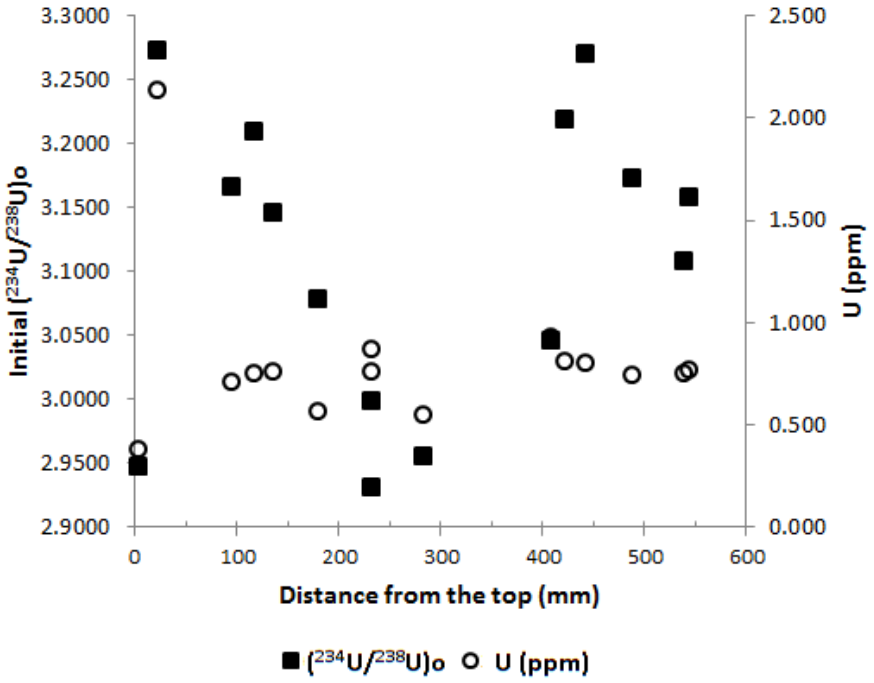

Fig. 5.1 Changes in the initial ($^{234}U/^{238}U$) activity ratio and uranium concentration (in ppm) along the vertical length of BL1

Directly above a depositional layer at 12 mm (from the top) there are light grey (5Y 6/1) crystals suspected to be composed of aragonite. The subsample taken from this section of BL1 dates to 23.0 ± 5.7 ka. To test for the presence of aragonite the intention was to use two methods. The first is Feigl's solution which differentiates between aragonite and calcite by staining aragonite (Friedman 1959) while X-ray diffraction (XRD) assists in identifying the mineral and crystal phases in the sample (Moore & Reynolds 1989). Due to time constraints this task could not be completed.

The presence of aragonite and calcite in the same sample has important implications for interpretations of the dating results and isotopic data. If for example the calcite in BL1 is in fact re-crystallised aragonite then this could indicate uranium mobilisation under non-equilibrium or open system

conditions (Hölzkamper *et al.* 2009). This would in turn reduce the reliability and sensitivity of the $^{230}Th/^{234}U$ age estimates (Lachniet 2012).

Experimental studies and natural observations of calcite-aragonite relationships indicate that aragonite is enriched in ^{18}O and ^{13}C relative to calcite. Average enrichment values of 0.6 ‰ from inorganic aragonite (Tarutani *et al.* 1969) and aragonitic foraminifera (Grossman & Ku 1986) are reported for $\delta^{18}O$ at 25°C. A slightly higher average enrichment value of 1.0‰ is reported for $\delta^{18}O$ at 25°C and comes from aragonitic coral sponges (Böhm *et al.* 2000) and stalagmites from Grotte de Clamouse (Frisia *et al.* 2002). For $\delta^{13}C$ at 25°C aragonite enrichment values of 2.7‰ are reported from Grotte de Clamouse (Frisia *et al.* 2002). This value for $\delta^{13}C$ enrichment has also been reported for inorganic aragonite at temperatures of 10°C, 25°C and 40°C (Romanek *et al.* 1992). In contrast, Zheng (1999) noted that aragonite is depleted relative to calcite with a fractionation factor of 4.5‰ at 25°C.

While the nature of calcite-aragonite interaction is somewhat contentious there is a possibility of an isotope offset. For BL1 this potential isotope offset could complicate the interpretation of the $\delta^{18}O$ and $\delta^{13}C$ data and preclude using them as temperature and vegetation proxies, respectively. For this reason, an acid-fractionation factor of 1.0‰ for aragonite at 75°C is applied to the $\delta^{18}O$ data from the suspected aragonitic layers of the sample (Kim *et al.* 2007; Lachniet *et al.* 2013). For the corresponding $\delta^{13}C$ data a fractionation factor of +1.7‰ is applied (Romanek *et al.* 1992).

With regards to the initial $^{234}U/^{238}U$ activity ratio- denoted as $(^{234}U/^{238}U)_0$ – the values appear to be fairly uniform. These values range between 2.9304 and 3.2721 with an average activity ratio value of 3.1112 (Table 5.1). Based on these observations, it is fair to deduce that the integrity of the uranium system in the BL1 sample has not been altered through preferential leaching of ^{234}U. Moreover ,the data do not indicate any post-depositional changes in the precipitated speleothem carbonate. The observed presence of suspected aragonitic layers and their replacement

by calcite in the sample probably suggests some degree of open system conditions.

Thorium activity ratios

The $^{230}Th/^{234}U$ ratio relates to the proportion of radiogenic thorium (hereafter Th) to uranium (hereafter U). For the major growth phase, represented by layers between 545.5 mm and 97 mm (from the top), which are dated from *c.* 82.6 ka to 69.3 ka, the $^{230}Th/^{234}U$ activity ratio values are between 0.4981 and 0.5851 (Fig. 5.2). These values are significantly higher than those at 24 mm (from the top) with an activity ratio value of 0.3237, that corresponds to the post-hiatus dated at 40.8 ka (Table 4.1). The lowest $^{230}Th/^{234}U$ activity ratio value of 0.1938 comes from the youngest subsample layers between 0 and 9 mm (from the top) that date to around 23 ka (Fig. 5.2 & Table 5.1).

In BL1 the $^{230}Th/^{232}Th$ activity ratio values are between 338 and 11878 with an average of 4597. These activity ratio values collectively exceed the standard baseline of 300 which is typically used to correct U-Th ages measured by ICPMS (see Chapter 3 section 3.3). The $^{230}Th/^{232}Th$ activity ratio is conventionally used to evaluate the contribution of detrital thorium (as initial detrital ^{230}Th & detrital ^{232}Th). Detrital thorium is also known to influence the uranium series age determinations by producing spurious ages that are out of sync with the stratigraphy of the sample. This leads to, for example, ages estimates that are inverted with regards to the sample stratigraphy (*e.g.,* Smart & Frances 1991).

For BL1 the $^{230}Th/^{232}Th$ activity ratios values closer to the base are much higher than those found at the top of the sample. Thorium activity ratio values in the basal layers range between 1473 and 11878 with an average of 5179. In the uppermost layers the $^{230}Th/^{232}Th$ activity ratio value is 338 and correspond to the post-hiatus section which dates to *c.* 40.8 ka. The

combination of high uranium and high ^{232}Th found in this section of BL1 suggests that the post-hiatus growth layers contain excess uranium and thorium. These extra U-Th nuclides were probably introduced by clay minerals. This is because thorium is typically incorporated into speleothem carbonate by adsorption onto clay particles found within the soil above the cave.

The terminal growth section of BL1, corresponding to the layers between 0 and 9 mm (from the top) is dated at *c.* 23.0 ka and has a ^{230}Th/^{232}Th activity ratio value of 1294. The age determinations obtained for the base of the sample are for the most part in stratigraphic order. This means the stalagmite becomes older with increasing distance from the top (Fig. 5.3). Notable exceptions to this occur at three places along the vertical length of the BL1 stalagmite; at 180.5 mm, 285 mm and at 422.5 mm. In these subsampled layers the corresponding ages appear to be marginally older than the subsamples lying either directly above or below it. This apparent discrepancy may be attributed to any number of factors, but not limited to, instrument precision on the day of the sample run and incomplete sample dissolution. This is investigated in more detail in subsequent sections of the chapter.

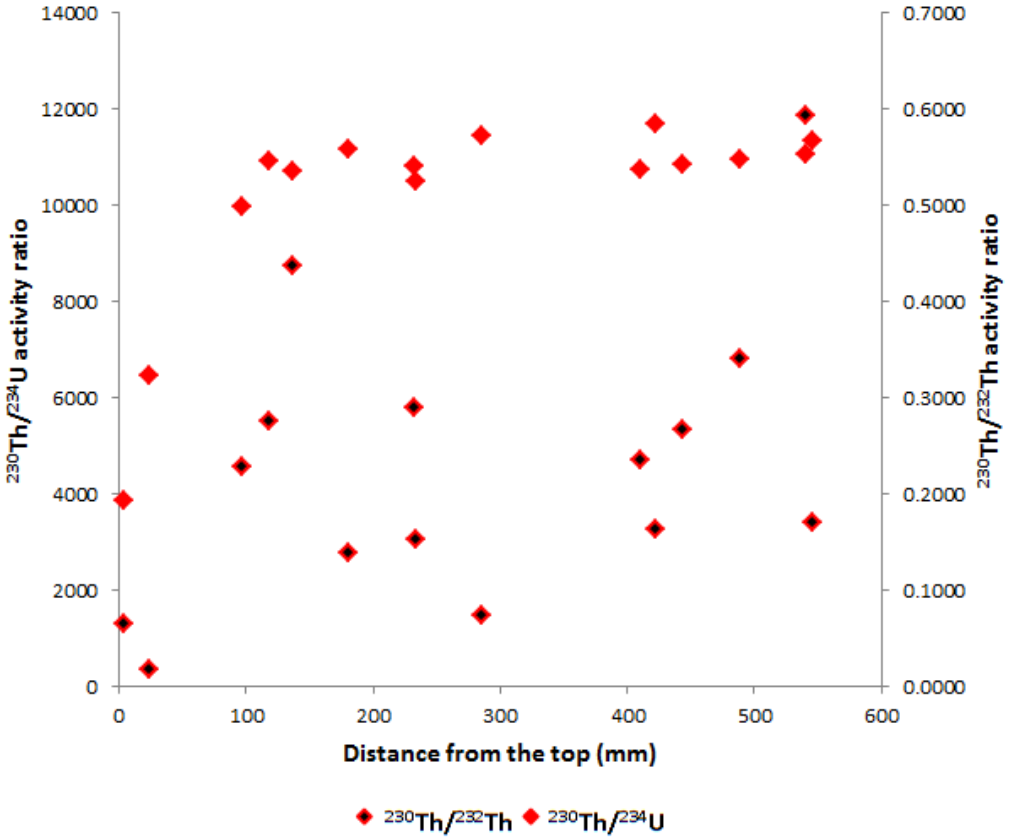

Fig. 5.2 Changes in the $^{230}Th/^{234}U$ and $^{230}Th/^{232}Th$ activity ratios as a function of stratigraphy in the BL1 stalagmite

Twelve of the fifteen dated subsamples taken along the length of BL1 show stratigraphic coherence and have correspondingly high $^{230}Th/^{232}Th$ activity ratios. This applies mainly to the subsamples taken from the section of BL1 that dates from *c.* 82.6 ka to 69.3 ka. Each of the $^{230}Th/^{232}Th$ activity ratio values for these particular subsamples falls within an accepted range for ICPMS because for $^{230}Th/^{232}Th$ ratios ≥ *c.* 50, correction for detrital Th is less than 1σ and is therefore not performed. For values < 50, the corrected age will deviate more than 1σ from the uncorrected"raw" age.)For this reason contamination by detrital thorium is considered negligible. From the geochemical data obtained in the older part of BL1 the effects of leaching and post-depositional alteration are also thought to be negligible. Based on these inferences the raw ages are not

corrected to account for a possible contribution from allogenic thorium (See Chapter 3 for details).

On the other hand, in the post-hiatus layers which date to *c.* 40.8 ka there is an organic rich layer at 23 mm (from the top). The presence of organics suggests that this layer may contain humic-rich (detritus) materials. Thorium is easily adsorped onto clay minerals and in this stratigraphic layer significant amounts of excess uranium and ^{232}Th may have been introduced into the sample. As a result the age estimates for the post-hiatus layers could be compromised.

Nevertheless, the age estimates for the older part of BL1 are assumed to be accurate and reliable (Fig. 5.3). An age model was generated for the growth history of the BL1 stalagmite using the StalAge algorithm. Details about the age model, its assumptions and its application to the BL1 data are presented below.

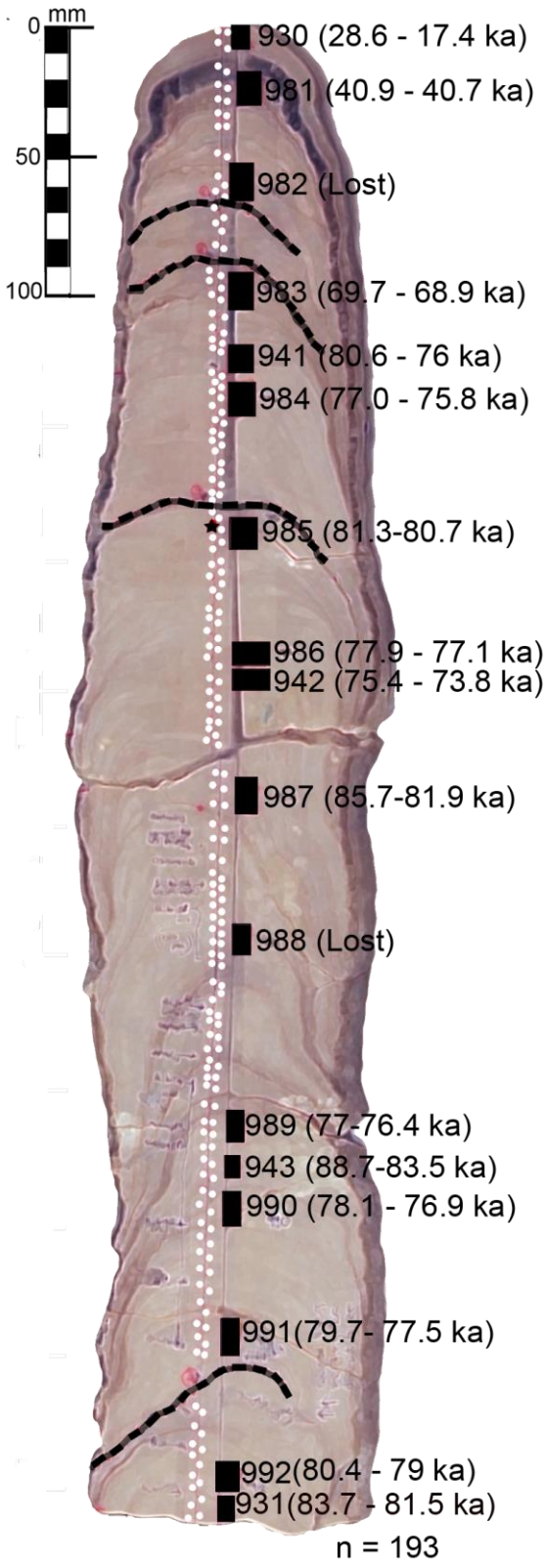

Fig. 5.3 Stratigraphic position for each of the uranium series age determinations obtained for the BL1 sample from Bloukrantz Cave. The associated U-Th lab journal numbers are also shown. Uranium-series dated intervals are presented in

ka and missing values are denoted as *Lost*. Individual isotope subsamples taken along the vertical length of the sample are shown as white dots (●). Black stars (★) represent those isotope points that were either lost or too small for measurement. The Hendy test traverses are represented by solid dark lines (-).

Age models

The StalAge algorithm discussed in the previous chapter (Chapter 3 section 3.3.7) was used to model the growth of the BL1 stalagmite. The data used to produce this age model is highlighted in Table 5.1 and the final age model is presented in Fig. 5.4 below:

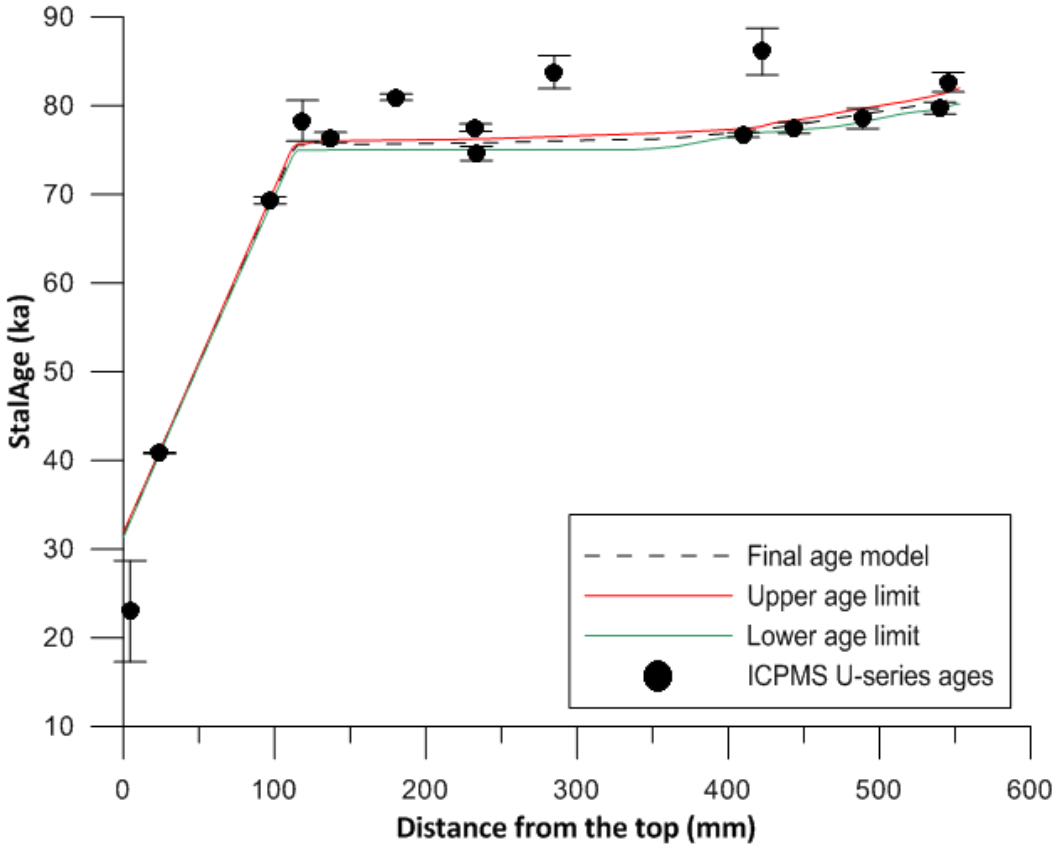

Fig. 5.4 The age model obtained for the BL1 sample from Bloukrantz Cave showing the final age model (dashed black line). Corresponding 95% confidence limits for the StalAge model are denoted by age upper limit (solid red line) and age lower limit (solid green line). The U-series ages measured by ICPMS are also shown (black dots) along with the corresponding 2σ errors.

In the simulated growth interval between 86 ka and 77 ka, four of the original U-Th age determinations were not included in the final model

(Table 5.1). These apparent outliers were discarded as they may have been compromised by instrument stability issues that were experienced on separate occasions during the analytical runs. The original dataset of U-Th ages does not however contain any significant age inversions. From the StalAge model simulations and the corresponding U-Th ages the BL1 stalagmite is thought to have grown fast between 82 ka and 76 ka and slower between 76 ka and 74 ka (Fig. 4.4). Based on the ages it appears that most of BL1, from 100 mm to 400 mm, was deposited within a very short interval of only a few hundred years (Fig. 4.4). While this is quite interesting, it is also rather unusual because stalagmites are typically slow growing and fast growing forms generally have a messy stratigraphy and tend to have a characteristic broomstick or spindly shape. BL1 does not have any of these features in its structure. It is quite possible that BL1 could have been deposited from a highly alkaline solution, which would to some extent explain its remarkable fast growth in such a short period of time. However, this could not be tested since Bloukrantz Cave is inactive and there are no actively dripping stalactites. Thus, it was not possible to test the pH of the dripwater in the cave. Further work on the luminescence characteristics of the BL1 growth layers, such as those conducted on fast growing stalagmites in Britain and Scandinavia, could provide insight into the growth history of BL1 (Baker *et al.* 1993, 2008; Sundqvist *et al*. 2005).

In the age model, the assumed trend of slower growth continued from 74 ka until 69 ka when growth stopped completely. From its onset at 69 ka the presumed hiatus persisted until *c.* 41 ka. Growth may have resumed slowly between *c.* 41 ka and *c.* 23 ka but it is difficult to determine this with any certainty. This is because there is no data for the interval either directly above the subsample at *c.* 41 ka or below the subsample at *c.* 23 ka. The subsample dated to *c.* 41 ka is also thought to be compromised by extra U and Th. Since this data point was retained when generating the age model the width of the corresponding confidence limits were increased accordingly. As a result there is greater uncertainty for the simulated post-

hiatus growth around *c.* 41 ka. By *c.* 23 ka the BL1 stalagmite stopped growing completely.

The simulated growth history of BL1 during the period from *c.* 82 ka to *c.* 23 ka was also used to anchor the stable isotope proxy data. The stable carbon and oxygen isotope data are presented in section 5.3 of this chapter.

Table 5.1 Results from ICPMS U-Th analyses of the BL1 stalagmite from Bloukrantz Cave

J. No.	Level	Centre position (mm)	mm interval	^{238}U (ppm)	$^{230}Th/^{234}U$		σ	$^{234}U/^{238}U$		σ	$^{230}Th/^{232}Th$		σ	$(^{234}U/^{238}U)_0$		σ	kyr		+σ		-σ
930	T	4.5	0-9	0.3732	0.1938	±	0.044	2.8246	±	0.070	1294	±	292	2.9471	±	0.073	23.0	+	5.8	-	5.6
981	T	24	18-30	2.1328	0.3237	±	0.005	3.0244	±	0.017	338	±	38	3.2721	±	0.018	40.8	+	0.1	-	0.1
983	M	97	89-105	0.7020	0.4981	±	0.002	2.7803	±	0.007	4556	±	29.1	3.1657	±	0.008	69.3	+	0.4	-	0.4
941	M	118.5	115-122	0.7456	0.5461	±	0.012	2.7703	±	0.024	5519	±	111	3.2088	±	0.028	78.3	+	2.3	-	2.3
984	M	137	130-144	0.7521	0.5359	±	0.003	2.7278	±	0.007	8729	±	62.6	3.1444	±	0.008	76.4	+	0.6	-	0.6
985	M	180.5	175-186	0.5615	0.5588	±	0.002	2.6524	±	0.005	2776	±	19.6	3.0773	±	0.006	81.0	+	0.3	-	0.3
986	M	233	228-238	0.7585	0.5404	±	0.002	2.5505	±	0.006	5799	±	34.0	2.9304	±	0.006	77.5	+	0.4	-	0.4
942	M	233.5	230-237	0.8636	0.5257	±	0.004	2.6178	±	0.010	3056	±	30.8	2.9977	±	0.012	74.6	+	0.8	-	0.8
987	M	285	279-291	0.5437	0.5721	±	0.009	2.5426	±	0.020	1473	±	39.0	2.9549	±	0.023	83.8	+	1.9	-	1.8
989	B	410	405-415	0.9224	0.5369	±	0.001	2.6468	±	0.005	4712	±	28.4	3.0456	±	0.006	76.7	+	0.3	-	0.3
943	B	422.5	420-425	0.8095	0.5851	±	0.013	2.7392	±	0.022	3269	±	69.0	3.2185	±	0.025	86.1	+	2.6	-	2.6
990	B	443.5	438-449	0.7941	0.5423	±	0.003	2.8225	±	0.010	5350	±	52.6	3.2688	±	0.011	77.5	+	0.6	-	0.6
991	B	489	483-495	0.7394	0.5471	±	0.006	2.7394	±	0.010	6817	±	82.3	3.1718	±	0.012	78.6	+	1.1	-	1.1
992	B	540	535-545	0.7434	0.5528	±	0.003	2.6820	±	0.008	11878	±	83.1	3.1072	±	0.009	79.7	+	0.7	-	0.7
931	B	545.5	541-550	0.7632	0.5677	±	0.005	2.7080	±	0.014	3402	±	39	3.1574	±	0.016	82.6	+	1.1	-	1.1

5.2.2 BL3 Sample

Uranium concentration and activity ratios

Thirteen U-Th ages were obtained for the BL3 stalagmite and the data are summarised in Table 4.2. Values are given for the uranium concentration and each of the activity ratios of uranium ($^{234}U/^{238}U$, $(^{234}U/^{238}U)_0$), thorium ($^{230}Th/^{232}Th$) and the activity ratio of $^{230}Th/^{234}U$. The stratigraphic position of each of the subsamples is denoted either by T (top), M (middle) or B (base). Errors are 1σ and ages are reported as kyr (thousand years).

In BL3 the uranium concentration is quite variable throughout the vertical length of the sample. The lowest uranium content, between 0.0728 and 0.3082 ppm, is found in the oldest part of the stalagmite corresponding to the layers from 187 to 417 mm (from the top). This older part of BL3 is represented by a smaller stalagmite occurring within the larger form of the sample. This stalagmite- within- a- stalagmite is dated to between *c.* 45.2 ka and *c.* 47.9 ka. Taken as a whole there appears to be a trend of decreasing uranium content along the length of BL3 and this is illustrated in Fig. 5.5.

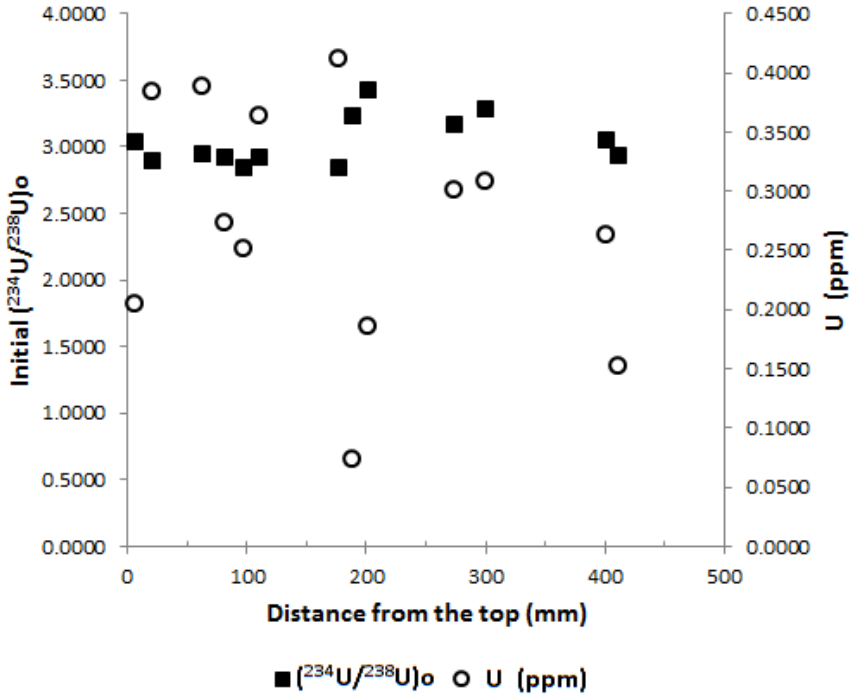

Fig. 5.5 Changes in the initial ($^{234}U/^{238}U$) activity ratio and uranium concentration (in ppm) along the length of BL3

For BL3 the initial ($^{234}U/^{238}U$) activity ratio values are fairly stable and occur within a tight range from 2.8400 to 3.4231 with an average of 3.0342 which is comparable with those of BL1. Post-depositional changes and preferential leaching of ^{234}U from the host rock is therefore not inferred from the pattern in the initial ($^{234}U/^{238}U$) activity ratio values.

Thorium activity ratios

The oldest part of BL3 represents the main growth phase of this sample. Here the $^{230}Th/^{234}U$ activity ratio values are fairly uniform with minor deviations during the period from *c.* 45.2 ka to 47.9 ka, which is represented by the growth layers between 182 and 417 mm (from the top) (Table 4.2 & Fig. 4.6). This region represents the main growth phase in BL3. In the post-hiatus section of BL3, starting at around 97.5 mm (from the top) the $^{230}Th/^{234}U$ activity ratio values are lower than those observed for the main growth phase.

In this post-hiatus section, represented by layers from 97.5 to 7.5 mm (from the top), the $^{230}Th/^{234}U$ activity ratio values range between 0.0188 and 0.0578. This is unusual because the basic tenet of the $^{230}Th/^{234}U$ dating method is that ^{230}Th accumulates in a sample because of radioactive decay of ^{234}U. It is therefore reasonable to expect that younger layers will have lower $^{230}Th/^{234}U$ activity ratio values compared to older ones. Sometimes discrepancies arise when excess uranium and thorium are introduced into a sample. This can occur during or after carbonate deposition. For this reason it is suspected additional uranium and possibly thorium may have been incorporated into the speleothem fabric when the younger, post-hiatus layers were formed. This was confirmed by looking at the corresponding $^{230}Th/^{232}Th$ activity ratio.

From the $^{230}Th/^{232}Th$ it is possible to determine the extent to which the ages are compromised by the addition of detrital thorium. In BL3 the $^{230}Th/^{232}Th$ activity ratios range between 72 and 10738 (Table 5.2). Three subsamples from the post-hiatus section have activity ratio values that fall below the standard baseline of 300. This baseline value is conventionally used to correct ICPMS U-Th age determinations. Activity ratio values for the post-hiatus section of BL3 show a general pattern of low $^{230}Th/^{232}Th$ activity ratio values and high uranium concentrations (Table 5.2). This suggests that both detrital Th and U were likely introduced into the post-hiatus section. Organic matter and humic acids are thought to be the primary sources of excess U and Th in this particular sample. This is because the growth layers representing post-hiatus growth consist of finely laminated calcite with discoloured bands in shades of cream (10YR 8/2), pale brown (5YR 5/2) and white (10YR 8/1) (Fig. 5.7). The discolourations are attributed to the presence of some sort of organic material in the calcite. Overall, the subsample area representing post-hiatus growth in BL3 is thought to be significantly compromised by the addition of extra U and Th nuclides.

The BL3 stalagmite is thought to have stopped growing with the onset of a hiatus(es) which lasted (presumably) until the Holocene. There are however problems with several age determinations occurring in this part of the sample. The ages for the layers at 7 mm and 22.5 mm (from the top) are too large and produce negative age estimates (Table 5.2). These negative ages result in negative growth rates and this is nonsensical. These ages were therefore discarded. The ages for the post-hiatus section of the sample are also for the most part out of stratigraphic order and imprecise when compared to the rest of BL3 (Fig. 5.7). As a result the post-hiatus ages do not appear to reflect the true age of post-hiatus growth in BL3.

The $^{230}Th/^{232}Th$ activity ratio values representing the older section of BL3 range between 1303 and 10738. All the dated layers in this part of BL3 are well above the baseline value of 300. These values are also higher than the activity ratio values obtained for the post-hiatus part of BL3. The high $^{230}Th/^{232}Th$ activity ratio values suggest a minor contribution from detrital thorium in these particular subsamples. Furthermore, the corresponding uranium series ages all overlap within error intervals and are in stratigraphic order with increasing age towards the base (Table 5.2 & Fig. 5.6).

It is as yet unclear what factors are responsible for the lower uranium content observed in the subsamples from the basal part of BL3. Analytical problems with stabilising the Element 2 and incomplete sample dissolution during chemical preparation could in part explain the lower U concentrations. These factors do not however fully explain the pattern of low U concentrations and correspondingly high $^{230}Th/^{232}Th$ activity ratio values. Overall the age estimates for the older section of BL3 are thought to be reliable. This is based on the high $^{230}Th/^{232}Th$ activity ratio values and the stratigraphic coherence of the uranium series ages.

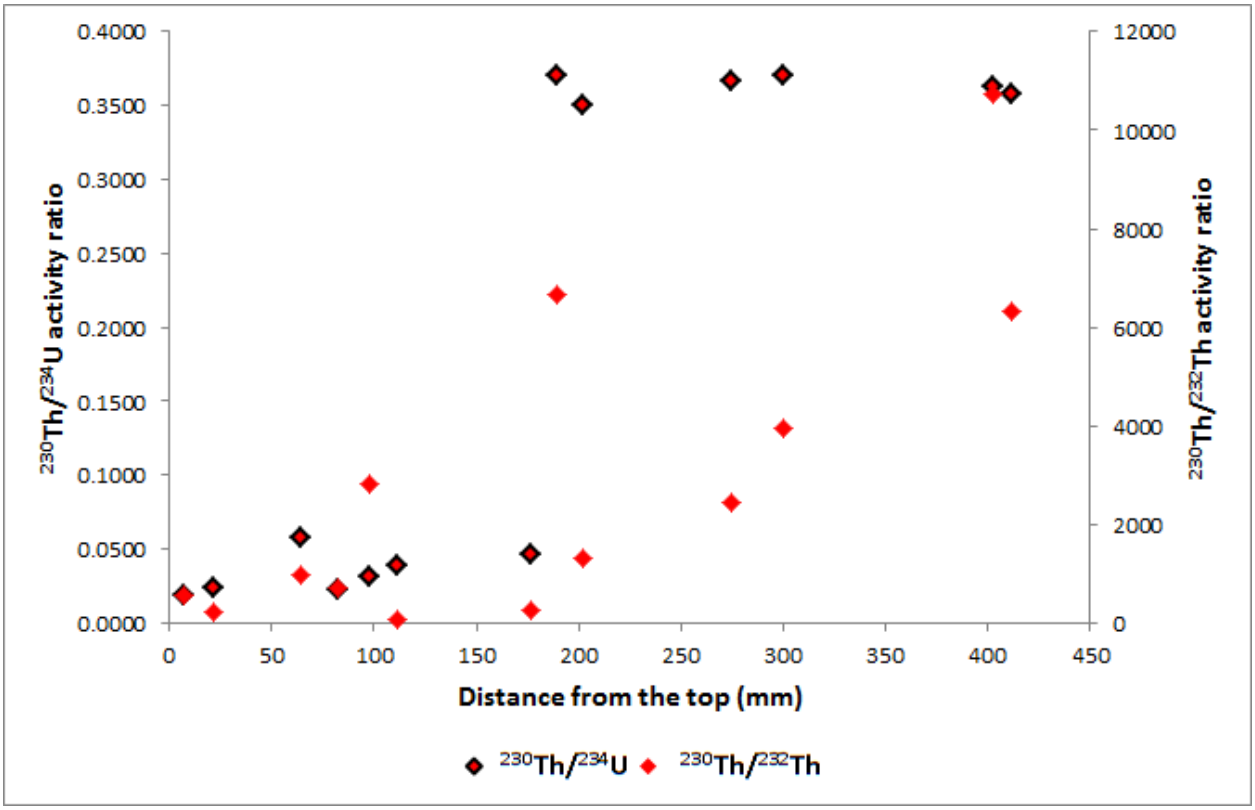

Fig. 5.6 Changes in the $^{230}Th/^{234}U$ and $^{230}Th/^{232}Th$ activity ratios along the length of BL3

An age model was simulated for the growth history of BL3 using the StalAge algorithm. The model was applied in the same manner described for BL1. The data used to generate the age model is highlighted in Table 5.2 and the resultant model is presented in the subsection below.

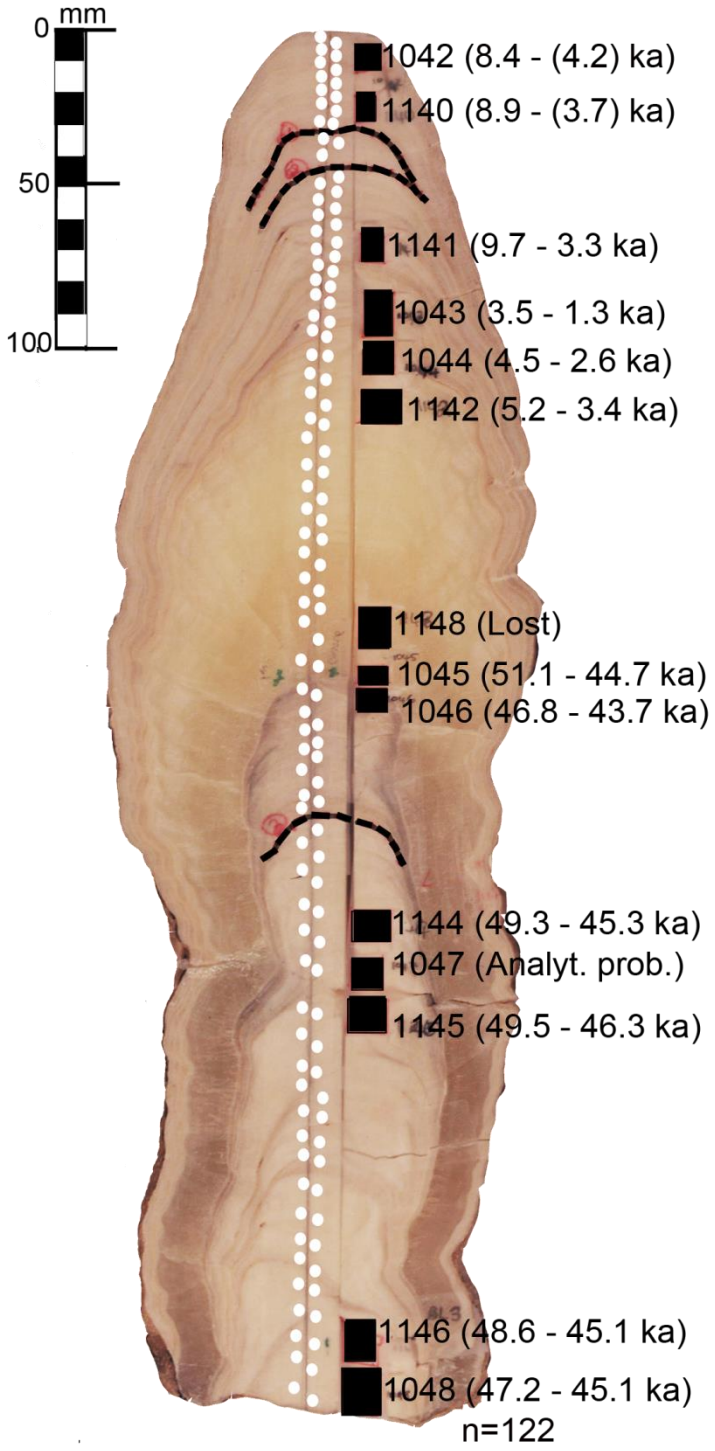

Fig. 5.7 Stratigraphic position of each of the uranium series age determinations obtained for the BL3 sample from Bloukrantz Cave. The associated U-Th lab journal numbers are also shown. Uranium-series dated intervals are presented in *ka* and missing values are denoted as *Lost*. Individual isotope subsamples taken along the vertical length of the sample are shown as white dots (●).The Hendy test traverses are represented by solid dark lines (-).

Age models

Using the same procedure for the BL1 stalagmite an age model was produced for the BL3 sample and is shown in Fig. 5.8 below. The data used to produce the age model for this sample is highlighted in Table 5.2. The ICPMS age determinations obtained for BL3, for the most part, fall within the 95% confidence intervals of the age model. Those age determinations that fall outside of these confidence limits were recognised as outliers. Three outliers occur at the very top of the stalagmite and are found in the growth layers at 64 mm, 21 mm and 7 mm from the top.

BL3 is thought to have grown fast from *c.* 47.9 ka to *c.* 46.0 ka and slower between *c.* 46.0 ka to 45.2 ka when growth stopped completely. The onset of a major hiatus, or possibly several hiatuses, *c.* 45.2 ka lasted until *c.* 5.1 ka when growth presumably resumed. Post-hiatus growth is thought to have been fast between 4.3 and 2.4 ka which correspond to the growth layers between 111 mm and 82 mm. The StalAge algorithm predictably identified the subsample at 64 mm which dates to *c.* 6.4 ka as an outlier. Since this data point was retained when generating the age model the width of the corresponding confidence limits were increased. As a result there is greater uncertainty for the simulated growth region dated to *c.* 6.4 ka.

As expected there is also greater uncertainty for the uppermost section of BL3. This section is represented by layers located between 21 mm and 7 mm and dated between *c.* 2.6 ka and 2.1 ka. Although these earlier ages are very similar and quite precise, the large error margins suggest that these ages could be doubtful. As for many of the ages corresponding to the entire post-hiatus section of BL3 where there are large errors when compared to the other subsamples obtained for the stalagmite. As mentioned in the preceding section, excess U and Th were likely introduced into these post-hiatus growth layers and this compromised the integrity of the resultant ages. Since there are issues concerning the reliability of these ages the dates for the upper part of BL3 are not very

informative. As a result it is not clear when growth resumed following the onset of a hiatus at *c.* 45.2 ka. Further investigation of the post-hiatus samples, perhaps with duplicate dating subsamples, could help refine the age model for the earlier part of BL3. However, based on the presently available data and the current uncertainty regarding the post-hiatus growth in BL3 the StalAge model could not be used to anchor the corresponding stable isotope proxy data. The isotope data representing the post-hiatus is therefore not considered further. Only the isotope data for the older part of BL3 was retained for further analysis and is presented in section 4.3 of this chapter.

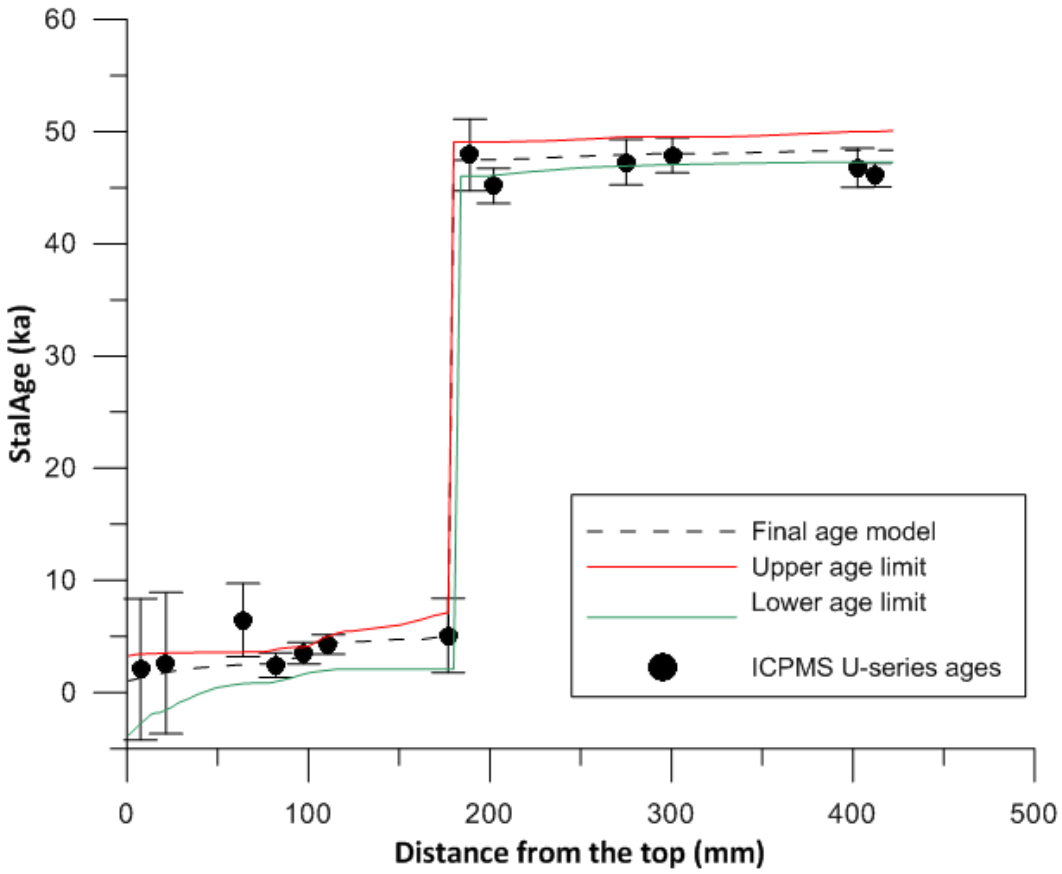

Fig. 5.8 The age model obtained for the BL3 sample from Bloukrantz Cave showing the final age model (dashed black line). Corresponding 95% confidence limits for the StalAge model are denoted by age upper limit (solid red line) and age lower limit (solid green line). The U-series ages measured by ICPMS are also shown (black dots) along with the corresponding 2σ errors.

Table 5.2 Results from ICPMS U-Th analyses of the BL3 stalagmite from Bloukrantz Cave

J. No.	Level	Centre position (mm)	mm interval	^{238}U (ppm)	$^{230}Th/^{234}U$		σ	$^{234}U/^{238}U$		σ	$^{230}Th/^{232}Th$		σ	$(^{234}U/^{238}U)_0$		σ	kyr		+σ		-σ
1042	T	7.5	4-11	0.2045	0.0188	±	0.057	3.0189	±	0.057	548	±	54	3.0308	±	0.057	2.07	+	6.4	-	6.2
1140	M	21.5	17-26	0.3833	0.0239	±	0.056	2.8762	±	0.039	243	±	577	2.8902	±	0.039	2.63	+	6.4	-	6.1
1141	M	64	60-68	0.3884	0.0578	±	0.029	2.9069	±	0.058	979	±	483	2.9421	±	0.059	6.46	+	3.3	-	3.2
1043	M	82	77-87	0.2731	0.0222	±	0.010	2.9001	±	0.015	703	±	311	2.9139	±	0.015	2.44	+	1.1	-	1.1
1044	M	97.5	93-102	0.2503	0.0318	±	0.008	2.8218	±	0.016	2831	±	755.7	2.8400	±	0.016	3.51	+	1.0	-	0.9
1142	M	111	107-115	0.3631	0.0388	±	0.008	2.8858	±	0.020	72	±	14	2.9089	±	0.020	4.30	+	0.9	-	0.9
1143	M	177	172-182	0.4107	0.0458	±	0.029	2.8164	±	0.014	244	±	156	2.8428	±	0.014	5.10	+	3.4	-	3.3
1045	M	189	182-196	0.0728	0.3706	±	0.021	2.9444	±	0.067	6647	±	336	3.2265	±	0.074	47.9	+	3.2	-	3.2
1046	M	202	199-205	0.1849	0.3502	±	0.010	3.1327	±	0.059	1303	±	29.0	3.4231	±	0.064	45.2	+	1.6	-	1.5
1144	B	275	270-280	0.3008	0.3663	±	0.013	2.8968	±	0.044	2455	±	80.5	3.1679	±	0.048	47.3	+	2.0	-	2.0
1145	B	300.5	296-305	0.3082	0.3706	±	0.010	2.9856	±	0.041	3936	±	96.2	3.2734	±	0.045	47.9	+	1.6	-	1.6
1146	B	402.5	398-407	0.2630	0.3628	±	0.011	2.7969	±	0.040	10738	±	300.9	3.0509	±	0.044	46.8	+	1.8	-	1.7
1048	B	412	407-417	0.1514	0.3583	±	0.007	2.6981	±	0.034	6319	±	92.4	2.9346	±	0.037	46.1	+	1.1	-	1.0

5.2.3 BL4 Sample

Uranium concentration and activity ratios

Twelve U-Th ages were obtained for the BL4 stalagmite. One subsample (J. No. 1053) was lost during measurement. The data for the remaining eleven ages is summarised in Table 5.4. Values are given for each of the activity ratios of uranium ($^{234}U/^{238}U$, $(^{234}U/^{238}U)_0$), thorium ($^{230}Th/^{232}Th$) and the activity ratio of $^{230}Th/^{234}U$. Changes in the latter ratio form the basis for the dating method used in this study. The stratigraphic position of each of the subsamples is denoted either by T (top), M (middle) or B (base). Errors are 1σ and ages are reported as kyr (thousand years).

The BL4 stalagmite sample is thought to have grown between *c*. 51.8 and *c*. 59.4 ka. The uranium concentration values for this growth period range from 0.1531 ppm to 0.4324 ppm with an average of 0.3139 ppm (Table 5.4). Taken as a whole there is a very weak trend of increasing uranium content along the length of BL4 and this is illustrated in Fig. 5.9. The corresponding initial $^{234}U/^{238}U$ activity ratio (denoted as $(^{234}U/^{238}U)_0$) is fairly consistent with values ranging from 3.1685 to 3.7438. Only minor deviations are noted around the mean activity ratio value of 3.5197 (Table 5.4 & Fig. 5.9). This average initial activity ratio value of 3.5197 is comparable to the $(^{234}U/^{238}U)_0$ values obtained from BL1 and BL3. The apparent similarity in the initial $^{234}U/^{238}U$ activity ratio values for the Bloukrantz Cave samples (*i.e.*, BL1, BL3 & BL4) suggests that the groundwater ($^{234}U/^{238}U$) feeding the cave had a fairly constant $^{234}U/^{238}U$ ratio.

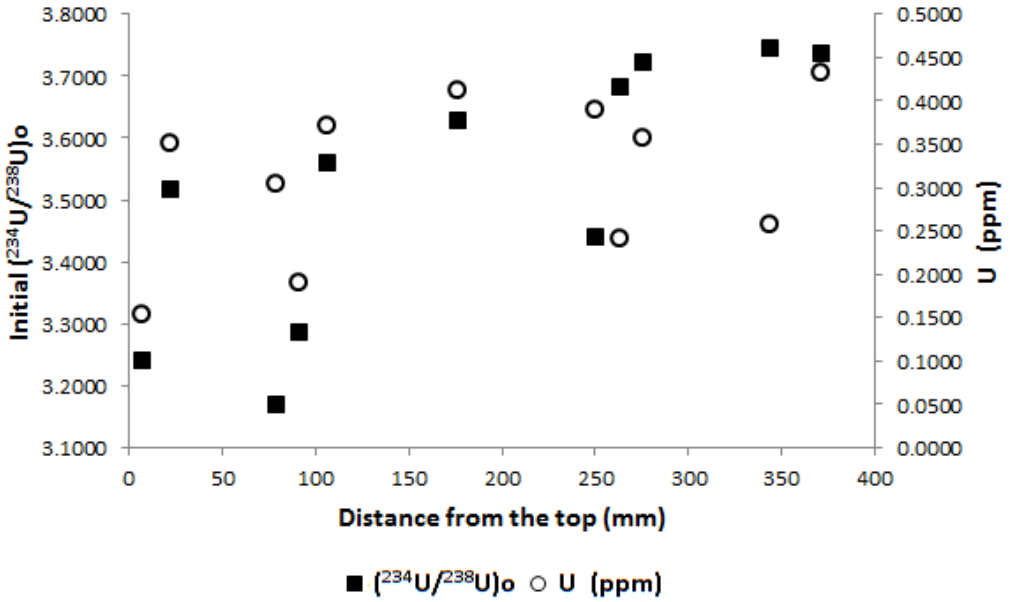

Fig. 5.9 Changes in the initial ($^{234}U/^{238}U$) activity ratio and uranium concentration (in ppm) along the length of BL4

Thorium activity ratios

The $^{230}Th/^{234}U$ activity ratios are fairly constant with an average of 0.4209 and a range from 0.3950 to 0.4426 (Table 5.4 & Fig. 5.10). The corresponding $^{230}Th/^{232}Th$ activity ratio is more variable with values between 236 and 7524 and an average of 2416. The majority of the BL4 subsamples meet the standard baseline of 300 for correcting U-Th age determinations measured by ICPMS. The one exception, located at 7 mm from the top, has a $^{230}Th/^{232}Th$ activity ratio value of 236. This suggests that detrital contamination may be present in this layer (Table 4.4 & Fig. 4.11). Taken as whole, the $^{230}Th/^{232}Th$ activity ratio values are generally higher in the lower part of the sample and occur in layers at 251 mm (from the top) towards the base at 371.5 mm (from the top). Here the stratigraphic layers are clearly banded and (mostly) creamy white (10YR 8/2) in colour (Fig. 5.11). In the upper part of the sample, represented by layers at 176.5 mm to 7 mm (from the top), activity ratio values are comparatively lower and range between 236 and 1804. This upper part of BL4 is characterised by a stratigraphy with growth layers arranged in

stacked bands growing in wavy ripples that alternate in colour between creamy white (10YR 8/2) and light brown (5YR 6/4) (Fig. 5.11).

The corresponding $^{230}Th/^{232}Th$ activity ratio is more variable with values between 236 and 7524 and an average of 2416. The majority of the BL4 subsamples meet the standard baseline of 300 for correcting U-Th age determinations measured by ICPMS. The one exception, located at 7 mm from the top, has a $^{230}Th/^{232}Th$ activity ratio value of 236. This suggests that detrital contamination may be present (Table 5.4 & Fig. 5.11). Taken as whole, the $^{230}Th/^{232}Th$ activity ratio values are generally higher in the basal layers where values ranging between 1078 and 7524 (Fig. 5.10).

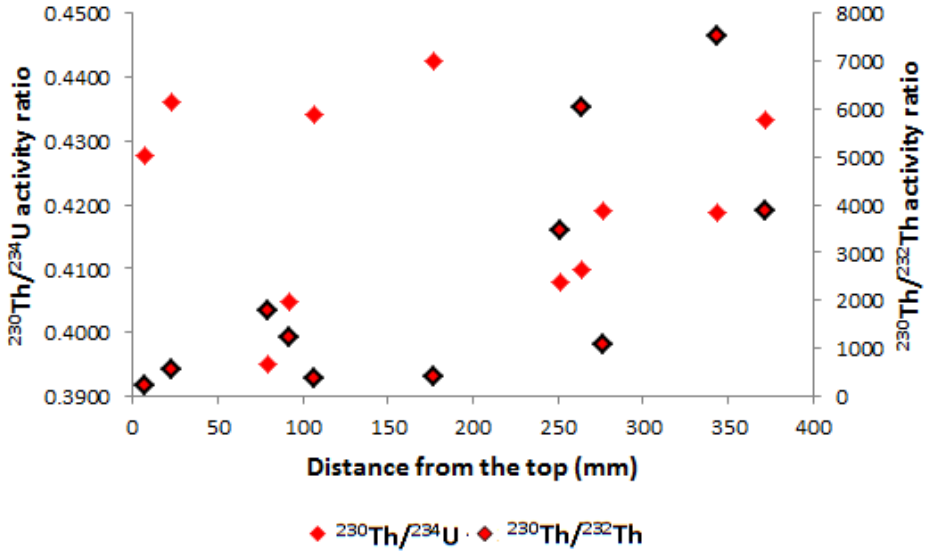

Fig. 5.10 Changes in the $^{230}Th/^{234}U$ and $^{230}Th/^{232}Th$ activity ratios in the BL4 stalagmite

In the upper part of the sample the layers from 176.5 mm (from the top) to 7 mm (from the top) have comparatively lower $^{230}Th/^{232}Th$ activity ratio values. In this part of BL4 the activity ratio values range between 236 and 1804. The layers in upper part of BL4 occur as wavy, ripple-like laminations that are arranged in stacked bands. These layers alternate in colour between creamy white (10YR 8/2) and light brown (5YR 6/4) (Fig. 5.11). Discoloured growth laminations are thought to represent organic

content in the calcite. Some contribution from non-radiogenic (detrital) thorium is therefore inferred from the presence of discoloured layers and relatively lower $^{230}Th/^{232}Th$ activity ratio. The inferred presence of detrital thorium may in part explain the low precision of some of the age estimates (J.o. 1052, 1137, 1150 & 1134) (Table 5.4).

At a whole sample level the uranium series ages do however overlap within error limits of each other. For this reason, corrections were not applied to any of the eleven dated subsamples.

Overall, BL4 is thought to have grown within a period of *c*. 7.6 kyr between *c.* 51.8 ka and *c*. 59.4 ka and an age model was simulated using the StalAge algorithm. The same procedure described for BL1 and BL3 was applied to the data from BL4 and the age model is presented in the subsection below

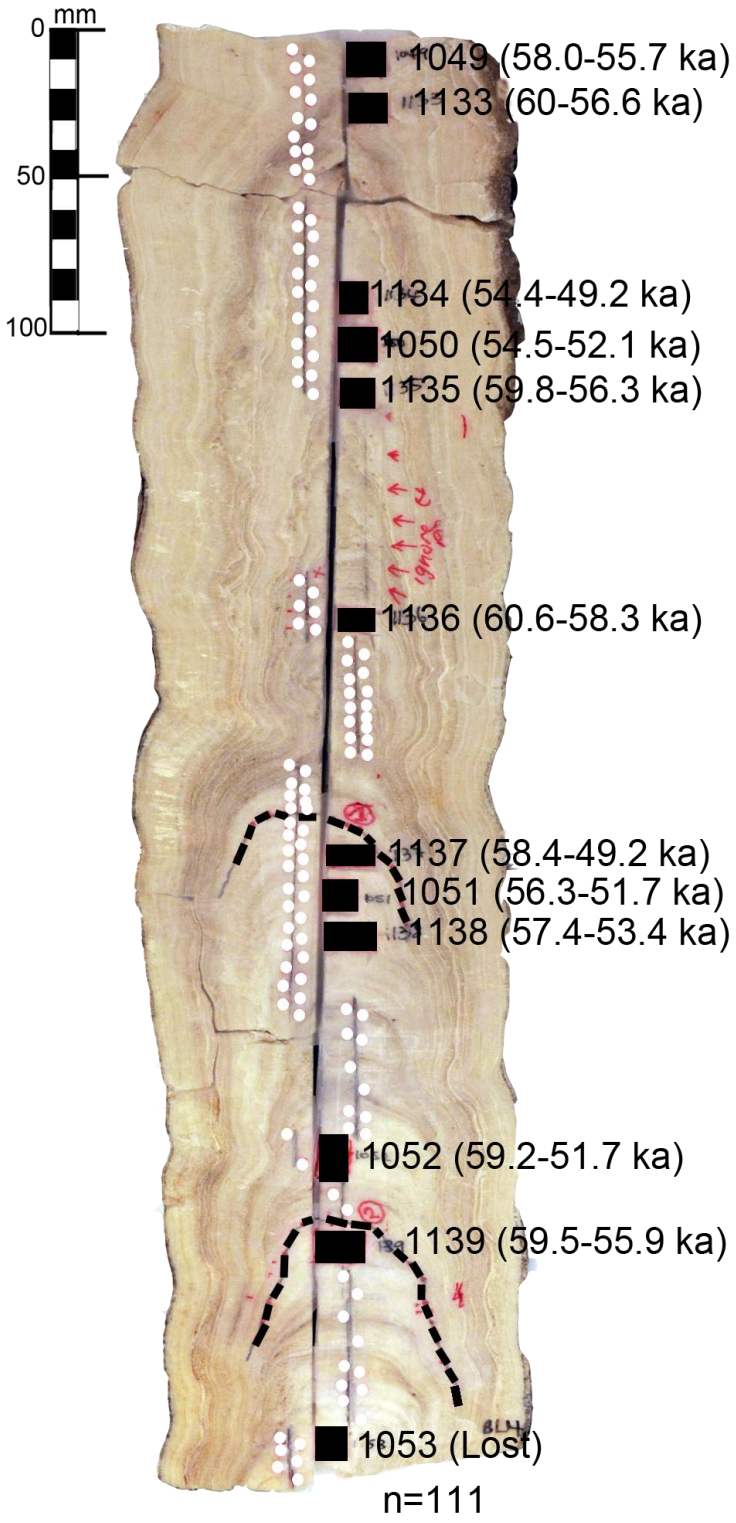

Fig. 5.11 Stratigraphic position of each of the uranium series age determinations obtained for the BL4 sample from Bloukrantz Cave. The associated U-Th lab journal numbers are also shown. Uranium-series dated intervals are presented in ka. Individual isotope subsamples taken along the vertical length of the sample

are shown as black dots (●).The Hendy test traverses are represented by solid dark lines (-).

Age models

Using the same procedure described for the previous samples (*i.e.*, BL1 & BL3) an age model was produced for the BL4 stalagmite and is shown in Fig. 5.12 below. The data used to produce the age model for this sample is highlighted in Table 5.3. Three of the eleven original ICPMS age determinations fall within the 95% confidence intervals of the age model. The remaining eight age determinations fall outside of these confidence limits and StalAge identified four of these as outliers. Two outliers occur closest to the top of the stalagmite and are found in the growth layers at 7 mm and 22.5 mm (from the top). These layers date respectively to 56.0 ± 1.1 ka and 58.3 ± 1.7 ka (Fig. 5.12a). Additional outliers were recognised in layers at 107 mm and 176.5 mm (from the top) which date to 58.0 ± 1.7 ka and 59.4 ± 1.1 ka, respectively (Fig. 5.12a). In the lower half of the stalagmite there are four U-Th ages that fall outside the lower 95% confidence limit of the age model. These ages have poor precision and are found in the growth layers at 251 mm (53.7 ± 4.6 ka), 276 mm (55.4 ± 1.0 ka) and 344 mm (55.4 ± 3.7 ka) (from the top) (Fig. 5.12a). Because of the relatively large uncertainties on these ages the width of the corresponding confidence limits were increased on the age model. Based on this model, it is assumed that BL4 grew continuously between 55 ka and 59 ka. From 55 ka to 52 ka growth is thought to have been slower (Fig. 5.12a).

The age model in Fig. 5.12a was subsequently refined using the dates associated with the section of BL3 from 79.5 mm to 371.5 mm (from the top) and by omitting the dates corresponding to the layers at 107 mm (58 ka) and 176.5 mm (59.4 ka). The refined model, presented in Fig. 4.12b, follows the linear trend in the BL3 ages more closely than the model presented in Fig. 5.12a. This is evident from the five younger dates for the region of BL3 from 77 mm through to 371.5 mm (from the top). These dates cover an interval from 51.8 ka to 57.7 ka (Table 5.3). Overall, this

revised model suggests that BL3 grew continuously between 51.5 ka and 58.5 ka.

The StalAge model of the growth history of BL4 was also used to anchor the stable isotope proxy data for the sample. This stable carbon and oxygen isotope data are presented in section 5.3 of this chapter.

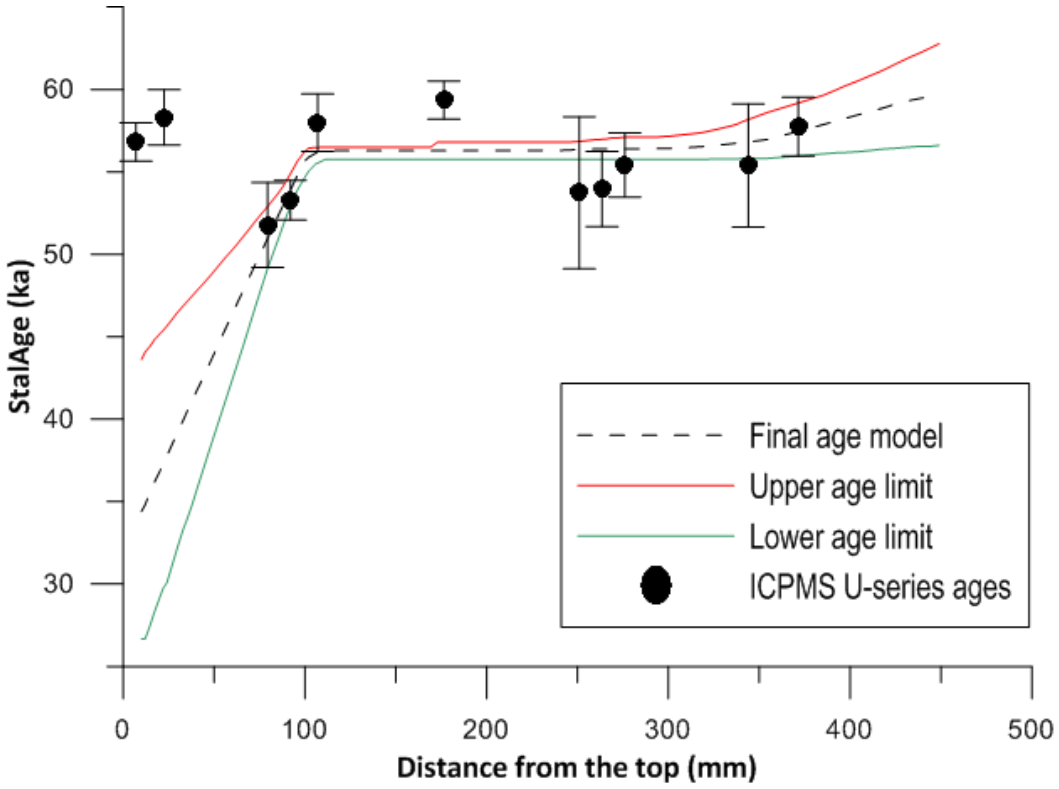

Fig. 5.12a The age model obtained for the BL4 sample from Bloukrantz Cave showing the final age model (dashed black line). Corresponding 95% confidence limits for the StalAge model are denoted by age upper limit (solid red line) and age lower limit (solid green line). The U-series ages measured by ICPMS are also shown (black dots) along with the corresponding 2σ errors.

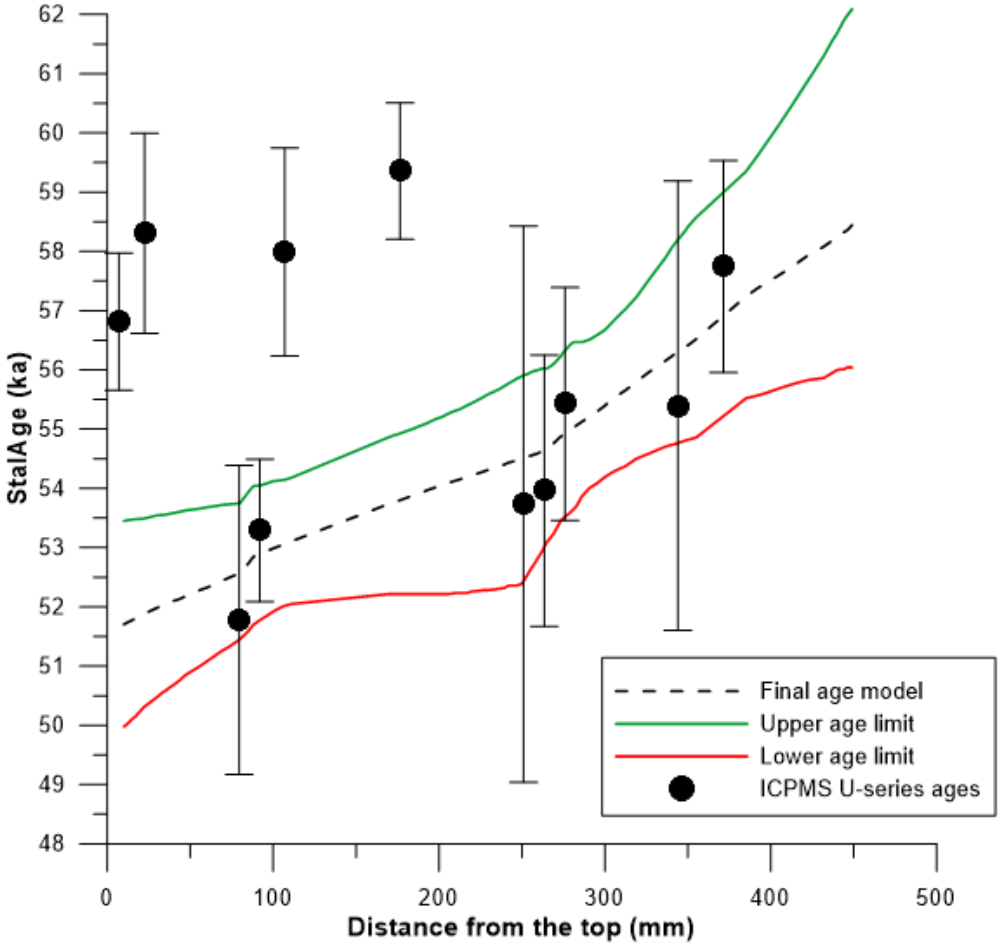

Fig. 5.12b The age model obtained for the BL4 sample from Bloukrantz Cave showing the final age model (dashed black line). Corresponding 95% confidence limits for the StalAge model are denoted by age upper limit (solid red line) and age lower limit (solid green line). The U-series ages measured by ICPMS are also shown (black dots) along with the corresponding 2σ errors.

Table 5.3 Results from ICPMS U-Th analyses of the BL4 stalagmite from Bloukrantz Cave

J. No.	Level	Centre position (mm)	mm interval	^{238}U (ppm)	$^{230}Th/^{234}U$		σ	$^{234}U/^{238}U$		σ	$^{230}Th/^{232}Th$		σ	$(^{234}U/^{238}U)_0$		σ	kyr		+σ		-σ
1049	T	7	0-14	0.1531	0.4278	±	0.007	2.906	±	0.015	236	±	5.0	3.2395	±	0.017	56.8	+	1.2	-	1.1
1133	T	22.5	20-25	0.3490	0.4360	±	0.010	3.134	±	0.033	551	±	13	3.5162	±	0.037	58.3	+	1.7	-	1.7
1134	M	79.5	75-84	0.3025	0.3950	±	0.016	2.873	±	0.026	1804	±	72.4	3.1685	±	0.028	51.8	+	2.6	-	2.6
1050	M	92	86-98	0.1898	0.4048	±	0.007	2.967	±	0.020	1229	±	22	3.2863	±	0.022	53.3	+	1.2	-	1.2
1135	M	107	103-111	0.3709	0.4342	±	0.010	3.173	±	0.034	374	±	8.8	3.5599	±	0.038	58.0	+	1.8	-	1.7
1136	M	176.5	172-181	0.4108	0.4426	±	0.007	3.222	±	0.023	391	±	6.8	3.6279	±	0.026	59.4	+	1.2	-	1.1
1137	B	251	248-254	0.3892	0.4079	±	0.029	3.095	±	0.052	3460	±	235	3.4380	±	0.058	53.7	+	4.7	-	4.5
1051	B	263.5	257-270	0.2411	0.4099	±	0.014	3.301	±	0.027	6050	±	203	3.6799	±	0.030	54.0	+	2.3	-	2.3
1138	B	276	273-279	0.3568	0.4191	±	0.012	3.328	±	0.035	1078	±	29.3	3.7222	±	0.039	55.4	+	2.0	-	1.9
1052	B	344	339-349	0.2572	0.4189	±	0.023	3.346	±	0.070	7524	±	381	3.7438	±	0.079	55.4	+	3.8	-	3.7
1139	B	371.5	367-376	0.4324	0.4332	±	0.011	3.323	±	0.023	3880	±	94.1	3.7343	±	0.026	57.7	+	1.8	-	1.8

5.2.4 KDS Sample

Uranium concentration and activity ratios

Twenty U-Th ages were obtained for the KDS stalagmite although one subsample (J. No. 1038) was omitted due to an analytical problem. The data for the remaining nineteen U-Th ages is summarised in Table 5.4. Values are given for each of the activity ratios of uranium ($^{234}U/^{238}U$, $(^{234}U/^{238}U)_0$), thorium ($^{230}Th/^{232}Th$) and the activity ratio of $^{230}Th/^{234}U$. Changes in the latter ratio form the basis for the dating method used in this study. The stratigraphic position of each of the subsamples is denoted either by T (top), M (middle) or B (base). Errors are 1σ and ages are reported as kyr (thousand years). In this stalagmite the speleothem fabric is characterised by growth layers of variable thickness that occur in various shades of brown. The KDS stalagmite is thought to have formed between *c.* 64.6 and *c.* 70.4 ka. In the top part of the sample, represented by growth layers between 2.5 mm and 9.5 mm (from the top) the uranium content ranges between 0.3465 and 0.8785 ppm. In the middle layers, between 25 mm and 44.5 mm (from the top), the uranium content is more uniform with values ranging between 0.8240 and 0.8356 ppm. At the base, in layers between 56 mm and 85 mm (from the top), the uranium content ranges between 0.4533 and 0.7390 ppm and these values are comparable with those obtained in the upper layers. However, when taken as a whole the uranium concentration values from the top, middle and basal layers occur within overlapping ranges and are therefore indistinguishable (Fig. 5.13).

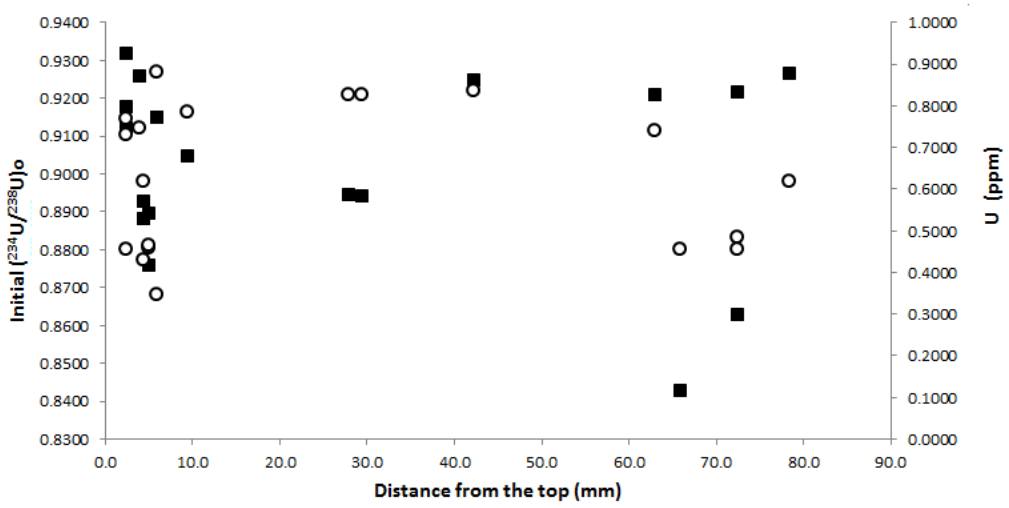

Fig. 5.13 Changes in the initial ($^{234}U/^{238}U$) activity ratio and uranium concentration (in ppm) along the length of the KDS stalagmite from Klipdrift Shelter

The initial ($^{234}U/^{238}U$) activity ratio is fairly uniform throughout the sample with little variation observed between subsamples from the top, middle and base of the KDS stalagmite. These $(^{238}U/^{234}U)_0$ activity ratio values range between 0.8428 and 0.9317 with an average activity ratio value of 0.9029. This is considerably lower than the values from the Bloukrantz Cave samples (discussed previously in this chapter). Nevertheless, from the absence of significant variation in the KDS activity ratio values the general inference is that the groundwater source remained stable during the period the stalagmite formed. Visual inspection of the stratigraphic layers to some extent supports this interpretation. This is because no visible hiatuses, which can (generally) indicate a decrease in groundwater recharge as a result of changes in precipitation above the cave, were observed. Definitive evidence can come from petrographic analysis of magnesium (Mg) and strontium (Sr) trace elements (*e.g.*, Railsback *et al*. 2002) but this approach is absent from this study.

Thorium activity ratios

The $^{230}Th/^{234}U$ activity ratios range between 0.4435 and 0.6095 with an average of 0.4823. Seventeen of the nineteen subsamples have activity ratio values that fall within a range from 0.4435 and 0.4997. Two exceptions come from subsamples with activity ratio values of 0.6095 (J.No. 1205) and 0.5649 (J. No. 1204). The vast majority of the KDS subsamples were taken from similar stratigraphic positions and presumed to be of similar age (Fig. 5.14).

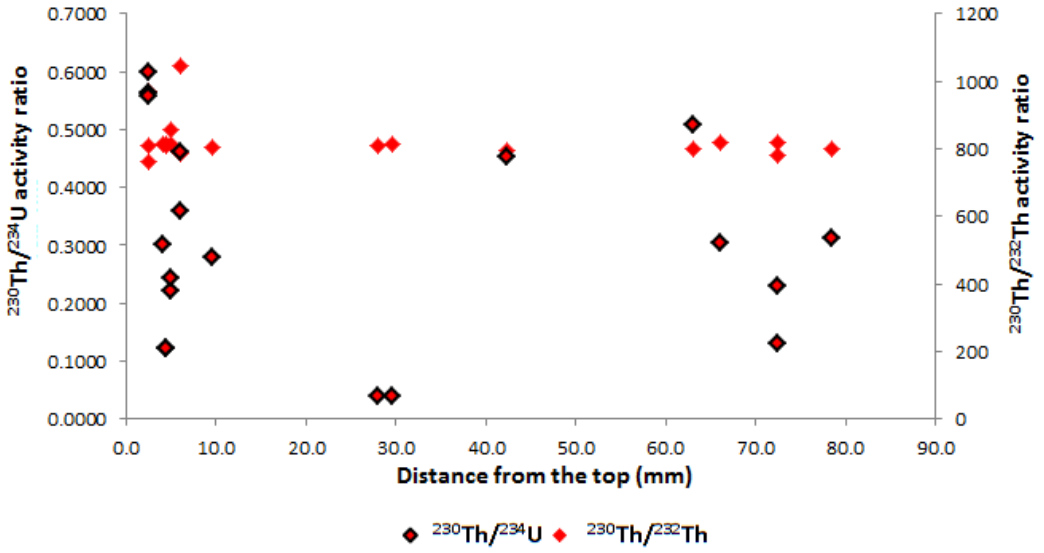

Fig. 5.14 Changes in the $^{230}Th/^{234}U$ and $^{230}Th/^{232}Th$ activity ratios along the length of the KDS stalagmite

The corresponding $^{230}Th/^{234}U$ activity ratio values were expected to reflect this with subsamples from the middle and upper part of KDS having lower activity ratio values with higer values occurring at in subsamples at the base. The $^{230}Th/^{232}Th$ activity ratio values are generally quite low and range between 67 and 1027 with a mean of 527. This is substantially lower than the range of values obtained for subsamples from Bloukrantz Cave. Fourteen of the KDS subsamples meet the ICPMS baseline value of 300. Five subsamples (J. No. 1033, 1034, 955, 977 & 1040) do not meet this criterion (Table 5.4). These subsamples have low activity ratio values and this can suggest contamination or post-depositional uranium loss but these

factors may not be an overriding issue in this instance. This is because the low $^{230}Th/^{232}Th$ activity ratios occur in conjunction with low initial ($^{234}U/^{238}U$) activity ratios. The implication is that the KDS subsamples contain similarly low levels of radiogenic thorium which can produce spurious ages. In addition, analytical issues are thought to play a role in the poor precision of many of the ages (excl. J.No. 954, 976, 978, 979, 980, 1037 & 1202). This is because subsamples with especially large errors (> 6 kyr) were run on the Element 2 shortly after a sample containing ^{232}Th levels of 500,000 cps was analysed. The integrity of subsequent sample runs may have been compromised if the excess thorium was not completely removed from the instrument. Twelve problematic ages were identified because of issues relating to the integrity of the ages (all unshaded J.No in Table 5.4). The remaining seven ages (all highlighted J.No in Table 5.4) did not exhibit the same problems and these were retained. Corrections were not applied to the spurious dates and these were instead omitted from the analysis.

Based on the ages that are deemed reliable KDS is thought to have grown between *c.* 64.6 ka and *c.* 70.4 ka. An age model was simulated for the growth history of KDS using the StalAge algorithm by applying the same procedure described for the Bloukrantz Cave samples. This age model is presented in the subsection below.

Age models

Using the same procedure used for the Bloukrantz Cave samples (described in Chapter 3 section 3.3.7) an age model was produced for the KDS stalagmite and is shown in Fig. 5.15. Due to the extremely low precision and accuracy of the vast majority of the ages only seven of the original ages were retained. The uranium series ages were selected from subsamples with relatively small age uncertainties of less than 6 kyr. This benchmark was selected as it represents the spread of error on the ages for the data from all the stalagmites (*i.e.*, BL1, BL3 & BL4 & KDC 5) discussed in this chapter. Suitable KDS subsamples that fulfil this requirement are J.No. 1037, 954, 976, 978 to 980 and 1202 (Table 5.4). Three of these subsamples have ages that fall within the 95% confidence limits of the model (Fig. 5.15). Two ages were identified as outliers are found in growth layers at 2.5 mm and 6 mm (from the top). These layers date respectively to 64.6 ± 4.3 ka and 67.6 ± 3.9 ka (Fig. 5.15). The two ages that fall outside the upper confidence limits of the model are also found in layers at 2.5 mm and 9.5 mm from the top (Fig. 5.15). These layers date respectively to 70.4 ± 1.4 ka and 70 ± 1.2 ka. Based on the StalAge model it is inferred that the KDS stalagmite grew continuously although slowly between *c.* 69.5 ka and *c.* 68 ka. This age model was used to anchor the stable isotope proxy data and the carbon and oxygen isotope data for KDS is presented in section 5.3 of the chapter.

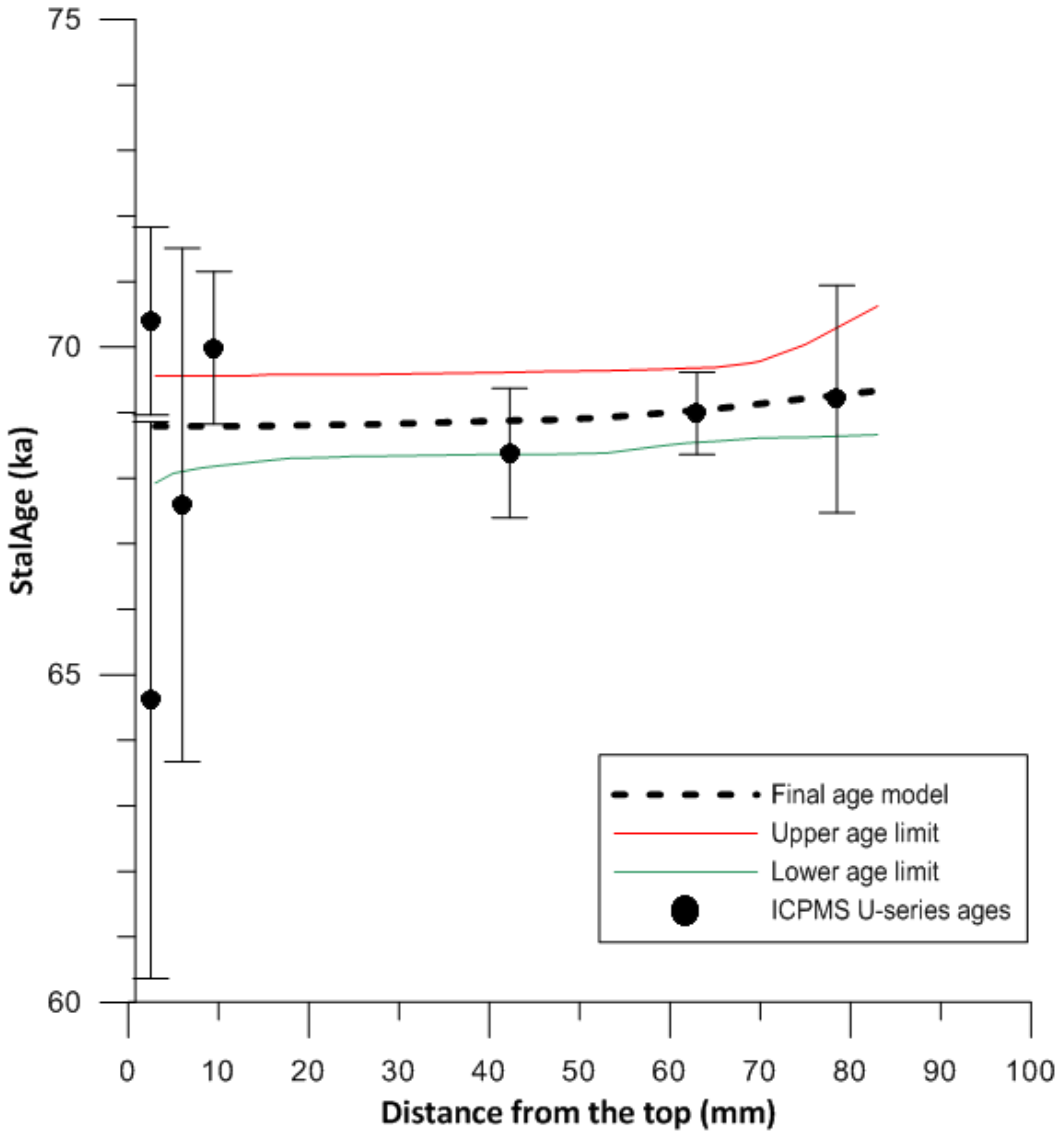

Fig. 5.15 The age model obtained for the KDS sample from Klipdrift Shelter showing the final age model (dashed black line). Corresponding 95% confidence limits for the StalAge model are denoted by age upper limit (solid red line) and age lower limit (solid green line). The U-series ages measured by ICPMS are also shown (black dots) along with the corresponding 2σ errors.

Table 5.4 Results from ICPMS U-Th analyses of the KDS stalagmite from Klipdrift Shelter with problematic ages shaded.

J. No.	Level	mm interval	Centre position (mm from top)	^{238}U (ppm)	$^{230}Th/^{234}U$		σ	$^{234}U/^{238}U$		σ	$^{230}Th/^{232}Th$		σ	$(^{234}U/^{238}U)_0$		σ	kyr		+σ		-σ
1037	T	0-5	2.5	0.4534	0.4435	±	0.020	0.9265	±	0.022	964	±	37	0.9118	±	0.022	64.6	+	4.4	-	4.1
1202	T	0-5	2.5	0.7300	0.4719	±	0.008	0.9324	±	0.006	1027	±	16.6	0.9175	±	0.006	70.4	+	1.7	-	1.2
1204	T	0-5	2.5	0.7679	0.5649	±	0.037	0.9473	±	0.035	955	±	52	0.9317	±	0.034	91.8	+	11	-	9.6
1203	T	0-8	4.0	0.7449	0.4744	±	0.028	0.9392	±	0.019	514	±	28	0.9257	±	0.019	70.9	+	6.3	-	5.9
1033	T	0-9	4.5	0.4281	0.4739	±	0.067	0.9086	±	0.044	210	±	28	0.8882	±	0.043	71.1	+	16	-	14
1034	T	0-9	4.5	0.6167	0.4722	±	0.063	0.9121	±	0.035	210	±	27	0.8927	±	0.034	70.7	+	15	-	13
1035	T	0-10	5.0	0.4580	0.4752	±	0.082	0.9097	±	0.049	378	±	62	0.8896	±	0.048	71.4	+	21	-	17
1036	T	0-10	5.0	0.4647	0.4997	±	0.077	0.8999	±	0.064	415	±	57	0.8756	±	0.062	76.9	+	21	-	17
1205	T	0-12	6.0	0.3465	0.6095	±	0.020	0.9366	±	0.015	615	±	19	0.9148	±	0.014	104.3	+	6.6	-	6.1
954	T	2-10	6.0	0.8785	0.4583	±	0.018	0.9296	±	0.014	792	±	30	0.9148	±	0.013	67.6	+	4.0	-	3.8
976	T	0-19	9.5	0.7840	0.4702	±	0.005	0.9217	±	0.005	480	±	9.3	0.9046	±	0.005	70.0	+	1.2	-	1.2
955	M	25-31	28.0	0.8241	0.4712	±	0.064	0.9134	±	0.037	67	±	9	0.8943	±	0.036	70.5	+	15	-	13.1
977	M	24-35	29.5	0.8240	0.4735	±	0.063	0.9134	±	0.037	67	±	9	0.8942	±	0.036	71.0	+	15	-	13
978	M	40-44.5	42.3	0.8356	0.4626	±	0.004	0.9380	±	0.009	776	±	12	0.9248	±	0.009	68.4	+	1.0	-	1.0
979	B	56-70	63.0	0.7390	0.4653	±	0.003	0.9347	±	0.004	869	±	8.9	0.9207	±	0.004	69.0	+	0.63	-	0.6
1041	B	64-68	66.0	0.4533	0.4775	±	0.062	0.8718	±	0.069	520	±	53	0.8428	±	0.067	72.4	+	16	-	13
1039	B	70-75	72.5	0.4538	0.4762	±	0.170	0.8881	±	0.128	394	±	130	0.8628	±	0.124	71.9	+	53	-	32
1040	B	70-75	72.5	0.4816	0.4568	±	0.035	0.9349	±	0.045	221	±	13	0.9213	±	0.044	67.2	+	8.1	-	7.3
980	B	72-85	78.5	0.6172	0.4666	±	0.008	0.9396	±	0.011	536	±	19	0.9265	±	0.011	69.2	+	1.8	-	1.7

5.2.5 KDC 5 Sample

Uranium concentration and activity ratios

Twelve U-Th ages were obtained for the KDC 5 stalagmite and the data are summarised in Table 5.5. Values are given for the uranium concentration and each of the activity ratios of uranium ($^{234}U/^{238}U$, $(^{234}U/^{238}U)_0$), thorium ($^{230}Th/^{232}Th$) and the activity ratio of $^{230}Th/^{234}U$. Changes in the latter ratio form the basis for the dating method used in this study. The stratigraphic position of each of the subsamples is denoted either by T (top), M (middle) or B (base). Errors are 1σ and ages are reported as kyr (thousand years).

In the KDC5 stalagmite the uranium content ranges between 0.658 and 2.877 ppm with a mean of 1.292 ppm. The vertical distribution of the uranium content is indistinguishable between the top, middle and basal layers in this sample (Fig. 4.16). The corresponding initial $^{234}U/^{238}U$ activity ratio - denoted as $(^{234}U/^{238}U)_0$ - exhibits minor variations around the mean activity ratio value of 0.7522 (Fig. 5.16). Slightly higher activity ratio values occur in subsample layers at the base while the activity ratio values in the middle and top layers are marginally lower. Taken as a whole these activity ratio values do not exhibit any significant variation.

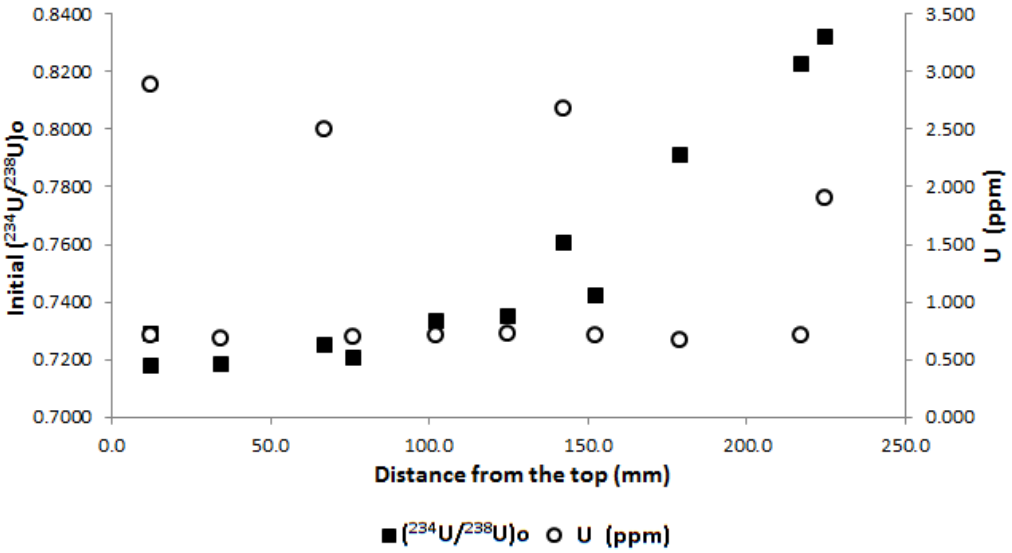

Fig. 5.16 Changes in the initial ($^{234}U/^{238}U$) activity ratio and uranium concentration (in ppm) along the length of the KDC5 stalagmite

Thorium activity ratios

The $^{230}Th/^{234}U$ activity ratio values range between 0.070 and 0.279 with an average of 0.105. There is a strong linear trend of decreasing $^{230}Th/^{234}U$ activity ratio values along the length of KDC5 with similar aged subsamples exhibiting similar activity ratio values. Notable exceptions to this pattern occur at three instances in the data. Problematic samples were identified in layers at 12.5 mm, 142.5 mm and at 152.5 mm (from the top) (Fig. 5.18).

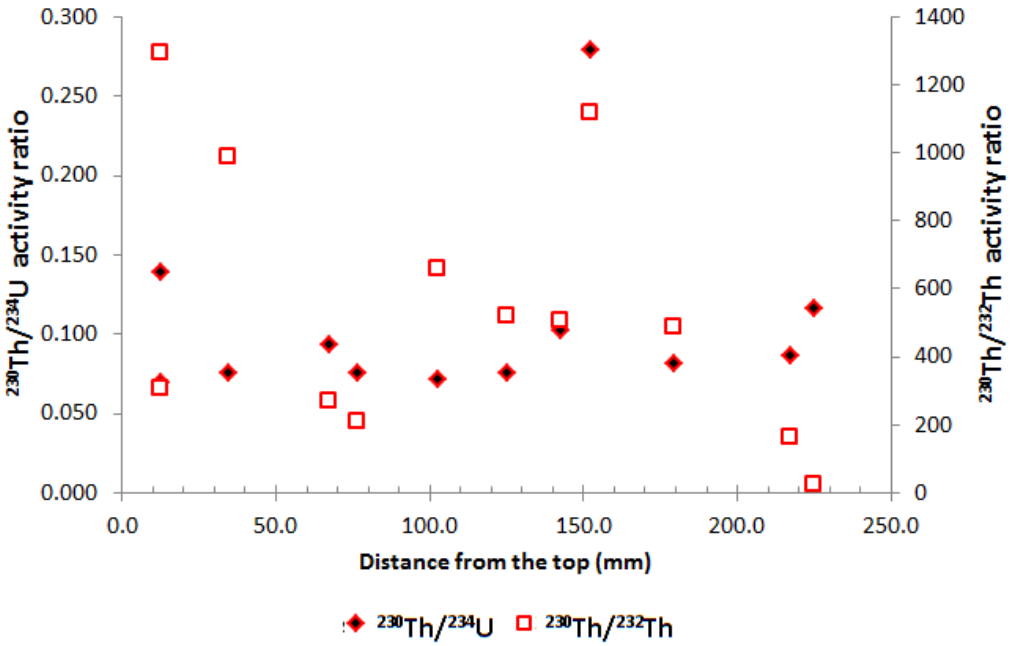

Fig. 5.17 Changes in the $^{230}Th/^{234}U$ and $^{230}Th/^{232}Th$ activity ratios along the length of KDC 5

The layer at 12.5 mm has an activity ratio value of 0.139 and dates to 16.5 ± 2.8 ka. This sample has an older age than the subsamples taken from the basal layers. The layer at 142.5 mm has an activity ratio value of 0.102 and dates to 11.9 ± 11 ka. The subsample from the layer directly below at 152.5 mm has an activity ratio of 0.279 and dates to 36.4 ± 2.3 ka (Fig. 5.18). This particular subsample is significantly older than the other dated KDC5 subsamples.

The $^{230}Th/^{232}Th$ activity ratio values range between 22 and 1291 and are significantly lower than the values recorded for the other stalagmite samples (*i.e.*, BL1, BL3, BL4 & KDS) from the study area. Eight of the twelve KDC5 subsamples have activity ratio values that exceed the standard baseline of 300 (Table 5.5 & Fig. 5.17). The remaining four subsamples do not fulfil this requirement. The implication is that these particular samples (J.No 923, 958, 963 & 921) may be compromised by the presence of non-radiogenic thorium. On the other hand, the ages for these low thorium samples fall within error limits with the majority of the dated subsamples obtained for the stalagmite. The $^{230}Th/^{232}Th$ activity

ratio values that exceed the baseline value of 300 (J.No 924, 956, 957, 959, 960, 922, 961, 963 & 921), range between 305 and 1291 with an average of 733. Three of these eight subsamples (J. No 924, 961 & 922) appear to be problematic. The uppermost layer at 12.5 mm (from the top) dates to 16.5 ± 2.8 ka and is older than the layer at the base dating to 13.6 ± 1.9 ka (Fig.4.18). This apparent stratigraphic inversion also occurs in the layer at 152.5 mm (from the top) dating to 36.4 ± 2.3 ka. Another subsample located at 142.5 mm (from the top) has very large error limits. As a result the age is not precise and this renders the particular subsample useless (Table 5.5 & Fig. 5.17). The presence of humic acids is inferred from dark visible growth layers and the low thorium values measured for the KDC5 subsamples could be related to this (Fig. 5.18).

Overall for the KDC5 stalagmite, eleven of the twelve ages were retained and used to model the growth history of KDC5 (all highlighted J.No in Table 5.5). One exception is the subsample corresponding to J. No 922 which has poor precision and large errors (> 6 kyr). Corrections were however not applied to the inverted age. For the KDC5 stalagmite the StalAge algorithm was applied to the data using the same procedure described for the previous samples and the model is presented in the subsection below..

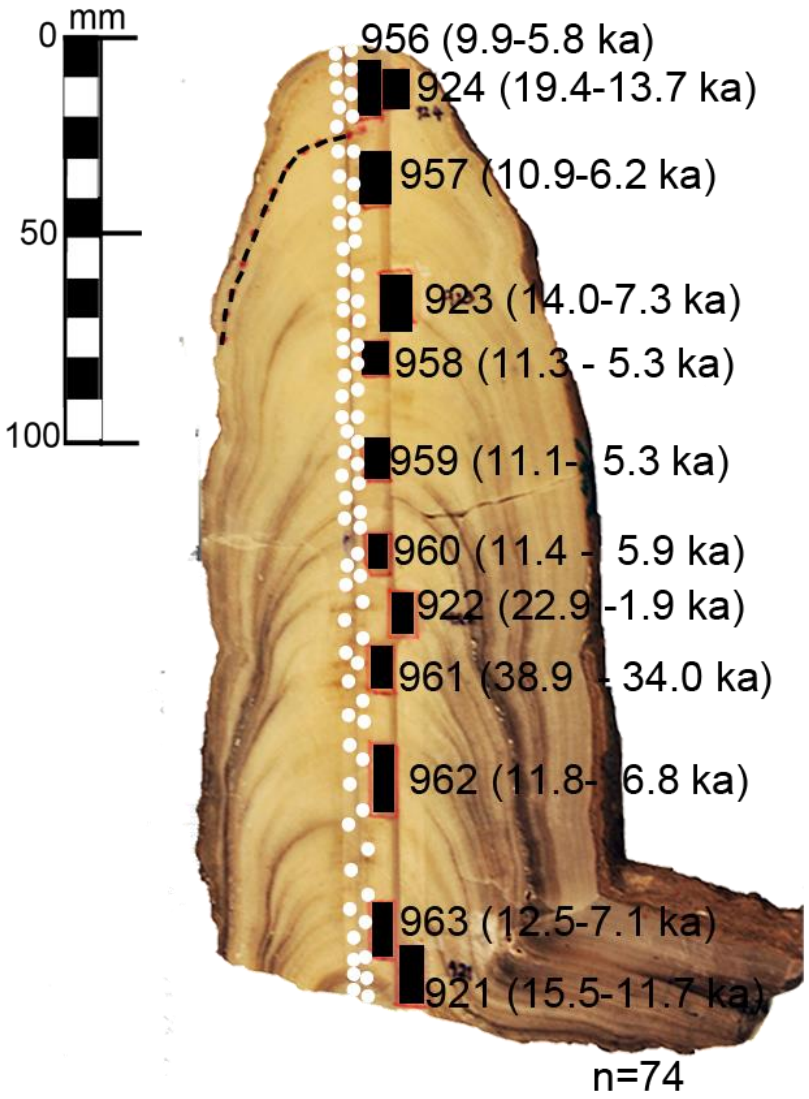

Fig. 5.18 Stratigraphic position of each of the uranium series age determinations obtained for the KDC 5 sample from Klipdrift Cave. The associated U-Th lab journal numbers are also shown. Uranium-series dated intervals are presented in *ka.* Individual isotope subsamples taken along the vertical length of the sample are shown as black dots (●).The Hendy test traverse is represented by solid dark lines (-)

Age models

The age model for the growth of the KDC5 stalagmite is shown in Fig. 4.19. The data used to produce this model is highlighted in Table 4.5. The majority of the original ages appear to fall within the 95% confidence limits of the model (Fig. 5.19). From these simulations the first period of growth is thought to have occurred between 13 ka and 9 ka. Slower growth is

interpreted for the period from *c.* 9 ka until 8 ka when KDC5 probably stopped growing. The subsample at 217.5 mm (from the top) which dates to *c*. 9.8 ka falls just outside the lower confidence limit of the model.

The subsample from the layer at 142.5 mm (from the top) is imprecisely dated and falls marginally within the upper confidence limit of the age model. A second subsample at 67.5 mm (from the top) dates to *c*. 10.8 ka and also falls just within the upper confidence limit. As expected, the subsamples at 152.5 mm and 12.5 mm (from the top) which date to *c*. 36.4 ka and 16.5 ka, respectively, were identified as outliers. It is unclear why the subsample at 152.5 mm appears to be much older than the rest of the KDC5 subsamples. The very low sample weight (< 0.5 g) for the subsample in the layer at 12.5 mm (from the top) may have affected the accuracy of the age determination for this subsample. Overall, this stalagmite appears to be of Holocene age. Based on the uranium series age estimates KDC5 formed between *c*. 13 ka and 8 ka.

The StalAge model simulations for KDC5 were used to anchor the stable isotope proxy data for the sample and the data are presented in section 5.3 of the chapter.

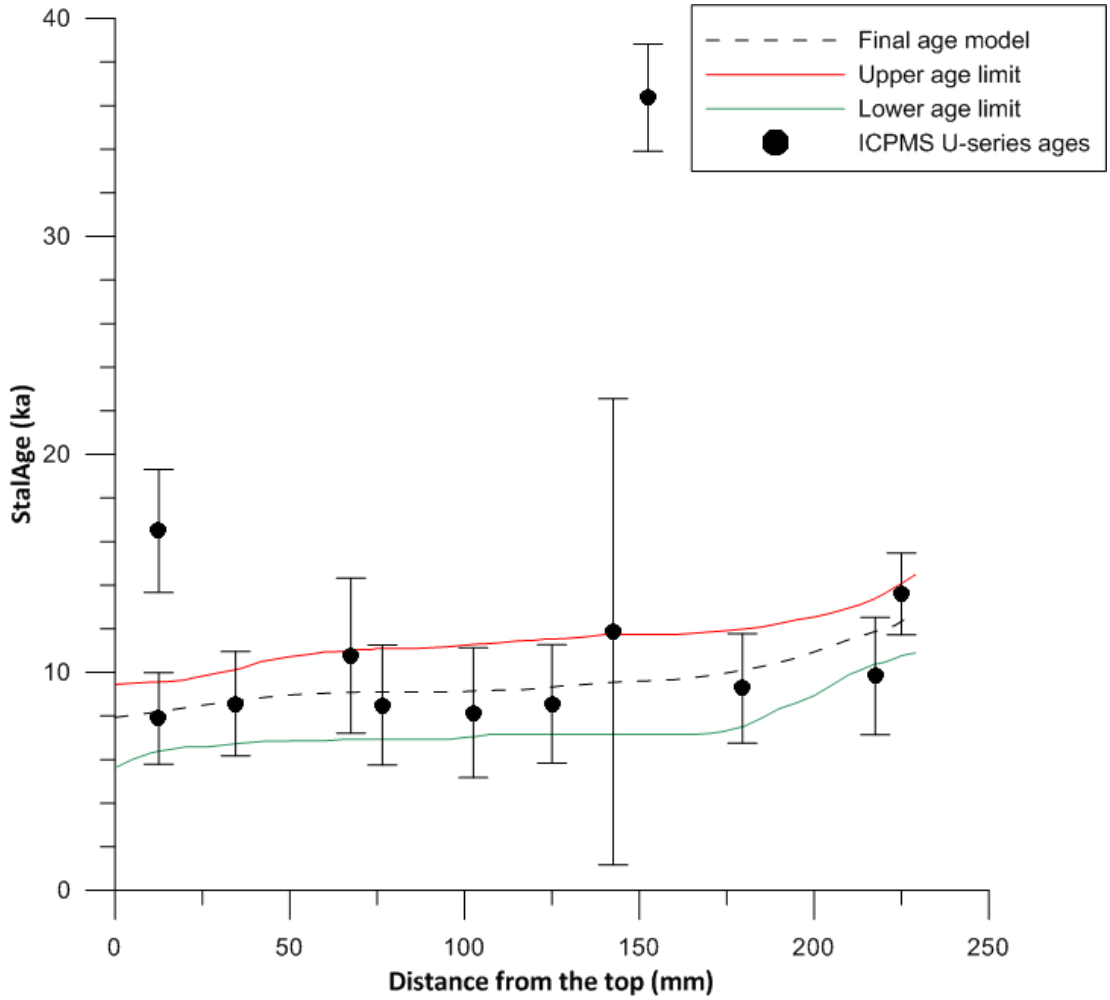

Fig. 5.19 The age model obtained for the KDC 5 sample from Klipdrift Sea Cave showing the final age model (dashed black line). Corresponding 95% confidence limits for the StalAge model are denoted by age upper limit (solid red line) and age lower limit (solid green line). The U-series ages measured by ICPMS are also shown (black dots) along with the corresponding 2σ errors

Table 5.5 Results from ICPMS U-Th analyses of the KDC 5 stalagmite from Klipdrift Sea Cave with problematic ages shaded.

J. No.	Level	Centre position (mm)	mm interval	^{238}U (ppm)	$^{230}Th/^{234}U$		σ	$^{234}U/^{238}U$		σ	$^{230}Th/^{232}Th$		σ	$(^{234}U/^{238}U)_0$		σ	kyr		+σ		-σ
924	T	12.5	5-20	2.877	0.139	±	0.02	0.7411	±	0.035	1291	±	192	0.7287	±	0.034	16.5	+	2.9	-	2.8
956	T	12.5	6-19	0.709	0.070	±	0.02	0.7236	±	0.003	305	±	77	0.7174	±	0.003	7.89	+	2.1	-	2.1
957	T	34.5	29-40	0.682	0.075	±	0.02	0.7250	±	0.007	985	±	263	0.7182	±	0.007	8.56	+	2.4	-	2.4
923	M	67.5	60-75	2.485	0.093	±	0.03	0.7331	±	0.004	270	±	84	0.7249	±	0.004	10.8	+	3.6	-	3.5
958	M	76.5	72-81	0.694	0.075	±	0.02	0.7272	±	0.005	210	±	65	0.7206	±	0.005	8.50	+	2.8	-	2.7
959	M	102.5	98-107	0.704	0.072	±	0.03	0.7389	±	0.010	659	±	230	0.7329	±	0.010	8.15	+	3.0	-	2.9
960	M	125	119-131	0.716	0.075	±	0.02	0.7414	±	0.005	519	±	157	0.7351	±	0.005	8.55	+	2.8	-	2.7
922	B	142.5	135-150	2.672	0.102	±	0.09	0.7685	±	0.014	503	±	425	0.7606	±	0.014	11.9	+	11	-	10
961	B	152.5	145-160	0.704	0.279	±	0.02	0.7673	±	0.009	1118	±	60.8	0.7421	±	0.008	36.4	+	2.5	-	2.4
962	B	179.5	170-189	0.658	0.081	±	0.02	0.7963	±	0.006	484	±	125	0.7909	±	0.006	9.27	+	2.5	-	2.5
963	B	217.5	205-230	0.697	0.087	±	0.02	0.8275	±	0.005	164	±	42	0.8226	±	0.005	9.83	+	2.7	-	2.7
921	B	225.0	220-230	1.901	0.117		0.02	0.8384	±	0.007	22	±	8	0.8321	±	0.007	13.6	+	1.9	-	1.9

5.3 Stable isotopes of Carbon and Oxygen

Stable isotopes of carbon and oxygen obtained from speleothems are widely used to make inferences about environmental conditions above the cave at the time when the speleothems were forming. Vegetation changes are inferred from the $\delta^{13}C$ ratio while the corresponding $\delta^{18}O$ ratio is used to make interpretations of rainfall and temperature. Processes such as kinetic fractionation effects can however cause isotopic shifts and weaken the interpretive value of the ^{13}C and ^{18}O signals. It is therefore important to determine whether or not fractionation effects influenced the isotope signal in the speleothem calcite. The Hendy Test is conventionally used for this purpose of evaluating isotope ratios and these results are presented for each of the samples (*i.e.*, BL1, BL3, BL4, KDS & KDC5) (Pickering *et al.* 2007, 2010; Bar-Matthews *et al.* 2010; Noah 2010).

The StalAge algorithm that was used to produce age models for the growth history of each of the stalagmites also provided temporal constraint of the ^{13}C and ^{18}O records. For each stalagmite the algorithm simulated growth using the U-Th ages, the centre position (in mm) of the age and the distance measurement (in mm) for each isotope point. In this way the algorithm calculated an age (in ka) for each of the isotope distance measurements and these stable isotope time series profiles are presented after the Hendy Test results.

The $\delta^{13}C$ values are interpreted using the data from the Cango Cave stalagmite record (Talma & Vogel 1992). Talma and Vogel (1992) calculated the proportion of ^{13}C input by C_4 plants by using relative C_4 abundance estimates reported by Cowling (1983). Cowling's estimates were determined from a botanical survey undertaken across the Humansdorp region of the south-eastern Cape. He estimated the relative percentages of C_3 and C_4 vegetation in three different vegetation types, grassy fynbos, dune fynbos and south coast Renosterveld (Cowling 1983). Cowling's (1983) relative estimates of *c.* 40% C_4 vegetation cover for

south coast Renosterveld were used as a baseline by Talma and Vogel (1992). They predicted that this would correspond to a $\delta^{13}C$ value of -7‰ for calcite and -17‰ for soil (Talma & Vogel 1992:211). To test this prediction they measured $\delta^{13}C$ values from four soil samples "*from the same vegetation zone nearby*" (Talma & Vogel 1992: 211). They obtained a mean $\delta^{13}C$ value of -16.7‰ for soil organic matter which is in agreement with their prediction. The $\delta^{13}C$ value of calcite sampled from the top of the stalagmite was -6.4‰ which is also close to the predicted value of -7‰. Talma and Vogel (1992) therefore proposed that the $\delta^{13}C_{calcite}$ signal from the Cango Cave stalagmite could be linked to changes in the abundance of C_4 photosynthesising plants.

The proportion of ^{13}C input from C_4 plants in the past was then calculated in percentage terms using the baseline of 40% C_4 cover (Cowling 1983) and the corresponding $\delta^{13}C_{calcite}$ value of -7‰. From these modern benchmark values Talma and Vogel (1992) presumed average enrichment of +3‰ for $\delta^{13}C$ for every 20‰ *increase* in the relative abundance of C_4 vegetation (Talma & Vogel 1992: 211). For example, based on present-day estimates for the Cango Cave a $\delta^{13}C_{calcite}$ value of -7‰ equates to 40% C_4 cover. Assuming a +3‰ enrichment for C_4 a $\delta^{13}C_{calcite}$ value of -4‰ would be equivalent to a 60% input of ^{13}C from C_4 plants. Similarly for every 20% *decrease* in C_4 dominance the direction and sign of these estimates will be opposite. For example, Talma and Vogel (1992: 208) equate a $\delta^{13}C_{calcite}$ value of -10‰ to a 20% input from C_4 plants. These relative percentages are estimated on the assumption that the $\delta^{13}C_{calcite}$ values only reflect changes in the dominant vegetation above the cave (Talma & Netterberg 1983; Talma & Vogel 1992: 211).

More recent speleothem work on kinetic effects (Mickler *et al.* 2004, 2006) and soil processes (Genty *et al.* 2006) indicates that these variables can also influence the $\delta^{13}C_{calcite}$ signal (see Chapter 3 section 3.3.2). While the controls on $\delta^{13}C_{calcite}$ are more complex than apparent in Talma and Vogel's (1992) assessment their data provides a useful benchmark for

interpreting variations in $\delta^{13}C_{calcite}$ signals in stalagmites. Indeed, their data are widely used as a frame of reference in other speleothem studies from South African contexts (see below).

Here Talma and Vogel's (1992) estimates are used to relate the $\delta^{13}C_{calcite}$ signal from the De Hoop stalagmites to shifts in the abundance of C_3, C_4 and potentially CAM plants to provide results comparable to other similar studies (see below). This approach is consistent with other speleothem studies from South African contexts where vegetation changes are generally interpreted using Talma and Vogel's (1992) $\delta^{13}C$ ratios as a comparative benchmark (*e.g.*, Bar-Matthews *et al.* 2010; Holmgren *et al.* 2003; Hölkzkamper *et al.* 2009; Noah 2010; Pickering 2006). At Cango Cave C_3 type vegetation is inferred from a lower (less positive) $\delta^{13}C_{calcite}$ value of -12.8‰. This is proposed for $\delta^{13}C$ in calcite with a 100% C_3 signal. Therefore it is assumed that the probable $\delta^{13}C$ range representing C_3 plants would be from -12 to -7‰. C_4 type vegetation is inferred from higher (more positive) $\delta^{13}C_{calcite}$ values with an estimated value of +1.2‰ for calcite with a pure C_4 signal (Talma & Vogel 1992: 211). The assumption made here is that the $\delta^{13}C$ range representing C_4 plants would be from -7‰ to -4‰. Chase (*pers. comm.* September 2013) advises that CAM values should be considered as well when interpreting $\delta^{13}C_{calcite}$ values in calcite because they are abundant in some areas such as the southern Cape. Modern vegetation in the Cango Valley is dominated by C_3 and C_4 types and therefore Talma and Vogel (1992) did not consider any input from CAM plants.

In the southern Cape common C_3-photosynthesing vegetation are sclerophyllous Fynbos, proteas (Proteaceae), asteraceous shrubs (*e.g.*, *Elytropappus rhinocerotis*), Cape reeds (Restionaceae) and cool season grass species (*e.g.*, *Pentaschistis eriostoma, Erharta calycina & Merxmuellera stricta*) (Milton 2004). C_4-type vegetation is dominated by warm season grasses (*e.g.*, *Themeda triandra & Cymbopogon marginatus*) and geophytic bulbs for example (Milton 2004).

The succulent species of *Crassula umbellata*, *Crassula nudicaulis* and *Mesembryanthamum crystallinum* are relatively abundant above the Klipdrift Sea Cave and Klipdrift Shelter (*personal observation*). These are the sites where the KDS and KDC5 stalagmites were taken. The aforementioned succulent plants are also observed at West Cave where the dripwater samples were obtained. Since CAM species are present in the vicinity of the De Hoop Caves a potential input from CAM plants into the $\delta^{13}C_{calcite}$ is quite plausible. *C. umbellata* and *C. nudicaulis* are typical CAM species (Raimondo *et al.* 2009) while *M. crystallinum* exhibits C_3-like CAM photosynthesis (Lüttge 1998). Species from the *Portulacaria* genus occur in parts of South Africa with succulent karoo, thicket and bushveld vegetation and are known to alternate between C_4 and CAM photosynthesis (Guralnick 1984; Guralnick *et al.* 2008). *Portulacaria* and *Portulaca* are the only documented genera of plants with the ability to use C_4 and CAM photosynthesis but these succulents do not occur in the southern Cape (Guralnick 1984; Guralnick *et al.* 2008; Lambers *et al.* 2008). Based on this it is suggested that a contribution from CAM photosynthesisng plants also be included. This is because, as previously mentioned CAM plants are present at De Hoop and occur as geophytes in fynbos and as succulents in thicket and strandveld vegetation (Quick 2013). Therefore, for the purpose of this study variations in $\delta^{13}C_{calcite}$ are not strictly interpreted in terms of C_3 and C_4. Instead, contributions from CAM photosynthesising plants are taken into consideration by interpreting speleothem $\delta^{13}C$ in terms of C_3/C_3-like CAM (also C_3/CAM) and C_4/CAM.

The $\delta^{18}O$ values that correspond to the $\delta^{13}C$ values are used as a broad rainfall and temperature proxy. In this study, variations in the $\delta^{18}O$ values corresponding to the $\delta^{13}C$ values are interpreted using the data from the Crevice Cave stalagmite record from Pinnacle Point in Mossel Bay (Bar-Matthews *et al.* 2010). Bar-Matthews and colleagues (2010) collected sixty-four precipitation samples between January 2006 and April 2007 and used the distribution of $\delta^{18}O$ in current precipitation as a modern reference

for interpreting the $\delta^{18}O_{calcite}$ signal (Bar-Matthews *et al.* 2010: Supplementary Data Table S3). They report higher (more positive) values from -1.6‰ up to +0.13‰ in present-day summer rain and lower (more negative) $\delta^{18}O$ values between -6.1‰ and -2.9‰ in current winter rain above the cave (Bar-Matthews *et al.* 2010: 2137). Bar-Matthews and colleagues (2010: 2138) then used the range of $\delta^{18}O$ variation in their modern precipitation samples to make inferences about changes in $\delta^{18}O_{calcite}$ of the Crevice Cave stalagmite by interpreting these values in terms of rainfall seasonality. Bar-Matthews *et al.*'s (2010) interpretations are based on the assumption that the seasonal variation in^{18}O input from summer and winter rain, determined from their modern precipitation samples, is preserved through time and reflected in the $\delta^{18}O_{calcite}$ of the Crevice Cave stalagmite. They did not however collect dripwater samples from within the cave to further test this assumption.

Based on the Crevice Cave data ^{18}O input from winter rain into the stalagmite calcite is interpreted from lower (less positive) $\delta^{18}O_{calcite}$ values between -4.0‰ and -5.5‰. A summer rainfall signal is inferred from higher (more positive) values between -3.5‰ up to -1.5‰. Using these values as a baseline it is therefore assumed that the probable $\delta^{18}O_{calcite}$ range for winter rainfall would be from -4.0‰ to -5.5‰.

The controls on ^{18}O fractionation is however more complex than considered by Bar-Matthews and colleagues (2010). This is because there are various factors that might influence the ^{18}O isotope signal. These include, for example, evaporation, altitude, rainfall amount and the type of precipitation (*e.g.*, snow, hail & rain), kinetic effects and variable drip rates (See Chapter 3 section 3.5.2 for details). Nevertheless, Bar-Matthews and colleagues (2010) Crevice Cave $\delta^{18}O_{calcite}$ record does provide a useful comparative benchmark for interpreting variations observed in the De Hoop stalagmite $\delta^{18}O$ signals. Their data are also pertinent to the southern Cape because the majority of $\delta^{18}O$ speleothem records in South African contexts come from the summer rainfall areas (*e.g.*, Holmgren *et al.* 1999,

2001, 2003; Pickering *et al.* 2007; Hölzkamper *et al.* 2009). Since the southern Cape receives rainfall year round the $\delta^{18}O$ records from the interior of South Africa may not necessarily be applicable.

The De Hoop Nature Reserve, the Overberg, Mossel Bay and by extension the southern Cape, falls within South Africa's year round rainfall area. However Bar-Matthews *et al.* (2010) did not consider or identify a year round rainfall signal in the $\delta^{18}O_{calcite}$ values from the Crevice Cave record. Because the above-mentioned areas presently fall under a year round rainfall regime, it is assumed that rainfall dynamics in the past were similar. Therefore, it is suggested that speleothem $\delta^{18}O$ signals not be interpreted strictly in terms of winter and summer rainfall and that a possible year round influence be considered. Using the $\delta^{18}O_{calcite}$ values for winter and summer rainfall (after Bar-Matthews *et al.* 2010) as a baseline, the assumption here is that a year round rainfall signal would straddle the range of winter and summer rain.

Therefore, for the purpose of this study variations in $\delta^{18}O_{calcite}$ are interpreted in terms of summer, winter and year round rainfall to take in account a possible ^{18}O input from all seasons precipitation. This approach provides results that are comparable to other similar studies from the southern Cape where rainfall seasonality is generally interpreted using the $\delta^{18}O$ values from Bar-Matthews and colleagues (2010) (*e.g.*, Braun *et al.* 2012; Braun 2014; Noah 2010).

To further constrain interpretations of the $\delta^{18}O_{calcite}$ records current meterological data, $\delta^{18}O$ data in current precipitation and cave dripwater are also used. The meterological data used to infer paleorainfall and temperature comes from the Still Bay weather station and the data are used to determine the variability in the annual and seasonal rainfall patterns. This provides information on the variability in the modern rainfall dynamics which is then used to extrapolate back in time.

The $\delta^{18}O$ values in rainfall are obtained from the International Atomic Energy Agency (IAEA) Global Networks of Isotopes in Precipitation (GNIP) database (http://www.iaea.org/water). The GNIP $\delta^{18}O$ data provides some information about the isotopic signal and how it relates to various meteorological patterns. Taken together this data gives an indication of the isotope signature of the different types of precipitation that could be hypothesised in the groundwater feeding the cave.

The comparative Cave dripwater samples come from West Cave and the Klipdrift Sea Cave. The dripwater $\delta^{18}O$ is compared to rainfall $\delta^{18}O$ to determine if the dripwater ^{18}O signal reflects changes in surface rainfall (Feng *et al.* 2012; Lachniet *et al.* 2012). The $\delta^{18}O$ in the dripwater is also used to evaluate whether or not the $\delta^{18}O_{calcite}$ are deposited in isotopic equilibrium with their dripwater $\delta^{18}O$. This is an important consideration as isotopic shifts can be caused by non-climatic factors such as kinetic processes and incorrectly explained in relation to rainfall and temperature. In this study variations in $\delta^{18}O_{calcite}$ and $\delta^{18}O_{dripwater}$ are used to make inferences about surface temperatures in the past using the equation proposed by Demény *et al.* (2010). The dripwater results and temperature reconstructions are presented after the discussion of the $\delta^{13}C$ and $\delta^{18}O$ records.

5.3.1 BL1 Sample

Hendy Test

A detailed discussion of the Hendy Test and its assumptions and limitations are provided in Chapter 3. In short, a negative Hendy test result is based on covariance between $\delta^{18}O$ and $\delta^{13}C$ along a single growth layer. This implies that the stalagmite isotope data cannot be confidently interpreted in terms of changes in climate. On the other hand, where linear plots of $\delta^{18}O$ and $\delta^{13}C$ do not show positive correlations this may indicate

deposition under equilibrium conditions. As a result the data can be interpreted in terms of general climate.

This test is a somewhat contentious measure for determining whether or not calcite was deposited under equilibrium conditions and the limitations of the Hendy Test and its assumptions are reviewed by Dorale and Liu (2009). An alternative known as the replication approach has been proposed as a more robust method of evaluating isotopic equilibrium. While the replication approach is preferred in this study, the Hendy Test is also used for the sake of completeness. For the BL1 stalagmite sixty-five subsamples were taken for the Hendy Test. These subsamples were taken along four different growth layers between 65 and 66 mm, at 87 mm, at 175 mm and at 513 mm (from the top) (Fig. 5.7). For each sampled layer the $\delta^{18}O$ values were plotted against the corresponding $\delta^{13}C$ values (Fig. 5.20).

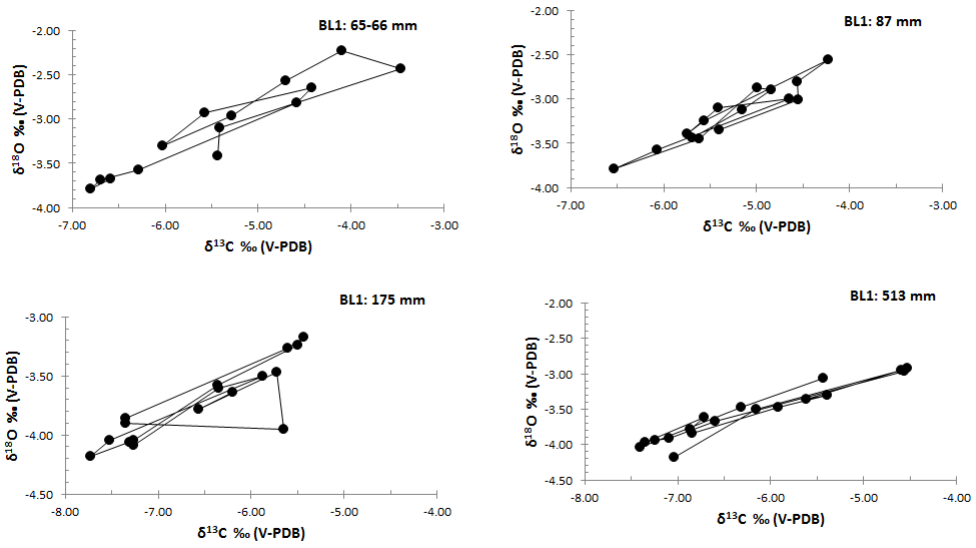

Fig. 5.20 Hendy Test results from the post-hiatus growth layers at 65-66 mm, at 87 mm and at 175 mm and at the growth layer at 513 mm from the BL1 stalagmite at Bloukrantz Cave.

Hendy Test results indicate that the $\delta^{18}O$ and $\delta^{13}C$ values occur in a very similar range of variation. Across all four sampled lamina there appears to be a lack of correlation between $\delta^{18}O$ and $\delta^{13}C$ which is suggestive of deposition in isotopic equilibrium.

Carbon isotope analyses

The $\delta^{13}C$ data from the BL1 stalagmite provide a discontinuous stable isotope record for the period from 81 ka to 74 ka (Fig. 5.21a) with a hiatus from *c.* 73 ka to 46 ka with growth resuming from 45 ka until *c.* 31 ka (Fig. 5.21b).

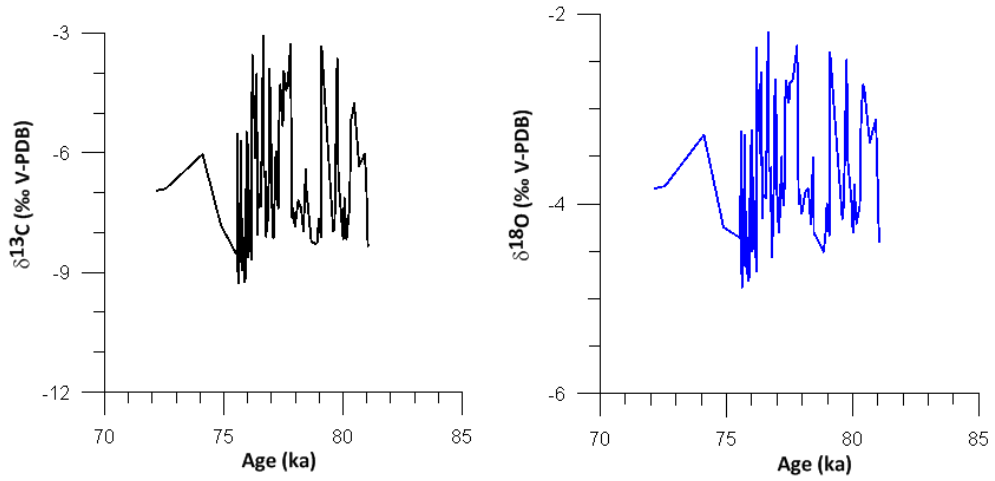

Fig. 5.21a $\delta^{13}C$ and $\delta^{18}O$ isotope age curve for the BL1 stalagmite for the interval isotope age curve for the BL1 stalagmite for the interval from 81.5 ka to 74 ka.

Between 81.5 ka and 81 ka there is an increasing trend in $\delta^{13}C$ towards slightly higher values from -8.5‰ up to -4.8‰ (Fig. 5.21a). Based on Talma and Vogel's (1992) estimates this equates to a shift in C_4 vegetation cover from 25% *c.* 81.5 ka to *c.* 55% by 81 ka. By 80.5 ka $\delta^{13}C$ drops down to a lower value of -8‰ which could reflect 30‰ C_4 cover at this time. Between 80.5 ka and 80 ka $\delta^{13}C$ increases again with a peak at -3.5‰ which could reflect a stronger input from C_4 type vegetation into the $\delta^{13}C$ signal by 80 ka. An abrupt vegetation change occurs between 79 ka and 78 ka with $\delta^{13}C$ showing an increasing trend towards higher values with a peak at -3.5‰. This value falls outside the upper limit of Talma and Vogel's (1992) $\delta^{13}C$ range but equates to about 70% C_4 vegetation. For

the period between 80 ka and 78 ka a somewhat similar trend is shown in the Little Karoo $\delta^{13}C$ records from Efflux Cave and Melville Pot with values increasing from -7‰ up to -4.5‰ (Braun *et al.* 2012). Braun (2014: 74) has however cautioned that large variations (of up to 2‰) in $\delta^{13}C$ between different samples from the Little Karoo have made interpretations from this signal tentative at best. Along the coast the $\delta^{13}C$ record for Crevice Cave shows an opposite pattern to BL1 with $\delta^{13}C$ values around -10‰ reported between 79 ka and 78 ka (Bar-Matthews *et al.* 2010 Supplementary Data Table S2).

In the BL1 record a minor decrease in $\delta^{13}C$ from -3.5‰ to -5.5‰ occurs around 77 ka but the values still fall within the theoretical range of C_4 type vegetation estimated by Talma and Vogel (1992). These values are similar to values between -4‰ and -6‰ reported for the Little Karoo $\delta^{13}C$ record at this time (Braun *et al.* 2012 but see Braun 2014). The $\delta^{13}C$ values from BL1 and the Little Karoo *c.* 77 ka fall within Talma and Vogel's (1992) range of C_4 vegetation. This pattern is contrary to that from the coeval Crevice Cave record where the $\delta^{13}C$ values for the same period fall within the range of C_3 vegetation (Bar-Matthews *et al.* 2010 Supplementary Data Table S2). This suggests that at least *c.* 77 ka, conditions were warmer in De Hoop (and by extension the Overberg) and in the Little Karoo during this part of MIS 5a. According to Braun (2014) interpretations of the Little Karoo $\delta^{13}C$ content is however compromised by the significant range of variation between coeval samples. As a result, firm interpretations of the $\delta^{13}C$ signal from the Little Karoo record is considered tentative at best.

Between 77 ka and 75 ka the BL1 $\delta^{13}C$ data shows a general decreasing trend towards a lower value of -9.5‰ which equates to around 25% C_4 plants (Fig. 5.21a). In other words this suggests a much stronger input of around 70% C_3 vegetation by 75 ka, possibly indicating wetter conditions. The $\delta^{13}C$ value observed here is comparable with the values from the contemporaneous period, between 77.3 ka and 74.6 ka, from Crevice Cave where $\delta^{13}C$ values are between 8.1‰ and 10‰ (Bar-Matthews *et al.*

2010). For the short interval between 75 ka and 74 ka, the BL1 stalagmite shows a 0.5-1 kyr periodicity in vegetation change between C_3/C_3-like CAM and C_4 plants. These fluctuations seem to have occurred rapidly, frequently and in a short period of time. Based on this pattern, is appears that environmental conditions were seemingly quite variable throughout MIS 5a and at the transition to MIS 4. It is also worth noting that the abrupt isotopic variations evident in this part of BL1 can be easily smoothed out when comparing high resolution records with more general proxy records such as ice cores and SST curves.

There is a break in the BL1 sequence from *c.* 73 ka due to a hiatus which lasted until *c.* 46 ka when growth resumed (Fig. 5.21b). The long duration of this hiatus is not present in its entirety in the BL3 and BL4 stalagmites that come from the same cave as BL1. BL3 records a hiatus from *c.* 45 ka –*c.* 5 ka (Fig. 5.22) whereas no visible hiatuses were observed in BL4 during the contemporaneous period between *c.* 60 ka and 34 ka (Fig. 5.23). The hiatus in the BL1 sample is also not present in the Crevice Cave stalagmite record which is dated from *c*. 90 ka to 53 ka (Bar-Matthews *et al.* 2010), in the composite record at Pinnacle Point dated from *c.* 114 ka – 40 ka or in the KDS stalagmite which grew between *c*. 69.8 ka and 69.4 ka (Fig. 5.24). Based on this pattern, the long hiatus in BL1 most likely reflects changes in the local hydrology of the cave.

In the BL1 sample growth resumed after the hiatus by *c.* 46 ka and this part of the sample is suspected of containing aragonite. Appropriate corrections were applied to make the younger aragonite section directly comparable with the older calcite section. Post-hiatus $\delta^{13}C$ values range between -5‰ and +3.5‰ and are higher than those values from the older of part of BL1 (Fig. 5.21b). At 46 ka, $\delta^{13}C$ peaks at -0.5‰ before decreasing abruptly to –3.0‰ around 44 ka. Between 44 ka and 40 ka there is an increasing trend towards higher (more positive) $\delta^{13}C$ values from -3.0‰ up to +3.0‰. This range of $\delta^{13}C$ variation in the aragonite part

of BL1 is most similar to that of the Wolkberg Cave record that also contains a stalagmite with mixed mineralogy (Hölkzkamper *et al.* 2009).

At Wolkberg Cave $\delta^{13}C$ values between 0‰ and +2‰ occur between *c.* 49 ka and 46 ka (Hölkzkamper *et al.* 2009). Similarly high values between +1‰ and +2‰ are also reported around 40 ka from the same stalagmite (Hölkzkamper *et al.* 2009). In the BL1 $\delta^{13}C$ record there is a high amplitude drop to lower values from +3.0‰ down to -5.0‰ occurring between 40 ka and 35 ka. From the Cango Cave there are two data points with $\delta^{13}C$ values between -10.5‰ and -11‰ that fall within this time period (Talma & Vogel 1992). At the Cango Cave a weak C_4 vegetation signal comprising less than 20% C_4 type plants is interpreted for the interval between 40 kcal BP and 38 kcal BP (Talma & Vogel 1992). At Cango Cave, this translates to stronger presence of C_3 type plants whereas the opposite pattern is reflected in the BL1 $\delta^{13}C$ data during the same period. By 34 ka the BL1 record shows $\delta^{13}C$ increasing again towards a higher value of +0.5‰ before declining incrementally to a lower value of -2.0‰ by 31 ka (Fig. 5.21b). While these values fall outside the upper limit of Talma and Vogel's (1992) $\delta^{13}C$ range of C_4 vegetation they suggest an input from C_4 type vegetation of more than 60% around this time.

Oxygen isotope analyses

Variations in the $\delta^{18}O_{calcite}$ signal of BL1 follow the same pattern as the $\delta^{13}C$. Between 81.5 ka and 81 ka there is a trend towards higher (more positive) $\delta^{18}O$ values with $\delta^{18}O$ increasing from -4.2‰ up to -2.8‰ (Fig. 5.21a). Based on Bar-Matthews *et al*.'s (2010) estimates this equates to a stronger summer rainfall signal. The increasing trend observed in the BL1 $\delta^{18}O$ record for this interval is also present at Crevice Cave (Bar-Matthews *et al.* 2010). This could suggest that similar rainfall conditions were present along the coast at De Hoop and Crevice Cave around this time. The pattern observed in the BL1 and Crevice Cave records is not present in the Little Karoo stalagmite which is located further inland from the other two sites (Braun 2014). At this site the smoothed $\delta^{18}O$ record shows the opposite pattern with a signal of *c.* 5.3‰ which falls within Bar-Matthews *et al.*'s (2010) $\delta^{18}O$ range of winter rainfall.

Between 80.5 ka and 80 ka there is an abrupt decreasing trend towards lower values with $\delta^{18}O$ dropping from -2.8‰ to -4.2‰ (Fig. 5.21a). Values in this lower range are suggestive of a stronger input of ^{18}O from winter rain. This drop in BL1 $\delta^{18}O$ is also present at Crevice Cave (Bar-Matthews *et al.* 2010) and in the Little Karoo $\delta^{18}O$ record (Braun *et al.* 2012). At all three sites $\delta^{18}O$ is equated with a winter rainfall signal based on the $\delta^{18}O_{calcite}$ estimates of Bar-Matthews *et al.* (2010). From the comparable pattern of $\delta^{18}O$ variation exhibited by all three records it is therefore reasonable to infer that similar winter rainfall conditions were present in these areas at this time.

While $\delta^{18}O$ increases again back towards a higher value of -2.4‰, suggestive of summer rainfall, around 79 ka, between 79 ka and 78 ka $\delta^{18}O$ shows a generally decreasing trend (Fig. 5.21a). During this period, values are between -4.1‰ and -4.3‰ suggesting that more winter rain was falling in the vicinity of the cave during at this time. In the period between 77 ka and 75 ka, $\delta^{18}O$ increases from -3.2‰ *c.* 77 ka to peak at -

2.2‰ *c.* 76 ka before dropping down to -5‰ by 75 ka. For the short interval between 75 ka and 74 ka,, $\delta^{18}O$ tracks changes in $\delta^{13}C$, suggesting that rapid changes in vegetation cover above the cave coincided with changes in local rainfall dynamics. These abrupt, short-term changes in the BL1 $\delta^{18}O$ are not evident in the Crevice Cave $\delta^{18}O$ data or in the smoothed $\delta^{18}O$ record for the Little Karoo. It is not clear whether or not these rapid changes in $\delta^{18}O$ represent real variation in the BL1 isotopic signal. This is explored further in Chapter 6.

Around 73 ka BL1 growth is interrupted by a hiatus which lasted until *c*. 46 ka (Fig. 5.21a). Aragonite corrections were applied to the post-hiatus $\delta^{18}O$ values. These values show a high degree of variation with $\delta^{18}O$ ranging from -3.5‰ up to +1.0‰. At 46 ka, $\delta^{18}O$ peaks at -0.5‰ before declining to a lower value of -2.0‰ around 44 ka. Between 44 ka and 40 ka, $\delta^{18}O$ shows a general increasing trend towards higher values, between 0‰ and +1‰ (Fig. 5.21b). The BL1 $\delta^{18}O$ values for this period are highly variable and similar variability is not shown in coeval records from Pinnacle Point, Sandkraal Cave and the Little Karoo (Braun 2014). Unlike BL1, the Pinnacle Point composite $\delta^{18}O$ record shows fairly stable $\delta^{18}O$ values around -4.0‰ which suggests summer rainfall input, between 52.5 ka and 40 ka. While the Sandkraal Cave record shows a hiatus *c.* 50 ka until *c.* 40 ka, the post-hiatus period between 40 ka and 30 ka shows $\delta^{18}O$ between -2.5‰ and -3.5‰ (Braun 2014) (Fig. 5.21b). These values are also suggestive of ^{18}O input from summer rainfall. Here $\delta^{18}O$ is comparable with Pinnacle Point and significantly lower than the values recorded at BL1. At the inland Little Karoo site there is also a hiatus *c.* 50 ka until 47 ka which is comparable with the one recorded at Sandkraal Cave (Braun 2014). While the Little Karoo $\delta^{18}O$ values for 45 ka increases from -6.0‰ up to -3.5‰, implying a shift from winter to summer rainfall, these values remain lower than BL1.

Between 40 ka and 35 ka, BL1 $\delta^{18}O$ decreases abruptly from +1.0‰ to -3.0‰ before increasing back towards a higher value of -1.5‰ around 35

ka. While $\delta^{18}O$ peaks and dips during this interval the $\delta^{18}O$ values remain within the range of summer rain (after Bar-Matthews *et al.* 2010). By 34 ka, $\delta^{18}O$ is at -1.5‰, still suggestive of more summer rain, but decreases marginally to -2.5‰ by 31 ka (Fig. 5.21b). This latter value is still indicative of summer rain during the terminal growth of BL1.

As a whole, the pattern of stable isotope variation in BL1 is not expressed at either of the other southern Cape sites discussed here. Taken together, these comparative sites exhibit $\delta^{18}O$ values that generally fall within an overlapping range. While the BL1 $\delta^{18}O$ values also suggest a strong summer rainfall input, $\delta^{18}O$ does not fall within the same range of variation. Although an appropriate aragonite correction was applied to BL1, the discrepancy in the $\delta^{18}O$ values possibly relate to the presence of aragonite in the sample. This is because aragonite typically produces more enriched isotope values. While the BL1 $\delta^{18}O$ values indicate a stronger summer rainfall signal in De Hoop relative to Pinnacle Point and the Little Karoo this interpretation is tentative at best. Further comparisons of BL1 with BL3 and BL4, which come from the same cave and are also correlated with MIS 3, will provide further insight. This is discussed in Chapter 6.

5.3.2 BL3 Sample

Hendy Test

For the BL3 stalagmite 53 subsamples were taken for the Hendy Test. These subsamples were taken along growth layers at 31 mm, at 44 mm and at 245 mm (from the top) (Fig. 5.7) and Hendy Test results are illustrated in Figure 5.22 below.

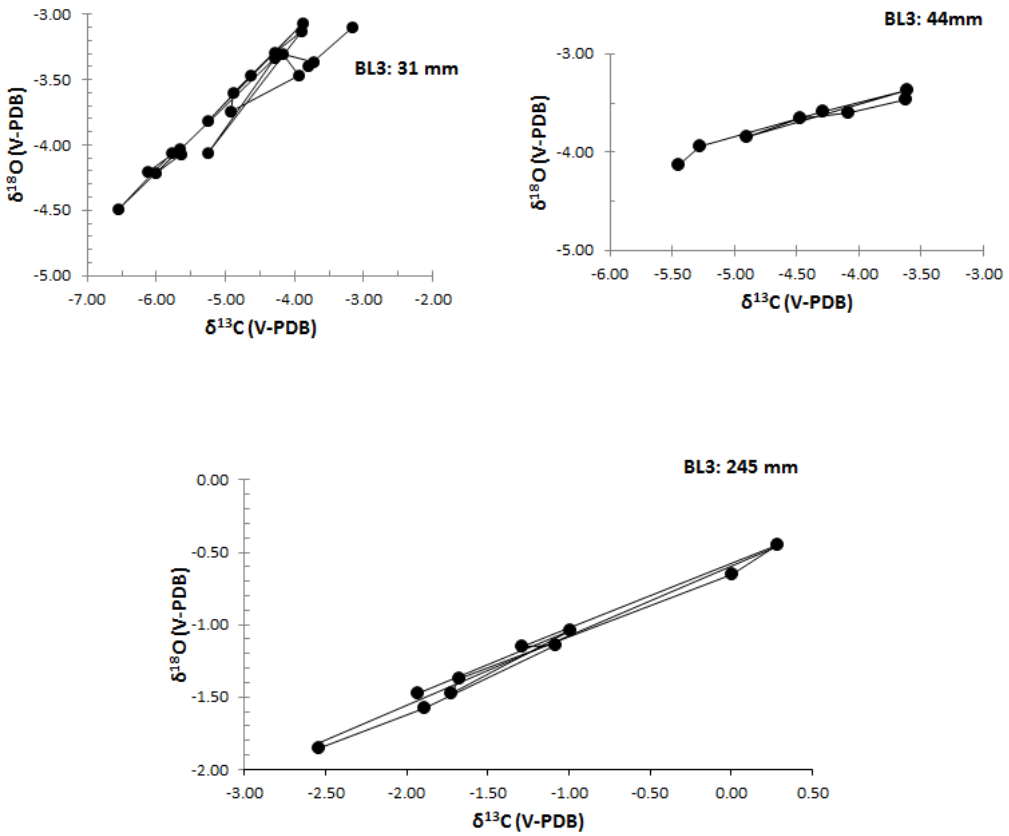

Fig. 5.22 Hendy Test results from the post-hiatus growth layers at 31 mm and 44 mm and at the growth layer at 245 mm in the BL3 stalagmite from Bloukrantz Cave

In the layer at 31 mm there is an increasing trend between $\delta^{18}O$ and $\delta^{13}C$ along the growth lamina which is suggestive of kinetic effects. In contrast the layer at 44 mm does not exhibit this pattern and instead shows a lack of correlation between $\delta^{18}O$ and $\delta^{13}C$. This suggests depositon in isotopic equilibrium and negligible kinetic effects. However, in the layer at 245 mm there is a clear increasing trend between $\delta^{18}O$ and $\delta^{13}C$ that is comparable with the pattern in layer at 31 mm. This suggests that kinetic effects could have occurred in this part of BL3.

Kinetic fractionation is largely caused by cave processes such as cave air temperature, cave ventilation, evaporation and degassing of drips (Tremaine *et al.* 2011; Cuthbert *et al.* 2014). Of these, the two most likely

causes are usually rapid degassing of CO_2 and evaporation from the stalagmite cap (Hendy 1971; Mickler *et al.* 2004, 2006). Under kinetic fractionation conditions the $\delta^{18}O$ data would be an unreliable rainfall and palaeotemperature proxy while the corresponding $\delta^{13}C$ data would be equally contentious.

On the other hand, the pattern between the $\delta^{13}C$ and $\delta^{18}O$ data can also be influenced by common environmental factors. Some of the environmental factors that could fractionate the ^{18}O and ^{13}C isotopes include changes in climate, hydrological changes in the amount and type of precipitation and soil productivity (White 2004, 2007). At this stage, it is not clear if the correlation between the $\delta^{18}O$ and $\delta^{13}C$ results are caused by kinetic or climatic factors. However since there are other stalagmites of similar age available from the Bloukrantz Cave (BL1, BL3 & BL4) comparing these records may help resolve the conflict (See Chapter 6).

Overall, the Hendy Test results for BL3 therefore suggest that the BL3 stalagmite was likely deposited under non-equilibrium conditions. <EXPAND>

Carbon isotope analyses

Based on the stratigraphy of BL3 a major hiatus or several hiatuses possibly occurs around 45 ka with growth resuming much later by *c.* 5 ka. However, because the U-Th ages in the younger post-hiatus section of the stalagmite have poor resolution a chronology cannot be established for the stable isotope results coming from this section of BL3 (see discussion in 5.2.2 for details). The focus instead shifted towards those regions in the base of the stalagmite with relatively precise, high-resolution U-Th ages. This region of BL3 dates between 47.5 ka and 46.5 ka and the stable isotope data provides a remarkably high resolution record for this 1000 year period (Fig. 5.23).

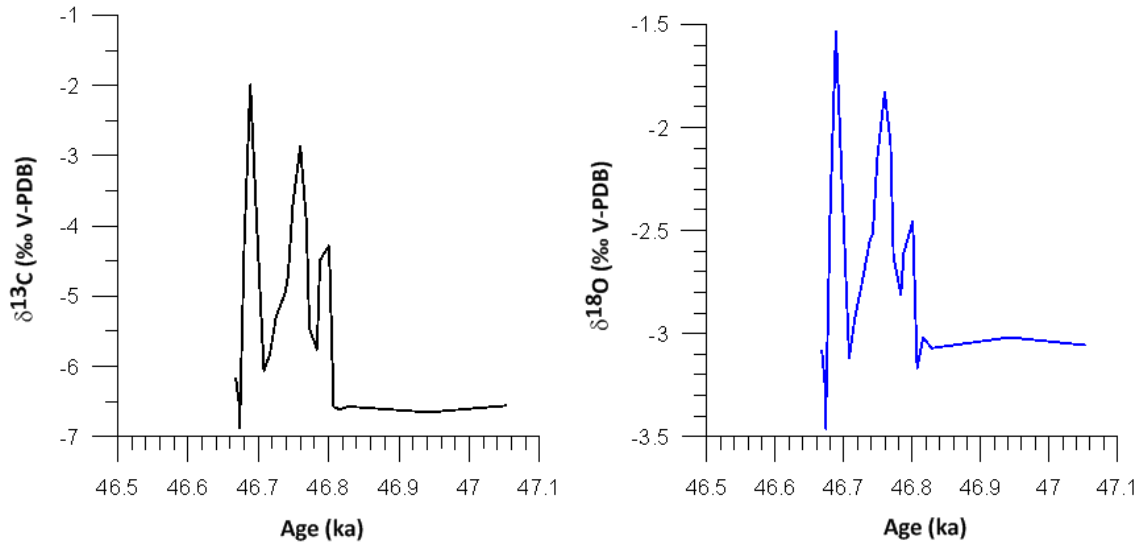

Fig. 5.23 $\delta^{13}C$ and $\delta^{18}O$ isotope age curve for the older part of the BL3 stalagmite.

The $\delta^{13}C$ signal in the older part of BL3 is fairly stable around -6.5‰ in the 250 years between 47.06 ka and 46.82 ka (Fig. 5.23). Based on Talma and Vogel's (1992) estimates this equates to an input of around 45% from C_4 vegetation (as discussed above in section 5.3). In other words this suggests a constant input from a strongly C_3/C_3-like CAM signal into the calcite at this time. Shortly after, around 46.8 ka, there is an abrupt jump towards a heavier value of -4.5‰ which equates to a strong input of up to 60% from C_4-type vegetation. By 46.78 ka, there is a minor decrease to a lower value of -5.8‰ that is followed by an increase towards a higher value of -2.8‰ by 46.76 ka. Between 46.76 ka and 46.7 ka, $\delta^{13}C$ decreases rapidly down to a lower value of -6‰ before increasing again to peak at -2‰ around 46.68 ka. These higher values fall outside Talma and Vogel's (1992) range of variation for $\delta^{13}C$. However, based on their estimates $\delta^{13}C$ values above -3.0‰ would equate to a 70% input from C_4 plants. After 46.68 ka, $\delta^{13}C$ decreases abruptly again towards a lower value of -6.9‰ by 46.67 ka. This value falls within the modern baseline for $\delta^{13}C$ in the Cango Valley and equates to a 40% contribution from C_4 plants (Cowling 1983a, b; Talma & Vogel 1992). Based on this trend it seems

that there was a decrease in the input from C_4 plants from 70% down to 40% during the terminal growth of BL3 (Fig. 5.23).

Overall the $\delta^{13}C$ record for BL3 shows that rapid changes in $\delta^{13}C$ took place within a short period of time (*c.* 1 ka) (Fig. 5.23). The peaks and dips observed in the $\delta^{13}C$ signal most probably indicate abrupt changes in the relative representation of C_3, C_4 and CAM vegetation above the cave through time in this period. Throughout the period when this section of BL3 was forming conditions at the surface seem to have shifted dramatically within several hundred years in favour of either C_4/CAM or C_3 type plants. Conditions favourable for C_4/CAM plants appear to have lasted for only brief periods at a time and conditions favouring C_3 plants were possibly of equally short duration. It is tempting interpret the rapid changes in $\delta^{13}C$ in terms of vegetation changes but the possible influence of kinetic enrichment inferred from the Hendy Test results may also be important. The BL3 $\delta^{13}C$ results and potential kinetic effects are further discussed in Chapter 6 in the context of coeval speleothem records available from Pinnacle Point (Braun 2014), Cango Cave (Talma & Vogel 1992) and Sandkraal Cave (Braun 2014).

Oxygen isotope analyses

Variations in the $\delta^{18}O$ signal for the older part of BL3 exhibit similar trends to those observed in the $\delta^{13}C$ record. For the period between 47.06 ka and 46.82 ka $\delta^{18}O$ shows no variation around -3.1‰ (Fig. 5.23). This suggests that rainfall and temperature were potentially stable during this part of the BL3 sequence.

Around 46.8 ka, $\delta^{18}O$ peaks at -2.5‰ that is suggestive of an increase in summer rainfall influence. While there is a minor decrease in $\delta^{18}O$ to -2.8‰ by 46.78 ka, $\delta^{18}O$ peaks again at a higher value of -1.9‰ by 46.76 ka. Between 46.76 ka and 46.7 ka, $\delta^{18}O$ shows a decreasing trend towards a lower value of -3.2‰ which falls within the range of summer rain

(after Bar-Matthews *et al.* 2010). This value is also comparable with the present-day $\delta^{18}O$ of -3.0‰ for MAP in the southern Cape as a whole, and might be suggestive of a shift to year round rainfall conditions at this time (discussed further in Chapter 6). Around 46.68 ka, $\delta^{18}O$ peaks abruptly at -1.5‰. Here a strong summer rainfall component is inferred based on Bar-Matthews *et al.*'s (2010) $\delta^{18}O_{calcite}$ data that indicates that warm rain was present at this time. By 46.67 ka, $\delta^{18}O$ decreases rapidly again towards a lower value of *c.* -3.5‰ which still falls within the theoretical range of summer rain although this value might potentially reflect increases in year round rainfall (as discussed in section 5.3 above) (Fig. 5.23). As a whole, $\delta^{18}O$ in BL3 show abrupt short-term changes which could be related to shifts in the rainfall dynamics above the cave.

Comparative $\delta^{13}C$ and $\delta^{18}O$ data comes from the BL4 stalagmite (further discussed below). How the $\delta^{18}O$ data from this study compare to results from other southern Cape speleothems is discussed further in Chapter 6. These speleothems are from Pinnacle Point, Sandkraal Cave, the Little Karoo and Cango Cave (Talma & Vogel 1992; Bar-Matthews *et al.* 2010; Braun *et al.* 2012; Braun 2014).

5.3.3 BL4 Sample

Hendy Test

For the BL4 stalagmite 52 subsamples were taken for the Hendy Test. These subsamples were taken along growth layers at 244 mm and 370 mm (from the top) (Fig. 5.24). In the Hendy Test layer at 244 mm there is an increasing trend between $\delta^{18}O$ and $\delta^{13}C$ suggestive of kinetic effects with a similar trend reflected in the layer at 370 mm where ^{18}O and ^{13}C increasing in concert along the growth lamina. Overall, for BL4 the Hendy Test results indicate non-equilibrium deposition, most likely due to kinetic

effects, with a pattern that is consistent with the the Hendy Test data from the BL3 sample. The implication of this is that at least part of these isotopic records would not be reliable and thus unsuitable for making inferences about past environmental conditions. However, as discussed previously in Chapter 3 section 3.3.2, the Hendy Test may not be an accurate indicator of non-equilibrium deposition of speleothem calcite. As per the Replication Test, corroborating evidence from other southern Cape speleothems and similar trends between coeval parts of the BL3 and BL4 isotopic records should help clarify this. Further discussion follows in Chapter 6.

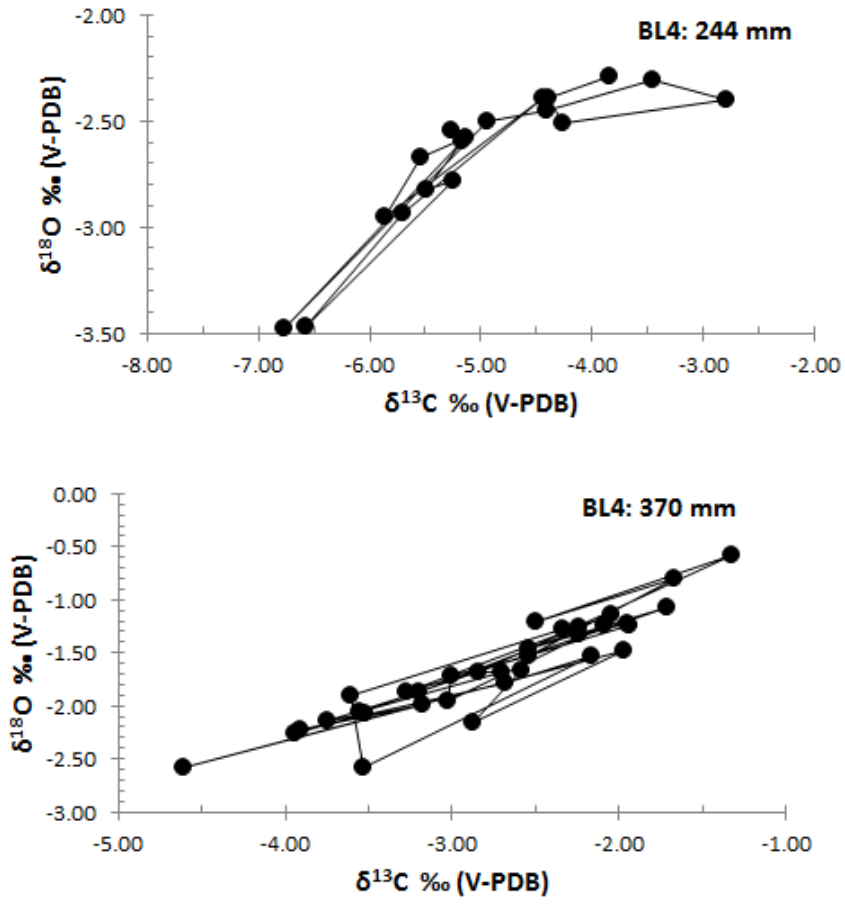

Fig. 5.24 Hendy Test results from the growth layers at 244 mm and 370 mm in the BL4 stalagmite at Bloukrantz Cave.

Carbon isotope analyses

The $\delta^{13}C$ signal from BL4 provides a sequence of environmental change from 59 ka to 34 ka (Fig. 5.25). This data shows rapid changes in isotopic variability throughout the period although general trends are also evident.

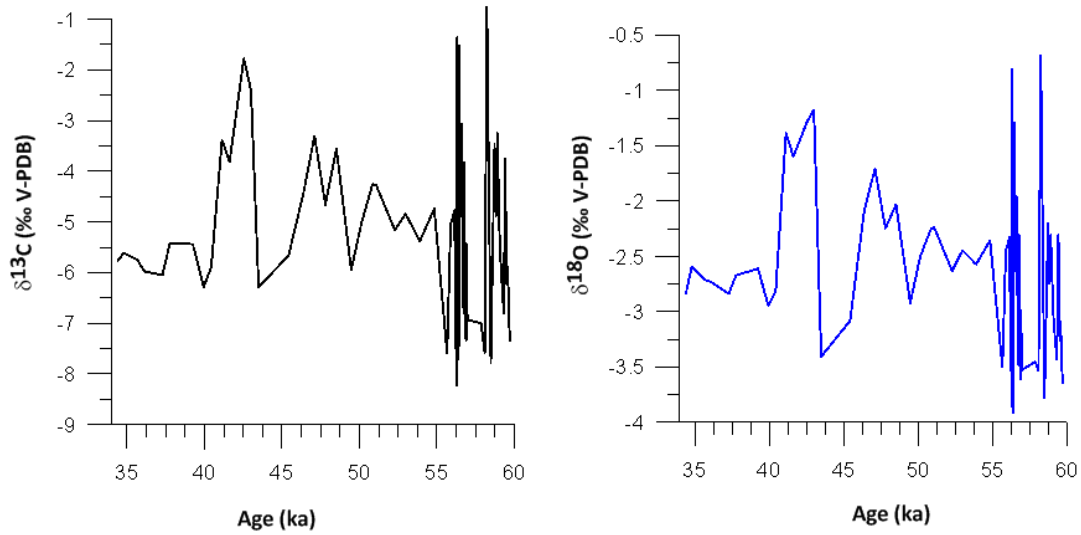

Fig. 5.25 $\delta^{13}C$ and $\delta^{18}O$ isotope age curve for the BL4 stalagmite

Oxygen isotope analyses

The $\delta^{18}O$ signal for the BL4 fragment (Fig. 5.25) is shows a similar pattern to the one observed for $\delta^{13}C$. Between 59 ka and 55 ka, $\delta^{18}O$ tracks changes in $\delta^{13}C$ with values between -0.5‰ and -3.9‰ which suggests rapid changes in local rainfall dynamics at this time. These values fall within the range of summer (-3‰ to -2‰) and winter rain (-4‰ to -5‰) (after Bar-Matthews *et al.* 2010).

These highly variable $\delta^{18}O$ values coupled with the corresponding peaks and dips in the $\delta^{13}C$ values point to a transition episode characterised by unstable environmental conditions. Between 55 ka and 47 ka, $\delta^{18}O$ follows an increasing trend towards higher values from -2.5‰ up to -2.75‰

around 50 ka (Fig. 5.25). This possibly reflects increases in precipitation derived from summer sources (after Bar-Matthews *et al.* 2010). Generally higher values occurring in this part of the BL4 sequence suggests warm conditions possibly with increases in summer rain or year round rainfall (see discussion in section 5.3). While $\delta^{18}O$ decreases to a lower value of -3‰ by 49 ka, still within the summer rainfall range of Bar-Matthews *et al.* (2010), values peak at -1.75‰ by 47 ka. By 45 ka, $\delta^{18}O$ has declined towards lower values to reach -3.75‰, before increasing rapidly to values between -1.25‰ and -1.5‰ around 42 ka. Based on Bar-Matthews *et al.*'s (2010) range of $\delta^{18}O_{calcite}$ variation this suggests a weak shift from winter to increasing summer component rain. After 42 ka, $\delta^{18}O$ decrease again to a lower value of -3‰ (Fig. 5.25). Between 40 ka and 34 ka, $\delta^{18}O$ in BL4 shows minor variations around a marginally lower value of -2.75‰ which possibly indicates an increase in either summer or year round rainfall.

In Chapter 6 the BL4 isotope data are discussed further in comparison to coeval stalagmite records available from Pinnacle Point (Braun 2014), Sandkraal Cave (Braun 2014) and Cango Cave (Talma & Vogel 1992).

5.3.4 KDS Sample

Hendy Test

In each of the Hendy Test lamina at 23 mm and 36 mm (from the top) there is a general increasing trend in $\delta^{18}O$ and $\delta^{13}C$ which indicates an influence of kinetic effects which suggests that the stalagmite could have been deposited under non-equilibrium conditions.

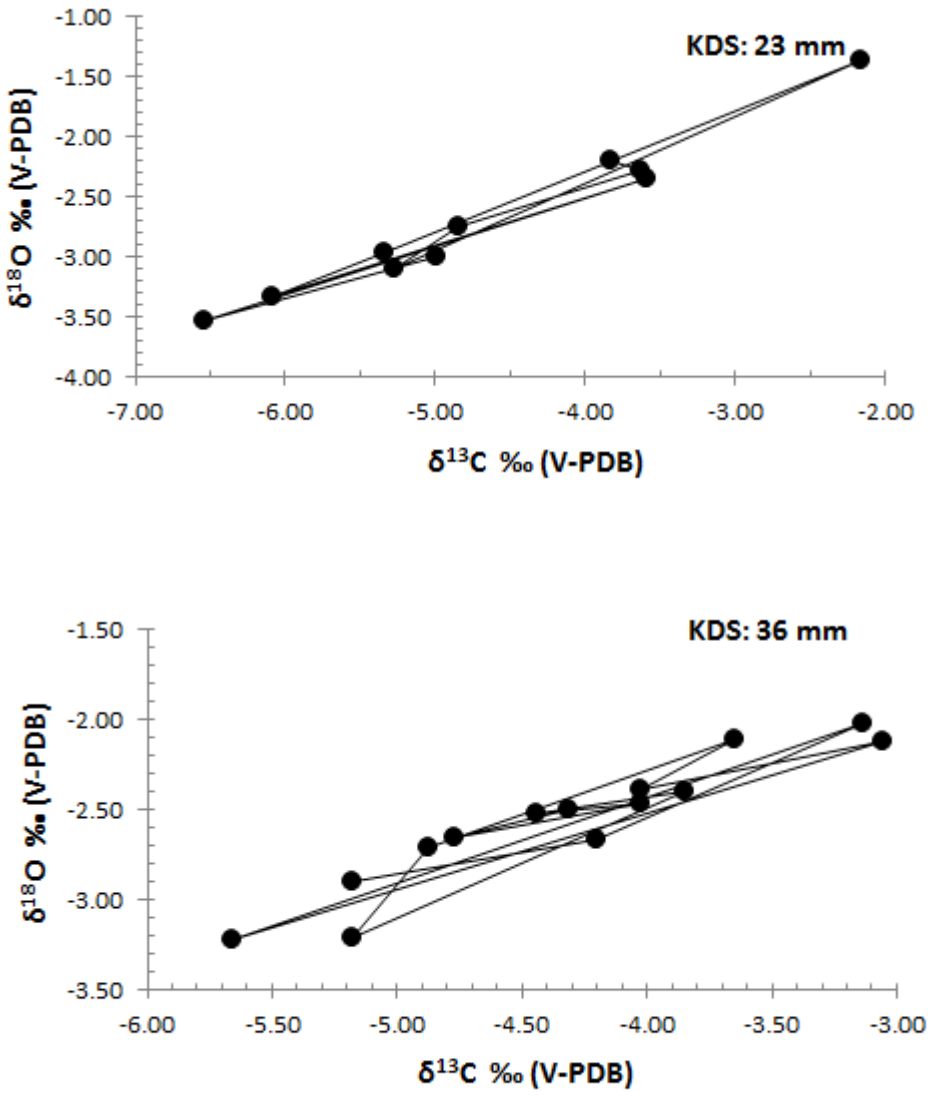

Fig. 5.26 Hendy Test results from the growth layers at 23 mm and 36 mm in the KDS stalagmite at Klipdrift Shelter.

Carbon isotope analyses

Between 69.4 ka and 69.2 ka $\delta^{13}C$ shows an increasing trend towards higher values with a high amplitude peak in $\delta^{13}C$ at -4‰ (Fig. 5.27). This value equates to a 60% input from C_4 vegetation.

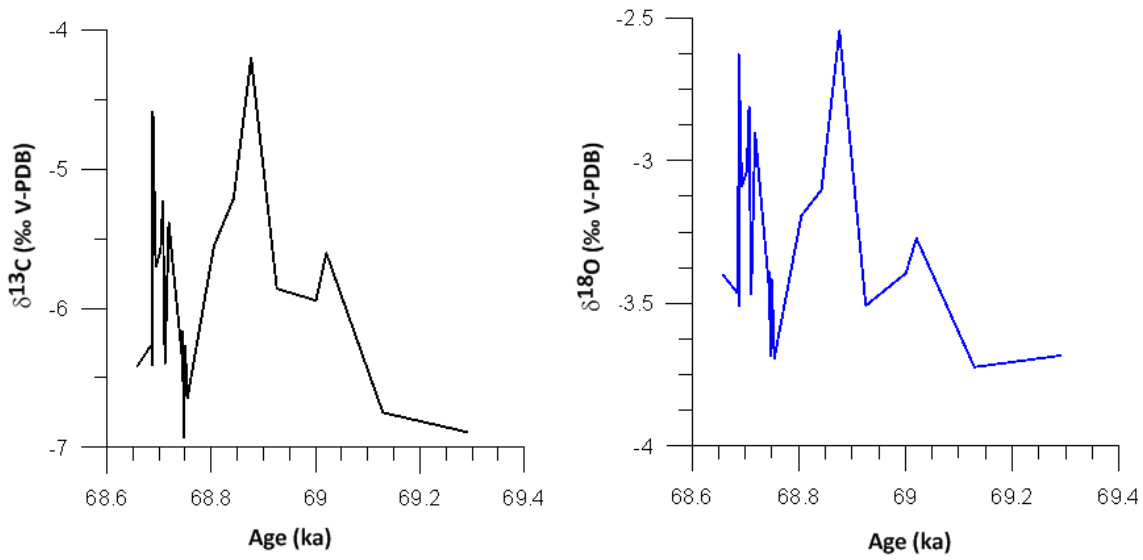

Fig. 5.27 $\delta^{13}C$ and $\delta^{18}O$ isotope age curve for the KDS stalagmite.

An alternative explanation is that the higher values are in part influenced by kinetic enrichment effects (inferred from the Hendy Test results). Kinetic fractionation processes such as evaporation may in turn be related to a decrease in vegetation cover above the cave. In this scenario evaporation from the soil could cause an increase in CO_2 uptake from the atmosphere and produce calcite that is more enriched in ^{13}C (Hölzkamper *et al.* 2009).

After the high amplitude shift to more positive (higher) values there is a sudden drop in $\delta^{13}C$ down to -7‰ which Talma and Vogel (1992) equates to a 40% contribution from C_4 vegetation. In other words this may indicate an abrupt shift in conditions favourable to C_3 type vegetation such as high water availability, low salinity and mild temperatures (Shah 1998). After 69ka there is a gradual increasing trend towards more positive values until *c.* 68.9ka when there is a slight dip from -5.5‰ to -6.5‰. Based on Talma and Vogel's (1992) estimates these $\delta^{13}C$ values indicate inputs from C_4 vegetation component between 55% and 45%. By 68.8 ka $\delta^{13}C$ values are increasing incrementally up to -4.5‰ by *c.* 68.7 ka (Fig. 5.27). This suggests an increase in the relative proportion of C_4 and possibly CAM plants above the cave at this time. After 68.7 ka there is a small amplitude dip in $\delta^{13}C$ from -4.5‰ down to -6.5‰ which is still within the range of C_4

determined by Talma and Vogel (1992). Between 68.7 ka and 68.6 ka $\delta^{13}C$ values occur within a fairly tight range hovering just between -5.5‰ and -6.5‰ which equates to a shift in C_4 type vegetation of up to 45% (Talma & Vogel 1992). Overall the $\delta^{13}C$ signal appears to be highly variable with rapid changes occurring over a very short period of time between 69.4 ka and 68.6 ka.

Oxygen isotope analyses

The trend observed in the $\delta^{13}C$ signal is reflected in the $\delta^{18}O$ signal although the magnitude of these isotopic shifts is not as strong. From 69.4 ka to 69.2 ka there is a trend towards more positive (higher) $\delta^{18}O$ values from -3.7‰ with a jump in $\delta^{18}O$ up to -2.5‰ by 69.2 ka (Fig. 5.27). According to Bar-Matthews *et al.*'s (2010) range of variation for $\delta^{18}O$ this may indicate a shift towards warm conditions with summer rain.

After 69 ka there is a downward trend towards relatively lower $\delta^{18}O$ values around -3.7‰ which may indicate a slight dip in ^{18}O input from summer rainfall. This is followed by a gradual increase towards more positive values from -3.7‰ up to -2.9‰ between 69.1 ka and *c.* 68.9 ka which reflects warmer conditions with more seasonal summer rain (Fig. 5.27). After 68.9 ka there is a small amplitude dip in $\delta^{18}O$ to -3.5‰ followed almost immediately by an increase in $\delta^{18}O$ up to -2.8‰ with a minor dip in $\delta^{18}O$ just after 68.8 ka. These minor dips still fall within the range of summer rain determined by Bar-Matthews *et al.* (2010) and may suggest that inputs from summer rain persisted throughout this period. $\delta^{18}O$ peaks at -2.4‰, which falls within the range of summer rain, before dipping down to -3.5‰ around 68.7 ka (Fig. 5.27). After this time the $\delta^{18}O$ values lie between -3.5‰ and -2.9‰. Based on Bar-Matthews *et al.*'s (2010) data this translates into a summer rainfall signal.

Overall the $\delta^{18}O$ signal observed in the KDS stalagmite is highly variable with shifts between high and low values occurring throughout (Fig. 5.27).

Rapid peaks and dips in $\delta^{18}O$ is strongly correlated with changes in $\delta^{13}C$ which suggests a shared response to changing environmental conditions. An interpretation of both isotopic signals is however complicated by the presence of presumed kinetic effects and will be discussed further in a broader palaeoenvironmental context in Chapter 7.

5.3.5 KDC 5 Sample

Hendy Test

For the KDC5 stalagmite ten Hendy Test subsamples were taken along a single growth layer at 22 mm (from the top) (Fig. 5.28). The Hendy Test data indicates a strong monotonic relationship between $\delta^{18}O$ and $\delta^{13}C$ which suggests a clear influence by kinetic processes. The most likely processes are usually rapid degassing which causes enrichment in both ^{13}C and ^{18}O or evaporation from the stalagmite cap which causes enrichment in ^{18}O relative to ^{13}C (Hendy 1971; Mickler *et al.* 2004, 2006). In this instance both processes may be possible.

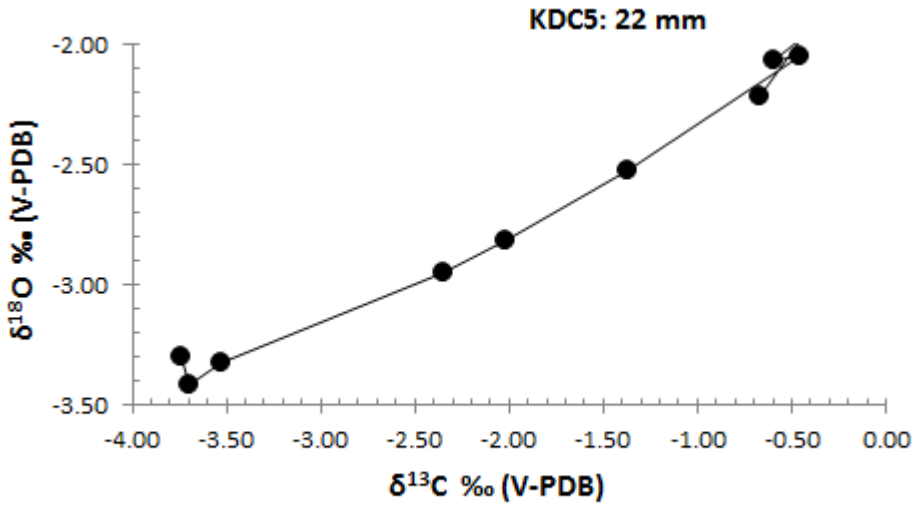

Fig. 5.28 Hendy Test result from the growth layer at 22 mm in the KDC5 stalagmite at Klipdrift Cave.

Carbon isotope analyses

Between 13.8 ka and 12.8 ka $\delta^{13}C$ values show minor fluctuations in the range of -4‰ to -2.5‰ (Fig. 5.29). Based on Talma and Vogel's (1992) estimates this $\delta^{13}C$ signal reflects a strong input from C_4 vegetation above the cave.

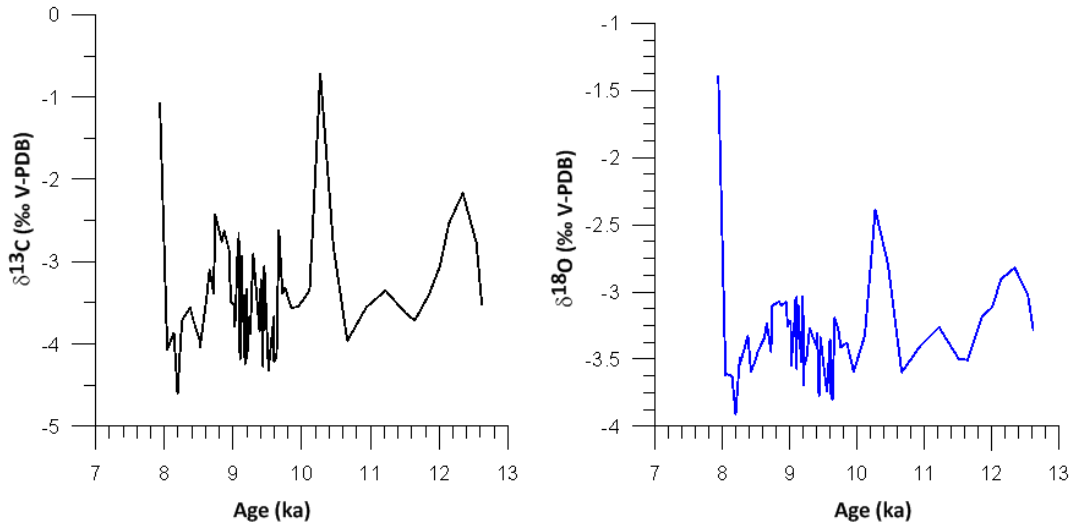

Fig. 5.29 $\delta^{13}C$ and $\delta^{18}O$ isotope age curve for the KDC5 stalagmite.

Around 12.4ka there is a high amplitude jump in $\delta^{13}C$ up to -0.5‰ which equates to a significant input from C_4 type vegetation (Fig. 5.29). This suggests either an abrupt transition to a significantly strong C_4/CAM signal or a sudden decrease in vegetation above the cave which can also be influenced by kinetic effects. Although this shift in the $\delta^{13}C$ isotopic signal can be explained by inputs from different factors it appears that significant changes in environmental conditions took place around 12.4 ka. This rapid shift towards more positive $\delta^{13}C$ values may strongly correlate with other regional episodes of climate change documented for the Pleistocene-Holocene boundary (Parkington 1987; Deacon 1995; Mitchell *et al.* 1998; Scott & Lee-Thorp 2004; Roberts 2013). After the onset of the inferred transition episode the $\delta^{13}C$ values are fairly stable. During this period from 11.7 ka to 8.6 ka there are only minor fluctuations in the range between *c.*

-3.7‰ and -3‰. This range indicates a predominant input from C_4/CAM plants into the $\delta^{13}C$ signal of the calcite with an estimated contribution from C_4/CAM of up to 75%. Between 8.6 ka and 8 ka there is a weak decreasing trend towards $\delta^{13}C$ values between -2.5‰ and -4.5‰. These values fall outside the Holocene range of $\delta^{13}C$ variation reported for the Cango Cave stalagmite (Talma & Vogel 1992). The peak in $\delta^{13}C$ up to -1‰ is thought to mark the end of the sequence and does not reflect real variation (Fig. 5.29).

Overall the $\delta^{13}C$ signal in the KDC5 stalagmite provides a record of isotopic variability from 13.8 ka to 7.8 ka. A sudden jump to higher values *c.* 12.4 ka may indicate a transition episode that coincides with the Pleistocene-Holocene boundary. After 12.4 ka $\delta^{13}C$ values are relatively uniform and fall within the range of C_4 and C_3-like CAM plants. This suggests environmental conditions were fairly stable throughout the period between 12.4 ka and 7.8 ka.

Oxygen isotope analyses

Isotopic variability observed in the $\delta^{18}O$ signal follow a similar trajectory to those observed in the $\delta^{13}C$ signal although the magnitude of the shifts are much smaller (<1‰). Between 13.8 ka and 13 ka $\delta^{18}O$ values show minor fluctuations around the modern $\delta^{18}O$ MAP value of -3‰ (http://www.iaea.org/water) (Fig. 5.29). This value equates to a summer rainfall signal based on the theoretical range adopted from Bar-Matthews *et al.*'s (2010) $\delta^{18}O$ data. A peak in $\delta^{18}O$ to -2.3‰, which could indicate warm summer rain, marks the onset of a transition that may represent the Pleistocene-Holocene boundary. After this episode the $\delta^{18}O$ values show little variation with only minor deviations between -3.7‰ and -2.9‰ with an average of 3.3‰ for the period from 11.8 ka to 8.4 ka. This range of $\delta^{18}O$ values which fluctuate between -3.7‰ and -2.9‰ straddles the range of $\delta^{18}O$ variation associated with winter (-4‰ to -5‰) and summer (-3‰ to -2‰) rain of Bar-Matthews *et al.* (2010) and Braun (2014). This suggests,

at least superficially, that between 11.8 ka and 8.4 ka present-day rainfall conditions could have been present at this time (Fig. 5.29).

5.4 West Cave and Klipdrift Sea Cave dripwater isotopic values

5.4.1 Dripwater $\delta^{18}O$

At West Cave eight drip sites were initially selected for water collection (discussed in Chapter 3 section 3.3.5). The water samples for WCD3 to WCD5 and WCD7 was however lost during transit from South Africa to the laboratory in Norway. For this reason there are no $\delta^{18}O$ dripwater, calcite data or temperature estimates from these localities. The $\delta^{18}O$ content for the dripwater ($\delta^{18}O_w$) and calcite ($\delta^{18}O_c$) of the remaining dripwater sites at West Cave is reported relative to V-PDB and summarised in Table 5.6. Across all the drip sites in West Cave $\delta^{18}O_w$ is highly variable with values from -31.8‰ to -28.5‰ (Table 5.6). The corresponding $\delta^{18}O_c$ content shows similar variability with values from -1.12‰ up to +0.04‰.

At Klipdrift Sea Cave, seven drip water sites were initially setup but at the end of the sampling period, there was insufficient data from KDCD1 and KDCD7. As a result, the $\delta^{18}O$ dripwater and calcite data from the remaining sites was retained and used to determine the temperature estimates. The $\delta^{18}O$ content of the dripwater ($\delta^{18}O_w$) and calcite ($\delta^{18}O_c$) for the Klipdrift Sea Cave samples are reported relative to V-PDB and summarised in Table 5.7. The data from Klipdrift Sea Cave shows a similar pattern of variability to that observed at West Cave with $\delta^{18}O_w$ between -32.4‰ and -24.3‰ (Table 5.7). The associated $\delta^{18}O_c$ tracks changes in $\delta^{18}O_w$ with values from -2.86‰ up to +1.46‰.

As a whole, the Klipdrift Sea Cave data exhibits the same variability in both $\delta^{18}O_w$ and $\delta^{18}O_c$ as West Cave. This implies that similar in-cave

processes are influencing the $\delta^{18}O$ dripwater and calcite ($\delta^{18}O$ & $\delta^{13}C$) signals at these two sites. The XY plots of recent calcite from both West Cave (Fig. 5.30) and Klipdrift Sea Cave (Fig. 5.31) in part support this inference. Each plot shows the extent of $\delta^{18}O$ and $\delta^{13}C$ variation within each cave. The main variables contributing to this in-cave variability are variable drip rates, cave ventilation and kinetic fractionation effects. Based on the linear trend these effects appear to be significant in both West Cave and Klipdrift Sea Cave. The implication is that recent calcite, at least from these two caves, might not be preserving a $\delta^{18}O$ signal that can be precisely correlated with rainfall and temperature conditions above the cave. This is explored further in the temperature reconstruction sub-section below.

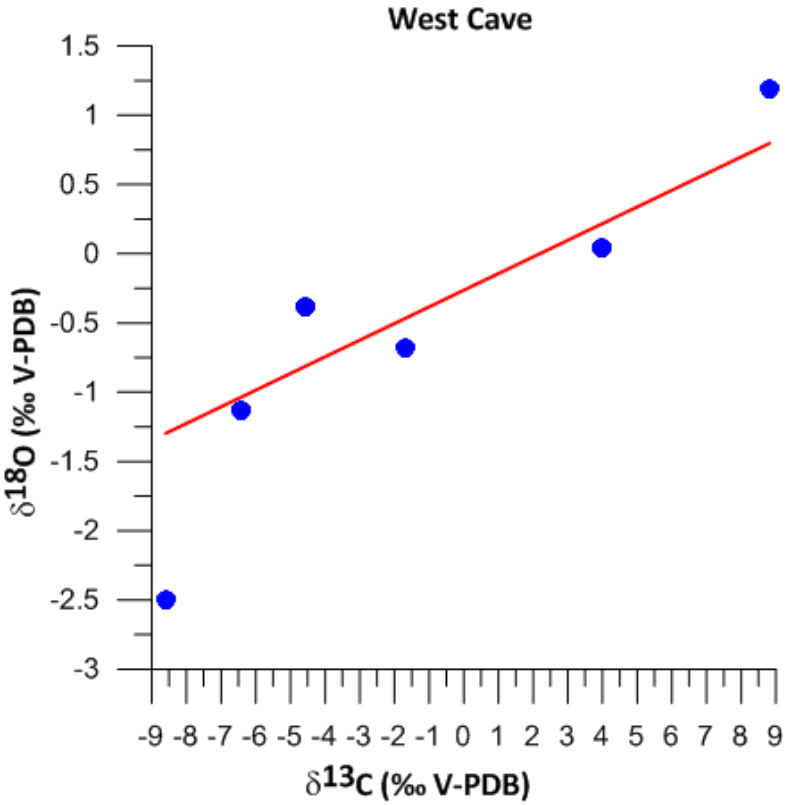

Fig. 5.30 $\delta^{18}O$ and $\delta^{13}C$ plot of recent calcite from four of the eight drip locations (WCD1, WCD2, WCD6 & WCD8) inside West Cave. This plot also includes multiple or replicate samples from single drip locations such as WCD2 & WCD8

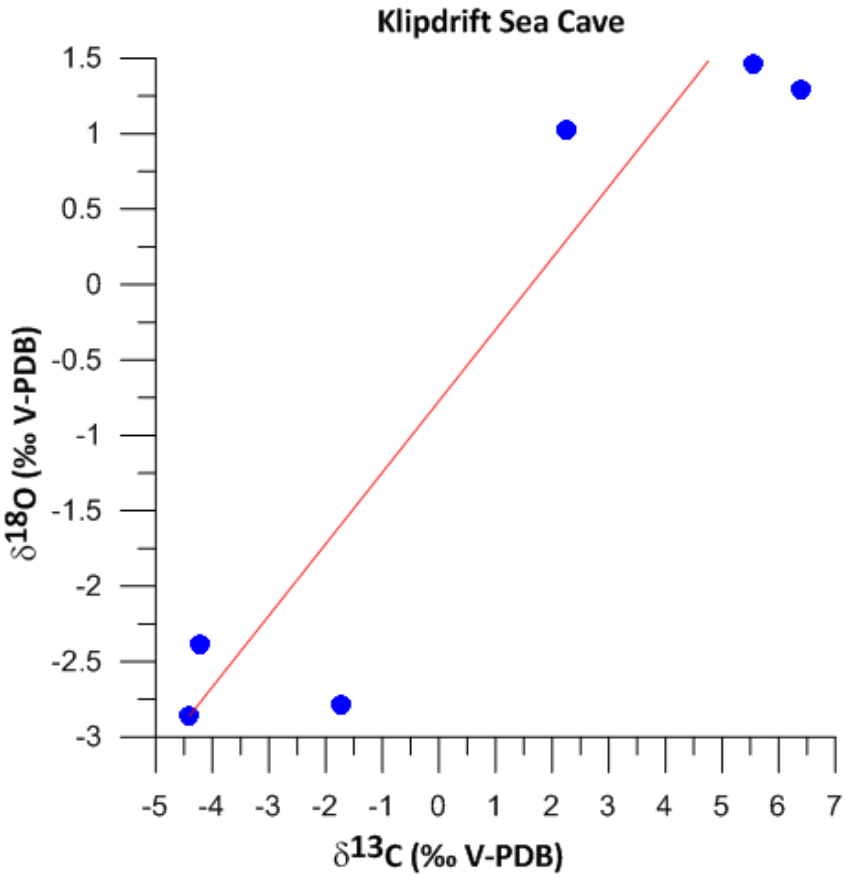

Fig. 5.31 $\delta^{18}O$ and $\delta^{13}C$ plot of recent calcite sampled at six different drip locations inside Klipdrift Sea Cave

Table 5.6 Summary of the dripwater and stalactite tip data collected for the West Cave samples collected during the 12-month sampling period from February 2012 to March 2013. The calculated temperatures (ºC) are also shown. Extreme temperature values, that are very clearly incorrect, were also obtained and these are highlighted in grey.

Sample ID	Sampling Interval (mm/yy)	Sampling Season	Sample Collection (mm/yy)	$\delta^{13}C_c$ (‰ V-PDB)	$\delta^{18}O_c$ (‰ V-PDB)	$\delta^{18}O_w$ (‰ V-SMOW)	$\delta^{18}O_w$ (‰ V-PDB) (Converted)	Temperature (ºC)
WCD1	Feb-12-Apr-12	Autumn	May-12	-6.42	-1.13	-1.82	-31.05	17.0
WCD2	Feb-12-Apr-12	Autumn	May-12	-4.56	-0.38	-1.11	-30.36	16.8
WCD1	May-12-July-12	Autumn/Winter	Aug-12	-6.42	-1.13	0.72	-28.58	29.8
WCD2	May-12-July-12	Autumn/Winter	Aug-12	-4.56	-0.38	-0.34	-29.61	20.6
WCD2	May-12-July-12	Autumn/Winter	Aug-12	-4.56	-0.38	0.008	-29.27	22.3
WCD8	May-12-July-12	Autumn/Winter	Aug-12	3.97	0.04	-0.13	-29.41	19.5
WCD8	May-12-July-12	Autumn/Winter	Aug-12	3.97	0.04	-0.55	-29.81	17.5
WCD8	May-12-July-12	Autumn/Winter	Aug-12	3.97	0.04	-0.07	-29.34	19.9
WCD1	Aug-12-Oct-12	Late Winter/Early Spring	Nov-12	-6.42	-1.13	-2.65	-31.85	13.1
WCD1	Aug-12-Oct-12	Late Winter/Early Spring	Nov-12	-6.42	-1.13	-2.25	-31.46	14.9
WCD2	Aug-12-Oct-12	Late Winter/Early Spring	Nov-12	-4.56	-0.38	-0.65	-29.91	19.1
WCD2	Aug-12-Oct-12	Late Winter/Early Spring	Nov-12	-4.56	-0.38	-0.55	-29.82	19.6
WCD8	Aug-12-Oct-12	Late Winter/Early Spring	Nov-12	3.97	0.04	-1.74	-30.97	11.8
WCD8	Aug-12-Oct-12	Late Winter/Early Spring	Nov-12	3.97	0.04	-1.87	-31.10	11.2
WCD8	Aug-12-Oct-12	Late Winter/Early Spring	Nov-12	3.97	0.04	-1.75	-30.98	11.8
WCD2	Dec-12-Feb-13	Summer	Mar-13	-4.56	-0.38	-3.34	-32.52	6.5
WCD6	Dec-12-Feb-13	Summer	Mar-13	-8.60	-2.50	-1.37	-30.61	26.1
WCD8	Dec-12-Feb-13	Summer	Mar-13	3.97	0.04	-3.01	-32.20	6.1

Table 5.7 Summary of the dripwater and stalactite tip data for the Klipdrift Sea Cave samples collected during the 12-month sampling period from February 2012 to March 2013. The calculated temperatures (°C) are also shown**.** Extreme temperature values, that are very clearly incorrect, were also obtained and these are highlighted in grey.

Sample ID	Sampling Interval (mm/yy)	Sampling Season	Sample Collection (mm/yy)	$\delta^{13}C_c$ (‰ V-PDB)	$\delta^{18}O_c$ (‰ V-PDB)	$\delta^{18}O_w$ (‰ V-SMOW)	$\delta^{18}O_w$ (‰ V-PDB) (Converted)	Temperature (°C)
KDCD3	Feb-12-Apr-12	Autumn	May-12	6.38	1.29	-1.00	-30.25	9.6
KDCD4	Feb-12-Apr-12	Autumn	May-12	2.24	1.02	0.56	-28.74	18.2
KDCD6	Feb-12-Apr-12	Autumn	May-12	-1.74	-2.79	-3.10	-32.28	18.9
KDCD4	May-12-July-12	Autumn/Winter	Aug-12	2.24	1.02	5.08	-24.35	41.8
KDCD4	May-12-July-12	Autumn/Winter	Aug-12	2.24	1.02	5.07	-24.36	41.7
KDCD6	May-12-July-12	Autumn/Winter	Aug-12	-1.74	-2.79	1.29	-28.03	42.0
KDCD4	Aug-12-Oct-12	Late Winter/Early Spring	Nov-12	2.24	1.02	2.44	-26.91	27.6
KDCD4	Aug-12-Oct-12	Late Winter/Early Spring	Nov-12	2.24	1.02	2.47	-26.89	27.7
KDCD4	Aug-12-Oct-12	Late Winter/Early Spring	Nov-12	2.24	1.02	1.86	-27.47	24.6
KDCD5	Aug-12-Oct-12	Late Winter/Early Spring	Nov-12	-4.21	-2.38	-0.92	-30.17	27.8
KDCD5	Aug-12-Oct-12	Late Winter/Early Spring	Nov-12	-4.21	-2.38	-0.92	-30.18	27.8
KDCD6	Aug-12-Oct-12	Late Winter/Early Spring	Nov-12	-1.74	-2.79	-3.30	-32.47	17.9
KDCD2	Dec-12-Feb-13	Summer	Mar-13	-4.41	-2.86	-0.13	-29.41	34.6
KDCD3	Dec-12-Feb-13	Summer	Mar-13	6.38	1.29	-0.95	-30.20	9.8
KDCD4	Dec-12-Feb-13	Summer	Mar-13	2.24	1.02	1.04	-28.27	20.5
KDCED1	May-12-July-12	Autumn/Winter	Aug-12	0.76	-1.64	5.29	-24.15	58.9
KDCED2	Feb-12-Apr-12	Autumn	May-12	-0.54	-1.99	-0.35	-29.62	28.7

5.4.2 Temperature reconstructions

As discussed in Chapter 3 section 3.3.6, the oxygen isotope fractionation that occurs between calcite and its corresponding dripwater is thought be temperature dependent. Since the use of $\delta^{18}O$ as a palaeothermometer depends on the equilibrium deposition of calcite with its dripwater(s), this relationship between temperature, calcite ($\delta^{18}O_c$) and water ($\delta^{18}O_w$) has previously been modelled empirically and experimentally (Fairchild & Baker 2012). Demény *et al.* (2010) have produced the most recent equations to represent the temperature dependent calcite-water oxygen isotope fractionation for carbonates including stalagmites at 10^{o}C to 25^{o}C. This equation, which is shown below, is preferred here because it is based on stalagmites that show positive correlations between $\delta^{18}O$ and $\delta^{13}C$ (suggestive of kinetic fractionation) as well as those that do not exhibit correlations between carbon and oxygen (suggestive of equilibrium deposition)

$$1000 \ln \alpha = 17.5 (1000/T) - 29.89$$

In the context of the current study on the De Hoop speleothems where there appears to be a clear trend in $\delta^{18}O$ and $\delta^{13}C$ that may indicate kinetic isotope fractionation, it is more suitable to apply Demény *et al.*'s (2010) equation. This is primarily because it takes into account a wide range of $\delta^{18}O$ and $\delta^{13}C$ variability occurring in natural systems.

Comparisons between known temperatures from the Still Bay weather stations and the range of values calculated using the Demény *et al.* (2010) formula for the 12-month sampling period at the sites of West Cave and Klipdrift Sea Cave are illustrated in Figure 5.32 and Figure 5.33, respectively.

With regards to the dripwater values for West Cave, the lowest (less positive/more negative) $\delta^{18}O_w$ values are associated with the summer collections (Dec.-Feb.) with $\delta^{18}O_{w\ ranging}$ from -3.34 to -1.37 with an average of -2.57 (V-SMOW) (n=3). The highest (more positive/less negative) $\delta^{18}O_w$ values correspond to the autumn/winter collections (May-July) with values from -0.55 to +0.72 (V-SMOW) with a mean of -0.06 (V-SMOW) (n=6). For the autumn collection (Feb.-Apr.), dripwater values range from -1.82 to -1.11 (n=2) while for the late winter/early spring period (Aug.-Oct.) $\delta^{18}O_w$ shows high variability with values from -2.65 upto -0.55 (V-SMOW) with an average of -1.63 (n=7). At Klipdrift Sea Cave, the lowest values are associated with the autumn collections (Feb.-Apr.) with $\delta^{18}O_w$ from -3.10 to +0.56 (V-SMOW) with an average of -0.97 (V-SMOW) (n=4). This is contrary to West Cave where the autumn collections show significantly less variability and the lowest values occur in summer collection dripwaters. For the Klipdrift Sea Cave samples, the highest dripwater values corresponded to the autumn/winter collections where $\delta^{18}O$ content ranged from +1.29 to +5.29 with a mean of +4.18 (V-SMOW) (n=4). This trend was also observed at West Cave although the dripwater values from KDSC are much higher than those from West Cave. Although dripwaters from the KDSC summer collections range from -0.95 to +1.04 with a mean of -0.01 (V-SMOW) (n=3) are significantly higher than those from West Cave, the dripwater $\delta^{18}O$ content is not as high as in the KDSC autumn/winter collections. For the autumn collections, the dripwaters $\delta^{18}O_w$ ranges from -3.10 to +0.56 and average at -0.97 (V-SMOW) (n=4). The late winter/early spring dripwaters at KDSC show similarly high variability with the autumn dripwaters. In these samples (late winter/early spring) $\delta^{18}O_w$ values range from -3.30 upto +2.47 (V-SMOW) (n=6).

Comparable values, at least for the summer collection at KDSC, comes from $\delta^{18}O$ of rainfall collected above Crevice Cave between 2006 and 2007 (Bar-Matthews *et al.* 2010 Supplementary data Table S3). At the latter site, rainfall

corresponding to the summer collection (at West Cave & Klipdrift Sea Cave) ranged from -2.05 to +1.09 and occur in an overlapping range of varibility with the $\delta^{18}O$ in dripwaters from Klipdrift Sea Cave. This suggests that the dripwaters could be retaining an oxygen isotope signal that broadly reflects the isotopic content of precipitation at the surface. The Klipdrift Sea Cave dripwaters also appear to show good agreement with the rainfall oxygen isotope signal from Crevice Cave during the autumn sampling season (At De Hoop). At Klipdrift Sea Cave, the autumn period values are highly variable and rainfall $\delta^{18}O$, at least from Crevice Cave, shows a similar trend with values ranging from -7.51 to +3.82 (Bar-Matthews *et al.* 2010 Supplementary data Table S3). For the dripwaters corresponding to late winter/early spring, the West Cave samples (-2.65 to -0.55) showed some overlap with the $\delta^{18}O$ content of rainfall from Crevice Cave (-4.42 to -1.20). This suggests that the West Cave dripwaters, at least for the late winter/early spring season, could contain an isotope signal that is directly related to precipitation at the surface. The most variable dripwater values, at both West Cave and Klipdrift Sea Cave, comes from the autumn/winter samplings where there is a strong trend towards higher (more positive) values. The rainfall values from Crevice Cave (-12.09 to +4.25) show similar variability and also follow the trend to much higher values during this interval. Overall, the oxygen isotope content of dripwaters from Klipdrift Sea Cave and West Cave match to some extent with the oxygen isotope signal in rainfall from Crevice Cave which suggests that the isotopic content of the dripwaters broadly reflect the oxygen isotope signal of rainfall at the surface. This indicates that kinetic fractionation effects (*viz.* evaporation) might not have been as strong as previously suggested.

Based on the modern proxy data, it appears that the higher values in dripwater and rainfall tends to occur during the cooler months represented here by autumn/winter collections although values are highly variable across the sampling seasons. By assuming that similar conditions also existed in the

past, the palaeoenvironmental implication is that rainfall could have been just as important as temperature in influencing speleothem $\delta^{18}O$ variability. This interpretation is however tentative as it is based on the isotopic values of surface rainfall and dripwaters. Further monitoring of in-cave variables such as CO_2 levels, cave air temperature and drip rates is however necessary in order to firmly establish whether the variations observed in the modern samples from West Cave and Klipdrift Sea Cave reflect seasonal variability that can be correlated with present-day meterological records. With regards to the temperature reconstructions and the occurrence of extreme values, these have been attributed to analytical and experimental problems. This includes fractionation from the container headspace due to very low (<1 ml) sample volumes or evaporation due to leakage, that in turn compromised the resultant temperature calculations. Overall, direct temperature estimates obtained from the cave dripwater and recent calcite was not useful due to experimental and logistical problems.

When considered together, the results suggest that speleothem growth may have occurred in quasi-equilibrium and not under conditions of fully isotopic equilibrium. This would in part explain the evidence for some retention of a rainfall isotopic signal in the dripwaters from West Cave and Klipdrift Sea Cave (as discussed above). It is strongly suggested that further monitoring of in-cave factors such as CO_2 levels, cave air temperature and drip rates is needed to firmly establish the extent to which rainfall could be influencing speleothem growth. It will also provide an opportunity to identify other variables that, along with rainfall, could be affecting the oxygen isotope signal.

5.5 Summary

Uranium series ages were obtained from stalagmite samples from Bloukrantz Cave (BL1, BL2, BL3 & BL4), Klipdrift Shelter (KDS) and Klipdrift Sea Cave (KDC5). The BL1 sample is dated from *c.* 82 ka to *c.* 23 ka and is discussed in section 5.2.1 and 5.3.1. Spurious ages were obtained for the BL2 sample and because of the poor stratigraphic constraint BL2 was omitted from further analysis (see Appendix). The BL3 stalagmite dates between 47.9 ka and 46 ka and is discussed in section 5.2.2 and 5.3.2. The BL4 sample is dated between *c.* 59 ka and 52 ka and is discussed in section 5.2.3 and 5.3.3. The KDS sample comes from the archaeological site of Klipdrift Shelter after which it is named. This particular sampled formed during a very short period of time between *c.* 69.5 ka and 68 ka and is discussed in section 5.2.4 and 5.3.4. KDC5 is the youngest sample discussed here. It comes from the Klipdrift Sea Cave and is of Holocene age; dating between 13 ka and 8 ka. The UTh systematics for KDC5 is discussed in section 5.2.5 and the corresponding stable isotope data are interpreted in section 5.3.5. Age models were determined for each of the stalagmite samples using the StalAge algorithm adopted from Scholz and Hoffmann (2011). For the stable isotope data corresponding to each of the samples, the Hendy Test was used to evaluate whether or not the stalagmites were formed under equilibrium conditions. These results indicate that$\delta^{13}C$ and $\delta^{18}O$ are influenced by kinetic fractionation effects. The implication is that the De Hoop stalagmites could not be used to make palaeoenvironmental interpretations. This is however overcome by comparing the De Hoop $\delta^{18}O$ and $\delta^{13}C$ curves with isotope profiles from similar aged regional stalagmite records (see Chapter 6). These comparative records come from stalagmites in the southern Cape (Crevice Cave, Pinnacle Point, Sandkraal Cave & Cango Cave) and the Little Karoo. When compared with these published records the De Hoop samples exhibit a similar pattern of variation in $\delta^{18}O$ and $\delta^{13}C$. This suggests a shared response to environmental, and by extension, regional climatic

influences,(discussed in Chapter 5). Here the $\delta^{13}C_{calcite}$ signal for each of the stalagmites was interpreted in terms of C_3/CAM and C_4 vegetation using a theoretical range adopted from Talma and Vogel (1992). Variations observed in the $\delta\ ^{18}O_{calcite}$ signal that corresponds to the $\delta\ ^{13}C_{calcite}$ signal were interpreted in relation to summer and winter rainfall. A theoretical range for seasonal rainfall was obtained from Bar-Matthews *et al.* (2010). The variations exhibited in the isotopic signal of the Bloukrantz Cave samples (BL1, BL3 & BL4) are discussed individually in sections 5.3.1, 5.3.2 and 5.3.3. For Klipdrift Shelter (KDS) and Klipdrift Sea Cave (KDC5) the isotope data are discussed in section 5.3.4 and 5.3.5, respectively.The $\delta^{18}O_{calcite}$ signal for the older samples including KDC5 was further evaluated using modern $\delta\ ^{18}O$ values obtained from recently precipitated calcite and its corresponding dripwaters (see Table 5.6 & Table 5.7). Current dripwater $\delta\ ^{18}O$ data comes from West Cave (which was used as a proxy for Bloukrantz Cave) and also from Klipdrift Sea Cave. The data are interpreted in section 5.4.1. Overall the stalagmites presented here provide a discontinuous isotopic record from MIS 5 to MIS 3 and the Holocene. These data are discussed further in Chapter 6 in relation to proxy records available for the southern Cape.

Chapter 5 - SPELEOTHEM RECORDS FROM THE SOUTHERN CAPE FROM MIS 5 - MIS 3

The analysis of the De Hoop speleothem record discussed in Chapter 4, provided data on the isotopic composition of speleothems dated to between 81 ka and 30 ka and the Holocene. As a whole, this period is represented by the five stalagmites that form the core of this thesis and which come from Bloukrantz Cave, Klipdrift Sheleter and Klipdrift Sea Cave. The Bloukrantz Cave samples (denoted as BL1, BL3 & BL4) and from Klipdrift Shelter (KDS) and Klipdrift Sea Cave (KDC5) all show good agreement between the uranium-series ages and the stratigraphy. Taken together, they provide a high resolution record that covers the interval from MIS 5a through to MIS 3 and the Holocene. The Holocene is covered by the KDC5 stalagmite and is not discussed here (see Chapter 4 section 4.3.5). Instead, the intention in this chapter is to compare the $\delta^{18}O$ and $\delta^{13}C$ results from the stalagmite records for MIS 5a (section 5.2), MIS 4 (section 5.3) and MIS 3 (section 5.4) to other southern Cape speleothem records (Talma & Vogel 1992; Bar-Matthews *et al.* 2010; Braun 2014). The comparative records selected for discussion have also been analysed using the same methodology and uranium series dating techniques discussed in Chapter 3 (see also Braun 2014 & Bar-Matthews *et al.* 2010). One exception is Cango Cave where the stalagmite record was stratigraphically constrained using radiocarbon techniques (Talma & Vogel 1992).

For the purpose of this discussion, each of the above-mentioned stages from MIS 5a to MIS 3 is subdivided into early and late phases. The time periods covered by each of the speleothem records is illustrated in Fig. 5.1 and also tabulated in Table 5.1. Comparative $\delta^{13}C$ and $\delta^{18}O$ plots for De Hoop and

other southern Cape speleothems are shown in Fig. 5.2 and Fig. 5.3, respectively.

5.2.1 MIS 5a palaeoenvironmental evidence from speleothems

MIS 5a (85 ka - 74 ka, Martinson *et al.* 1987) in this study is represented by the calcite section of BL1 while comparative speleothem proxy data covering MIS 5a comes from the composite Pinnacle Point record, Crevice Cave, Herold's Bay and the Little Karoo $\delta^{18}O$ record. At Pinnacle Point, Braun (2014) compiled the composite record with recent data from Staircase Cave, PP29 and Crevice Cave. She also extended the existing Crevice Cave sequence (after Bar-Matthews *et al.* 2010) and put together the composite Herold's Bay and Little Karoo records with data from different samples.

In BL1, the stable isotope proxy record covers the period from *c.* 81 ka to 74 ka (Fig. 5.1 blue horizontal bars) this interval falls within MIS 5a (Table 5.1). In the Pinnacle Point record, denoted here as PP29, MIS 5a is dated from *c.* 84 ka to 75 ka. At Crevice Cave, this stage covers the period between *c.* 80 ka and 75 ka (Fig. 5.1; Table 5.1). In the Herold's Bay and Little Karoo records, MIS 5a similarly falls between 85 ka and 75 ka (Fig. 5.1; Table 5.1). As mentioned previously, the discussion here is subdivided into early MIS 5a (*c.* 85 ka – 80 ka) and late MIS 5a (*c.* 79 ka – 74 ka) and data pertinent to each of these sub-stages is discussed below.

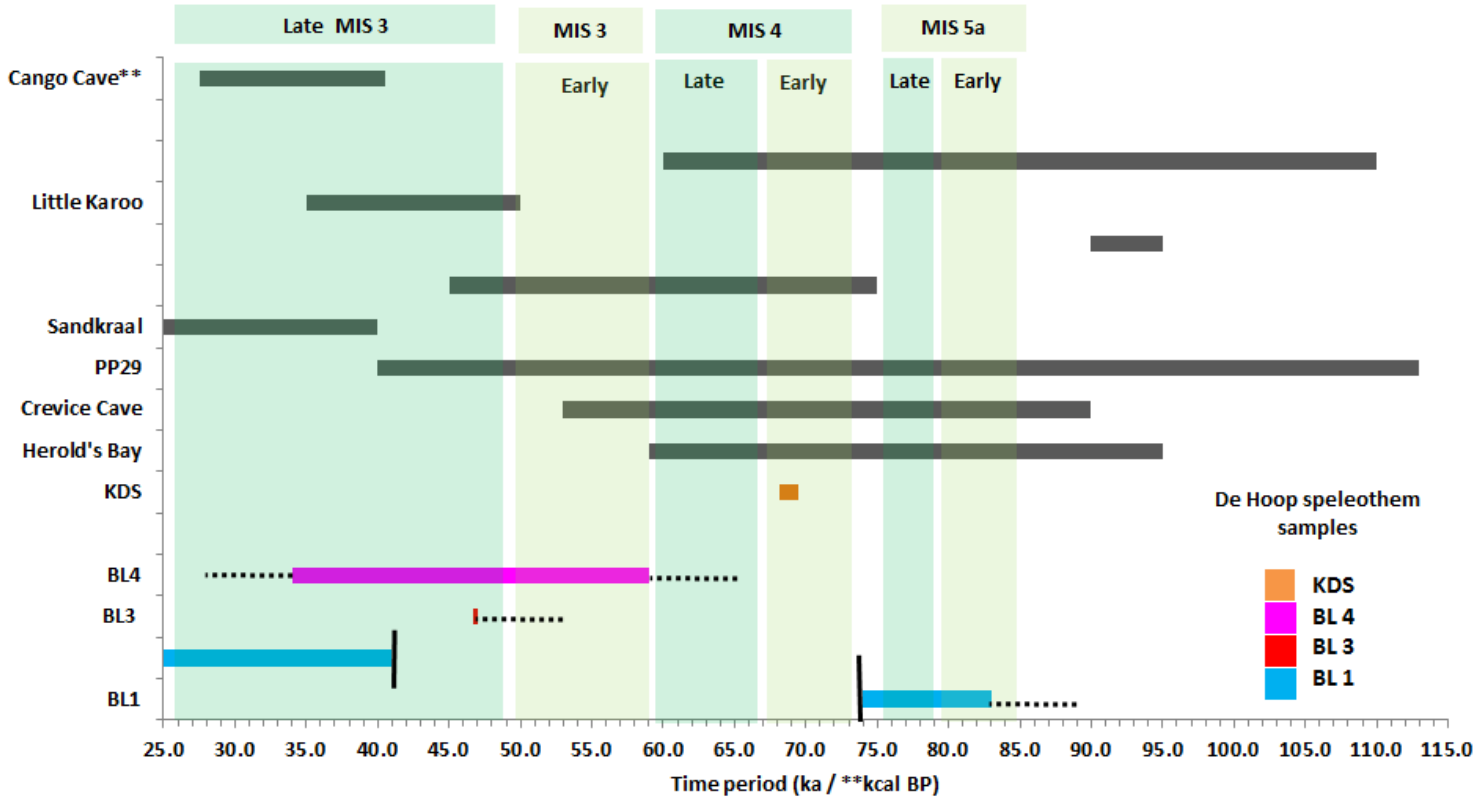

Fig. 5.1 Time periods represented by the De Hoop speleothem samples (KDS, BL4, BL3 & BL1) and comparative speleothem records from the southern Cape sites of Cango Cave, the Little Karoo, Sandkraal Cave, PP29 at Pinnacle Point, Crevice Cave and Herold's Bay. The time intevals are reported in ka with the exception of Cango Cave where age ranges are reported in kcal

BP. The data from the Little Karoo, Sandkraal Cave and Herold's Bay also represents composite records obtained from multiple samples whereas the PP29 record was compiled using data from Staircase Cave, PP29 and Crevice Cave. Those records from the De Hoop stalagmites (BL1, BL3, BL4 & KDS) and Cango Cave represent single samples. For the De Hoop stalagmites regions where the samples were broken are indicated by dashed lines (- - - -). These are areas where growth could have likely continued. The short black vertical lines (I) refers to regions where growth was interrupted by a hiatus(es).

Table 5.1 Time periods covered by speleothem isotopic records from De Hoop (BL1, BL3 & BL4), Klipdrift Shelter (KDS) and other southern Cape cave sites

Site	Period covered (ka/kcal BP)	Reference
BL1 (calcite section) **BL 1 (aragonite section)**	*c.* 81 ka – 74 ka (hiatus *c.* 73 ka – 46 ka) *c.* 46 ka – *c.* 31 ka	This study
BL3	*c.* 47.1 ka – *c.* 46.7 ka	This study
BL4	*c.* 59 ka – 34 ka	This study
KDS	69.4 ka – 68.6 ka	This study
KDC 5	*c.* 13.8 ka – 7.8 ka	This study
Pinnacle Point (PP29)	113 ka – 40 ka	Braun 2014
Crevice Cave	90 ka – *c.* 53 ka	Bar-Matthews *et al.* 2010
Herold's Bay	95 ka – 59 ka	Braun 2014
Sandkraal Cave	95 ka – 90 ka 75 ka – 49 ka (hiatus *c.* 48 ka – 41 ka) **40 ka – *c.* 25 ka	Braun 2014
Little Karoo	110 ka – 64 ka (hiatus *c.* 64 ka – 60 ka) 48 ka – 35 ka (hiatus *c.* 50 ka – 48 ka & *c.* 43 ka – 42 ka)	Braun *et al.* 2012; Braun 2014
Cango Cave	**40.5 kcal BP – 27.5 kcal BP	Talma & Vogel 1992

NOTES: For the De Hoop samples (BL1, BL3 & BL4), Klipdrift Shelter (KDS) and Klipdrift Sea Cave (KDC5), the time periods covered by each of the stalagmite records is based on the modelled growth phases derived from the U-Th ages. For the composite Sandkraal Cave record the main growth phase correlated with late MIS 3 is shown. While this particular proxy record covers the LGM and Holocene these periods are not pertinent to the current discussion. Similarly, for the Cango Cave stalagmite, the Holocene part of the sequence is omitted from the table above.

Early MIS 5a (*c.* 85 – 80 ka)

Between 81.5 ka and 81 ka, $\delta^{13}C$ in BL1 shows an increasing trend to higher values of around -4.8‰, indicating C_4 vegetation, in early MIS 5a (shown in orange in Fig. 5.2). The corresponding $\delta^{18}O$ signal tracks changes in $\delta^{13}C$ with a trend towards higher (more positive) values up to -2.8‰ indicating increasing summer rainfall (shown in orange in Fig. 5.3). In the composite Pinnacle Point (PP29) record there is an increasing trend in $\delta^{13}C$ towards higher values from -12‰ *c.* 84 ka to -8‰ by *c.* 80 ka (not illustrated in Figs 5.2 & 5.3, due to inaccessible raw data but shown in grey in Braun 2014: 119

Fig. 4.12). Values in this range are suggestive of more C_4 vegetation in early MIS 5a. The corresponding $\delta^{18}O$ signal in PP29 tracks changes in the $\delta^{13}C$ with $\delta^{18}O$ increasing from -4.5‰ *c.* 84 ka to -2.5‰ by *c.* 80 ka (shown in grey in Braun 2014: 119 Fig. 4.12). This indicates a summer rainfall influence in early MIS 5a. When compared to PP29, the overall pattern identified in BL1 appears to be consistent with the interpretation of C_4 vegetation and summer rain interpreted from the PP29 record. Both records therefore associate early MIS 5a with C_4 vegetation and summer rainfall.

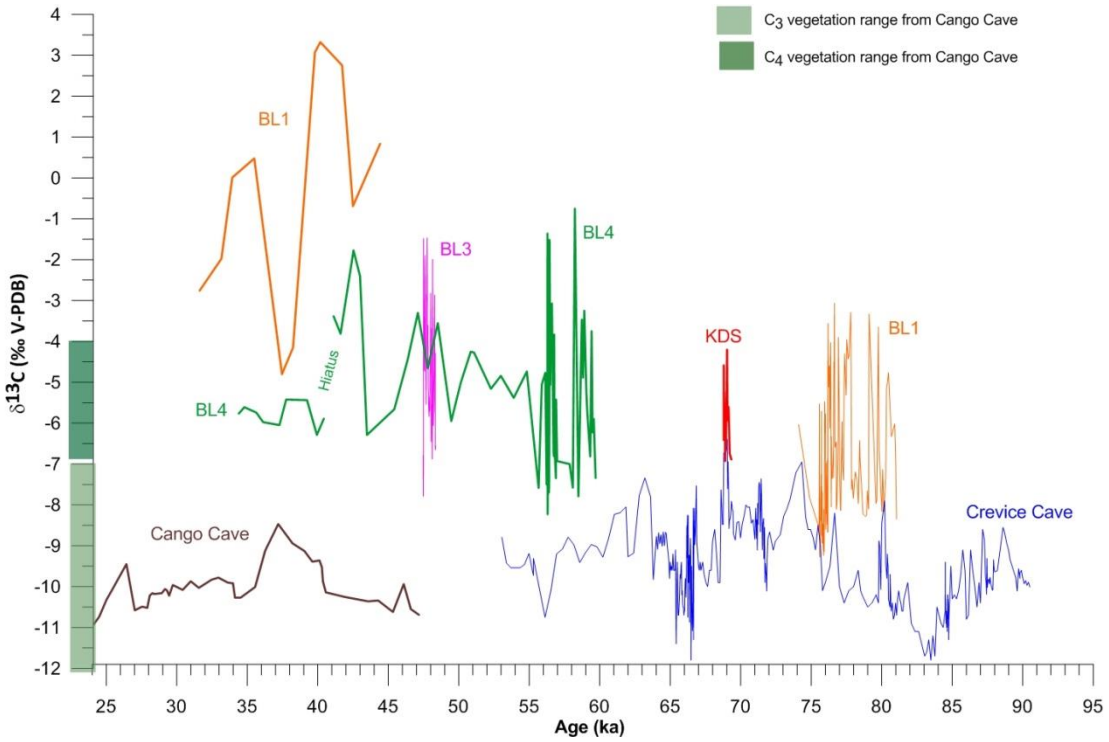

Fig. 5.2 Comparison of the $\delta^{13}C$ data from the De Hoop (BL1, BL3 & BL4) and Klipdrift Shelter (KDS) stalagmites with published speleothem records from the southern Cape (Cango Cave & Crevice Cave). The raw $\delta^{13}C$ data are shown with the exception of the Little Karoo where smoothed $\delta^{13}C$ values are used (after Braun *et al.* 2012). For the BL1 the raw aragonite corrected $\delta^{13}C$ data are plotted. Here the data from Pinnacle Point (PP29), Herold's Bay and Sandkraal Cave is not included as the author did not have access to the raw data generated for the composite records from these sites. Ages for the Cango Cave are in kcal BP. The theoretical range of $\delta^{13}C$ values for C_3/CAM and C_4 vegetation adopted from Talma and Vogel's (1992) estimates for Cango Cave are highlighted along the y-axis.

In contrast to BL1 and PP29, $\delta^{13}C$ from Crevice Cave shows a general decreasing trend from -9.5‰ *c.* 85 ka to -11.8‰ *c.* 83.5 ka (shown in dark blue in Fig. 5.2). These values are consistently within the the range of C_3 vegetation. While this interval is not represented in BL1, it is present in PP29, and in the latter record, $\delta^{13}C$ shows an increasing trend. While Crevice Cave $\delta^{13}C$ increases from -11.5‰ *c.* 83 ka upto -7.5‰ *c.* 81 ka, these values still fall within the range of C_3 vegetation (shown in dark blue in Fig. 5.2). The Crevice Cave $\delta^{13}C$ value of -7.5‰ for 81 ka is also lower than the respective values of -4.8‰ and -2.5‰ reported from BL1 and PP29 at this time. The corresponding $\delta^{18}O$ from Crevice Cave is relatively unstable between -3.5‰ and -4.75‰ for the period between *c.* 85 ka to *c.* 83.5 ka (shown in dark blue in Fig. 5.3). These values fall within the upper range of winter rainfall and just outside the lower limit of summer rainfall (after Bar-Matthews *et al.* 2010 & Braun 2014). Based on this range of variability, $\delta^{18}O$ possibly reflects a year round rainfall signal (as disussed in Chapter 4 section 4.3; shown in dark blue in Fig. 5.3). The implication is that for this part of early MIS 5a local precipitation at Crevice Cave might have been more variable compared to PP29. This is because PP29 exhibits a relatively strong summer rainfall signal which is not reflected in the coeval part Crevice Cave record. It is only from *c.* 83 ka to *c.* 81 ka that $\delta^{18}O$ at Crevice Cave tracks changes in $\delta^{13}C$ with $\delta^{18}O$ increasing to -2.5‰, indicating a trend towards more summer rainfall. As discussed above, this pattern of increasing summer rainfall influence is also evident in BL1 and PP29 *c.* 81 ka. Overall, it appears that for the early part of MIS 5a, dating from *c.* 83 ka to 81 ka, similar conditions occurred at BL1, PP29 and Crevice Cave. These conditions were characterised by more seasonal summer rainfall and C_4 vegetation.

In contrast to the above-mentioned sites, an opposite pattern is evident at Herold's Bay and the Little Karoo. At Herold's Bay, *c.* 45 km east of Pinnacle Point, there is a decreasing trend in $\delta^{13}C$ throughout the period from *c.* 85 ka

to 80 ka. During this period, values are between -10‰ and -12‰, suggestive of more C_3 vegetation above the site at this time (shown in black in Braun 2014: 119 Fig. 4.12). The Herold's Bay $\delta^{18}O$ mirrors the pattern observed in $\delta^{13}C$ with a trend towards lower $\delta^{18}O$ values, from -2.5‰ to -4.0‰ (shown in black in Braun 2014: 119 Fig. 4.12). These values are thought to reflect a weaker summer rainfall influence in early MIS 5a at this site. While Herold's Bay is a coastal site located in close proximity to Pinnacle Point, the changes in Herold's Bay $\delta^{13}C$ and $\delta^{18}O$ are comparable with those from the Little Karoo.

Although the Little Karoo, $\delta^{13}C$ record is considered problematic (Braun 2014), its corresponding $\delta^{18}O$ record is not. In this latter record, there is a general decreasing trend in $\delta^{18}O$ from -3.75‰ to -5.1‰, indicating a consistent input of ^{18}O from winter rainfall sources (shown in dark blue in Braun 2014: 130 Fig. 4.18). Braun (2014) attributes these lower values to the combined influence of orographic effects and evapotranspiration effects on the $\delta^{18}O$ signal of precipitation and cave dripwater. The general trend is that the orographic effect on rainfall $\delta^{18}O$ produces low values. Evapotranspiration effects on the other hand, affects the seasonality of groundwater recharge, which in turn affects the isotope values of cave dripwater (Mickler *et al.* 2004, 2006; Mattey *et al.* 2008; Lachniet 2009). Since the Little Karoo presently receives most of its rainfall in winter, groundwater recharge here is limited to the wet winter months. As a result, water feeding into the cave has a winter rainfall signal that is characterised by lower $\delta^{18}O$ values. Braun's (2014) inference is therefore reasonable given the current dynamics at the Little Karoo site.

Late MIS 5a (c. 79 ka – 74 ka*)*

Throughout late MIS 5a, $\delta^{13}C$ in BL1 fluctuates between high values, indicating C_4 vegetation, and low values, associated with C_3/C_3-like CAM vegetation (shown in orange Fig. 5.2). At 79 ka, $\delta^{13}C$ peaks at -3.5‰,

suggesting C_4 but this followed by a drop to a lower value of -7.5‰, suggesting a weaker C_4 signal relative to C_3/CAM *c.* 78 ka. In BL1 $\delta^{13}C$ of -9.5‰ remains within the range of C_3/CAM until *c.* 77 ka before increasing to -3.5‰, suggestive of C_4 vegetation, by *c.* 76 ka. By terminal MIS 5a, which is dated to between 75 ka and 74 ka in BL1, $\delta^{13}C$ shows abrupt, short-term fluctuations. These rapid changes possibly reflect an interval of vegetation instability at the transition to MIS 4. In BL1 the corresponding $\delta^{18}O$ signal tracks changes in $\delta^{13}C$ (shown in orange in Fig. 5.3). Warm summer rain is inferred from the higher $\delta^{18}O$ value of -2.4‰ at 79 ka which is consistent with the interpretation of C_4 vegetation in BL1 at this time. Around 78 ka $\delta^{18}O$ is at -4.3‰ and falls within the theoretical range of winter rain. By 77 ka, $\delta^{18}O$ is at -3.2‰ and within the lower boundary of summer rainfall but possibly reflects a year round rainfall influence (see Chapter 4 section 4.3 for details). By 76 ka, $\delta^{18}O$ peaks at -2.2‰ suggesting an increasing influence of summer rainfall at the site which corresponds with the C_4 vegetation signal. For the MIS 5a/4 boundary, $\delta^{18}O$ shows rapid changes which either signify a year round rainfall regime or possibly reflects abrupt changes in winter and summer rainfall dynamics.

In contrast to BL1, the comparative PP29 record does not exhibit comparable trends in late MIS 5a. Here $\delta^{13}C$ shows a minor peak at -9.7‰, indicating C_3 vegetation at 79 ka which is followed by a minor drop to -10.3‰ at *c.* 78 ka (shown in grey in Braun 2014: 119 Fig. 4.12). This value still falls within the range of C_3 plants. While there is a minor increase in $\delta^{13}C$ to -8‰ between 77 ka and 76 ka, these values remain within the range variability for C_3. By 75 ka, PP29 shows a weak decreasing trend to marginally lower values between -10.0‰ and -11.8‰, also suggesting C_3 at the transition to MIS 4 (shown in grey in Braun 2014: 119 Fig. 4.12). In PP29 the corresponding $\delta^{18}O$ signal tracks changes in $\delta^{13}C$ with minor peak at -3.0‰, associated with summer rainfall (after Bar-Matthews *et al.* 2010) but possibly year round rainfall as well

(as discussed in Chapter 4 section 4.3). At 78 ka there is a minor drop in $\delta^{18}O$ to -4.0‰, suggestive of increasing winter rainfall which is consistent with an interpretation of C_3 vegetation at this time. Between 77 ka and 76 ka, there is a weak increasing trend to a higher value of -3.0‰, reflecting a shift back to either summer or year round rainfall (shown in grey in Braun 2014: 119 Fig. 4.12).

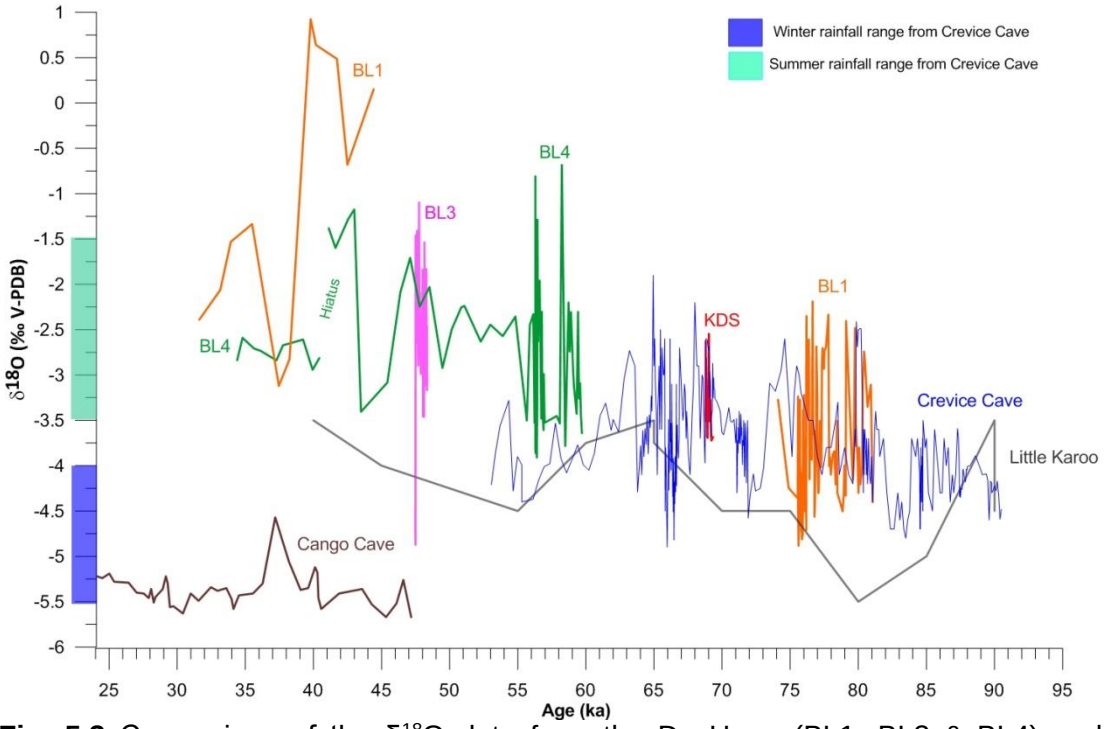

Fig. 5.3 Comparison of the $\delta^{18}O$ data from the De Hoop (BL1, BL3 & BL4) and Klipdrift Shelter (KDS) stalagmites with published speleothem records from the southern Cape (Cango Cave & Crevice Cave) and the Little Karoo. The raw $\delta^{18}O$ data are shown with the exception of the Little Karoo where smoothed $\delta^{18}O$ values are used. For the BL1 the raw aragonite corrected $\delta^{18}O$ data are plotted. Here the data from Pinnacle Point (PP29), Herold's Bay and Sandkraal Cave is not included as the author did not have access to the raw data generated for the composite records from these sites. Ages for the Cango Cave are in kcal BP. The theoretical range of $\delta^{18}O$ values for summer and winter rainfall adopted from Bar-Matthews *et al.*'s (2010) estimates for Crevice Cave are highlighted along the y-axis

By 75 ka, $\delta^{18}O$ in PP29 decreases back down to -4.0‰, suggesting a stronger winter rainfall influence at the transition to MIS 4. The general pattern of C_3 vegetation and winter rainfall during late MIS 5a at PP29 is also

mirrored at Crevice Cave. In this latter record, $\delta^{13}C$ increases to -9.5‰, suggesting C_3 vegetation, between 79 ka and 78 ka (shown in dark blue in Fig. 5.2). This is followed by a minor decrease to -10.5‰, still within the C_3 range, at 77 ka. Between 77 ka and 76 ka, there is a major peak to a relatively higher value of -8.0‰ which is still within the range of C_3 (shown in dark blue in Fig. 5.2). By 75 ka $\delta^{13}C$ peaks at 6.5‰, suggesting an increase in C_4 vegetation at the transition to MIS 4 which is not reflected in BL1 or at PP29. The corresponding $\delta^{18}O$ values show a decreasing trend from 79 ka to 77 ka, with values dropping from -3.25‰ to -4.1‰ (shown in dark blue in Fig. 5.3). This is suggestive of weaker summer/year round rainfall and thus a stronger winter rainfall influence. Between 77 ka and 76 ka, there is an increasing trend to higher values with a peak at -3.0‰. This trend is also evident in PP29 where an increase in either summer/year round rainfall is inferred. By 75 ka, $\delta^{18}O$ in Crevice Cave drops to -4.1‰, suggesting a stronger winter rainfall influence, which is also interpreted in the coeval part of PP29. However, in the Crevice Cave record, $\delta^{18}O$ peaks again at -2.75‰, suggesting a shift to more summer/year round rainfall by 74 ka (shown in dark blue in Fig. 5.3). Overall, the Crevice Cave record is fairly similar to PP29. This is because both records associate late MIS 5a with relatively more C_3 vegetation and a generally stronger winter rainfall influence relative to summer and possibly year round rainfall.

A similar inference of late MIS 5a conditions is also reflected at Herold's Bay which is in close proximity of *c.* 45 km to Pinnacle Point and Crevice Cave. For the interval from 79 ka to 75 ka, $\delta^{13}C$ at Herold's Bay ranges between -10.2‰ and -11.8‰ but falls consistently within the C_3 range (shown in black in Braun 2014: 119 Fig. 4.12). This suggests a uniform C_3 presence throughout late MIS 5a which is also evident at PP29. At the transition to MIS 4, Herold's Bay $\delta^{13}C$ shows a minor increasing trend to -10.0‰, but this value is still within the range of C_3 vegetation (shown in black in Braun 2014: 119

Fig. 4.12). Taken together, both PP29 and Herold's Bay associates late MIS 5a and the MIS 5a/4 boundary with C_3 vegetation and winter rainfall. A similar inference of winter rainfall in late MIS 5a also comes from the Little Karoo $\delta^{18}O$ record (shown in dark blue in Braun 2014: 130 Fig. 4.18). Here $\delta^{18}O$ values are fairly stable at around -5.0‰, suggesting a consistent winter rainfall influence in this area.

Taken together, the Mossel Bay (PP29 & Crevice Cave), George (Herold's Bay) and inland (Little Karoo) records link late MIS 5a with C_3 vegetation and winter rainfall. In contrast to these records, BL1 correlates late MIS 5a with abrupt changes in vegetation and rainfall dynamics. Here fluctuations in $\delta^{13}C$ and $\delta^{18}O$ appear to be more pronounced at the transition from MIS 5a to MIS 4 which is evident as a period of isotopic instability. The implication is that local conditions at De Hoop and by extension in the Overberg were relatively warmer and more variable compared to Mossel Bay and George. Based on the palaeo-$\delta^{18}O$ signal from the Little Karoo it has been suggested that this area received more rain during winter both in the past and present (Braun 2014: 129).

Conclusion

Overall, the speleothem proxy data presented here provides different snapshots of environmental conditions during MIS 5a. Taken as a whole, conditions during early MIS 5a (*c.* 85 ka to 80 ka) in the southern Cape appears to have been warm with more seasonal rain falling during summer. Vegetation proxies suggest habitats mainly comprising C_4 vegetation. Typical C_4 plants in the present day southern Cape include C_4 grasses such as *Themeda triandra* and *Cymbopogon marginatus* (Vogel *et al.* 1978; Cowling 1983a, b) which occur in South Coast Dune Fynbos and Renosterveld habitats (Cowling 1983a).

By late MIS 5a (*c.* 79 ka to 74 ka), conditions remained warm, particularly at De Hoop and the Overberg where local rainfall and vegetation was quite variable throughout this period. However, in the areas of Mossel Bay, George and the Little Karoo, late MIS 5a was seemingly not as warm compared to De Hoop. It appears that conditions during summer were relatively warm and dry as these areas received more rainfall during winter. Vegetation proxies suggest habitats consisting of C_3/CAM vegetation. This might have included fynbos, C_3 grasses such as *Erharta capensis*, *Elytropappus* shrubs, geophytes and possibly succulents (Vogel *et al.* 1978; Cowling 1983a, b).

As a whole, the speleothem evidence is generally complementary in implying that in MIS 5a surface conditions (*i.e.*, precipitation, temperature & vegetation coverage) were generally favourable for speleothem growth. However, based on the BL1 data from De Hoop, conditions in this part of the southern Cape were seemingly more variable.

5.2.2 MIS 4 palaeoenvironmental evidence from speleothems

MIS 4 (*c.* 73 ka – 57 ka; Martinson *et al.* 1987) in this study is represented by a small part of the BL1 stalagmite, dating to *c.* 72 ka (Fig. 5.1 & Table 5.1) and the Klipdrift Shelter stalagmite fragment, KDS, that dates to between 69.5 ka and 68.2 ka (Fig. 5.1 & Table 5.1). However, for BL1 there is no corresponding stable isotope data to complement the uranium series age of 72 ka. For this reason, only the proxy evidence from the KDS sample is discussed here. Other southern Cape speleothem proxies covering MIS 4 or part thereof come from Pinnacle Point (PP29) (*c.* 73 ka to 60 ka), Crevice Cave (*c.* 72 ka - 60 ka), Herold's Bay Cave (*c.* 72 ka - 61 ka) and Sandkraal Cave (*c.* 73 ka - 60 ka). Herold's Bay and Sandkraal Cave are located *c.* 30 km and 45 km east of Pinnacle Point, respectively (Braun 2014). While a part of the Little Karoo record, dating from *c.* 72.5 ka to 64 ka, falls within MIS 4,

the $\delta^{13}C$ part of the sequence is considered highly variable (Braun 2014: 74) and is not discussed further. In this section, the discussion focuses on comparing the $\delta^{18}O$ and $\delta^{13}C$ signals in the KDS record with those from the above-mentioned southern Cape speleothem records. Here interpretations of MIS 4 environmental conditions are sub-divided into early and late MIS 4. The discussion starts with early MIS 4 which is defined as the interval from *c.* 73 ka to 68 ka. Late MIS 4, which is discussed last, refers to the period between *c.* 67 ka and 60 ka.

Early MIS 4 (73 ka – 68 ka)

Early MIS 4 in KDS is dated to between 69 ka and 68.5 ka (Fig. 5.1). Here $\delta^{13}C$ shows a minor peak at -4‰, suggesting C_4 vegetation, before declining to -7‰ at 68.5 ka (shown in red in Fig. 5.2). These values are however within the Cango Cave Holocene range of C_4 vegetation. The corresponding $\delta^{18}O$ signal tracks changes in $\delta^{13}C$ with a local peak at -2.5‰ *c.* 69 ka. This suggests more seasonal summer rain and complements the $\delta^{13}C$ interpretation of C_4 vegetation. At 68.5 ka, $\delta^{18}O$ declines to -3.75‰ which is intermediate between the theoretical range of summer and winter rainfall (shown in red in Fig. 5.3). This possibly suggests a shift to year round rainfall in this part of early MIS 4. Broadly similar trends are evident in the comparative Pinnacle Point (PP29) record (shown in grey in Braun 2014: 119 Fig. 4.12). Between 73 ka and 72 ka, $\delta^{13}C$ shows a general increasing trend from -11‰ to -7‰, suggestive of more C_4 vegetation above the cave at this time. From 72 ka to 70 ka, $\delta^{13}C$ stabilises around -8.75‰ before peaking around -7‰ at 68 ka. This latter peak in PP29 is comparable with the one evident in the coeval part of KDS (as discussed above). The corresponding PP29 $\delta^{18}O$ signal mirrors changes in $\delta^{13}C$ with values increasing from -5‰ up to -3.5‰ between 73 ka and 72 ka (shown in grey in Braun 2014: 119 Fig. 4.12).

While these values fall within the Crevice Cave range of winter rainfall, there is a minor peak at -2.5‰ around *c.* 68 ka which suggests a shift to more summer rain at this time. When compared with KDS and PP29, the coeval part of the Crevice Cave record shows fairly similar trends. In this record, $\delta^{13}C$ is highly variable at 72 ka with values between -10‰ (associated with C_3) and -7.5‰ (which falls within the C_4 range) (Bar-Matthews *et al.* 2010; also shown in dark blue in Fig. 5.2). Bar-Matthews *et al.* (2010: 2140) refer to this part variation as a "…*high amplitude isotopic excursion…"* and interpret 72 ka as a period of C_3/C_4 instability. From 71 ka to 69.5 ka, $\delta^{13}C$ is fairly stable between -9‰ and -8‰, which possibly reflects more C_3 vegetation in this part of early MIS 4. This trend is not reflected in KDS, which only covers the terminal part of this interval and it is also not evident in PP29. However, at 69 ka, Crevice Cave $\delta^{13}C$ peaks at -6‰, which suggests increasing C_4 vegetation as inferred from the KDS and PP29 records at this time. The corresponding Crevice Cave $\delta^{18}O$ signal generally mirrors changes in $\delta^{13}C$. At 72 ka, $\delta^{18}O$ shows similar variability to $\delta^{13}C$ with values between -4.5‰ and -3.0‰ which straddles the range of winter and summer rainfall (shown in dark blue in Fig. 5.3). This is suggestive of abrupt shifts in winter and summer rainfall influences but possibly reflects a shift to a year round rainfall regime. From 71 ka to 69 ka, $\delta^{18}O$ falls between -3.0‰ and -3.5‰, which suggests increasing summer rain (Bar-Matthews *et al.* 2010). The corresponding Crevice Cave $\delta^{13}C$ is however interpreted in terms of more C_3 vegetation (Bar-Matthews *et al.* 2010). At 69 ka, $\delta^{18}O$ peaks around -2.5‰, suggesting summer rain. This trend is also clearly shown in the coeval part of KDS (as discussed above & also see Fig. 5.3).

In contrast to the records discussed above, the Herold's Bay, Sandkraal and Little Karoo records do not associate early MIS 4 with C_4 vegetation. At Herold's Bay, $\delta^{13}C$ is stable around -10‰, suggestive of C_3 vegetation between 72 ka and 70 ka (shown in black in Braun 2014: 119 Fig. 4.12).

While there is a weak decreasing trend to lower values (-11‰ & -12‰) at 68 ka, these remain within the range of C_3 vegetation. The associated $\delta^{18}O$ values follow a similar trajectory to $\delta^{13}C$ and range between -2.5‰ and -2.0‰, suggesting more seasonal summer rain in the area in early MIS 4 (but see Braun 2014: 119 who suggests the $\delta^{18}O$ signal is enriched due to cave ventilation effects). This is however not consistent with an interpretation of C_3 vegetation and possibly reflects a contribution from CAM plants (as discussed in Chapter 4 section 4.3). At the nearby Sandkraal Cave, which is approximately 13 km northwest of Herold's Bay, $\delta^{13}C$ shows a comparable pattern. At Sandkraal Cave $\delta^{13}C$ for the period between 73 ka and 68 ka, is between -10‰ and -8.25‰ (shown in black in Braun 2014: 121 Fig. 4.13). This is suggestive of a consistent C_3 presence at the site in early MIS 4, which is also reflected at Herold's Bay Cave. The associated Sandkraal $\delta^{18}O$ signal shows a weak increasing trend with values increasing from -3.0‰ *c.* 73 ka up to -2.5‰ by 68 ka (shown in black in Braun 2014: 121 Fig. 4.13). At both of these sites, variations in $\delta^{18}O$ suggest warm conditions possibly with more seasonal summer rainfall. In contrast, in the Little Karoo, $\delta^{18}O$ is uniform at -5‰, suggestive of a stronger winter rainfall influence throughout early MIS 4 (and also for late MIS 4).

Taken together, the De Hoop and Mossel Bay records are broadly complementary in associating early MIS 4 with C_4 vegetation and summer/year round rainfall. While seemingly similar inferences of summer rainfall conditions are interpreted from the George $\delta^{18}O$ signal (Herold's Bay & Sandkraal Cave) these vegetation proxy records indicate a stronger C_3 signal. Based on this, it is possible that there is a contribution from CAM plants into the $\delta^{13}C$ signal (as discussed in Chapter 4 section 4.3). Further inland at the Little Karoo, winter rainfall is consistently associated with early MIS 4. This might suggest that coastal areas of the southern Cape experienced similar conditions that were not clearly expressed further inland.

Late MIS 4 (67 ka – 60 ka)

Although none of the De Hoop stalagmites covers late MIS 4 (Fig. 5.1) this period is represented in other southern Cape speleothems. In PP29, $\delta^{13}C$ shows values fluctuating between -12‰ and -7.8‰ between 67 ka and 65 ka, which covers the range of C_3 and C_4 plants (shown in grey in Braun 2014: 119 Fig. 4.12). At 64 ka, $\delta^{13}C$ peaks at -8‰ and this is followed by a steady decline to lower values between -10‰ and -9‰ around 63 ka. Throughout this latter interval, $\delta^{13}C$ falls within the Holocene range of C_3 vegetation (after Talma & Vogel 1992). By 62 ka, $\delta^{13}C$ peaks again at -7‰, suggestive of a weaker C_3 signal, before decreasing towards slightly lower values, between -8‰ and -9‰ around 60 ka leading to the transition from MIS 4 to MIS 3 (discussed further in MIS 3 section below). The corresponding $\delta^{18}O$ signal, tracks changes in $\delta^{13}C$ (shown in grey in Braun 2014: 119 Fig. 4.12). Here $\delta^{18}O$ fluctuates between -5‰ and -2‰ between 67 ka and 65 ka, covering the inferred range of winter and summer rainfall (after Bar-Matthews *et al.* 2010 & Braun 2014). This suggests that part of late MIS 4 was characterised by either a year round rainfall signal or abrupt local changes in rainfall dynamics. At 64 ka, $\delta^{18}O$ peaks at -2‰, suggestive of an increasing summer rain influence, before decreasing incrementally to lower values between -4.5‰ and -4.0‰ around 63 ka. The $\delta^{18}O$ values in this range imply weaker summer rain at this time. By 62 ka, $\delta^{18}O$ shows a minor peak at -2.8‰ but this is followed almost immediately by a decreasing trend towards lower values, between -4‰ and -5‰ around 60 ka (shown in grey in Braun 2014: 119 Fig. 4.12). Values in this range are suggestive of a stronger winter rainfall signal which continues through to the MIS 4/3 boundary.

In the coeval Crevice Cave record, $\delta^{13}C$ shows values between -12‰ and -7.5‰, during the period between 67 ka and 65 ka (shown in dark blue in Fig. 5.2). While these fluctuations are comparable with those shown in PP29 it is

thought to indicate a stronger C_4 grass presence (Bar-Matthews *et al.* 2010: 2140). Around 64 ka, $\delta^{13}C$ is stable around -9‰. Around 63.5 ka there is a minor increasing trend towards marginally higher values between -9‰ and -8.5‰. By 63 ka, Crevice Cave $\delta^{13}C$ peaks at -7.5‰, suggesting a weaker C_3 presence, before following a general decreasing trend back to lower values, between -9‰ and -8.5‰ from 62 ka to 60 ka. The corresponding Crevice Cave $\delta^{18}O$ values track changes in $\delta^{13}C$ and in this record, $\delta^{18}O$ ranges between -5.25‰ and -2.5‰ between 67 k and 65 ka (shown in dark blue in Fig. 5.3). While these values cover the range of winter and summer rainfall, the smoothed Crevice Cave $\delta^{18}O$ curves link these values with stronger summer rain (Bar-Matthews *et al.* 2010: 2139). Around 64 ka, $\delta^{18}O$ peaks at -1.75‰, suggestive of weaker winter rainfall influence relative to summer rain, before decreasing incrementally to -3.75‰ around 63.5 ka. By 63 ka Crevice Cave $\delta^{18}O$ peaked at -2.75‰ implying more summer rain. However, shortly thereafter, from 62 ka to 60 ka, $\delta^{18}O$ decreases to slightly lower values between -3.6‰ and -4.1‰, suggestive of a weaker summer rainfall signal (shown in dark blue in Fig. 5.3). As a whole, late MIS 4 in Crevice Cave is characterised by generally cooler conditions and associated with more C_4 grasses and summer rain (Bar-Matthews *et al.* 2010: 2139).

At Herold's Bay, there are comparable trends in late MIS 4 to those identified at PP29.The Herold's Bay $\delta^{13}C$ signal, for the period between 67 ka and 61 ka, shows minor variations around -11‰, and this has been associated with a uniform presence of C_3 plants (Braun 2014). The associated $\delta^{18}O$ signal tracks changes in $\delta^{13}C$ and shows a general decreasing trend with values declining from -2.5‰ to -3.5‰ (shown in black in Braun 2014: 119 Fig. 4.12). While $\delta^{18}O$ in this range is associated with summer rain, these elevated values were attributed to evaporative effects caused by cave ventilation (Braun 2014: 119). This potentially resulted in a muted palaeoenvironmental signal.

In the coeval part of the nearby Sandkraal Cave record, there are similar interpretations with PP29 and Herold's Bay (Braun 2014). At Sandkraal Cave, $\delta^{13}C$ is relatively stable around -8.5‰ for the interval between 67 ka and 65 ka (shown in black in Braun 2014: 121 Fig. 4.13). While there is a weak increasing trend between 65 ka and 60 ka to a marginally higher value of -8.25‰, $\delta^{13}C$ remains within the range of C_3 plants. The corresponding $\delta^{18}O$ signal for the interval between 67 ka and 65 ka is relatively stable throughout late MIS 4. Here values are uniform around -2.5‰, which is thought to reflect more summer rain (shown in black in Braun 2014: 121 Fig. 4.13). Between 65 ka and 60 ka, $\delta^{18}O$ shows a weak decreasing trend to a lower value of -3‰ which has been attributed to decreased amounts of summer rainfall (Braun 2014: 120).

When compared to the above-mentioned coastal records, the Little Karoo $\delta^{18}O$ record shows a weak decreasing trend to lower values between -4‰ and -5‰ (shown in dark blue in Braun 2014: 130 Fig. 4.18). Therefore, in contrast to the coastal records discussed above, the Little Karoo $\delta^{18}O$ signal associates late MIS 4 with generally increasing amounts of winter rain (Braun 2014). Based on this, the implication is that southern Cape coastal sites experienced relatively similar conditions that seemingly did not extend further inland.

As a whole, the coastal records from Mossel Bay (PP29 & Crevice Cave) and George (Herold's Bay & Sandkraal) are broadly complementary. Taken together these records generally associate late MIS 4 with variable rainfall and vegetation conditions that waxed and waned throughout this period. Interestingly, these speleothem records also seem to express a trend in favour of C_3 vegetation and winter rain at the MIS 4/3 boundary. This is discussed further below.

Conclusion

Overall, the Klipdrift Shelter, PP29 and Crevice Cave records exhibit similar trends in $\delta^{13}C$ and $\delta^{18}O$ during early MIS 4 (*c.* 73 ka – 68 ka). While Crevice Cave links the transition from MIS 5a to MIS 4, dating to *c.* 72 ka, with unstable conditions, this is not evident at Klipdrift Shelter and PP29. As a whole, early MIS 4 in the southern Cape appears to have been cooler than during MIS 5a but with generally more seasonal summer or year round rainfall. Vegetation proxies suggest similar habitats to those in early MIS 5a that favoured C_4 plants. By late MIS 4 (*c.* 67 ka – 60 ka), conditions remained cool, but were more variable than during the earlier part of this stage. This is particularly so in the coastal areas of Mossel Bay (PP29 & Crevice Cave) and George (Herold's Bay & Sandkraal) where local rainfall and vegetation seemingly fluctuated throughout this period. Although cooler conditions also extended into the Little Karoo during late MIS 4, rainfall appears to have been less variable than at the coast. While conditions along the coast were seemingly more variable, the absence of speleothems formed between 64 ka and 61 ka from the Little Karoo implies that inland conditions were less favourable for speleothem growth (Braun 2014).

5.2.3 MIS 3 palaeoenvironmental evidence from speleothems

Unlike the other marine oxygen isotope stages, MIS 3 is well represented in the De Hoop speleothem record with three stalagmites, BL1, BL3 and BL4, all from Bloukrantz Cave, linked to part of MIS 3 (Table 5.1 & Fig. 5.1). Comparative speleothem data comes from Pinnacle Point (*c.* 59 ka – 38 ka), Crevice Cave (*c.* 59 ka – 53 ka), Sandkraal Cave (*c.* 59 ka – 50 ka & 40 ka – 25 ka), the Little Karoo (*c.* 53 ka – 50 ka & 47 ka – 35 ka) and Cango Cave (*c.* 47.1 kcal BP – 24.1 kcal BP) (Fig. 5.1 & Table 5.1). In this section, the discussion focuses on comparing the $\delta^{18}O$ and $\delta^{13}C$ signals in the Bloukrantz stalagmite record with the above-mentioned southern Cape speleothems.

Here interpretations of MIS 3 environmental conditions are sub-divided into early and late MIS 3. The discussion starts with early MIS 3, defined as the interval from *c*. 59 ka to 50 ka, and late MIS 3 referring to the period between *c.* 49 ka and 24 ka.

Early MIS 3 (*c.* 59 ka – 50 ka)

At De Hoop, the base of BL4 that dates here to between *c.* 59 ka and 50 ka falls within early MIS 3 (shown in magenta in Fig. 5.1). Between 59 ka and 56 ka, $\delta^{13}C$ shows rapid fluctuations with values between -0.75‰ and -8.5‰, which is suggestive of abrupt shifts between C_3/C_3-like CAM and C_4 vegetation (shown in green in Fig. 5.2). By 55 ka, $\delta^{13}C$ is at -7.5‰, and falls in the upper Holocene range of C_3 plants (after Talma & Vogel 1992). During the period between 54 ka and 50 ka, $\delta^{13}C$ follows a general increasing trend towards higher values between -4.5‰ and -4.0‰. These values fall within the range of C_4 plants and suggest an increase in C_4 during this part of early MIS 3. The corresponding $\delta^{18}O$ signal tracks changes in $\delta^{13}C$ and shows variable $\delta^{18}O$ values, between -3.75‰ and -0.75‰, between 58 ka and 56 ka (shown in green in Fig. 5.3). These highly variable BL4 $\delta^{18}O$ values, suggest rapid shifts in local rainfall dynamics that coincided with changes in vegetation. By 55 ka, $\delta^{18}O$ is at -3.25‰, and within the lower limit of summer rainfall (after Bar-Matthews *et al.* 2010 & Braun 2014). Between 54 ka and 50 ka, $\delta^{18}O$ follows an increasing trend towards higher values, between -2.5‰ and -2.0‰. This is suggestive of an increasing summer rainfall influence, which complements the interpretation of C_4 vegetation at this time.

While the De Hoop record (from BL4) associates the interval between 59 ka and 56 ka with unstable conditions, this is not evident in the comparative PP29 record. In this latter record, the contemporaneous period between 59 ka and 56 ka, shows $\delta^{13}C$ decreasing to lower values between -9‰ and -11‰

(shown in grey in Braun 2014: 119 Fig. 4.12). At 55 ka, $\delta^{13}C$ increases marginally to -9‰ but values remain within the range of C_3 plants until *c.* 50 ka. In contrast to PP29, the BL4 record associates this part of early MIS 3 with increases in C_4 and summer rain. The corresponding PP29 $\delta^{18}O$ signal generally tracks changes in $\delta^{13}C$ (shown in grey in Braun 2014: 119 Fig. 4.12). Here $\delta^{18}O$ decreases to lower values between -3.5‰ and -4.5‰ during the interval between 59 ka and 56 ka. This is thought to reflect an increasing influence of winter rainfall at this time (Braun 2014). At 55 ka, there is a minor peak in $\delta^{18}O$ to -3.2‰, suggesting a marginally weaker but consistent input from winter rain. This trend continues until 50 ka (and into late MIS 3) when $\delta^{18}O$ show only minor fluctuations around -4‰ (shown in grey in Braun 2014: 119 Fig. 4.12).

When compared to BL4 and PP29, the Crevice Cave record shows comparable changes in $\delta^{13}C$ with PP29 between 59 ka and 56 ka. During this interval, these Mossel Bay records do not show rapid changes in $\delta^{13}C$, which is evident in BL4. Instead, the Crevice Cave $\delta^{13}C$ signal shows a decreasing trend from -9‰ to -11‰, suggestive of increasing C_3 vegetation (shown in dark blue in Fig. 5.2). At 55 ka, there is a weak increasing trend to higher values between -9.5‰ and -9.0‰, which is still indicative of C_3 plants (Bar-Matthews *et al.* 2010). While this trend is also evident in BL4, the amplitude of these peaks is relatively muted at Crevice Cave. In the latter Crevice Cave record, the increasing trend continues until 53 ka, which marks the terminal growth of the stalagmite (Bar-Matthews *et al.* 2010). During this interval, $\delta^{13}C$ values remain within the range of C_3 plants (after Talma & Vogel 1992). The associated $\delta^{18}O$ signal broadly tracks changes in $\delta^{13}C$. Between 59 ka and 56 ka, $\delta^{18}O$ shows a decreasing trend to lower values, from -3.5‰ to -4.5‰, which suggests a trend towards more winter rainfall during this part of early MIS 3 (shown in dark blue in Fig. 5.3). At 55 ka, $\delta^{18}O$ is between -4.5‰ and -4.0‰ but remains within the range of winter rain (after Bar-Matthews *et al.*

2010). By 53 ka, $\delta^{18}O$ peaks at -3.2‰ and is suggestive of weaker winter rain (Bar-Matthews *et al.* 2010: 2139) and possibly increasing year round rainfall (as discussed in Chapter 4 section 4.3).

Between 59 ka and 51 ka, the coeval part of the Sandkraal Cave record, shows $\delta^{13}C$ decreasing to values between -8‰ and -9‰, associated with C_3 plants (Braun 2014). Around 50 ka, there is a weak increasing trend to a marginally higher value of -7‰, suggestive of decreasing C_3 plants relative to C_4 just before a hiatus in the Sandkraal record (shown in black in Braun 2014: 121 Fig. 4.13). The corresponding $\delta^{18}O$ signal for the period between 59 ka and 51 ka is relatively stable around -3‰ (shown in black in Braun 2014: 121 Fig. 4.13). Around 50 ka, there is a minor peak in $\delta^{18}O$ to -2‰, which possibly reflects either increasing summer rainfall (Braun 2014) or a shift to year round rainfall.

As a whole, in early MIS 3, the coastal records reflect either variable rainfall conditions (*viz.* De Hoop) or generally more winter rain (*viz.* PP29, Crevice Cave & Sandkraal). In contrast, the Little Karoo record suggests consistent winter rain input. Here the Little Karoo $\delta^{18}O$ record only shows minor fluctuations around -4‰ in early MIS 3 (and into late MIS 3) (shown in dark blue in Braun 2014: 130 Fig. 4.18).

Taken together, there are apparent discontinuities between the De Hoop (BL4), Mossel Bay (PP29 & Crevice Cave), George (Sandkraal) and Little Karoo records. With the exception of the De Hoop record, there are more commonalities between the other coastal records. The implication is that local conditions at De Hoop during part of early MIS 3 were more variable compared to Mossel Bay and George. During the latter part of early MIS 3, when summer rain and C_4 vegetation occurs at De Hoop conditions were seemingly similar to those in early MIS 5a (as discussed in section 5.2.1).

Late MIS 3 (*c.* 49 ka – 24 ka)

Late MIS 3 is represented by the upper part of BL4, BL3 and the younger part of BL1 (Fig. 5.1). In BL4, late MIS 3 is dated between 50 ka and 34 ka (shown in magenta in Fig. 5.1) while in BL3 late MIS 3 falls between 47.1 ka and *c.* 46.7 ka and (shown in red in Fig. 5.1). In the younger part of BL1 the main growth phase correlated with late MIS 3 is dated to between *c.* 46 ka and 31 ka (shown in blue Fig. 5.1). Comparative speleothem records for late MIS 3 come from Pinnacle Point (PP29) (*c.* 49 ka - 40 ka), Sandkraal Cave (*c.* 40 ka - 25 ka), the Little Karoo (*c.* 48 ka to 35 ka) and Cango Cave (*c.* 47.1 kcal BP – 24.1 kcal BP) (Table 5.1 & Fig. 5.1).

At De Hoop, BL4 shows $\delta^{13}C$ between -3‰ and -6‰, during the period between 50 ka and 45 ka (shown in green in Fig. 5.2). These values cover the range of C_4 plants and are suggestive of increasing C_4 coverage at this time. The associated $\delta^{18}O$ signal shows comparable variation with values between -2.75‰ and -1.75‰ that reflect a stronger summer rainfall signal (shown in green in Fig. 5.3). A comparable pattern is also evident in BL3 where increases in C_4 occur throughout the coeval period between 47.1 ka and 46.7 ka (shown in pink in Fig. 5.2). The associated BL3 $\delta^{18}O$ signal also tracks changes in $\delta^{13}C$ with values between -3.5‰ and -1.5‰ which fall within a similar range to those from BL4 (shown in purple in Fig. 5.3). This suggests similar (summer) rainfall conditions above the cave during this part of late MIS 3. Both of these stalagmites come from the same cave, were formed during similar time periods and clearly express similar conditions in late MIS 3. Based on this, it is reasonable to infer that BL4 and BL3 have retained a palaeoenvironmental signal of late MIS 3 conditions at De Hoop and the Overberg. During this stage, the De Hoop records indicate warm, seasonal summer rain and C_4 vegetation.

In contrast to the De Hoop records which associate part of late MIS 3 with increases in summer rain and more C_4 plants the comparative PP29 record

does not exhibit this. In the contemporaneous part of PP29, dating between 49 ka and 45 ka, $\delta^{13}C$ is between -9‰ and -10‰ and firmly within the range of C_3 plants (shown in grey in Braun 2014: 119 Fig. 4.12). The associated $\delta^{18}O$ values, which are fairly stable between -4.0‰ and -3.5‰, and are thought to reflect year round rainfall conditions (Braun 2014: 159 also see Chapter 4 section 4.3). In the coeval Little Karoo record, there is a general increasing trend in $\delta^{18}O$ from -6‰ up to -4‰ between 48 ka and 44 ka (shown in dark blue in Braun 2014: 130 Fig. 4.18). These values are however consistently within the range of winter rainfall at this site (after Braun 2014). When compared to PP29 and the Little Karoo, the Cango Cave record shows more commonalities with these records than those from De Hoop (BL4 & BL3). Here $\delta^{13}C$ for the interval between 47.1 kcal BP and 44 kcal BP is similarly associated with increasing C_3 plants with values between -10.0‰ and -10.7‰ (shown in dark brown in Fig. 5.2). This pattern of C_3 vegetation is also evident in PP29 (as discussed above). While PP29 associates this part of late MIS 3 with year round rainfall, $\delta^{18}O$ at Cango Cave (-5.2‰ & -5.5‰) is thought to reflect a stronger winter rainfall signal (shown in dark brown in Fig. 5.3) that is comparable with the Little Karoo.

During the interval between 46 ka and 40 ka, the BL1 stalagmite from De Hoop shows $\delta^{13}C$ between -4.5‰ and +3.0‰ which are suggestive of a stronger C_4 vegetation signal (shown in orange in Fig. 5.2). The corresponding $\delta^{18}O$ values, between -3.0‰ and +1.0‰, are equally enriched and fall well outside the theoretical limit of summer rainfall (after Bar-Matthews *et al* .2010 & Braun 2014). In the contemporaneous part of BL4, dating between 44 ka and 40 ka, $\delta^{13}C$ is between -6.0‰ and -1.5‰ and similarly within the range of C_4 plants (shown in magenta in Fig. 5.2). The corresponding BL4 $\delta^{18}O$ values, between -3.5‰ and -1.25‰, also suggest generally stronger summer rain during this part of late MIS 3. Although BL1 and BL4 exhibit comparable trends, the $\delta^{13}C$ and $\delta^{18}O$ values from BL1 are

significantly higher than those from BL4. This is attributed to aragonite enrichment in BL1 (as discussed in Chapter 4 section 4.3.1). In contrast to the De Hoop records (BL1 & BL4), PP29 does not show a pattern of summer rainfall and C_4 plants between 44 ka and 40 ka. Instead, this latter record shows $\delta^{13}C$ values (between -9‰ & -10‰) which continue to favour C_3 plants and $\delta^{18}O$ (between -4.0‰ & -3.5‰,) that is suggestive of year round rainfall (shown in grey in Braun 2014: 119 Fig. 4.12). This interval is not represented in the Little Karoo $\delta^{18}O$ record as there is a brief hiatus between *c.* 43 ka and 42 ka (Fig. 5.1 & Table 5.1). In the Cango Cave record, there is a minor increasing trend in $\delta^{13}C$ during the period between 44.2 kcal BP and 40.1 kcal BP. At this time, $\delta^{13}C$ increases incrementally from -10.5‰ up to -9.5‰ which is suggestive of more C_3 plants relative to C_4 (shown in dark brown in Fig. 5.2). The corresponding $\delta^{18}O$ signal shows minor fluctuations during this period with values between -5.5‰ and -5.1‰ which remains within the range of winter rainfall (shown in dark brown in Fig. 5.2).

Between 40 ka and *c.* 31 ka, BL1 shows high amplitude changes in $\delta^{13}C$ with values decreasing dramatically from +3.5‰ at 40 ka down to -4.5‰ by 37 ka. The BL1 $\delta^{13}C$ peaks again at +0.5‰ *c.* 34 ka before decreasing progressively to a lower value of -2.0‰ by *c.* 31 ka (shown in orange in Fig. 5.2). While these values are highly variable they favour correlation with C_4 plants and suggest a variable but consistent presence of C_4 vegetation at this time. The corresponding $\delta^{18}O$ signal tracks changes in $\delta^{13}C$ with values decreasing abruptly from +1.0‰ at 40 ka down to -3.0‰ by 37 ka. Around 34 ka, $\delta^{18}O$ peaks at -1.5‰ but decreases incrementally to a lower value of -2.5‰ by 31 ka (shown in orange in Fig. 5.3). Although quite variable, these consistently high $\delta^{18}O$ values remain within the range of summer rain. This interval is also present in its entirey in BL4 which comes from the same cave as BL1 (and BL3). Unlike BL3, BL4 has no clearly defined hiatus (es) associated with this period (Fig. 5.1). In the contemporaneous period between 40 ka and 34 ka,

BL4 shows $\delta^{13}C$ falling with the range of C_4 plants with values between -5.5‰ and -6.0‰ (shown in magenta in Fig. 5.2). However, based on the estimates from Talma and Vogel (1992), these values equate to about 50% C_4. This implies an equal contribution from C_3/CAM plants into the $\delta^{13}C$ signal at this time. When compared to BL1, which shows increases in C_4, BL4 shows a markedly different pattern of vegetation change with a mosaic of both C_4 and C_3/CAM associated with this part of late MIS 3. The corresponding $\delta^{18}O$ values show very little variation during this interval with fairly stable values, around -2.75‰ which appears to suggest generally more summer rain (shown in magenta in Fig. 5.3). As a whole, there are some commonalities between BL1 and BL4 and also between BL3 and BL4. Based on this, kinetic fractionation effects, interpreted from the Hendy Test results (discussed in Chapter 4 section 4.2), did not seemingly compromise the De Hoop palaeoenvironmental signal to a significant extent. However, given the significantly higher $\delta^{13}C$ and $\delta^{18}O$ values in BL1 relative to BL4, it appears that aragonite enrichment could have compromised this particular record.

At Sandkraal Cave, the contemporaneous period between 40 ka and 30 ka shows $\delta^{13}C$ increasing from -10.5‰ to -8.5‰, which is suggestive of weak increases in C_4 plants (shown in black in Braun 2014: 121 Fig. 4.13). This is broadly similar to the pattern at De Hoop where C_4 plants are also interpreted during this part of late MIS 3 (discussed above). The corresponding $\delta^{18}O$ values tracks changes in $\delta^{13}C$ and show values fluctuating between -3.5‰ and -2.5‰ which falls within the range of summer rain (after Bar-Matthews *et al.* 2010). In the Little Karoo record, there is a general increasing trend towards higher $\delta^{18}O$ values, from -4.0‰ up to -3.5‰, during the coeval period between 40 ka and 35 ka (shown in dark blue in Braun 20014: 130 Fig. 4.18). While $\delta^{18}O$ values from the Little Karoo are primarily associated with winter rainfall (Braun 2014: 172), these values possibly reflect a weaker winter rainfall influence at this time. During the period between 40.5 kcal BP and

30.4 kcal BP, $\delta^{13}C$ in Cango Cave shows an increasing trend towards higher values with a local peak at -8.5‰ by 37.1 kcal BP (shown in dark brown in Fig. 5.2). This is followed by a decreasing trend to lower values, still within the range of C_3 plants, from *c*. 34 kcal BP to 30 kcal BP. The associated $\delta^{18}O$ values track changes in $\delta^{13}C$ and also show a local peak at a higher value of -4.5‰ by 37.1 kcal BP (shown in dark brown in Fig. 5.3). There is also a decreasing trend to lower values, which are associated with winter rain, from 34 kcal BP to 30 kcal BP. During this period $\delta^{18}O$ is fairly stable around -5.5‰. In contrast to the coastal records from De Hoop (BL1 & BL4) and George (Sandkraal), Cango Cave does not show comparable trends during this part of late MIS 3. The Cango record does however share a winter rainfall signal with the Little Karoo.

The terminal part of late MIS 3, dating to between 30 ka and 25 ka, is not present in the De Hoop records. With the exception of part of the Sandkraal Cave record, it is also absent in other coastal speleothem records discussed here. Part of the Cango Cave record also falls within this stage. At Sandkraal Cave, $\delta^{13}C$ shows an increasing trend towards higher values from -9‰ up to -6‰ (shown in black in Braun 2014: 121 Fig. 4.13). While the associated $\delta^{18}O$ values are less variable, contemporaneous values are between -2.0‰ and -3.0‰, and within the range of summer rain (shown in black in Braun 2014: 121 Fig. 4.13). In contrast to the Sandkraal record, the coeval part of the Cango record, dated to between 29.7 kcal BP and 24.5 kcal BP, does not show a comparable pattern. In this latter record, $\delta^{13}C$ shows a weak decreasing trend towards a lower value of -10.5‰ before peaking at -9.5‰ by 26.4 kcal BP (shown in dark brown in Fig. 5.2). By 24.5 kcal BP $\delta^{13}C$ decreases back down to a low value of -10.7‰ and remains within the range of C_3 plants through to MIS 2 and the Holocene (Talma & Vogel 1992). The corresponding $\delta^{18}O$ values are fairly stable throughout the terminal part of late

MIS 3 with values between -5.2‰ and -5.5‰, which are suggestive of a consistent input of ^{18}O from winter rain (shown in dark brown in Fig. 5.3).

To summarise, conditions at De Hoop during the earlier part of late MIS 3 appears to have favoured warm summer rains and C_4 vegetation. In contrast, at Mossel Bay (PP29), the Little Karoo and Cango Valley (Cango Cave), conditions were seemingly less variable than at De Hoop. Rainfall proxies from these sites suggest increases in either year round rainfall (PP29) or winter rainfall (Little Karoo & Oudtshoorn) while vegetation proxies suggest C_3 dominance at this time. Towards the later part of this stage, conditions at the coast appear to have become less variable, particularly between De Hoop (BL1 & BL4) and George (Sandkraal).

Conclusion

Overall, during early MIS 3 (*c.* 59 ka – 50 ka), the De Hoop record from Bloukrantz Cave (BL4) suggests variable and possibly unstable conditions based on rapid changes in $\delta^{13}C$ and $\delta^{18}O$. The abrupt shifts in vegetation and local rainfall dynamics evident in BL4 are not expressed in coeval southern Cape speleothem records dating to this period. While conditions were seemingly more variable at De Hoop the opposite pattern is reflected at Mossel Bay (PP29 & Crevice Cave) and George (Sandkraal Cave). As a whole, early MIS 3 in the southern Cape appears to have been as cool as in early MIS 4. However during this part of MIS 3, rainfall was more variable at De Hoop while seasonally wetter during winter at Mossel Bay and George. Further inland, winter rain also extended into the Little Karoo. Vegetation proxies from De Hoop suggest habitats comparable to those during MIS 5a/4 while at Crevice Cave and George the cool, wet winter conditions favoured habitats with C_3 plants. By late MIS 3 (*c.* 49 ka – 24 ka) conditions were seemingly less variable than during the earlier part of this stage. During this

period, the De Hoop records (BL1, BL3 & BL4) suggest a shift towards increases in summer rain and a consistent C_4 vegetation presence. A similar trend is expressed at Sandkraal in George where relatively warm conditions with more seasonal summer rain and C_4 plants are interpreted. Late MIS 3, at least in these parts of the southern Cape, is comparable with conditions in early MIS 5a (based on BL1) and early MIS 4 (based on KDS, PP29 & Crevice Cave). In contrast to De Hoop and George (Sandkraal), conditions at Mossel Bay (PP29), the Little Karoo and Cango Valley (Cango Cave), remained similar to those in early MIS 3. As a whole, the occurrence of MIS 3 speleothems from different parts of the southern Cape implies that conditions throughout this stage remained wet enough to favour speleothem growth.

5.3 Summary

This chapter provided an overview of the environmental interpretations for marine oxygen isotope stages MIS 5a, MIS 4, and MIS 3 obtained from speleothem records pertinent to the southern Cape. Here inferences of vegetation, rainfall, and temperature were presented for MIS 5a in section 5.2, for MIS 4 in section 5.3 and for MIS 3 in section 5.4. In each instance the data from this study, which comes from the De Hoop caves (BL1, BL3 & BL4) and Klipdrift Shelter (KDS), were discussed in relation to other speleothem proxy records. These comparative records come from Mossel Bay (Pinnacle Point & Crevice Cave), and George (Herold's Bay Cave & Sandkraal Cave), the Little Karoo and Cango Cave (Talma & Vogel 1992; Bar-Matthews *et al.* 2010; Braun *et al.* 2012; Braun 2014). In the next chapter (Chapter 6), each MIS stage represented by the De Hoop stalagmites and other pertinent speleothem records is considered in relation to archaeological proxies from the area. The main comparative proxy indicators used here are shellfish, micromammal fauna, large mammal faunal and ostrich eggshell. The above-mentioned proxies come from key southern Cape archaeological sites such as Blombos Cave, Klasies River, Die Kelders Cave, Klipdrift Shelter and Boomplaas.

Chapter 6 – THE PALAEOENVIRONMENTAL CONTEXT OF THE SOUTHERN CAPE FROM MIS 5a – 3: EVIDENCE FROM SPELEOTHEMS AND ARCHAEOLOGICAL PROXIES

6.1 Introduction

One of the major issues in South African Middle Stone Age archaeology is whether environmental change is correlated with cultural change. One of the ways to investigate this is to use detailed palaeoenvironmental records. In Chapter 2 I discussed whether there could be more high resolution site specific environmental data. New speleothem data from De Hoop which covers the period from MIS 5a to MIS 3 is discussed in Chapter 4. The extent to which the De Hoop data correlates to similar speleothem records from the southern Cape is the focus of Chapter 5. In this Chapter 6 comparisons are made between the interpretations derived from the speleothem records and selected archaeological proxies. In the southern Cape, the terrestrial archive of past environmental change comes primarily from the archaeological record. Here shellfish, micromammal remains, large mammal fauna, and ostrich eggshell (hereafter OES), are the main archaeological indicators used for inferring environmental change. The discussion presented here focuses on marine oxygen isotope stages MIS 5a (section 6.2), MIS 4 (section 6.4) and MIS 3 (section 6.6). A summary of the interpretations is also provided for each stage starting with MIS 5a (section 6.3), followed by MIS 4 (section 6.5) and concluding with MIS 3 (section 6.7).

6.2 Palaeoenvironmental synthesis for MIS 5a

At two sites in the southern Cape, Blombos and Klasies River, archaeological deposits fall within MIS 5a. Based on the recent OSL ages from Blombos and its associated error margins (Jacobs *et al.* 2013), the M1 and M2 levels are placed almost completely within MIS 5a. For this

reason the Blombos data presented here is only discussed in the context of MIS 5a.

In the Klasies sequence it is the upper part of the SAS member that dates to a part of early MIS 5a, with dates of *c.* 85 ka and *c.* 77 ka (Vogel 2001; Feathers 2002; Wurz 2002). In this section the discussion focuses on data from the shellfish, micromammal and large mammal fauna at Blombos and Klasies. The OES data are presently only available from Blombos and each of these proxies is discussed below.

Shellfish

At Blombos Cave, a higher shellfish density of 31.8 kg/m^3 in the older M2 compared with the 17.5 kg/m^3 for the M1 level is suggestive of the site being closer to the sea during the M2 occupation and further inland during M1 times (Henshilwood *et al.* 2001; Langejans *et al.* 2012). Shore distance estimates support this interpretation and place Blombos within *c.* 4.6 km of the coast in M2 times (Fisher *et al.* 2010). In contrast, during the M1 the site is placed further away with an average distance of up to 15 km from the coast (Fig. 6.1; Fisher *et al.* 2010).

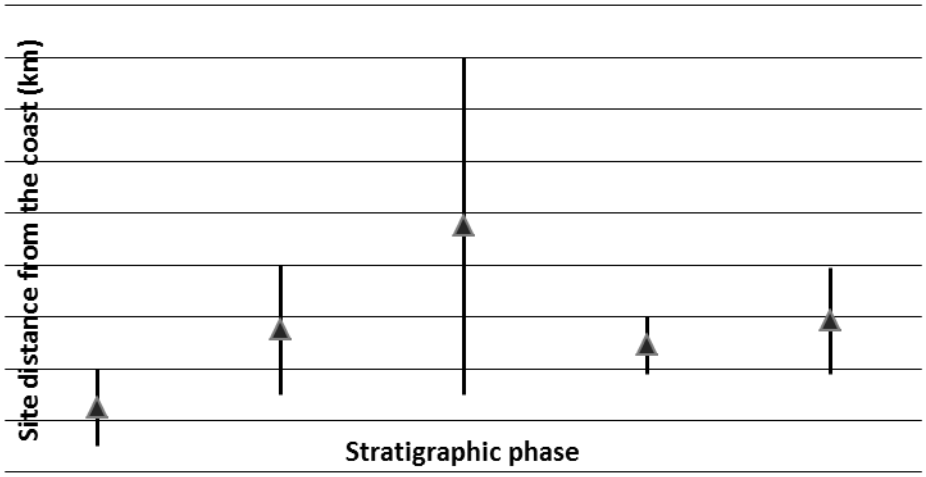

Fig. 6.1 Estimated distance from the coast during the occupations at Klasies River main site (denoted as KRM) (MSA II, Howiesons Poort & MSA III) and also

during the M2 and M1 occupations at Blombos Cave (denoted as BBC). The shoreline distance estimates presented above do not differentiate between the MSA II upper and MSA II lower and instead a combined range is used. Similarly for the M2 phase at Blombos Cave separate estimates are not provided for the M2 upper and M2 lower. (Modified after Langejans *et al.* 2012: 90 & 92)

In addition to the M1 level containing a lower concentration of shellfish, significant amounts of white mussel (*D. serra)*, a sandy beach indicator, also occurs in the M1. In contrast, the M2 levels do not contain any Donaxand are instead dominated by rocky shore indicator species of brown mussel (*P. perna*) (Henshilwood *et al.* 2001; Langejans *et al.* 2012). Rocky shores could also have been present during part of the M1 occupation since this level also contains brown mussel, turban shell (*Turbo sarmaticus*) and giant chiton (*Dinoplax gigas*), which favour rocky shores. These species occur in frequencies that are comparable to those in the M2 layers (Henshilwood *et al.* 2001; Langejans *et al.* 2012).

At the Klasies River main site, shoreline distance estimates also place the site within close proximity of *c.* 2.3 km to the sea throughout MIS 5 (Langejans *et al.* 2012). Unfortunately the MSA ll lower and upper have not been reported on separately , but this very close proximity of the site to the sea is reflected in the high density of shellfish (*c.* 3.9 kg/m^3 – 162.5 kg/m^3) that generally comes from the MSA ll in the SAS member (Thackeray 1988). The density of shellfish from the MSA II at Klasies is significantly higher than in the M1 at Blombos Cave. The *c.* 74 ka RF member on the other hand is described as sterile because it only contains a few shell fragments (Thackeray 1988). In the SAS member, rocky shore species of brown mussel (*P. perna*), turban shell (*T. sarmaticus*) and Patellids dominate and are suggestive of the shore being predominantly rocky (Thackeray 1988; Langejans *et al.* 2012). This interpretation is consistent with the surface topography at Klasies which has been characterised by steep cliffs with rocky horizons sloping steeply down to the shore by *c.* -50 m RSL (van Andel 1989: 143; Langejans *et al.* 2012).

Although rocky shore species generally dominate in the MSA II, there is a relative decrease in these species in the upper part of the MSA II

(Thackeray 1988), which relates to the data from BL1 (discussed in Chapter 5 section 5.2.1). Almost directly below the RF member, in the units associated with the upper MSA II in Cave 1A, there is a white mussel (*D.* serra) rich midden (Thackeray 1988). This midden occurs about one metre above Layer 30 dated to between 84.4 ka and 70.4 ka (Vogel 2001) whereas for the RF member, Layer 22, there is an OSL estimate of between 80 ka and 70 ka. The abundance of white mussel (*D. serra*) in the uppermost part of the MSA ll, is thus broadly contemporaneous with a part of the M1 at Blombos Cave where white mussel is also well represented.

The presence of white mussel in the upper MSA II and in the M1 level at Blombos therefore likely reflects lower sea levels at the transition from MIS 5a to MIS 4. This is consistent with shoreline distance estimates that place both sites further from the sea around *c.* 74 ka. During this period of relatively lower sea levels the suggestion is that conditions could have favoured sandy shore species.

While black mussel (*Choromytilus meridionalis*) occurs throughout the Klasies sequence, it is found in low frequencies, below 5%, in the upper MSA II (Thackeray 1988; Langejans *et al.* 2012). Black mussel (*C. meridionalis*) is ubiquitous along the west coast of South Africa where sea surface temperatures are often below 12^{o}C (Galimberti 2010). This mussel species has an affinity for cold water and is rare in the southern Cape. For this reason, its presence is generally used as a proxy for inferring cooler temperatures although? this species is not widely regarded as a reliable SST indicator (see Langejans *et al.* 2012). Nevertheless, from its consistently low occurrence in the MSA at Klasies main site, black mussel is considered indicative of cooler temperatures (relative to modern conditions) along the southern Cape coast (Thackeray 1988: 31).

Overall, the shellfish proxy data from Blombos Cave (M1 & M2) and the upper MSA II at Klasies River show that similar species occurred in varying abundances at both sites. Rocky shorelines that are linked to sea level transgression in late MIS 5a are inferred from the abundance of rocky

shore species. At Blombos Cave, rocky shore species are abundant in the M2 level and in part of the MSA II at Klasies. A different pattern emerges for the transition from MIS 5a to MIS 4. During this period, sandy shore white mussel becomes prominent in the M1 level at Blombos and in the midden below the RF member (correlated with the upper part of the MSA II at Klasies). At Blombos and Klasies sandy shorelines are inferred from the presence of white mussel (*D. serra*) and other sandy shore indicator species such as *Bullia* and giant chiton (*D. gigas*). The occurrence of molluscs with a preference for sandy substrates has also been related to regressing seas associated with the transition from MIS 5a to MIS 4.

Micromammals

In the context of MIS 5a, the micromammal assemblage from Blombos Cave and Klasies River main site are most pertinent and discussed below. Based on the similar diversity index values (*H*) corresponding to M1 (1.8 – 2.5), lower M2 (1.8 – 2.4) and upper M2 (2.1 – 2.3) the Blombos area is thought to have supported a diverse micromammal community throughout MIS 5a (Hillestad-Nel 2013). At Klasies, micromammal diversity is generally lower in the upper MSA II compared to the lower MSA II and MSA I. For the MSA II levels, *H* values were between 1.9 and 2.2 (Avery 1987) and recently refined to between 1.2 and 1.6 for the upper MSA II (Hillestad-Nel 2013). Based on this index alone, the implication is that during MIS 5a conditions in the Blombos area may have been more equable (non-seasonal) compared to Klasies. It is worth keeping in mind that diversity indices are sensitive to sample size and interpretations might be tentative (Hillestad-Nel 2013). For this reason, interpretations based on taxonomic habitat indices and multivariate analyses are usually preferred.

In the lower M2 and upper M2 at Blombos dense vegetation and closed, moist environments are inferred from low ratios (< 1.0) of gerbils to murines and from the abundance of shrews (*M. varius*), vlei rats (*O. irroratus*) and striped mouse (*R. pumilio*) (in the lower M2 CG-CGAA unit)

(Reed 2007; Hillestad-Nel 2013: 199). Fynbos vegetation is interpreted in the M2 (upper & lower) from the fynbos endemic Cape spiny mouse (*Acomys subspinosus*) and Verreaux's mouse (*Myomyscus verreauxii*) in part of the upper M2 (CFD & CF-CFA) (Avery *et al.* 1987; Hillestad-Nel 2013). Grassy vegetation is also represented in the M2 (upper & lower) and is interpreted from the abundance of climbing mouse (*Dendromus mesomelas*). With regards to rainfall, equable, less seasonal rainfall has been suggested from the relative abundance of vlei rats (*O. irroratus*) (Avery 1987: 416; Avery *et al.* 2005; Hillestad-Nel 2013: 211).

In the M1, the abundance of the pygmy mouse (*Mus minutoides*) and climbing mouse (*D. mesomelas*) suggests more open (grassland) habitats with little fynbos and sandy soils (Hillestad-Nel 2013). At the transition from MIS 5a to MIS 4 in the M1 (unit CA-CCC), dating to *c.* 73 ka, shrub vegetation is interpreted from the abundance of Kreb's fat mouse (*Steatomys krebsii*) and Saunder's vlei rat (*Otomys saundersiae*) (Hillestad-Nel 2013). This is thought to indicate slightly cooler conditions at this time. Moist conditions with dense vegetation has however been interpreted for much of MIS 5a at Blombos including the M1 based on a consistently low gerbil-to-murine ratio (Hillestad-Nel 2013).

At the Klasies River main site the micromammal assemblage from the SASW member in the upper MSA II falls within MIS 5a. In this member, moist conditions and dense vegetation are implied from vlei rats (*Otomys irroratus*) and laminate vlei rats (*Otomys laminatus*) (Hillestad-Nel 2013). Cape dune mole rats (*Bathyergus suillus*), imply Renosterveld vegetation (Avery 1987), and occur in low frequencies (0-9%) throughout the MSA phases at Klasies. It has been suggested that Renosterveld vegetation occurred in the vicinity of Klasies River throughout MIS 5 times including in MIS 5a (Hillestad-Nel 2013). The absence of fynbos endemics such as Cape spiny mouse (*Acomys subspinosus*), Namaqua rock rat (*Aethomys namaquensis*) and Verreaux's white-footed rat (*Myomyscus verreauxii*) is

suggestive of a weak fynbos presence at Klasies. These species do however occur in the M2 levels at Blombos.

As a whole, in the upper MSA II, moist habitats close to streams and springs with grassy vegetation are inferred from the taxonomic microhabitat indices and from the abundance of African marsh rat (*Dasymys incomtus*) which favours areas close to natural waters (Hillestad-Nel 2013). With regards to rainfall, seasonally drier conditions with irregular or unequable rainfall is interpreted from the low frequency of shrews and from the absence of Duthie's golden mole (*Chlorotalpa duthieae*) (Hillestad-Nel 2013 but *cf.* Avery (1987) who previously identified this species in the upper MSA II.

Taken together, broadly similar inferences are made regarding the general vegetation and habitat conditions at Blombos (M1, upper & lower M2) and the upper MSA II at Klasies River. There does however seem to be minor discrepancies in the vegetation and rainfall interpretations between these sites. For example, the weak representation of fynbos in the upper MSA II at Klasies is not reflected at Blombos where fynbos is inferred from the consistent presence of endemic taxa in the M2. Although fynbos is poorly represented in the upper MSA II at Klasies River and absent in the M1 at Blombos these two phases are not contemporaneous. Also, at Klasies Renosterveld vegetation is inferred from the low frequency of Cape dune mole rats (*B.* suillus) in the upper MSA II (and older phases of the MSA). This inference is not made for Blombos.

With regards to inferences of rainfall seasonality, which are informed by the known reproductive and breeding season behaviour of abundant taxa, there are also some contradictions. For example, in the M1 and M2 at Blombos generally equable rainfall, which is evenly distributed throughout the year, is interpreted from the abundance of vlei rats (*O. irroratus*). In contrast, at Klasies River it is proposed that rainfall was more irregular (Hillestad-Nel 2013: 219). At Blombos notable exceptions do however come from part of the upper M2 (CGAC) and also in the M1 (CA-CCC).

Here it is suggested that rainfall may have been more seasonal at least for a short period of MIS 5a and during the transition from MIS 5a to MIS 4 (Hillestad-Nel 2013).

Based on the micromammal data from Blombos and Klasies River, MIS 5a is associated with generally warm, moist conditions with habitats mainly comprising grassy vegetation. It is worth keeping in mind that interpretations based on micromammals can seemingly be complicated by an over reliance on a few indicator species and the relative presence or absence of others. In the section below the large mammal fauna associated with MIS 5a are discussed.

Large mammal fauna

Large mammal faunal remains associated with MIS 5a come primarily from Blombos Cave and part of the upper MSA II at Klasies River . At Blombos, large mammal faunal remains from the M1 and M2 levels were previously described by Klein (Henshilwood *et al.* 2001). Unlike the micromammal data from the M2 levels the large fauna was not initially separated into the upper and lower M2 (Henshilwood *et al.* 2001). More recent taphonomic analyses of the Blombos fauna have however sub-divided the M2 levels into the upper and lower M2 (Reynard 2011; Reynard *et al.* 2014; Thompson & Henshilwood 2011, 2014a, b).

In the upper M2 at Blombos, bushy vegetation is interpreted from the presence of the common duiker (*Sylvicapra grimmia*) while closed habitats are suggested from grysbok (*Raphicerus melanotis*) and steenbok (*Raphicerus campestris*) (Henshilwood *et al.* 2001; Thompson & Henshilwood 2011). Across the M2, grysbok (*R. melanotis*) and steenbok (*R. campestris*) are well represented and extant species are endemic to the Cape Floral Region where habitats are dominated by fynbos. The M2 as a whole is also associated with wet conditions which is interpreted from the water-dependent southern reedbuck (*Redunca arudinum*)

(Henshilwood *et al.* 2001). Overall, the large mammal fauna indicates that in the M2 conditions were relatively moist with habitats mainly consisting of dense vegetation with tall grass, some bush and fynbos elements. From the ubiquity of small browsing antelope in the M2 (upper & lower) conditions are thought to have favoured small bovids relative to larger animals (Thompson & Henshilwood 2011). As a whole, the interpretations for conditions in the M2, based on the micromammals, are broadly complementary with those derived from the associated large mammal fauna.

While small bovid bones are most abundant in the M2 this pattern is not reflected in the M1 where larger (size class 4) animals are more abundant (Reynard 2011; Thompson & Henshilwood 2011). Here in the M1 grassy vegetation is interpreted from the relative abundance of black wildebeest (*Connochaetes gnou*) and hartebeest (*Alcelaphus buselaphus*) (Henshilwood *et al.* 2001). While these species are atypical of the present-day fynbos habitat in the area they are water dependent and imply moist and grassy conditions during part of the M1. Similar conditions in the M1 are suggested from the presence of the extinct, water-dependent, blue antelope (*Hippotragus leucophaeus*), which was endemic to the southern Cape and had a dietary preference for grass. Wet conditions during the M1 are further implied from southern reedbuck (*R. arudinum*) which occurs in similar frequencies in the M1 relative to the M2 (Henshilwood *et al.* 2001). Grysbok (*R. melanotis*) and steenbok (*R. campestris*), which are generally associated with fynbos, occur in lower frequencies in the M1 and may indicate a weak fynbos presence. This supports the previous interpretations from the micromammal data where fynbos is absent and generally moist conditions with grassy vegetation are associated with the M1.

At Klasies River, the upper part of the SAS member falls broadly within MIS 5a. The large mammal fauna identified in this member was previously divided into the SAS t, SAS m and SAS b to differentiate between fauna

from the top, middle and base (van Pletzen 2000). The SAS t relates to MIS 5a, and here the faunal remains are dominated by grazers and mixed feeders that occur in frequencies of 38% and 55%, respectively (van Pletzen 2000). As a whole, the SAS member has a higher frequency of browsers relative to grazers which is suggestive of closed habitats (van Pletzen 2000). A similar pattern was previously identified by Klein (1976) during his analysis of the Klasies fauna. While he focused on the MSA II as a whole, he also observed a decline in the relative frequencies of open habitat species to closed habitat species.

Although large size class bovids such as Cape buffalo (*Syncerus caffer*) and eland (*Taurotragus oryx*) also occur within the SAS member, small size class antelope (Klein 1976) dominate the fauna in this member. Here, small size class antelope account for approximately 86% of the MSA II faunal remains (Klein 1976). With regards to the SAS member, the inference of closed habitats is further supported by the abundance of blue duiker (*Philantomba monticola*) (van Pletzen 2000). This browsing antelope only occurs in the SAS divisions and is associated with forest and woodland habitats (Klein 1976). Dense (closed) vegetation is also interpreted from common duiker (*S. grimmia*), steenbok (*R. campestris*) and Cape grysbok (*R. melanotis*) in the SAS divisions (van Pletzen 2000). Overall, small browsing antelope that prefer closed vegetation dominate the fauna from the SAS member in the upper MSA II at Klasies River. The co-occurrence of terrestrial fauna comprising browsers and mixed feeders is suggestive of habitats with vegetation comprising grass and bush elements. Throughout the accumulation of the SAS member, including the top, conditions near the site were likely moist and local micro-habitats could support several water-dependent species (*e.g.*, southern reedbuck (*R. arudinum*) & blue antelope (*H. leucophaeus*).

When compared with the MIS 5a fauna at Blombos Cave, similar habitat and vegetation indicator species occur at both sites. These include, amongst others, grysbok (*R. melanotis*), steenbok (*R. campestris*),

common duiker (*S. grimmia*), klipspringer (*Oreotragus oreotragus*), blue antelope (*H. leucophaeus*), southern reedbuck (*R. arudinum*) and eland (*T. oryx*). While these species occur in varying abundances at both sites, small bovids dominate the faunal assemblages in the M2 (upper & lower) at Blombos and in the SAS member at Klasies. Since micro-habitats at Blombos and Klasies supported similar types of animals during MIS 5a it is reasonable to infer that environmental conditions were fairly similar here. Different habitats are however inferred from the relative abundance of large size class fauna in the M1 level at Blombos and in the Upper member at Klasies.

Ostrich eggshell (OES)

In the context of the southern Cape, Roberts (2013) undertook the only known study that uses $\delta^{13}C$ and $\delta^{18}O$ from OES as an environmental proxy. As part of his dissertation, Roberts (2013) analysed OES from Blombos Cave, Klipdrift Shelter and Klipdrift Cave. The Klipdrift Shelter samples come from deposits dated between 65.5 ka and 59.4 ka and is correlated to MIS 4 (Henshilwood *et al.* 2014). The Klipdrift Cave deposits are of Holocene age and cover the period between 11.8 ka and 9.7 ka (Ryano 2014). With regards to MIS 5a, only OES from the M1 and M2 (upper & lower) phases at Blombos are considered. In his analysis $\delta^{13}C_{OES}$ values between -10‰ and -8‰ are associated with C_4 vegetation while C_3 vegetation is reflected in values between -13‰ and -11‰. With regards to the corresponding $\delta^{18}O_{OES}$ values these were primarily interpreted in terms of relative humidity and aridity and linked to the effects of evapotranspiration on the plant-water response (Roberts 2013).

In the Blombos 1 group (representing the M1 & M2), $\delta^{13}C_{OES}$ values are between -9.9‰ and -9.3‰ suggesting a C_4 dietary input with the corresponding $\delta^{18}O_{OES}$ values falling between 2.4‰ and 1.6‰. Here, higher $\delta^{18}O_{OES}$ values (+5.0‰ to +0.1‰) are suggestive of ostriches eating vegetation with low moisture which is in turn linked to warm, summer season conditions associated with high evapotranspiration (Roberts 2013:

73). Lower values $\delta^{18}O_{OES}$ (+1.4‰ to -1.5‰) are in contrast associated with relatively cool, winter season conditions which generally reflect low evapotranspiration in plants. The weak increasing trend towards higher (more positive) values in the Blombos 1 group, comprising the M1 and M2, is however suggestive of relatively warm, arid local conditions during part of MIS 5a (Roberts 2013: 67).

Overall, the $\delta^{13}C_{OES}$ and $\delta^{18}O_{OES}$ data from Blombos are thought to indicate an increasing input of C_4 vegetation into the ostrich diet. The inferred expansion of C_4 vegetation coincides with relatively arid local conditions (inferred from the $\delta^{18}O_{OES}$ signal) that are attributed to seasonal summer rainfall in the area. There is however some disparity between the OES records and those from the small and large mammal remains. The latter records from Blombos and the Upper MSA II at Klasies River main site are complementary in suggesting MIS 5a conditions were warm and moist with dense and grassy vegetation. While the OES data primarily reflects conditions during the ostrich breeding season it suggests that local conditions may have been seasonally drier and possibly warmer than initially inferred.

6.3 Summary for MIS 5a

Interpretations of the micromammal and large mammal fauna from Blombos Cave and Klasies River suggest that conditions were relatively warm and humid during MIS 5a. Further evidence to support an inference of warm conditions in MIS 5a times comes from higher $\delta^{18}O$ values in the Blombos OES. Inferences about rainfall conditions derived from the MIS 5a faunal remains is somewhat tentative although the OES proxy data indicates that rainfall could have been more seasonal due to summer aridity.

When compared with the archaeological proxies that associate MIS 5a as a whole with warm, dry conditions, the speleothem records mainly associate these conditions with earlier parts of MIS 5a (85 ka – 80 ka).

The speleothem data corresponding to this interval comes from PP29 and Crevice Cave in Pinnacle Point and from BL1 in Bloukrantz Cave at De Hoop Nature Reserve. As a whole, more seasonal summer rain is interpreted from the high $\delta^{18}O$ values in each of these records and C_4 vegetation from the corresponding $\delta^{13}C$ values. From the speleothem records for PP29, Crevice Cave and Herold's Bay conditions in late MIS 5a (79 ka – 74 ka) were seemingly humid due to increases in winter rain and C_3 vegetation interpreted from the $\delta^{18}O$ and $\delta^{13}C$ signals, respectively. By the transition to MIS 4 conditions were more humid than during early MIS 5a, at least in the vicinity of Mossel Bay (PP29 & Crevice Cave) and George (Herold's Bay Cave). However, at De Hoop (BL1), and by extension the Overberg, local conditions appear to have been warmer and more variable.

Faunal proxy data indicates that MIS 5a habitats, at least those in the vicinity of Blombos and Klasies River, comprised dense vegetation suitable for both small browsing antelope and rodent micromammals. Varying abundances of large fauna and mixed feeders in the MIS 5a faunal assemblage is however suggestive of habitats with heterogeneous vegetation, possibly comprising C_3 and C_4 elements. While the small and large mammal fauna provides a broad overview of habitat conditions during MIS 5a, the OES data focuses specifically on conditions during the ostrich breeding season. While the OES $\delta^{13}C$ signal primarily reflects C_4 vegetation input in MIS 5a times, the speleothem $\delta^{13}C$ values only link C_4 vegetation to early MIS 5a. In the speleothem records from Mossel Bay and George, C_3/C_3-like CAM vegetation is thought to have been more abundant during later parts of MIS 5a and at the transition from MIS 5a to MIS 4. Here, interpretations of faunal remains and $\delta^{13}C$ signals in OES and speleothems indicate vegetation dominated by C_3 and possibly C_3-like CAM plants.

6.4 Palaeoenvironmental synthesis for MIS 4

In the southern Cape, key archaeological sites correlated with MIS 4 are Die Kelders Cave, Boomplaas Cave, Klipdrift Shelter, Pinnacle Point Cave PP5-6 and the Howiesons Poort at the Klasies River main site. Previous ages for the M1 at Blombos Cave dated the terminal part of this phase to *c.* 73 ka, the upper M2 at 76 ka and the lower M2 phase is dated to *c.* 85 ka (Jacobs *et al.* 2003a, b; 2006; Henshilwood *et al.* 2011). Together, the M1 phase falls within the MIS 5a/4 boundary and the M2 (as a whole) within MIS 5a. Recently OSL age determinations have also placed these layers towards the boundary of MIS 5a (Jaocbs *et al.* 2013). The proxies from these layers have therefore been discussed above. Further afield, along the South African west coast, archaeological proxy evidence pertinent to MIS 4 comes from Diepkloof Rock Shelter (Tribolo *et al.* 2013; Porraz *et al*. 2013) and Klein Kliphuis (Mackay 2006, 2011). For the purpose of this discussion, only archaeological proxy evidence from the southern Cape is considered.

Shellfish

The shellfish remains from the Howiesons Poort archaeological deposits correlated with MIS 4 are discussed here. These come from the Upper Member at Klasies River main site and from Klipdrift Shelter. While Pinnacle Point caves PP5-6 contains deposits dating to MIS 4 the sample of shellfish remains are as yet too small for analysis (Galimberti 2010; Brown *et al.* 2012).

At Klasies River the most abundant species in the Upper Member *(i.e*., Howiesons Poort & MSA III) are white mussel (*Donax serra*), *Bullia*, abalone (*Haliotis midae*), crown turban (*Turbo cidaris*) and giant chiton (*Dinoplax gigas*) (Thackeray 1988; Galimberti 2010; Langejans *et al*. 2012). Black mussel (*Choromytilus meridionalis*), which occurs almost exclusively along the west coast, is also found in consistently low frequencies (< 5%) throughout the Klasies sequence (Thackeray 1988:

28). As environmental indicators, white mussel (*D. serra*), *Bullia* and giant chiton (*D. gigas*) have a common preference for sandy beach substrates (Galimberti 2010). On the other hand abalone (*H. midae*), brown mussel (*Perna perna*), turban shell (*Turbo sarmaticus*) and crown turban (*T. cidaris*) typically occur either on rocks or in pools in the intertidal zone (Galimberti 2010; Langejans *et al.* 2012). Rocky shore indicator species, particularly brown mussel (*P. perna*) and turban shell (*T. sarmaticus*), are however more abundant in the MSA I and in the SAS member of the MSA II. In these depositional phases (*i.e*. MSA I & MSA II) shellfish densities are also higher compared to those associated with the Howiesons Poort and MSA III (Thackeray 1988). In the Howiesons Poort there is a decreasing trend towards lower values with a mean shellfish density of 5 kg/m^3 (Thackeray 1988). This is much lower than in the densities reported for the overlying MIS 5 layers. The occurrence of low shellfish densities during the accumulation of the Upper Member has often been linked to regressive seas that would have placed the site further from the sea (Deacon & Geleijnse 1988). For example, during MIS 4 times it is estimated that the Klasies main site could have been between 4.8 km and 5.6 km from the coast (Langejans *et al*. 2012: 92). Inferences have also been made that sandy shores exposed during MIS 4 sea level regressions provided a favourable habitat for molluscs that live on and in sandy substrates (Thackeray 1988).

At Klipdrift Shelter the shellfish densities (from units PCA, PBE, PBD & PBC) range from 25 kg/m^3 up to 183 kg/m^3 and show an increasing trend until *c*. 65.5 ka (unit PBC). By *c*. 60 ka there is a significant decline in shellfish density at the top of the sequence in units PBA/PBB (32 kg/m^3), PAZ (16 kg/m^3) and PAY (3 kg/m^3) (Henshilwood *et al.* 2014). Preliminary shellfish densities from Klipdrift Shelter also show a trend of shell diminution in the Howiesons Poort which is comparable with that at Klasies (Henshilwood *et al.* 2014). In this assemblage giant chiton (*D. gigas*), turban shell (*T. sarmaticus*) and abalone (*H. midae*) are the most common species across units PCA to PAY (Henshilwood *et* al. 2014). Brown

mussel (*P. perna*), another rocky shore indicator species, also occurs in consistently low frequencies while black mussel (*C. meridionalis*) is not present. This is contrary to the pattern at Klasies where the black mussel (*C. meridionalis*), suggestive of slightly cooler water temperatures during MIS 4, is present.

In the lowermost PCA unit of the Klipdrift Shelter sequence, turban shell (*T. sarmaticus*) represents 65% of the marine molluscs whereas abalone is more ubiquitous in PBE (50%) and PBD (64%). Overall, animals that favour rocky shores occur more frequently across the Howiesons Poort units PCA to PBD. One exception is unit PBC, in the middle of the sequence, where the sandy shore giant chiton, and rocky shore abalone, is present in similar frequencies of 39% and 41%, respectively (Henshilwood *et al*. 2014). The shellfish densities corresponding to each of these units (PCA, PBE, PBD & PBC) range from 25 kg/m^3 up to 183 kg/m^3 and show an increasing trend until *c*. 65.5 ka (unit PBC). By *c*. 60 ka there is a significant decline in shellfish density at the top of the sequence in units PBA/PBB (32 kg/m^3), PAZ (16 kg/m^3) and PAY (3 kg/m^3) (Henshilwood et al. 2014).

Overall, similar shellfish species are found in the Howiesons Poort assemblages from the Upper Member of the Klasies River main site and at Klipdrift Shelter. While shellfish densities at Klipdrift Shelter are siginificantly higher than those reported for the Howiesons Poort at Klasies River, both assemblages show a comparable trend in shell dimunition. Each assemblage is however dominated by seemingly different indicator species. In the Klasies sequence for example, sandy shore species such as white mussel (*D. serra*), *Bullia* and giant chiton (*D. gigas*) are more abundant. This implies that local conditions could have been sandy in the vicinity of Klasies during late MIS 4. In contrast, in the lower Howiesons Poort at Klipdrift Shelter, abalone (*H. midae*) and turban shell (*T. sarmaticus*), which are rocky shore species occurs more frequently. However in the upper Howieons Poort levels at Klipdrift Shelter giant

chiton dominates. While sandy beaches could have been present at Klipdrift Shelter during the late part of the Howiesons Poort it seems that for part of the Howiesons Poort rocky shorelines also occurred in the vicinity of Klipdrift Shelter. This suggests that relatively more rocky shorelines than those inferred at Klasies occurred during late MIS 4 for at least part of the Howiesons Poort.

Micromammals

Micromammal remains from MIS 4 contexts in the southern Cape also comes from part of the Klasies River main site sequence, from Die Kelders Cave and more recently from Klipdrift Shelter. While micromammal remains from Blombos Cave are associated with the MIS 5a/4 boundary these do not favour correlation with MIS 4. For this reason, the current discussion focuses on micromammals from Klasies River, Die Kelders Cave and Klipdrift Shelter. At the Klasies site, the earliest micromammal analyses initially placed the Howiesons Poort and MSA III deposits within MIS 5 (Avery 1982, 1987, 1988). This association has however been refined and the Howiesons Poort has been firmly correlated with MIS 4 (Jacobs *et al.* 2008). While a more recent, fine-grained study of the Klasies small mammal assemblage included taxonomic habitat indices and multivariate analyses, it focused on the MSA I and MSA II phases and did not focus on either the Howiesons Poort or MSA III (Hillestad-Nel 2013). Inferences of past environmental conditions during the Howiesons Poort and MSA III are therefore based on the study of Avery (1982, 1987) using species diversity and relative abundance measures. The latter measure has also been used as a temperature proxy for the Howiesons Poort and MSA II phases at the site (Thackeray 1987).

From her analysis, Avery (1987) noted that although vlei rats (*Otomys irroratus*) occur in other stratigraphic units at Klasies they were especially common in the Howiesons Poort (and MSA III). As proxy indicators, vlei

rats (*O. irroratus*) tend to occur in moist habitats with dense herbaceous vegetation (Avery 1987; Hillestad-Nel 2013). They have also been associated with Afrotemperate (Afromontane) forest found in the present-day Klasies area (Hillestad-Nel 2013). Fairly similar types of micromammal species occur in the Howiesons Poort and MSA III although in varying relative abundances. The main species are Saunder's vlei rats (*Otomys saundersiae*), Hottentots golden mole (*Amblysomus hottentotus*) and the xeric four striped mouse (*Rhabdomys pumilio*). Saunder's vlei rat (*O. saundersiae*) is associated with shrublands and has a preference for mountain fynbos (Avery 1987).

On the other hand, the golden mole (*A. hottentotus*) typically occurs in habitats with moist soils such as coastal dunes and tends to favour grassland vegetation (Thackeray 1987). The xeric four-striped mouse (*R. pumilio*) has a wide habitat tolerance but is more abundant in habitats with shrub vegetation (Avery 1987; Hillestad-Nel 2013). Taken together, these three species are relatively more abundant in the MSA III than in the underlying Howiesons Poort, suggesting more open habitats during the Howiesons Poort compared to the MSA III (Avery 1987).

The corresponding large mammal fauna, from the Upper Member as a whole, to some extent supports the inference of open habitats during parts of MIS 4 (see discussion on large mammal fauna section below). This is because typical grassland taxa occur more frequently in the Upper Member, and presumably in the Howiesons Poort, than in either the MSA I or MSA II (Klein 1976; van Pletzen 2000). There is however some disagreement between interpretations derived from species abundance measures and diversity index values. Although the latter implies that local conditions were similar throughout the Klasies sequence (Avery 1987: 415) more recent taphonomic analyses have cautioned against the use of diversity index values for palaeoenvironmental inferences (Hillestad-Nel 2013).

Large mammal fauna

In the southern Cape context, large mammal remains correlated with MIS 4 comes from Die Kelders Cave, in the Upper Member of the Howiesons Poort levels at Klasies River and from Klipdrift Shelter. MIS 4 fauna are found in the MIS 4 deposits at Diepkloof Rock Shelter on South Africa's west coast although these are not pertinent to the current discussion on the southern Cape. With the exception of the Diepkloof Rock Shelter, environmental interpretations derived from large mammal fauna at the above-mentioned sites is discussed below. There are also small mammal remains in the layers from Die Kelders and Klipdrift Shelter.

At Die Kelders Cave the large mammal faunal assemblage is represented by layers 4, 6, 8, 10, 12 and 14 (Grine *et al.* 1991; Marean *et al*. 2000). In these MSA layers, the Cape grysbok (*R. melanotis*) is the most abundant browser although browsers are not common at the site compared to grazers (Klein 1972; Marean *et al.* 2000). At Die Kelders, open habitats with grassy vegetation are interpreted from extralimital grazers such as springbok (*Antidorcas marsupialis*), Cape hartebeest (*Alcelaphus bucelaphus*) and black wildebeest (*Connochaetes gnou*) (Klein & Cruz-Uribe 2000). In layers 10 and 11, grassy vegetation is also suggested from the abudance of grazers which represent 86% and 93% of the Die Kelders fauna in these layers (Marean *et al.* 2000). The interpretation of grassy, vegetated habitats during part of MIS 4 complements previous inferences of similar conditions derived from the abundance of Cape hares (*Lepus capensis*) (discussed above).

At Die Kelders, wet conditions are also interpreted from southern reedbuck (*Redunca arudinum*), blue antelope (*Hippotragus leucophaeus*), black wildebeest (*C. gnou*) and hartebeest (*A. bucelaphus*) which are all water dependent species. Hippopotamus (*Hippopotamus amphibius*) remains were also found in the MSA layers at the site and also implies moist conditions in MIS 4 (Marean *et al*. 2000). The inference of wet conditions is further supported by the relatively large average size of Cape dune mole

rats (*Bathyergus suillus*) at the site (as discussed in the previous section). Overall, interpretations derived from the small and large mammal faunal remains at Die Kelders Cave are fairly complementary. Both records imply generally cool and moist local conditions with habitats mainly comprising grassy vegetation. This is in stark contrast to the present-day vegetation in the area which is dominated by sclerophyllous fynbos.

At Klasies River main site, the Upper Member contains MSA III and Howiesons Poort deposits. In previous analyses of the main site fauna, zooarchaeologists did not differentiate between the Howiesons Poort and MSA III. References are instead made to the MSA III (Klein 1976) or Upper Member deposits (van Pletzen 2000). Environmental inferences based on faunal evidence therefore only broadly correlates with MIS 4. In his initial analysis of the Klasies River fauna, Klein (1976) linked the occurrence of open habitats in the MSA III to the abundance of grazing indicator species. Van Pletzen (2000) subsequently analysed the large mammal fauna from the site and also noted that grazers dominated the Upper Member and interpreted this as indicating open (grassland) habitats. Chi-squared test statistics did however indicate that similar proportions of closed and open habitat indicator species were present in the Upper Member (Van Pletzen 2000). Based on this, Van Pletzen (2000) suggested that vegetation around the Klasies site potentially supported a heterogeneous community of animals. This inference is to some extent supported by the occurrence of mixed feeders such as eland (*T. oryx*) in the MSA III. The abundance of Cape buffalo (*Syncerus caffer*), which tends to occur in a wide variety of habitat types, similarly implies variable local habitats at Klasies.

At Boomplaas Cave the large mammal fauna was previously analysed by Klein (1978) and more recently by Faith (2013). In his preliminary analysis, Klein (1978) focused primarily on the fauna from the Holocene and Last Glacial members, but and also grouped the MIS 4, OCH and LOH members, into the Earlier Upper Pleistocene 1 (Klein 1978). From his

analysis, Klein (1978) found that grazing species, which are suggestive of grassy vegetation, were generally less abundant in the Earlier Upper Pleistocene 1. Faith (2013) identified a similar pattern of increasing grazing species richness from the base of the sequence through to the LGM. Unlike Klein (1978), Faith (2013) retained the original stratigraphic designations of Deacon (1979, 1995) and identified southern reedbuck (*R. arudinum*) and mountain reedbuck (*R. fulvorufula*) as the most common grazers in the MIS 4 members (*i.e.* OCH & LOH) but also in the MIS 3 (BOL & OLP members).

As a whole, grazers are weakly represented in the MIS 4 part of the Boomplaas sequence where they occurred in relative frequencies of 12.5% and 28%, respectively (Faith 2013). Browsers were however more ubiquitous. From the abundance of Cape grysbok (*Raphicerus melanotis*) and steenbok (*Raphicerus campestris*), habitats with dense closed, fynbos vegetation are interpreted. At Boomplaas, rocky or mountainous habitats with some grassy vegetation are also inferred by the co-occurrence of klipspringer (*Oreotragus oreotragus*) and grey rhebok (*Pelea capreolus*) (Kingdon *et al.* 2013). As a whole, the large mammal fauna suggests that in MIS 4, conditions at Boomplaas were favourable to browsers and local habitats contained a heterogeneous mixture of shrubs and grass (Faith 2013).

In the Klipdrift Shelter faunal assemblage, bones are highly fragmented and identified species are represented by animals from size class 1 through to 4. Due to the small sample sizes, the preliminary faunal analysis by Henshilwood *et al.* (2014) only focused on stratigraphic layers PAY, PAZ, PBA/PBB, PBC, PBD, PBE and PCA. Faunal remains from this site also include burnt and unburnt tortoise bone mainly identified as angulate tortoise (*Chersina angulata*) (Henshilwood *et al*. 2014). From Henshilwood *et al.*'s (2014) analysis, grazers are generally more abundant in PBC and PBA/PBB where they respectively account for 79% and 80% of the identified fauna. Grazing species are generally indicative of open,

grassy habitats such as grassland and savannah environments. Conditions favourable to grassy vegetation is further implied by the occurrence of Leoporids in the Klipdrift Shelter micromammal assemblage (as discussed previously). Browsing fauna is however more common in the older *c*. 64.6 ka PBD unit, accounting for 75% of the identified fauna.

In PBD, closed fynbos-type vegetation is interpreted from Cape grysbok (*R. melanotis*) and steenbok (*R. campestris*) while dense, woody vegetation are also interpreted from the grey duiker (*S. grimmia*) and black rhinoceros (*Diceros bicornis*) (Pienaar 1974; Buk & Knight 2010). Rocky, mountain slope habitats are however inferred from grey rhebok (*P. capreolus*). The micromammal remains from the Klipdrift Shelter sequence, which also includes rock hyrax (*P. capensis*), to some extent support an inference of local micro-habitats comprising dense vegetation and rocky slopes.

While the large mammal fauna from PBC and PBA/PBB is associated with grassland type habitats conditions were seemingly more heterogeneous during the deposition of PBD. This is because the fauna from the two units directly above PBD mainly contain grazers whereas in PBD browsers are more abundant (Henshilwood *et al*. 2014). It generally seems that during MIS 4 conditions at Klipdrift Shelter were favourable for grazers and local habitats were relatively open, wet and grassy. The high frequency of browsers in PBD does however imply that subtle environmental changes also occurred with micro-habitats supporting fauna with a preference for rocky habitats and woody vegetation.

Taken as a whole, the faunal evidence presented here shows that fairly similar grazing and browsing species occurred in the southern Cape during MIS 4 times. During early MIS 4 (*c.* 72 ka – 68 ka), grassland alcelaphines are abundant at Die Kelders Cave which indicates wet and grassy conditions around this time. By mid-to-late MIS 4 (*c*. 66 ka – 62 ka), mixed feeders and grazing fauna are well represented relative to browsers in the Upper Member at Klasies River main site. This is contrary to the

pattern at Boomplaas where browsers are better represented in the coeval part of the sequence correlated to late MIS 4. While interpretations of the Klipdrift Shelter faunal assemblage are based on preliminary assessments, similar variability, comparable to the Klasies River main site, is observed between browsing and grazing fauna. At Klipdrift Shelter grazing ungulates occur more frequently in unit PBD *c*. 65 ka and in unit PBA/PBB *c*. 59 ka. Here the latter unit correlates to the MIS 4/3 boundary. However, unlike in PBC where grazers are well represented, browsers are more common in the similar aged, underlying PBD unit. Based on these trends, the general inference is that by late MIS 4, conditions at Klipdrift Shelter were suitable enough for heterogeneous communities of grazers and browsers to co-exist. This may be attributed to a variety of environmental factors. The mostly likely variables relates to habitat productivity, adequate vegetation for foraging, annual precipitation and the opening up of new habitats as a result of changes in local topography (Shipley 1999; Janis *et al.* 2000).

With regards to the small mammal remains pertinent to MIS 4 these come from Die Kelders Cave and Klipdrift Shelter. At Die Kelders, small mammal remains, such as dune mole rats and rock hyrax, are particularly abundant in layers 5, 7, 9, 11, 13 and 15 (Klein 1986; Grine *et al*. 1991). As a whole, the MSA small mammal assemblage is dominated by four key indicator species. These are Cape dune mole rats (*B. suillus*), grey mongoose (*Galerella pulverulenta*), hares (*Lepus*) and rock hyrax (*Procavia capensis*) (Klein 1986; Grine *et al.* 1991; Cruz-Uribe & Klein 1998; Marean *et al*. 2000). Cape dune mole rats (*B. suillus*) are ubiquitous at southern Cape archaeological sites and typically occur in sandy coastal areas receiving MAP above 500 mm (Henshilwood 1997; Bennett & Faulkes 2000). Here the abundance of relatively large sized Cape dune mole rats (*B. suillus*) imply wet conditions with sandy habitats containing grass and geophytic bulbs in fynbos vegetation (Klein 1986; Jarvis & Bennett 1990; Bennett &

Faulkes 2000; Klein & Cruz-Uribe 2000; Henshilwood *et al.* 2001; Hart *et al.* 2006).

Slightly cooler temperatures are interpreted from the relative abundance of large sized grey mongoose (*G. pulverulenta*) which also has a preference for fynbos. Vegetated and grassy local habitats are however also interpreted from Cape hares (*Lepus capensis*) in MSA layers 15 to 12 and 6 to 4 (Klein 1986; Klein & Cruz-Uribe 2000). Like Cape dune mole rats (*B. suillus*), size variation in rock hyraxes (*P. capensis*) is also positively correlated with rainfall (Klein & Cruz-Uribe 1996b). From the occurrence of this species in part of the MSA sequence at Die Kelders rocky habitats (*e.g.* outcrops, rocky hillsides, cliffs) with bushes, shrubs and trees are inferred (Klein & Cruz-Uribe 1996b; Skinner & Chimimba 2005; Carr *et al.* 2010; Meadows *et al.* 2010; Chase *et al*. 2012). Taken together, conditions in MIS 4 at Die Kelders were seemingly favourable to a diverse community of mcromammals and small mammals.

At Klipdrift Shelter, the most common species identified in the small mammal assemblage are rock hyrax (*P. capensis*), Cape dune mole rat (*B. suillus*), scrub hare (*Lepus saxatilis*) and other unidentified leporids (Henshilwood *et al*. 2014). With the exception of other rabbit and hare species, these taxa are also abundant in the Die Kelders Cave assemblage. When compared to Klasies River, where open, presumably grassland, habitats are associated with MIS 4, relatively cool and wet conditions with dense vegetation is interpreted at Die Kelders Cave. Since Klipdrift Shelter shows a comparable pattern of small mammal diversity to Die Kelders, similar conditions during MIS 4 are also inferred at this site.

Ostrich eggshell (OES)

At Klipdrift Shelter, twenty-four OES samples obtained from units PDA, PCA, PBC, PBA/PBB and PAZ, comprising burnt and engraved fragments were analysed by Roberts (2013). This is the only known study from the

southern Cape where OES has been used to make interpretations about past environmental conditions. Here $\delta^{13}C_{OES}$ values ranged between -8.5‰ and -10.3‰ with a weak increasing trend from PAZ through to PBA/PBB. A peak at PBC and a slightly lower value in PCA and an increase in PDA follows this (Roberts 2013: 78). The corresponding $\delta^{18}O_{OES}$ values track changes in $\delta^{13}C_{OES}$ and ranges between 4.5‰ and 0.9‰ with the lowest values also occurring in PAZ. According to Roberts (2013: 76), $\delta^{18}O_{OES}$ values in this range reflect increasingly warm evaporative (summer) conditions (Roberts 2013: 76). Overall, the $\delta^{13}C_{OES}$ data are thought to reflect fluctuations between the dietary contribution from C_4 and C_3 vegetation while warm, dry conditions are inferred from the corresponding $\delta^{18}O_{OES}$ signal. The $\delta^{13}C_{OES}$ signal which implies shifts between C_4 and C_3 vegetation complements the interpretations derived from the large mammal remains at Klipdrift Shelter (as discussed previously). While generally grassy, wet conditions are inferred from the small mammal remains, the large mammal fauna that comprises a mosaic of browsers and grazers imply variable local conditions.

6.5 Summary for MIS 4

Interpretations of the micromammals from Klasies River are suggestive of generally more open habitats in MIS 4 times. However, varying abundances of vlei rats in the Upper Member could be suggestive of moist conditions with dense vegetation. In contrast, small mammal evidence from Die Kelders and Klipdrift Shelter suggests variable conditions in MIS 4. This is to some extent supported by interpretations of the large mammal fauna. At Die Kelders the faunal evidence suggests that in early MIS 4 (*c.* 72 ka - 68 ka), conditions were cool and wet with habitats supporting dense vegetation. Similar inferences come from the large mammal evidence for Klasies River and Klipdrift Shelter. Here, the suggestion is that during mid-to-late MIS 4 (*c.* 66 ka - 62 ka) (at Klasies) and by late MIS

4 (at Klipdrift Shelter), habitats supported both grazers and browsers. Further evidence to support an inference of environmental heterogeneity, at least during late MIS 4, comes from fluctuating $\delta^{13}C_{OES}$ values in the Klipdrift Shelter OES data. Inferences about rainfall conditions derived from the OES data are however suggestive of warm, dry conditions, at least during the (summer) ostrich breeding season. This interpretation of warm conditions, at least during part of MIS 4, also comes from temperature indices derived from the Klasies micromammals in the Howiesons Poort of the Upper Member (Thackeray 1987; Thackeray & Avery 1990 also see discussion in Chapter 2 section 2.3.2).

While the faunal evidence from Die Kelders associates early MIS 4 with heterogeneous habitats, the speleothem data links conditions of variable rainfall and vegetation mainly with late MIS 4. For early MIS 4, speleothem evidence comes from De Hoop Nature Reserve (KDS) and Mossel Bay (PP29 & Crevice Cave). During this part of MIS 4, high $\delta^{13}C$ values and increases in $\delta^{18}O$ are linked to increases in C_4 vegetation and either more summer or year-round rain, respectively. From the interpretations of the speleothem records, conditions in early MIS 4 were comparable with those in MIS 5a where warm, seasonally dry conditions are associated with early MIS 5a. Interpretations derived from the speleothem records are therefore contrary to those from the micromammal and large mammal fauna, at least for earlier parts of MIS 4.

Faunal evidence for later parts of MIS 4 suggests mosaic habitats and conditions suitable for diverse communities of rodents, and browsing and grazing fauna. Speleothem data from Mossel Bay (PP29 & Crevice Cave and George (Sandkraal Cave & Herold's Bay) supports this interpretation. Here high variability in $\delta^{18}O$ and $\delta^{13}C$ is thought to reflect fluctuations in rainfall and vegetation with generally cooler conditions in late MIS 4 compared to early MIS 4.

6.6 Palaeoenvironmental synthesis for MIS 3

In the southern Cape, archaeological deposits correlated to MIS 3 presently comes from two MSA sites. These are the MSA III (post-Howiesons Poort) in the Upper Member at the Klasies River main site and Boomplaas Cave (Mitchell 2008). Across the rest of the Western Cape Province, other sites with some MIS 3 deposits are Diepkloof Rock Shelter, Klein Kliphuis, Elands Bay Cave and possibly Ysterfontein 1 (Parkington 1980; Parkington & Poggenpoel 1987; Halkett *et al.* 2003; Mackay 2006, 2011; Avery *et al.* 2008). Further afield, in other parts of South Africa, MIS 3 sites include Wonderkrater Cave, Rose Cottage Cave, Sibudu and Umhlatuzana (Kaplan 1989; Wadley 1991; Wadley & Jacobs 2006; Backwell *et al.* 2014). However, for the purpose of this discussion, only archaeological proxy evidence from the southern Cape is considered. As discussed previously in Chapter 2 section 2.3.2 and in Chapter 5 section 5.2.3, MIS 3 is a fairly long stage and here it is sub-divided into early MIS 3 (*c.* 59 ka – 50 ka) and late MIS 3 (*c.* 48 ka – 24 ka).

Shellfish

Early MIS 3 (c. 59 ka – 50 ka*)*

In the southern Cape, shellfish remains from archaeological deposits correlated with MIS 3 come primarily from the Upper Member at Klasies River main site. While the Boomplaas deposits date to MIS 3, shellfish has only been recovered from some of the younger, Later Stone Age members (Deacon 1995). At Klasies, the Upper Member contains the Howiesons Poort and MSA III deposits. Here the latter sub-stage correlates with late early MIS 3 and is also known as the post-Howiesons Poort (Wurz 2002; Villa *et al*. 2010). In the MSA III white mussel (*D. serra*), giant chiton (*D. gigas*) and *Bullia*, all sandy beach indicator species, are most abundant relative to the rocky shore brown mussel (*P. perna*) and black mussels (*C. meridionalis*) (Thackeray 1988; Langejans *et al*. 2012). Based on this, the implication is that sandy shores were present throughout MIS 3 at this site.

In this period the rocky shore species, such as black mussel (*C. meridionalis)* are either absent, or occur in very low frequencies (≤ 10%), as in the case of brown mussels (*P. perna*) and true limpets (*Patella vulgata*) (Langejans *et al*. 2012). Of these species, the true limpet (*P. vulgata*) is particularly sensitive to sand inundation and is typically absent in sandy areas (Lubke & de Moor 1998). Taken together, the weak representation of rocky shore molluscs supports an inference that rocky shores were either absent or not very extensive in MIS 3 (Langejans *et al*. 2012).

As a whole, MSA III shellfish is comparable with those found in the Howiesons Poort, suggesting similar conditions in the vicinity of Klasies during MIS 4 and MIS 3. The lowest shellfish density of 1.0 kg/m^3 at the Klasies main site comes from the MSA III (Thackeray 1988). This trend of shell diminution from MIS 4 through to MIS 3 is suggestive of the site being further from the coast. This inference is supported by palaeo-shoreline distance estimates that place the Klasies River main site further from the sea during the accumulation of the Upper Member (Fisher *et al.* 2010; Langejans *et al*. 2012).

Micromammals

Micromammal remains pertinent to MIS 3 in the southern Cape presently come from the MSA III at Klasies River main site and part of the Boomplaas Cave sequence. In the MSA III at Klasies, the small mammal assemblage is attributed to predatory bird accumulation and palaeoenvironmental inferences are based on species diversity and relative abundances.

Early MIS 3 (c. 59 ka - 50 ka*)*

In the MSA III, cool and wet conditions associated with Afromontane forest and mountain fynbos are interpreted from the abundance of vlei rats (*O. irroratus*) and Saunder's vlei rat (*O. saundersiae*) (Avery 1987). Local

habitats with dune fynbos is also implied by the abundance of Hottentot's golden mole (*Amblysomus. hottentotus*) From the relative abundance of these taxa, early MIS 3 at Klasies River is associated with dense vegetation and humid conditions (Avery 1987; Hillestad-Nel 2013).

Late MIS 3 (c. 48 ka – 24 ka*)*

A slightly different pattern emerges from the micromammals at Boomplaas that comes from the BOL, OLP and BP members which correlate to late MIS 3. In BOL high abundances of Saunder's vlei rat (*O. saundersiae*) and Karoo bush rat (*Myotomys unisulcatus*), imply open vegetation characterised by semi-arid shrubland in the valley and grass on the hill slopes (Avery 1982). Cold and dry conditions are also interpreted from the low diversity index values (*H*) and the large sized shrews (*Myosorex varius*). The spindly growth habitat of identified wood from BOL also supports an inference of cold and dry conditions in late MIS 3 which is described as "…*very cold, dry and harsh*…"(Scholtz 1986: 179). This interpretation is however not supported by the associated large mammal fauna from BOL which is dominated by browsers (Klein 1983; Faith 2013) (see discussion below).

In the OLP member, dating to between *c.* 48 kcal BP and 40 kcal BP, there appears to be good agreement between the micromammal and large mammal fauna. Here the small mammal fauna correlates with relatively dense vegetation and results from fossil charcoal analysis (Scholtz 1986), which associates OLP with wet and mesic conditions. The large mammal fauna, which is dominated by browsers and mixed feeders, complements this interpretation (Klein 1983; Faith 2013). Cool and wet conditions are also inferred from the abudance of Saunder's vlei rat (*O. saundersiae*) and forest shrews (*Myosorex varius*) in the younger BP member (*c.* 38.6 kcal BP – 36.0 kcal BP) (Avery 1982).Contradictory evidence does however come from the absence of woody vegetation taxa and small, spindly shrubs identified in the BP charcoal which is associated with cold and dry conditions (Scholtz 1986: 70).

Taken together, the micromammal evidence from the MSA III at Klasies River suggests relatively cool and wet conditions with dense vegetation in early MIS 3. In contrast, conditions in late MIS 3, was seemingly colder and drier with more open habitats interpreted for part of the Boomplaas Cave sequence (BOL & BP).

Large mammal fauna

In the southern Cape, faunal remains associated with deposits dating to MIS 3 are relatively scarce. There are however large mammal assemblages from the MSA III in the Upper Member at Klasies River main site and Boomplaas Cave.

Early MIS 3 (c. 59 ka – 50 ka*)*

In the MSA III, Klein (1976) linked the occurrence of open habitats to the abundance of grazing indicator species. Here equids and antelope account for 53% and 47% of the fauna, respectively and the comparatively high frequency of equids is associated with the presence of dry grasses (Klein 1976; van Pletzen 2000; Faith 2013).

Late MIS 3 (c. 48 ka – 24 ka*)*

In Klein's (1978) analysis of the Boomplaas fauna, the Earlier Upper Pleistocene 3 was represented by the OLP, BP, YOL and LPC members. Although YOL is undated, these members are broadly associated with late MIS 3. With the exception of OLP, where browsers and mixed feeders are common, grazers represent 78%, 52% and 75% of the fauna in the other late MIS 3 members (Faith 2013). In OLP browsers imply dense, bushy vegetation while grey rhebok (*P. capreolus*) and klipspringer (*O. oreotragus*) suggest rocky habitats with some grassy vegetation. During this part of the Boomplaas sequence, it is thought that winter rainfall dominated and that conditions were relatively stable (Faith 2013: 725). In contrast to OLP, the BP and LPC members mainly contain typical grassland indicator species such as greater kudu (*Tragelaphus*

strepsiceros), blue antelope (*H. leucophaeus*), giant Cape horse (*Equus capensis*) and long-horned African buffalo (*Pelorovis antiquus*). During this part of MIS 3, conditions presumably shifted in favour of animals with a dietary preference for grass. When compared to the micromammal data, the large mammal fauna from Boomplaas loosely supports an inference of cold and dry conditions in late MIS 3. As a whole, conditions at this time seem to have been generally cooler and favourable to grazers and small mammals with an affinity for cool conditions.

Taken together, the large mammal fauna from the MSA III at Klasies River implies open habitats with relatively dry, grassy vegetation in early MIS 3. This inference is contrary to that of the micromammals from the site which associate this part of MIS 3 with generally wet conditions and dense vegetation. Compared to Klasies, grazing fauna is also well represented in the late MIS 3 members at Boomplaas Cave, suggesting broadly similar habitats favouring grazers throughout MIS 3.

Ostrich eggshell (OES)

While ostrich eggshell beads have not been recovered from the Klasies River main site (Klein 2002) eggshell fragments are found in the SAS and RF members of the MSA II (Rightmire & Deacon 1991). There is however no associated OES in either the MSA I or MSA III with the latter containing the post-Howiesons Poort lithic technology which is correlated with MIS 3 (Wurz 2002). From the occurrence of OES in the older MSA I and MSA II local habitats with suitable conditions for ostriches have been inferred (Rightmire & Deacon 1991). A similar inference cannot be made for the MSA III where there is an absence of evidence for ostriches. Because of this, palaeoenvironmental inferences come primarily from interpretation of the shellfish and faunal remains (discussed above). Unlike at Klasies River main site, ostrich eggshell, mainly interpreted as beads, is found in the OLP member at Boomplaas Cave (Deacon 1979; Deacon 1995). As mentioned above, this member is dated between 48 kcal BP and 40 kcal

BP and falls within late MIS 3. Despite this, the Boomplaas ostrich eggshell has only been used for dating purposes and not as an environmental proxy (Deacon 1995; Miller *et al*. 1999). As a result there are no palaeoenvironmental interpretations associated with the OES at the site.

While OES is not widely applied for palaeoenvironmental reconstruction, ostrich remains generally imply C_4 vegetation while the $\delta^{18}O$ content of eggshells typically indicates arid conditions (Johnson *et al.* 1997, 1998; Lee-Thorpe & Sponheimer 2007; Roberts 2014). In the context of Boomplaas Cave, the OES in the OLP member might imply drier conditions in late MIS 3. This interpretation is however not consistent with the associated large mammal fauna which is dominated by browsers and mixed feeders.

6.7 Summary for MIS 3

In summary, the micromammal and large mammal evidence provides variable and somewhat contradictory interpretations for MIS 3. In the southern Cape, early MIS 3 is represented by archaeo-proxy evidence from the MSA III at Klasies River main site while stratigraphic units at Boomplaas Cave correlate with late MIS 3. Micromammal evidence for the early MIS 3 at Klasies River implies humid conditions and closed habitats with dense vegetation. This interpretation is to some extent supported by speleothem data from Pinnacle Point, Crevice Cave and Sandkraal Cave. These stalagmites indicate C_3 vegetation and winter rainfall in early MIS 3 (*c.* 60 ka to 40 ka). In contrast, the associated MSA III large mammal fauna, which is dominated by equid grazers, correlates with open habitats and dry grassy or shrub vegetation. Here the faunal evidence is complemented by isotope data from the BL4 stalagmite in De Hoop which indicates C_4 vegetation and either summer or year-round rainfall at this time. Proxy temperature data derived from the MSA III rodent fauna offers some support for this interpretation. This is because temperature

estimates for the MSA III correlate with early MIS 3 at Klasies River main site with an interval of warming (see Chapter 2 section 2.3.2).

With regards to late MIS 3 (*c.* 49 ka – 24 ka), this interval is represented by the OLP and BOL members from Boomplaas Cave. During late MIS 3 the large mammal fauna is dominated by browsers which are associated with wet conditions and habitats with dense, bushy vegetation. By late MIS 3, the micromammal species imply cool conditions with open vegetation characterised by shrubs and grasses. Evidence from fossil charcoal supports this inference of cool, dry conditions. Further support comes from the occurrence of grazers in the Boomplaas layers corresponding to late MIS 3. Evidence from coastal speleothem records correlated with late MIS 3 complement the interpretations derived from the Boomplaas large mammal fauna. Here both the Sandkraal Cave and De Hoop stalagmites imply warm conditions with either summer or year-round rainfall and habitats with a strong C_4 vegetation presence in late MIS 3. In contrast, a different pattern is shown by the interior Cango Cave and Little Karoo records which link conditions in late MIS 3 with C_3 vegetation and winter rainfall, respectively.

Overall, the palaeoenvironmental implication is that in MIS 3, local habitat conditions were quite variable. This variability seems to have been expressed at different parts along the coast and also between the coast and more interior parts of the southern Cape. Despite these local variations, conditions throughout the early and later parts of MIS 3 were consistently favourable for speleothem growth in terms of temperature, relative humidity and vegetation cover. This implies that contrary to previous interpretations, MIS 3 was relatively wet and not likely a period of cold, dry conditions.

6.8 Summary

In this chapter comparisons were made between interpretations derived from selected archaeological proxies (*viz.* shellfish, micromammals, large mammal fauna & OES) and the evidence from the stalagmite records discussed in Chapter 4 and Chapter 5 of this thesis. The discussion of the past environmental conditions in the southern Cape presented here focuses specifically on marine oxygen isotope stage (MIS) 5a, MIS 4 and MIS 3 since these are the periods covered by the De Hoop speleothems. In the next chapter, Chapter 7, the evidence for environmental change discussed in Chapter 6 is placed within a broader archaeological context. This is presented in the final chapter by relating the environmental evidence with the potential archaeological implications (in terms of cultural change).

Chapter 7 – CONCLUSION & RECOMMENDATIONS FOR FUTURE WORK

General introduction

The primary objectives of this study were to reconstruct past environmental conditions in the southern Cape during the Middle Stone Age and to attempt to relate these conditions to the evolution of behaviour, and in particular subsistence practices, of early *Homo sapiens* who hunted, gathered and fished in this region after 75 ka. By using proxy data for vegetation and rainfall derived from the geochemical analysis of speleothems collected in De Hoop Nature Reserve, the intention was to relate this data to the lives of our early ancestors. This includes, but is not limited to, the Still Bay and Howiesons Poort and the post-Howiesons Poort. In this final chapter, I discuss the hypotheses initially set out in Chapter 1 and suggest recommendations for future work. In reference to the hypotheses, each of these are evaluated and its implications discussed in the context of the speleothem proxy evidence presented in Chapter 5 and Chapter 6 of this thesis.

Evaluation of hypotheses

The BL1 stalagmite from De Hoop indicates that MIS 5a (c. 85 ka - 74 ka) was characterised by warmer temperatures and increased summer rainfall that favoured C_4 vegetation

The BL1 stalagmite record covers the interval from 81 ka to 74 ka. For early MIS 5a (*c.* 85 ka – 80 ka), high $\delta^{18}O$ values are associated with ^{18}O derived from summer rainfall and are therefore suggestive of warmer temperatures. The $\delta^{13}C$ values corresponding to the BL1 $\delta^{18}O$ signal for early MIS 5a tracks changes in $\delta^{18}O$ and is suggestive of more C_4 vegetation above the cave. The proxy data from the BL1 stalagmite

therefore indicates that early MIS 5a was characterised by warm conditions with more seasonal summer rain. Habitats during this part of MIS 5a appear to have been dominated by C_4 vegetation. Evidence to support this interpretation, at least for the earlier part of MIS 5a, comes from the PP29 record in Pinnacle Point which mirrors the trends observed in the BL1 record.

While warm conditions with summer rain and C_4 vegetation occurred in early MIS 5a, the BL1 stalagmite record indicates that by late MIS 5a (*c.* 79 ka – 74 ka), conditions were more variable. This is interpreted from rapid, short-term changes in $\delta^{18}O$ and $\delta^{13}C$ which suggests that late MIS 5a, at least in the vicinity of De Hoop, was a period of variable local rainfall and vegetation.

Micromammal and large mammal faunal data from Blombos Cave and Klasies River main site indicate dense vegetation that could have supported small browsing antelope and rodent micromammals. The data are suggestive of heterogeneous vegetation with both C_3 and C_4 elements and complements the interpretation of habitat heterogeneity and variable environmental conditions from the De Hoop speleothems. The higher $\delta^{18}O$ values in the OES from Blombos corroborate warmer conditions and summer rainfall, at least in the vicinity of Blombos and De Hoop, in early MIS 5a. The upper part of the SAS Member containing the MSA II at Klasies River main site, which dates to early MIS 5a (Vogel 2001; Feathers 2002; Wurz 2002) also seemingly occurred during a warming interval with variable environmental conditions.

The Still Bay industry from Blombos Cave occurs in the M1 and upper M2 levels. .These levels have been dated by luminescence techniques (OSL & TL) to 72.7 ± 3.1 ka for the upper part of the M1 phase (Jacobs *et al.* 2003a, b) with TL dates of between 74 ± 5 ka and 78 ± 6 ka (Tribolo *et al.* 2006). The upper M2 is dated by OSL to 76.8 ± 3.1 ka (Jacobs *et al*. 2006a). The Still Bay levels were recently resampled for OSL dating and

the new ages place these levels towards the boundary of MIS 5a/4 (Jacobs *et al*. 2013).

Based on these dates, the Still Bay therefore falls within MIS 5a as a whole when environmental, and by extension climatic conditions were initially warm with seasonal summer rain and C_4 vegetation but became more variable towards the boundary of MIS 5a. Towards the end of MIS 5a, when the Still Bay occurred, environmental conditions were more variable than in early MIS 5a when the MSA ll upper occurred.

The KDS stalagmite from Klipdrift Shelter links MIS 4 (c. 72 ka - 62 ka) with cooler temperatures and wetter conditions due to stronger winter rains as suggested by Chase (2010). Under these cooler MIS 4 conditions, C_3 vegetation cover was favoured.

The KDS stalagmite dates to between 69.5 ka and 68.2 ka. The interval covered by this stalagmite is correlated with early MIS 4 (*c.* 72 ka – 68 ka). During this part of MIS 4, the KDS $\delta^{18}O$ values fall within the Crevice Cave range of summer rainfall (after Bar-Matthews *et al.* 2010) and is suggestive of warm conditions in early MIS 4. The corresponding $\delta^{13}C$ values are associated with C_4 vegetation and fall within the Holocene range of C_4 vegetation for Cango Cave. This interpretation of warm conditions with summer rain and C_4 vegetation in early MIS 4 is supported by evidence from the PP29 speleothem record for Pinnacle Point which shows similar trends in $\delta^{18}O$ and $\delta^{13}C$ at this time. Temperature indices derived from the Klasies rodent micromammals similarly link the Howiesons Poort in the Upper Member with relatively warm local conditions (Thackeray 1987; Thackeray & Avery 1990). The earlier phase of the Howiesons Poort that occurs at Klasies River thus falls within a relatively warmer period when the De Hoop speleothem records indicate summer rain and C_4 vegetation.

In contrast, at Die Kelders Cave and Klipdrift Shelter similar conditions with relatively cool and wet conditions favouring diverse communities of

small and large animals is inferred during MIS 4. Variable habitat conditions, at least within the vicinity of Klipdrift Shelter, are also interpreted from fluctuating $\delta^{13}C$ signal in ostrich eggshell (OES) (Roberts 2013). Comparative evidence from other coastal speleothem records at Crevice Cave, Sandkraal Cave and Herold's Bay further support this interpretation of cool and wet conditions in MIS 4. While the evidence from the Die Kelder and Klipdrift Shelter archaeo-proxies and from the Mossel Bay and George speleothem records support the inference that conditions in MIS 4 (as a whole) were humid and cool (after Chase 2010), the De Hoop speleothem records and faunal evidence from Klasies River do not. Taken together, the implication is that at least for the earlier part of MIS 4, represented by the De Hoop speleothem records and the Klasies River data, the hypothesis set (and that of Chase (2010)) is not supported. Since there are speleothem records that indicate cool and wet conditions in MIS 4, it may be that these conditions also occur during later phases of the Howiesons Poort at Klasies River and elsewhere in the southern Cape, regardless of the De Hoop speleothem records not indicating a cool and humid signal at this time.

In MIS 3 (c. 59 ka – 24 ka), the De Hoop stalagmites from Bloukrantz Cave (BL1 ,BL3 & BL4) indicate generally cooler and seasonally drier conditions due to a decrease in winter rainfall (Chase 2010) with variable vegetation.

Early MIS 3 is covered by the base of the BL 4 stalagmite that dates from 59 ka to 56 ka and this interval is associated with rapid changes in both $\delta^{18}O$ and $\delta^{13}C$. This is suggestive of abrupt shifts in local rainfall dynamics and vegetation.

The archaeological signal in the southern Cape represented by this period occurs at Klasies River main site in the MSA III or post-Howiesons Poort. Micromammal data from Klasies River associates the early MIS 3 with

cool, humid conditions and dense vegetation that included C_3 vegetation elements of Afrotemperate forest and mountain fynbos. Evidence from other coastal speleothems (PP29, Crevice Cave and Sandkraal) also indicates cool and wet conditions in early MIS 3. Taken together, the proxy evidence from the MSA III at Klasies River main site and from coastal speleothems at Mossel Bay indicate that in the vicinity of Tsitsikamma and Mossel Bay conditions during the post-Howiesons Poort were cool and humid with habitats mainly comprising dense C_3 vegetation. In contrast, the De Hoop records suggest that conditions, at least in the vicinity of the Overberg, could have been warmer but seasonally wetter in summer. This data indicates that in early MIS 3 conditions during the post-Howiesons Poort (MSA III) at the southern Cape coast were quite variable.

Similar inferences are also made for late MIS 3 (*c.* 49 ka – 24 ka) which is an interval represented by the post-Howiesons Poort at Boomplaas Cave and Die Kelders. At Boomplaas Cave the post-Howiesons Poort is dated to between 48 kcal BP and 40 kcal BP and falls within late MIS 3 (*c.* 49 ka – 24 ka). Micromammal evidence for this interval indicates open habitats with grassy vegetation and cold and dry conditions. This is interpreted from low diversity index values and large sized shrews. The spindly growth habit of identified wood in the Boomplaas BOL member supports an inference of cold and dry conditions in late MIS 3 (Scholtz 1986). At De Hoop there are three speleothem records that cover the period correlated to late MIS 3 and these are the upper parts of BL4, BL1 and BL3. These speleothem records all indicate that conditions in late MIS 3 were characterised by increases in summer rain and C_4 vegetation. Some support for this interpretation comes from the Sandkraal Cave record in George dating to between 40 ka and 30 ka where the $\delta^{18}O$ content is suggestive of more summer rain and the $\delta^{13}C$ points to a weak C_4 signal. However, other comparative speleothem records from further inland, particularly the Little Karoo and Cango Cave indicate cooler and wetter conditions in late MIS 3 due to increases in winter rain which favoured C_3 vegetation.

Considered together, the De Hoop speleothem records analysed here indicate somewhat different conditions to those interpreted during the post-Howiesons Poort at Boomplaas. The discrepancy with the Boomplaas record may be due to a slightly different time period covered or strong regional variability. This needs further investigation. Overall the data does show strong regional differences throughout MIS 3 in the southern Cape, supporting hypothesis 3.

Limitations of using speleothems for palaeoenvironmental interpretations and recommendations for future work

The results from this study have provided a broad record of environmental and climatic variations from MIS 5a through to MIS 3 as discussed in the preceding chapters xxxx.

With regards to the limitations of the study and the use of speleothems for palaeoenvironmental interpretations, a number of concerns were highlighted in this study. The main issues being, (1) inverted U-Th ages, (2) mineralogical changes and (3) non-equilibrium fractionation (kinetic fractionation effects) and (4) additional chemical analyses of dripwaters. Each of these points are discussed further below.

1. *Inverted U-Th ages*: In many instances the U-Th ages were out of stratigraphic order and this resulted in either shortening of the speleothem record or the sample being disregarded completely (in the case of BL2). In each of the speleothem samples analysed in this study, the uranium content was sufficiently high enough and thorium contamination negligible. These are two important theoretical considerations for ICPMS analysis. Despite this, there were a number of instances where the U-Th ages were out of stratigraphic order. This resulted in shortening of the speleothem record or a sample being disregarded completely (in the case of BL2). Future work could address this by, for example, taking

duplicate subsamples and improving on the laboratory analyses with additional calibrations. This approach should also help to improve the error margins obtained on the ages such as those for KDC5 and KDS.

2. *Mineralogical changes:* In reference to the suspected mineralogical changes from calcite to aragonite in part of BL1, it is nearly imposible to assess something like this in the field. In certain instances, mineralogical changes from calcite to aragonite have been linked to dry conditions (Frisia *et al.* 2002). However, the lesson learned here is that speleothems with internal structures that show signs of recrystallisation and mineralogical changes such as those in BL1 are too problematic and should be avoided.

3. *Non-equilibrium fractionation*: For speleothems to be reliable indicators of past environmental, and by extension, climatic changes, it is important that calcite deposition occurs under equilibrium conditions or close to it. Kinetic fractionation effects are frequently recognised for having a major impact on the interpretative value of $\delta^{18}O$ and $\delta^{13}C$ isotopic records. In speleothem research, the Hendy Test is traditionally used to assess this based on the assumption that kinetic effects will produce covarying isotopic records. However, real-life natural systems rarely behave under conditions that satisfy theoretical prerequisites and the suitability of the Hendy Test for assessing non-equilibrium deposition is increasingy being questioned. In this study, every effort was made to collect samples from the deeper parts of the cave such as Klipdrift Sea Cave (KDC5) and Bloukrantz Cave. From the Hendy Test plots presented in Chapter 5 it appears that kinetic fractionation effects may have compromised the reliability of at least part of the isotopic records for BL1, BL3, BL4 and KDS. However, future work on additional samples from Bloukrantz Cave,

which is relatively deeper and with a more restricted entrance, could help to validate and strengthen the interpretations presented in this thesis.

4. *Chemical analyses of dripwaters*:

General conclusion

In this thesis speleothems collected in the De Hoop Nature Reserve, southern Cape that contained palaeoclimate records from MIS 5a to MIS 3 were analysed. The data I present indicates shifting palaeoenvironmental conditions across this time period with warmer relatively stable conditions in early MIS 5a. In late MIS 5a and early MIS 4 there is greater variability in comparison with early MIS 5a. However, MIS 3 is the most variable period recorded here. In this study I have emphasised that much greater control is needed on in-cave variables, for example air temperature and atmospheric CO_2. This is particularly relevant to the interpretation of the ^{18}O signal in terms of temperature and rainfall. I also indicate that the ages for some of the known archaeological data for this region, especially from the older excavations, is not sufficiently accurate to allow for direct comparison with the speleothem signals. This integration will become more productive as a fine-grained understanding of the ages of the archaeological deposits becomes available.

Perhaps the key message I would like to emphasise in this thesis is that *Homo sapiens* in this region faced highly variable environmental and climatic conditions during MIS 5a to MIS 3. Yet, despite this variability it seems that these early humans were highly adaptable, both in terms of changing technologies but also in their demographic and subsistence patterns. This might be one of the reasons that when *Homo sapiens* left Africa at *c.* 60 ka they so easily adapted to the very variable conditions found in other continents.

Chapter 8 – REFERENCES

Affek, H. P., Bar-Matthews, M., Ayalon, A., Matthews, A. & Eiler, J. M. (2008). Glacial/interglacial temperature variations in Soreq cave speleothems as recorded by 'clumped isotope' thermometry. *Geochimica et Cosmochimica Acta* **72**: 5351-5360.

Armitage, S.J., Jasim, S.A., Marks, A.E., Parker, A.G., Usik, V.I. & Uerpmann, H.P. (2012). The southern route "out of Africa": evidence for an early expansion of modern humans into Arabia. *Science* **331**: 453-456.

Alcaraz-Pelegrina, J. M. & Martínez-Aguirre, A. (2005). Isotopic fractionation during leaching of impure carbonates and their effect on uranium series dating. *Quaternary Science Reviews* **24**: 2584-2593.

Asrat, A., Baker, A., Mohammed, M. U., Leng, M. J., Calsteren, P. V. & Smith, C. (2007). A high-resolution multi-proxy stalagmite record from Mechara, Southeastern Ethiopia: palaeohydrological implications for speleothem palaeoclimate reconstruction. *Journal of Quaternary Science* **22**: 53-63.

Avery, D.M. (1987). Late Pleistocene coastal environment of the Southern Cape Province of South Africa: micromammals from Klasies River Mouth. *Journal of Archaeological Science* **14**: 405-421.

Avery, D.M. (1982). Micromammals as palaeoenvironmental indicators and an interpretation of the late Quaternary in the southern Cape Province, South Africa*. Annals of the South African Museum* **85**: 183-374.

Avery, D.M., Avery, G. & Palmer, N.G. (2005). Micromammalian distribution and abundance in the Western Cape Province, South Africa, as evidenced by barn owls *Tyto alba* (Scopoli). *Journal of Natural History* **39**: 2047-2071.

Backwell, L. R., McCarthy, T. S., Wadley, L., Henderson, Z., Steininger, C. M., Barré, M., Lamothe, M., Chase, B.M., Woodborne, S., Susino, G. J., Bamford, M. K., Sievers, C., Brink, J. S., Roussouw, L., Pollarolo, L., Trower, G., Scott, L. & d'Errico, F. (2014). Multiproxy record of late Quaternary climate change and Middle Stone Age human occupation at Wonderkrater, South Africa. *Quaternary Science Reviews* **99**: 42-59.

Baker, A., Smith, C. L., Jex, C., Fairchild, I. J., Genty, D. & Fuller, L. (2008). Annually laminated speleothems: a review. *International Journal of Speleology* **37**: 4.

Baker, A., Smart, P. L., Edwards, R. L., & Richards, D. A. (1993). Annual growth banding in a cave stalagmite. *Nature* **364**: 518-520.

Baldini, J.U.L., McDermott, F. & Fairchild, I.J. (2006). Spatial variability in cave drip water hydrochemistry: implications for stalagmite palaeoclimate records. *Chemical Geology* **235**: 390-404.

Bar-Matthews, M., Marean, C. W., Karkanas, P., Jacobs, Z., Fisher, E., Herries, A. I. R., Brown, K., Williams, H.M., Bernatchez, J., Ayalon, A. &Nilssen, P.J. (2010). High resolution and continuous isotopic speleothem record of palaeoclimate and palaeoenvironment from 92–55 ka from Pinnacle Point, South Africa. *Quaternary Science Reviews* **29**: 2131-2145.

Bateman, M.D., Holmes, P.J., Carr, A.S., Horton, B.P. & Jaiswal, M.K. (2004). Aeolianite and barrier dune construction spanning the last two glacial-interglacial cycles from the southern Cape coast, South Africa. *Quaternary Science Reviews* **23**: 1681-1698.

Beck, W. C., Grossman, E. L. & Morse, J. W. (2005). Experimental studies of oxygen isotope fractionation in the carbonic acid system at 15, 25, and 40 C. *Geochimica et Cosmochimica Acta* **69**: 3493-3503.

Bennett, N.C. & Faulkes, C. G. (2000). Introduction to the Bathyergidae. **In**: Bennett, N.C. & Faulkes, C.G. (eds) *African mole-rats: ecology and eusociality*. United Kingdom: Cambridge University Press. pp. 1-28.

Bischoff, J. L. & Fitzpatrick, J. A. 1991. U-series dating of impure carbonates: an isochron technique using total-sample dissolution. *Geochimica et Cosmochimica Acta* **55**: 543-554.

Blome, M. W., Cohen, A. S., Tryon, C. A., Brooks, A. S. & Russell, J. (2012). The environmental context for the origins of modern human diversity: a synthesis of regional variability in African climate 150,000–30,000 years ago. *Journal of Human Evolution* **62**: 563-592.

Böhm, F., Joachimski, M. M., Dullo, W. C., Eisenhauer, A., Lehnert, H., Reitner, J., & Wörheide, G. (2000). Oxygen isotope fractionation in marine aragonite of coralline sponges. *Geochimica et Cosmochimica Acta* **64**: 1695-1703.

Bonotto, D. M. & Andrews, J.N. (2000). The transfer of uranium isotopes^{234}U and ^{238}U to the waters interacting with carbonates from Mendip Hills area (England). *Applied Radiation & Isotopes* **52**: 965-983.

Bourdon, B., Turner, S., Henderson, G. M. & Lundstrom, C. C. (2003).Introduction to U-series geochemistry. *Reviews in Mineralogy and Geochemistry* **52**: 1-21.

Braun, K. (2014). Influence of the Agulhas Current on the terrestrial climate of South Africa as derived from speleothems. Unpublished PhD Thesis. Jerusalem: Hebrew University of Jerusalem.

Braun, K., Bar-Matthews, M., Ayalon, A., Marean, C., Herries, A. I. R., Zahn, R., & Matthews, A. (2012). Influences of the Agulhas Current on South African terrestrial climate as inferred from speleothem stable isotope records. **In**: *EGU General Assembly Conference Abstracts*.

Brennecka, G. A., Borg, L. E., Hutcheon, I. D., Sharp, M. A. & Anbar, A. D. (2010). Natural variations in uranium isotope ratios of uranium ore concentrates: Understanding the $^{238}U/^{235}U$ fractionation mechanism. *Earth & Planetary Science Letters* **29**1: 228-233.

Brown, K. S., Marean, C. W., Jacobs, Z., Schoville, B. J., Oestmo, S., Fisher, E. C., Bernatchez, J., Karkanas, P. & Matthews, T. (2012). An early and enduring advanced technology originating 71 000 years ago in South Africa. *Nature* **491**: 590-593.

Buk, K.G. & Knight, M.H. (2010). Seasonal diet preferences of black rhinoceros in three arid South African National Parks. *African Journal of Ecology* **48**: 1064-1075.

Buck, C. E., Cavanagh, W. G. & Litton, C. D. (1996). *Bayesian approach to interpreting archaeological data*. Chichester: Wiley.

Butcher, A. (2010).*De Hoop caves*. Cape Peninsula Spelaeological Society. Available from http://cpss.caving.org.za/caves/western-cape/de-hoop [Accessed 22 May 2013]

Butzer, K.W. (2004). Coastal eolian sands, paleosols, and Pleistocene geoarchaeology of the south-western Cape, South Africa. *Journal of Archaeological Science* **31**: 1743-1781.

Caley, T., Kim, J. H., Malaizé, B., Giraudeau, J., Laepple, T., Caillon, N., Charlier, K., Rebaubier, H., Rossignol, L., Castañeda, I.S., Schouten, S. & Sinninghe Damsté, J. S. (2011). High-latitude obliquity as a dominant forcing in the Agulhas current system. *Climate of the Past **7***: 1285-1296.

Carr, A. S., Bateman, M. D., Roberts, D. L., Murray-Wallace, C. V., Jacobs, Z. & Holmes, P. J. (2010). The last interglacial sea-level high stand on the southern Cape coastline of South Africa. *Quaternary Research* **73**: 351-363.

Carr, A. S., Bateman, M. D. & Holmes, P. J. (2007).Developing a 150ka luminescence chronology for the barrier dunes of the southern Cape, South Africa. *Quaternary Geochronology* **2**: 110-116.

Carr, A. S., Thomas, D. S. & Bateman, M. D. (2006). Climatic and sea level controls on Late Quaternary eolian activity on the Agulhas Plain, South Africa. *Quaternary Research* **65**: 252-263.

Carto, S. L., Weaver, A. J., Hetherington, R., Lam, Y. & Wiebe, E. C. (2009). Out of Africa and into an ice age: on the role of global climate

change in the late Pleistocene migration of early modern humans out of Africa. *Journal of Human Evolution* **56**: 139-151.

Cerling, T. E., Harris, J. M., MacFadden, B. J., Leakey, M. G., Quade, J., Eisenmann, V. & Ehleringer, J. R. (1997). Global vegetation change through the Miocene/Pliocene boundary. *Nature* **389**: 153-158.

Chacko, T. & Deines, P. (2008). Theoretical calculation of oxygen isotope fractionation factors in carbonate systems. *Geochimica et Cosmochimica Acta* **72**: 3642-3660.

Chase, B.M., Lim, S., Chevalier, M., Boom, A., Carr, A.S., Meadows, M.E. & Reimer, P.J. (2015). Influence of tropical easterlies in southern Africa's winter rainfall zone during the Holocene. *Quaternary Science Reviews* **107**: 138-148.

Chase, B. M. (2010). South African palaeoenvironments during marine oxygen isotope stage 4: a context for the Howiesons Poort and Still Bay industries. *Journal of Archaeological Science* **37**: 1359-1366.

Chase, B. (2009). Evaluating the use of dune sediments as a proxy for palaeo-aridity: a southern African case study. *Earth-Science Reviews* **93**: 31-45.

Chase, B. M., & Meadows, M. E. (2007). Late Quaternary dynamics of southern Africa's winter rainfall zone. *Earth-Science Reviews* **84**: 103-138.

Cheng, H., Edwards, R. L., Hoff, J., Gallup, C. D., Richards, D. A. & Asmerom, Y. (2000). The half-lives of Uranium-^{234} and Thorium-^{230}. *Chemical Geology* **169**: 17-33.

Cherdyntsev, V. V. (1971). *Uranium-234* (No.IPST-Cat.--2313). John Wiley and Sons, Inc.: New York.

Choppin, G. R. & Stout, B. E. (1989).Actinide behavior in natural waters. *Science of the Total Environment* **83:** 203-216.

Cockcroft, M.J., Wilkinson, M.J. & Tyson, P.D. (1987).The application of a present-day climatic model to the late Quaternary in southern Africa. *Climatic Change* **10**: 161-181.

Compton, J. S. (2011). Pleistocene sea-level fluctuations and human evolution on the southern coastal plain of South Africa. *Quaternary Science Reviews* **30**: 506-527.

Compton, J.S. (2004). *The rocks and mountains of Cape Town.* Cape Town: Double Storey Books (Juta & Co.).

Constantin, S., Bojar, A. V., Lauritzen, S. E. & Lundberg, J. (2007). Holocene and Late Pleistocene climate in the sub-Mediterranean

continental environment: a speleothem record from Poleva Cave (Southern Carpathians, Romania). *Palaeogeography, Palaeoclimatology, Palaeoecology* **243**: 322-338.

Coplen, T. B. (2007). Calibration of the calcite–water oxygen-isotope geothermometer at Devils Hole, Nevada, a natural laboratory. *Geochimica et Cosmochimica Acta* **71**: 3948-3957.

Coplen, T. B. (1988). Normalization of oxygen and hydrogen isotope data. *Chemical Geology* **72**: 293-297.

Couchoud, I., Genty, D., Hoffmann, D., Drysdale, R. & Blamart, D. (2009). Millennial-scale climate variability during the Last Interglacial recorded in a speleothem from south-western France. *Quaternary Science Reviews* **28**: 3263-3274.

Cowling, R.M. (1990).Diversity components in a species-rich area of the Cape Floristic Region. *Journal of Vegetation Science* **1**: 699-710.

Cowling, R. M. & Pierce, S. M. (1988). Secondary succession in coastal dune fynbos: variation due to site and disturbance. *Vegetatio* **76**: 131-139.

Cowling, R.M. (1983).Phytochorology and vegetation history in the south-Eastern Cape, South Africa. *Journal of Biogeography* **10**: 393-419.

Craig, H. (1961). Isotopic variations in meteoric waters. *Science* **133**: 1702-1703.

Crançon, P. & van der Lee, J. (2003). Speciation and mobility of uranium(VI) in humic-containing soils. *Radiochimica Acta* **91**: 673-679.

Cruz-Uribe, K. & Klein, R. G. (1998). Hyrax and hare bones from modern South African eagle roosts and the detection of eagle involvement in fossil bone assemblages. *Journal of Archaeological Science* **25**: 135-147.

Cuney, M. (2009).The extreme diversity of uranium deposits. *Mineralium Deposita* **44**: 3-9.

Cuthbert, M. O., Baker, A., Jex, C. N., Graham, P. W., Treble, P. C., Andersen, M. S. & Acworth, I. R. (2014). Drip water isotopes in semi-arid karst: implications for speleothem paleoclimatology. *Earth and Planetary Science Letters* **395**: 194-204.

Daëron, M., Guo, W., Eiler, J., Genty, D., Blamart, D., Boch, R., Drysdale, R., Maire, R., Wainer, K. & Zanchetta, G. (2011).$^{13}C^{18}O$ clumping in speleothems: Observations from natural caves and precipitation experiments. *Geochimica et Cosmochimica Acta* **75**: 3303-3317.

Day, C. C. & Henderson, G. M. (2011).Oxygen isotopes in calcite grown under cave-analogue conditions. *Geochimica et Cosmochimica Acta* **75**: 3956-3972.

Deacon, H.J. & Deacon, J. (1999). *Human beginnings in southern Africa: uncovering the secrets of the Stone Age.* Claremont: David Philip Publishers. pp. 107-166.

Deacon, H. J. (2008). The context of the 1967-8 sample of human remains from Cave 1 Klasies River Main Site. *South African Archaeological Bulletin Goodwin Series* **10**: 143-149.

Deacon, H. J. (1995).Two late Pleistocene-Holocene archaeological depositories from the southern Cape, South Africa. *South African Archaeological Bulletin* **50**: 121-131.

Deacon, H.J. (1989).Late Pleistocene paleoecology and archaeology in the southern Cape, South Africa. **In**: Mellars, P. & Stringer, C. (eds), *The Human Revolution: behavioral and biological perspectives on the origins of modern humans*. Princeton: Princeton University Press. pp. 547-564.

Deacon, H. J. & Geleijnse, V. B. (1988). The stratigraphy and sedimentology of the main site sequence, Klasies River, South Africa. *South African Archaeological Bulletin* **43**: 5-14.

Deacon, J. & Lancaster, N. (1988).*Late Quaternary palaeoenvironments of southern Africa*. Oxford: Clarendon.

Deacon, H. J. & Thackeray, F. (1984).Late Pleistocene environmental changes and implications for the archaeological record in southern Africa. **In**: Vogel, J.C. (ed.) *Late Cenozoic palaeoclimates of the southern hemisphere*. Rotterdam: Balkema. pp. 375-390.

Deacon, H. J. (1979). Excavations at Boomplaas cave-a sequence through the upper Pleistocene and Holocene in South Africa. *World Archaeology* **10**: 241-257.

Demény, A., Kele, S., & Siklosy, Z. (2010). Empirical equations for the temperature dependence of calcite-water oxygen isotope fractionation from 10 to 70° C. *Rapid Communications in Mass Spectrometry* **24**: 3521-3526.

d'Errico, F., Henshilwood, C., Vanhaeren, M. & van Niekerk, K. (2005). *Nassarius kraussianus* shell beads from Blombos Cave: evidence for symbolic behaviour in the Middle Stone Age. *Journal of Human Evolution* **48**:3-24.

Dorale, J. A. & Liu, Z. (2009). Limitations of Hendy test criteria in judging the paleoclimatic suitability of speleothems and the need for replication. *Journal of Cave and Karst Studies* **71**: 73-80.

Dorale, J. A., Edwards, R. L., Alexander Jr, E. C., Shen, C. C., Richards, D. A. & Cheng, H. (2004). Uranium-series dating of speleothems: current techniques, limits, & applications. **In**: Sasowsky, I. D. & Mylroie, J. (eds), *Studies of cave sediments: physical and chemical records of paleoclimate*. New York: Kluwer Academic/Plenum Publishers. pp. 177-197.

Dorale, J. A., Edwards, R. L., Ito, E., & González, L. A. (1998). Climate and vegetation history of the midcontinent from 75 to 25 ka: a speleothem record from Crevice Cave, Missouri, USA. *Science* **282**: 1871-1874.

Douze, K., Wurz, S. & Henshilwood, C.S. (2015).Techno-cultural characterisation of MIS 5 (c. 105 – 90 ka) lithic industries at Blombos Cave, South Africa. DOI: 10.1371/journal.pone.0142151

Dusseldorp, G.L., Lombard, M. & Wurz, S. (2013). Pleistocene *Homo* and updated Stone Age sequence for South Africa. *South African Journal of Science* **109**. DOI: 10.1590/sajs.2013/20120042.

Eggins, S.M., Grün, R., McCulloch, M.T., Pike, A.W., Chappell, J., Kinsley, L., Mortimer, G., Shelley, M., Murray-Wallace, C.V., Spötl, C. & Taylor, L. (2005). In situ U-series dating by laser-ablation multi-collector ICPMS: new prospects for Quaternary geochronology. *Quaternary Science Reviews* **24**: 2523-2538.

Ehleringer, J. R., Bowling, D. R., Flanagan, L. B., Fessenden, J., Helliker, B., Martinelli, L. A. & Ometto, J. P. (2002). Stable isotopes and carbon cycle processes in forests and grasslands. *Plant Biology* **4**: 181-189.

Ehleringer, J. R., Cerling, T. E. & Helliker, B. R. (1997). C_4 photosynthesis, atmospheric CO_2, and climate. *Oecologia* **112**: 285-299.

Fairchild, I. J. & Baker, A. (eds). (2012). *Speleothem science: from process to past environments*. West Sussex: Wiley-Blackwell.

Faith, J. T. (2013).Taphonomic and paleoecological change in the large mammal sequence from Boomplaas Cave, Western Cape, South Africa. *Journal of Human Evolution* **65**: 715-730.

Feathers, J. K. (2002). Luminescence dating in less than ideal conditions: case studies from Klasies River main site and Duinefontein, South Africa. *Journal of Archaeological Science* **29**: 177-194.

Feathers, J. K., & Bush, D. A. (2000). Luminescence dating of Middle Stone Age deposits at Die Kelders. *Journal of Human Evolution* **38**: 91-119.

Feng, W., Banner, J. L., Guilfoyle, A. L., Musgrove, M. & James, E. W. (2012). Oxygen isotopic fractionation between drip water and speleothem calcite: A 10-year monitoring study, central Texas, USA. *Chemical Geology* **304**: 53-67.

Fisher, E. C., Bar-Matthews, M., Jerardino, A. & Marean, C. W. (2010). Middle and Late Pleistocene paleoscape modeling along the southern coast of South Africa. *Quaternary Science Reviews* **29**: 1382-1398.

Fleitmann, D., Burns, S. J., Neff, U., Mudelsee, M., Mangini, A. & Matter, A. (2004). Palaeoclimatic interpretation of high-resolution oxygen isotope profiles derived from annually laminated speleothems from Southern Oman. *Quaternary Science Reviews* **23**: 935-945.

Friedman, G. M. (1959). Identification of carbonate minerals by staining methods. *Journal of Sedimentary Research* **29***:*87-97.

Friedman, I.& O'Neil, J. R. (1977).*Compilation of stable isotope fractionation factors of geochemical interest* (Vol. 440). USGPO.Available from: http://www.osti.gov/scitech/servlets/purl/7314610#page=729 [Accessed 28 March 2015].

Frisia, S., Borsato, A., Drysdale, R. N., Paul, B., Greig, A. &Cotte, M. (2012).A re-evaluation of the palaeoclimatic significance of phosphorus variability in speleothems revealed by high-resolution synchrotron micro XRF mapping.*Climate of the Past* **8**: 2039-2051.

Frisia, S., Fairchild, I. J., Fohlmeister, J., Miorandi, R., Spötl, C., & Borsato, A. (2011). Carbon mass-balance modelling and carbon isotope exchange processes in dynamic caves. *Geochimica et Cosmochimica Acta* **75**: 380-400.

Frisia, S., Borsato, A., Fairchild, I. J., McDermott, F. & Selmo, E. M. (2002). Aragonite-calcite relationships in speleothems (Grotte de Clamouse, France): Environment, fabrics, and carbonate geochemistry. *Journal of Sedimentary Research* ***72***: 687-699.

Galimberti, M.G. (2010). *Investigating the use of oxygen and carbon isotopes and sclerochronology on Turbo sarmaticus and Donax serra for palaeoenvironment reconstruction at Pinnacle Point, South Africa.* Unpublished PhD Thesis. Cape Town: University of Cape Town.

Gascoyne, M. (1992a). Geochemistry of the actinides and their daughters. **In**: Ivanovich, M. & Harmon, R. S. (eds) *Uranium-series disequilibrium: applications to earth, marine, and environmental sciences*. Oxford: Clarendon Press. pp. 34-58.

Gascoyne, M. (1992b). Palaeoclimate determinations from cave calcite deposits. *Quaternary Science Reviews* **11**: 609-632.

Genty, D., Blamart, D., Ghaleb, B., Plagnes, V., Causse, C., Bakalowicz, M., Zouari, K., Chkir, N., Hellstrom, J., Wainer, K. & Bourges, F. (2006). Timing and dynamics of the last deglaciation from European and North African $\delta^{13}C$ stalagmite profiles—comparison with Chinese and South Hemisphere stalagmites. *Quaternary Science Reviews* **25**: 2118-2142.

Goldblatt, P. & Manning, J. (2000). *Cape plants: a conspectus of the Cape flora of South Africa*. National Botanical Institute.

Goldstein, S. J. & Stirling, C. H. (2003). Techniques for measuring uranium-series nuclides: 1992–2002. *Reviews in Mineralogy and Geochemistry* **52**: 23-57.

Grine, F.E. (2001). Implications of morphological diversity in early *Homo* crania from eastern and southern Africa. **In**: Tobias, P.V., Raath, M.A., Maggi-Cecchi, J. & Doyle, G.A. (eds) *Humanity from African naissance to coming millennia*. Florence: Florence University Press.pp. 107-115.

Grine, F. E., Klein, R. G. & Volman, T. P. (1991).Dating, archaeology and human fossils from the Middle Stone Age levels of Die Kelders, South Africa. *Journal of Human Evolution* **21**: 363-395.

Grossman, E. L., & Ku, T. L. (1986). Oxygen and carbon isotope fractionation in biogenic aragonite: temperature effects. *Chemical Geology: Isotope Geoscience Section* **59**: 59-74.

Guo, W., Mosenfelder, J. L., Goddard III, W. A. &Eiler, J. M. (2009). Isotopic fractionations associated with phosphoric acid digestion of carbonate minerals: insights from first-principles theoretical modeling and clumped isotope measurements. *Geochimica et Cosmochimica Acta* **73**: 7203-7225.

Guralnick, L. J., Cline, A., Smith, M. & Sage, R. F. (2008). Evolutionary physiology: the extent of C_4 and CAM photosynthesis in the genera Anacampseros and Grahamia of the Portulacaceae. *Journal of Experimental Botany* **59**: 1735-1742.

Guralnick, L. J., Rorabaugh, P. A. & Hanscom, Z. (1984). Seasonal shifts of photosynthesis in Portulacaria afra (L.) Jacq. *Plant Physiology* **76***:* 643-646.

Halkett, D., Hart, T., Yates, R., Volman, T. P., Parkington, J. E., Orton, J., Klein, R.G., Cruz-Uribe, K. & Avery, G. (2003). First excavation of intact Middle Stone Age layers at Ysterfontein, Western Cape Province, South Africa: implications for Middle Stone Age ecology. *Journal of Archaeological Science* **30**: 955-971.

Hall, G. & Woodborne, S. (2011). Chapter 5: Ecosystem change during MIS 4 and early MIS 3: evidence from the Middle Stone Age sites in South Africa. **In**: Runge, J. (ed.) *African palaeoenvironments and geomorphic landscape evolution.* Florida: CRC Press. pp. 79-106.

Harmon, R., Schwarcz, H.P., Gascoyne, M., Hess, J.W. & Ford, D.C. (2004).Palaeoclimate information from speleothems: the present as a guide to the past. **In**: Sasowsky, I. &Mylroie, J. (eds) *Studies of cave sediments.* Kluwer Academic/Plenum Publishers, New York. pp. 199-226

Hart, L., O'Riain, M. J., Jarvis, J. U. M. & Bennett, N. C. (2006). Is the Cape dune mole-rat, *Bathyergussuillus* (Rodentia: Bathyergidae), a seasonal or aseasonal breeder? *Journal of Mammalogy* **87***:* 1078-1085.

Hellstrom, J. (2006). U–Th dating of speleothems with high initial ^{230}Th using stratigraphical constraint. *Quaternary Geochronology* **1**: 289-295.

Hellstrom, J. (2003). Rapid and accurate U/Th dating using parallel ion-counting multi-collector ICP-MS. *Journal of Analytical Atomic Spectrometry* **18:** 1346-1351.

Hendy, C. H. (1971). The isotopic geochemistry of speleothems—I.The calculation of the effects of different modes of formation on the isotopic composition of speleothems and their applicability as palaeoclimatic indicators. *Geochimica et Cosmochimica Acta* **35**: 801-824.

Henshilwood, C. S., van Niekerk, K. L., Wurz, S., Delagnes, A., Armitage, S. J., Rifkin, R. F., Douze, K., Keene, P., Haaland, M.M., Reynard, J., Discamps, E. &Mienies, S. S. (2014). Klipdrift shelter, southern Cape, South Africa: preliminary report on the HowiesonsPoort layers. *Journal of Archaeological Science* **45**: 284-303.

Henshilwood, C. S. (2012). Late Pleistocene techno-traditions in southern Africa: a review of the Still Bay and Howiesons Poort, *c*. 75–59 ka. *Journal of World Prehistory* **25**: 205-237.

Henshilwood, C. S. & Dubreuil, B. (2011).The Still Bay and Howiesons Poort, 77–59 ka. *Current Anthropology* **52***:* 361-400.

Henshilwood, C.S., d'Errico, F., van Niekerk, K.L., Coquinot, Y., Jacobs, Z., Lauritzen, S.E., Menu, M. & García-Moreno, R. (2011). A 100,000-year-old ochre-processing workshop at Blombos Cave, South Africa. *Science* **334**: 219-222.

Henshilwood, C.S., d'Errico, F. & Watts, I. (2009). Engraved ochre from the Middle Stone Age levels at Blombos Cave, South Africa. *Journal of Human Evolution* **57**: 27-47.

Henshilwood, C.S. (2008). Winds of change: palaeoenvironments, material culture and human behaviour in the Late Pleistocene (~ 77 ka-48 ka) in the Western Cape Province, South Africa. *South African Archaeological Bulletin Goodwin Series* **10**: 35-51.

Henshilwood, C., d'Errico, F., Vanhaeren, M., van Niekerk, K. & Jacobs, Z. (2004). Middle Stone Age shell beads from South Africa. *Science* **304**: 404-404.

Henshilwood, C. S. & Marean, C. W. (2003).The origin of modern human behavior. *Current Anthropology* **44**: 627-651.

Henshilwood, C.S., d'Errico, F., Yates, R., Jacobs, Z., Tribolo, C., Duller, G.A., Mercier, N., Sealy, J.C., Valladas, H., Watts, I. & Wintle, A.G. (2002). Emergence of modern human behavior: Middle Stone Age engravings from South Africa. *Science* **295**: 1278-1280.

Henshilwood, C. S., Sealy, J.C., Yates, R., Cruz-Uribe, K., Goldberg, P., Grine, F.E., Klein, R.G., Poggenpoel, C., van Niekerk, K. & Watts, I. (2001). Blombos Cave, southern Cape, South Africa: preliminary report on the 1992–1999 excavations of the Middle Stone Age levels. *Journal of Archaeological Science* **28**: 421-448.

Henshilwood, C. S. (1997). Identifying the collector: evidence for human processing of the Cape Dune Mole-Rat, *Bathyergussuillus*, from Blombos Cave, southern Cape, South Africa. *Journal of Archaeological Science* **24**: 659-662.

Herries, A. I. (2006). Archaeomagnetic evidence for climate change at Sibudu Cave. *Southern African Humanities* **18**: 131-147.

Hilkert, A.W. & Avak, H. (2004).Finnigan Gas Bench II: *^{18}O-Equilibration on water, fruit juice and wine.* Bremen: Thermo Electron Corporation (Application Note 30048_E11/04C). Available from: www.joytech.com.tw/uploads/ass/11280977725877.pdf [Accessed 25 April 2013]

Hillestad-Nel, T. (2013).*Micromammals, climate change and human behaviour in the Middle Stone Age, southern Cape, South Africa: examining the possible links between palaeoenvironments and the cognitive evolution of Homo sapiens.* Unpublished PhD Thesis. Norway: University of Bergen.

Hoffmann, D. L., Spötl, C. & Mangini, A. (2009). Micromill and in situ laser ablation sampling techniques for high spatial resolution MC-ICPMS U-Th dating of carbonates. *Chemical Geology* **259**: 253-261.

Holmes, P.J. & Meadows, M.E. (2012). Southern African geomorphology: recent trends and new directions. Stellenbosch: Sun Press.

Holmes, P.J., Bateman, M.D., Carr, A.S. & Marker, M.E. (2007).The place of Aeolian coversands in the geomorphic evolution of the southern Cape coast, South Africa. *South African Journal of Geology* **110**: 125-136.

Holmgren, K., Lee-Thorp, J.A., Cooper, G.R.J., Lundblad, K., Partridge, T.C., Scott, L., Sithaldeen, R., Talma, A.S. & Tyson, P.D. (2003).Persistent millennial-scale climatic variability over the past 25 000 years in southern Africa. *Quaternary Science Reviews* **22**: 2311-2326.

Holmgren, K., Tyson, P. D., Moberg, A., & Svanered, O. (2001). A preliminary 3000-year regional temperature reconstruction for South Africa: research letter. *South African Journal of Science* **97**: 49.

Holmgren, K., Karlén, W., Lauritzen, S.E., Lee-Thorp, J.A., Partridge, T.C., Piketh, S., Repinski, P., Stevenson, C., Svarnered, O. & Tyson, P.D. (1999). A 3000-year high-resolution stalagmite based record of palaeoclimate for northeastern South Africa. *The Holocene* **9**: 295-309.

Hua, Q., McDonald, J., Redwood, D., Drysdale, R., Lee, S., Fallon, S. &Hellstrom, J. (2012).Robust chronological reconstruction for young speleothems using radiocarbon. *Quaternary Geochronology* **14**: 67-80.

Ivanovich, M., & Harmon, R. S. (eds). (1982). *Uranium series disequilibrium: applications to environmental problems*. United States: Oxford University Press.

Jacobs, Z., Hayes, E. H., Roberts, R. G., Galbraith, R. F. & Henshilwood, C. S. (2013). An improved OSL chronology for the Still Bay layers at Blombos Cave, South Africa: further tests of single-grain dating procedures and a re-evaluation of the timing of the Still Bay industry across southern Africa. *Journal of Archaeological Science* **40**: 579-594.

Jacobs, Z. (2010). An OSL chronology for the sedimentary deposits from Pinnacle Point Cave 13B—a punctuated presence. *Journal of Human Evolution* **59**: 289-305.

Jacobs, Z. & Roberts, R. G. (2009). Were environmental or demographic factors the driving force behind Middle Stone Age innovations in southern Africa?. *South African Journal of Science* **105**: 333-334.

Jacobs, Z., Roberts, R.G., Deacon, H.J., Grün, R., Mackay, A., Mitchell, P., Vogelsang, R. & Wadley, L. (2008). Ages for the Middle Stone Age of southern Africa: implications for human behaviour and dispersal. *Science* **322**: 733-735.

Jacobs, Z., Duller, G. A., Wintle, A. G., & Henshilwood, C. S. (2006). Extending the chronology of deposits at Blombos Cave, South Africa, back to 140ka using optical dating of single and multiple grains of quartz. *Journal of Human Evolution* **51**: 255-273.

Jacobs, Z., Wintle, A. G., & Duller, G. A. (2003a). Optical dating of dune sand from Blombos Cave, South Africa: I—multiple grain data. *Journal of Human Evolution* **44**: 599-612.

Jacobs, Z., Duller, G. A., & Wintle, A. G. (2003b). Optical dating of dune sand from Blombos Cave, South Africa: II—single grain data. *Journal of Human Evolution* **44**: 613-625.

James, N.P. & Jones, B. (2015).*Origin of carbonate sedimentary rocks*. Chichester: John Wiley & Sons. pp. 1-37.

Janis, C.M., Damuth, J. & Theodor, J.M. (2000). Miocene ungulates and terrestrial primary productivity: where have all the browsers gone? *Proceedings of the National Academy of Sciences* **97**: 7899-7904.

Jarvis, J. U M. & Bennett, N.C. (1990).The evolutionary history, population biology and social structure of African mole-rats: family Bathyergidae. **In**: Nevo, E. & Reig, O.A. (eds) *Evolution of subterranean mammals at the organismal and molecular levels.* New York: Wiley & Sons. pp. 97–128.

Johnson, B. J., Fogel, M. L. & Miller, G. H. (1998). Stable isotopes in modern ostrich eggshell: a calibration for paleoenvironmental applications in semi-arid regions of southern Africa. *Geochimica et Cosmochimica Acta* **62**: 2451-2461.

Johnson, B. J., Miller, G. H., Fogel, M. L. & Beaumont, P. B. (1997).The determination of late Quaternary paleoenvironments at Equus Cave, South Africa, using stable isotopes and amino acid racemization in ostrich eggshell. *Palaeogeography, Palaeoclimatology, Palaeoecology* **136**: 121-137.

Johnston, V.E., Borsato, A., Spötl, C., Frisia, S. & Miorandi, R. (2013). Stable isotopes in caves over altitudinal gradients: fractionation behaviour and inference for speleothem sensitivity to climate change. *Climate of the Past* **9**: 99-118.

Kaplan, A., Guilderson, T. P., Fairbanks, T. W., Bloom, A. L., Grootesg, P. M. & Nadeaug, M. J. (2005). Radiocarbon calibration curve spanning 0 to 50,000 years BP based on paired $^{230}Th/^{234}U/^{238}U$ and ^{14}C dates on pristine corals. *Quaternary Science Reviews* **24**: 1781-1796.

Kaplan, J. M. (1989). 45,000 years of hunter-gatherer history in Natal as seen from Umhlatuzana Rock Shelter. *South African Archaeological Bulletin Goodwin Series* **6**: 7-16.

Kandel, A. W., Bolus, M., Bretzke, K., Bruch, A. A., Haidle, M. N., Hertler, C. &Märker, M. (2015). Increasing behavioral flexibility? An integrative macro-scale approach to understanding the Middle Stone Age of southern Africa. *Journal of Archaeological Method and Theory*: 1-46. Viewed 06 July 2015.http://dx.doi.org/10.1007/s10816-015-9254-y

Kigoshi, K. 1971. Alpha-recoil thorium-234: dissolution into water and the uranium-234/uranium-238 disequilibrium in nature. *Science* **173**: 47-48.

Kim, S. T., O'Neil, J. R., Hillaire-Marcel, C. & Mucci, A. (2007). Oxygen isotope fractionation between synthetic aragonite and water: Influence of temperature and Mg^{2+} concentration. *Geochimica et Cosmochimica Acta* **71**: 4704-4715.

Kingdon, J., Happold, D., Hoffmann, M., Butynski, T., Happold, M. & Kalina, J. (2013). *Mammals of Africa Volume I: introductory chapters and Afrotheria*. Bloomsbury Publishing: London.

Klein, R. G., Avery, G., Cruz-Uribe, K., Halkett, D., Parkington, J.E., Steele, T., Volman, T.P. & Yates, R. (2004). The Ysterfontein 1 Middle Stone Age site, South Africa, and early human exploitation of coastal resources. *Proceedings of the National Academy of Sciences* **101**: 5708-5715.

Klein, R.G. (2002). *The dawn of human culture*. New York: Wiley & Sons.

Klein, R. G. & Cruz-Uribe, K. (2000). Middle and later Stone Age large mammal and tortoise remains from Die Kelders Cave 1, Western Cape Province, South Africa. *Journal of Human Evolution* **38**: 169-195.

Klein, R. G.& Cruz-Uribe, K. (1996). Exploitation of large bovids and seals at Middle and Later Stone Age sites in South Africa. *Journal of Human Evolution*, **31**: 315-334.

Klein, R. G. (1986). Carnivore size and Quaternary climatic change in southern Africa. *Quaternary Research* **26***:* 153-170.

Klein, R.G. (1983). Palaeoenvironmental implications of Quaternary large mammals in the fynbos region. **In**: Deacon, H.J., Hendey, Q.B. &Lambrechts, J.J.N. (eds) *Fynbospalaeoecology: a preliminary synthesis*. Pretoria: CSIR National Scientific Programmes Unit. Report No. 75. pp. 116-138. [Accessed March 04, 2015] http://hdl.handle.net/10204/2324.

Klein, R. G. (1978). A preliminary report on the larger mammals from the Boomplaas Stone Age cave site, Cango Valley, Oudtshoorn District, South Africa. *South African Archaeological Bulletin* **33**: 66-75.

Klein, R. G. (1976). The mammalian fauna of the Klasies River mouth sites, southern Cape Province, South Africa. *South African Archaeological Bulletin* **31** 75-98.

Klein, R. G. (1972). The late Quaternary mammalian fauna of Nelson Bay Cave (Cape Province, South Africa): its implications for megafaunal extinctions and environmental and cultural change. *Quaternary Research* **2**: 135-142.

Klein, R. G., & Cruz-Uribe, K. (2000). Middle and Later Stone Age large mammal and tortoise remains from Die Kelders Cave 1, Western Cape Province, South Africa. *Journal of Human Evolution* **38**: 169-195.

Klein, R. G. & Cruz-Uribe, K. (1996).Size variation in the rock hyrax (*Procaviacapensis*) and Late Quaternary climatic change in South Africa. *Quaternary Research***46**: 193-207.

Kluge, T., Marx, T., Scholz, D., Niggemann, S., Mangini, A. & Aeschbach-Hertig, W. (2008). A new tool for palaeoclimate reconstruction: Noble gas temperatures from fluid inclusions in speleothems. *Earth and Planetary Science Letters* **269**: 408-415.

Kronfeld, J., & Adams, J. A. (1974). Hydrologic investigations of the groundwaters of central Texas using U-^{234}U-^{238} disequilibrium. *Journal of Hydrology* **22**: 77-88.

Ku, T. L. (1976). The uranium-series methods of age determination. *Annual Review of Earth and Planetary Sciences* **4**: 347-379.

Lachniet, M. S., Asmerom, Y., Bernal, J. P., Polyak, V. J. & Vazquez-Selem, L. (2013).Orbital pacing and ocean circulation-induced collapses of the Mesoamerican monsoon over the past 22,000 years. *Proceedings of the National Academy of Sciences* **110**: 9255-9260.

Lachniet, M. S., Bernal, J. P., Asmerom, Y. & Polyak, V. (2012). Uranium loss and aragonite-calcite age discordance in a calcitized aragonite stalagmite. *Quaternary Geochronology* **14**: 26-37.

Lachniet, M. S. (2009). Climatic and environmental controls on speleothem oxygen-isotope values. *Quaternary Science Reviews* **28**: 412-432.

Lambeck, K., Esat, T. M., & Potter, E. K. (2002). Links between climate and sea levels for the past three million years. *Nature* **419**: 199-206.

Lambers, H., Chapin III, F. S. & Pons, T. L. (2008). *Plant water relations*. Springer : New York. pp.163-223.

Langejans, G. H., van Niekerk, K. L., Dusseldorp, G. L. & Thackeray, J. F. (2012). Middle Stone Age shellfish exploitation: Potential indications for mass collecting and resource intensification at Blombos Cave and Klasies River, South Africa. *Quaternary International* **270**: 80-94.

Langmuir, D. (1978). Uranium solution-mineral equilibria at low temperatures with applications to sedimentary ore deposits. *Geochimica et Cosmochimica Acta* **42**: 547-569.

Langmuir, D. & Herman, J. S. (1980).The mobility of thorium in natural waters at low temperatures. *Geochimica et Cosmochimica Acta* **44**: 1753-1766.

Lauritzen, S.E. & Lundberg, J. (1999). Calibration of the speleothem delta function: an absolute temperature record for the Holocene in northern Norway. *Holocene* **9**: 659-669.

Lee-Thorpe, J. & Sponheimer, M. (2007). Chapter 9: contribution of stable light isotopes to palaeoenvironmental reconstruction. **In**: Henke, W.,

Tattersall, I. & Hardt, T. (eds) *Handbook of palaeoanthropology*. New York: Springer. pp. 289-310.

Linge, H., Lauritzen, S. E., Lundberg, J., & Berstad, I. M. (2001). Stable isotope stratigraphy of Holocene speleothems: examples from a cave system in Rana, northern Norway. *Palaeogeography, Palaeoclimatology, Palaeoecology* **167**: 209-224.

Linge, H., Baker, A., Andersson, C. & Lauritzen, S.E. (2009). Variability in luminescent lamination and initial $^{230}Th/^{232}Th$ activity ratios in a late Holocene stalagmite from northern Norway. *Quaternary Geochronology* **4**: 181-192.

Lombard, M., Wadley, L., Deacon, J., Wurz, S., Parsons, I., Mohapi, M., Swart, J. & Mitchell, P. (2012). South African and Lesotho Stone Age sequence updated. *South African Archaeological Bulletin* **67**: 123-14.

Lombard, M. & Parsons, I. (2011). What happened to the human mind after the Howiesons Poort? *Antiquity* **85**: 1433-1443.

Lombard, M. (2009). The Howieson's Poort of South Africa amplified. *South African Archaeological Bulletin* **64**: 4-12.

Lubke, R. & de Moor, I.J. (1998).*Field guide to the eastern and southern Cape coasts.* Cape Town: University of Cape Town Press.

Ludwig, K. R. (2003). Mathematical–statistical treatment of data and errors for $^{230}Th/U$ geochronology. *Reviews in Mineralogy and Geochemistry* **52**:1 631-656.

Ludwig, K. R. &Titterington, D. M. (1994). Calculation of ^{230}ThU isochrons, ages and errors. *Geochimica et Cosmochimica Acta* **58**: 5031-5042.

Lundberg, J. (1990). *U-Series dating of carbonates by mass spectrometry with examples of speleothem coral and shell*. Unpublished PhD thesis. Ontario: McMaster University.

Luo, S. & Ku, T. L. (1991). U-series isochron dating: a generalized method employing total-sample dissolution. *Geochimica et Cosmochimica Acta* **55**: 555-564.

Lüttge, U. (1998). *Physiological ecology of tropical plants.* Heildelberg: Springer-Verlag.

Mackay, A., Stewart, B. A. & Chase, B. M. (2014).Coalescence and fragmentation in the late Pleistocene archaeology of southernmost Africa. *Journal of Human Evolution* **72**: 26-51.

Mackay, A. (2011). Nature and significance of the Howiesons Poort to post-Howiesons Poort transition at Klein Kliphuis Rockshelter, South Africa. *Journal of Archaeological Science* **38**: 1430-1440.

Mackay, A. (2006). A characterization of the MSA stone artefact assemblage from the 1984 excavations at Klein Kliphuis, Western Cape. *South African Archaeological Bulletin* **61**: 181-188.

Macron, C., Pohl, B., Richard, Y. &Bessafi, M. (2014). How do tropical temperate troughs form and develop over southern Africa?.*Journal of Climate* **27**: 1633-1647.

Malan, J.A. (1989). Lithostratigraphy of the Waenhuiskrans Formation (Bredasdorp Group).*Department of Mineral and Energy Affairs, Republic of South Africa.*

Marean, C. W. (2010). Pinnacle Point Cave 13B (Western Cape Province, South Africa) in context: the Cape floral kingdom, shellfish, and modern human origins. *Journal of Human Evolution* **59**: 425-443.

Marean, C.W., Bar-Matthews, M., Bernatchez, J., Fisher, E., Goldberg, P., Herries, A.I., Jacobs, Z., Jerardino, A., Karkanas, P., Minichillo, T., Nilssen, P.J., Thompson, E., Watts, I. & Williams, H.M. (2007).Early human use of marine resources and pigment in South Africa during the Middle Pleistocene. *Nature* **18**: 905-908.

Marean, C. W., Abe, Y., Frey, C. J. & Randall, R. C. (2000).Zooarchaeological and taphonomic analysis of the Die Kelders Cave 1 Layers 10 and 11 Middle Stone Age larger mammal fauna. *Journal of Human Evolution* **38**: 197-233.

Marker, M. E. (2003). The Knysna Basin, South Africa: geomorphology, landscape sensitivity and sustainability. *Geographical Journal* **169**: 32-42.

Marker, M.E. & Holmes, P.J. (2010). The geomorphology of the coastal platform in the southern Cape. *South African Geographical Journal* **92**: 105-116.

Marker, M. E. & Holmes, P. J. (2005). Landscape evolution and landscape sensitivity: the case of the southern Cape. *South African Journal of Science* **101**: 53-60.

Marker, M. E. & Holmes, P. J. (1999). Laterisation on limestones of the Tertiary Wankoe Formation and its relationship to the African Surface, southern Cape, South Africa. *Catena* **38**: 1-21.

Martinson, D. G., Pisias, N. G., Hays, J. D., Imbrie, J., Moore, T. C. & Shackleton, N. J. (1987). Age dating and the orbital theory of the ice ages:

development of a high-resolution 0 to 300,000-year chronostratigraphy. *Quaternary Research* **27**: 1-29.

Mattey, D., Lowry, D., Duffet, J., Fisher, R., Hodge, E. & Frisia, S. (2008). A 53- year seasonally resolved oxygen and carbon isotope record from a modern Gibraltar speleothem: reconstructed drip water and relationship to local precipitation. *Earth & Planetary Science Letters* **269**: 80-95.

McBrearty, S. & Brooks, A. S. (2000). The revolution that wasn't: a new interpretation of the origin of modern human behavior. *Journal of Human Evolution* **39**: 453-563.

McCall, G. S. (2007). Behavioral ecological models of lithic technological change during the later Middle Stone Age of South Africa. *Journal of Archaeological Science* **34**: 1738-1751.

McDermott, F. (2004).Palaeo-climate reconstruction from stable isotope variations in speleothems: a review. *Quaternary Science Reviews* **23**: 901-918.

McGarry, S., Bar-Matthews, M., Matthews, A., Vaks, A., Schilman, B. &Ayalon, A. (2004).Constraints on hydrological and paleotemperature variations in the Eastern Mediterranean region in the last 140 ka given by the δD values of speleothem fluid inclusions. *Quaternary Science Reviews* **23**: 919-934.

Meadows, M. E., Chase, B. M. &Seliane, M. (2010). Holocene palaeoenvironments of the Cederberg and Swartruggens mountains, Western Cape, South Africa: pollen and stable isotope evidence from hyrax dung middens. *Journal of Arid Environments* **74**: 786-793.

Meadows, M. E. & Baxter, A. J. (1999). Late Quaternary palaeoenvironments of the southwestern Cape, South Africa: a regional synthesis. *Quaternary International* **57**: 193-206.

Mickler, P. J., Stern, L. A., & Banner, J. L. (2006). Large kinetic isotope effects in modern speleothems. *Geological Society of America Bulletin* **118**: 65-81.

Mickler, P. J., Banner, J. L., Stern, L., Asmerom, Y., Edwards, R. L. & Ito, E. (2004). Stable isotope variations in modern tropical speleothems: evaluating equilibrium vs. kinetic isotope effects. *Geochimica et Cosmochimica Acta* **68**: 4381-4393.

Miller, G. H., Beaumont, P. B., Deacon, H. J., Brooks, A. S., Hare, P. E. & Jull, A. J. T. (1999). Earliest modern humans in southern Africa dated by isoleucine epimerization in ostrich eggshell. *Quaternary Science Reviews* **18**: 1537-1548.

Millard, A. R. (2008). A critique of the chronometric evidence for hominid fossils: I. Africa and the Near East 500–50 ka. *Journal of Human Evolution* **54**: 848-874.

Millard, A. R. (2006). Bayesian analysis of ESR dates, with application to Border Cave. *Quaternary Geochronology* **1**: 159-166.

Milton, S. J. (2004). Grasses as invasive alien plants in South Africa: working for water. *South African Journal of Science* **100**: 69.

Mitchell, P. (2002). *The archaeology of southern Africa.* Cape Town: Cambridge University Press.

Mitchell, P. (2008). Developing the archaeology of Marine Isotope Stage 3.*South African Archaeological Bulletin Goodwin Series* **10**: 52-65.

Mitchell, P., Parkington, J. & Wadley, L. (1998). A tale from three regions: The archaeology of the Pleistocene/Holocene transition in the Western Cape, the Caledon Valley and the Lesotho Highlands, southern Africa. *Quaternary International* **49**: 105-115.

Moffett, R. O. & Deacon, H. J. (1977). The flora and vegetation in the surrounds of Boomplaas Cave: Cango Valley. *South African Archaeological Bulletin* **32**: 127-145.

Moore, D. M. & Reynolds, R. C. (1989). *X-ray Diffraction and the Identification and Analysis of Clay Minerals* (Vol. 378). Oxford: Oxford University Press.

Mourre, V., Villa, P. & Henshilwood, C. S. (2010). Early use of pressure flaking on lithic artifacts at Blombos Cave, South Africa. *Science* **330**: 659-662.

Mucina, L. & Rutherford, M.C. (2006). The vegetation of South Africa, Lesotho and Swaziland.*Strelitzia* **19**: 220-299.

Mühlinghaus, C., Scholz, D. & Mangini, A. (2009). Modelling fractionation of stable isotopes in stalagmites. *Geochimica et Cosmochimica Acta* **73**: 7275-7289.

Noah, J. S. (2010). *Reconstructing palaeoenvironments during the Middle Stone Age in the southern Cape, South Africa: stable isotope analysis of speleothems from the De Hoop Nature Reserve*. Unpublished MSc Dissertation. Johannesburg: University of the Witwatersrand.

Nürnberg, D. (2000). Taking the temperature of past ocean surfaces. *Science* **289**: 1698-1699.

Ortega, R., Maire, R., Devès, G. & Quinif, Y. (2005). High-resolution mapping of uranium and other trace elements in recrystallized aragonite–

calcite speleothems from caves in the Pyrenees (France): implication for U-series dating. *Earth and Planetary Science Letters* **237**: 911-923.

Osmond, J. K. & Cowart, J. B. (1976). The theory and uses of natural uranium isotopic variations in hydrology. *Atomic Energy Review* **14**: 621-679.

Osmond, J. K., Cowart, J. B. & Ivanovich, M. (1983).Uranium isotopic disequilibrium in ground water as an indicator of anomalies. *The International Journal of Applied Radiation and Isotopes* **34**: 283-308.

Parkington, J. (1987). Prehistory and palaeoenvironments at the Pleistocene-Holocene boundary in the Western Cape. **In:** *The Pleistocene Old World* . Springer: New York. pp. 349-363.

Parkington, J. &Poggenpoel, C. (1987). Diepkloof Rock Shelter. *BAR International Series* **332**: 269-293.

Parkington, J. E. (1980). The Elands Bay cave sequence: cultural stratigraphy and subsistence strategies. **In**: *Proceedings of the 8th Pan-African Congress of Prehistory and Quaternary Studies, Nairobi*. pp. 315-320.

Partridge, T. C. (1997). Cainozoic environmental change in southern Africa, with special emphasis on the last 200,000 years. *Progress in Physical Geography***21**: 3-22.

Partridge, T. C., Demenocal, P. B., Lorentz, S. A., Paiker, M. J. & Vogel, J. C. (1997). Orbital forcing of climate over South Africa: a 200,000-year rainfall record from the Pretoria Saltpan. *Quaternary Science Reviews* **16**: 1125-1133.

Partridge, T.C. & Maud, R.R. (1987). Geomorphic evolution of southern Africa since the Mesozoic. *South African Journal of Geology* **90**: 179-208.

Petersen, J.O., Deschamps, P., Hamelin, B., Goncalves, J., Michelor, J.L. &Zouari, K. (2013). Water-rock interaction and residence time of groundwater inferred by $^{234}U/^{238}U$ disequilibria in the Tunisian Continental Intercalaire aquifer system. *Procedia Earth & Planetary Sciences* **7**: 685-688.

Pickering, R. & Kramers, J. D. (2010). Re-appraisal of the stratigraphy and determination of new U-Pb dates for the Sterkfontein hominin site, South Africa. *Journal of Human Evolution* **59**: 70-86.

Pickering, R., Hancox, P.J., Lee-Thorp, J.A., Grün, R., Mortimer, G.E., McCulloch, M. & Berger, L.R. (2007). Stratigraphy, U-Th chronology and palaeoenvironments at Gladysvale Cave: insights into the climatic control of South African hominin-bearing cave deposits. *Journal of Human Evolution* **53**: 602-619.

Pickering, R. (2006). *The stratigraphy, chronology and palaeoenvironment of the Pleistocene Cave Fill, Gladysvale Cave, South Africa*. MSc Dissertation. Johannesburg: University of the Witwatersrand.

Pienaar, U. D. V. (1974). Habitat-preference in South African antelope species and its significance in natural and artificial distribution patterns. *Koedoe***17**:185-195.

Polag, D., Scholz, D., Mühlinghaus, C., Spötl, C., Schröder-Ritzrau, A., Segl, M. & Mangini, A. (2010). Stable isotope fractionation in speleothems: Laboratory experiments. *Chemical Geology* **279**: 31-39.

Porraz, G., Texier, J.P., Archer, W., Piboule, M., Rigaud, J.P. & Tribolo, C. (2013). Technological successions in the Middle Stone Age sequence of Diepkloof Rock Shelter, Western Cape, South Africa. *Journal of Archaeological Science* **40**: 3376-3400.

Quick, L.J. (2013). *Late Quaternary palaeoenvironments of the southern Cape, South Africa: palynological evidence from the coastal wetlands*. Unpublished PhD Thesis. Cape Town: University of Cape Town.

Rabassa, J. & Ponce, J. F. (2013). The Heinrich and Dansgaard-Oeschger climatic events during Marine Isotopic Stage 3: Searching for appropriate times for human colonization of the Americas. *Quaternary International* **299**: 94-105.

Railsback, L. B., Brook, G. A., Chen, J., Kalin, R., & Fleisher, C. J. (1994). Environmental controls on the petrology of a late Holocene speleothem from Botswana with annual layers of aragonite and calcite. *Journal of Sedimentary Research* **64**: 147-155.

Railsback, L. B., Dabous, A. A., Osmond, J. K. & Fleisher, C. J. (2002). Petrographic and geochemical screening of speleothems for U-series dating: an example from recrystallized speleothems from Wadi Sannur Cavern, Egypt. *Journal of Cave & Karst Studies* **64**: 108-116.

Raimondo, D., Staden, L.V., Foden, W., Victor, J.E., Helme, N.A., Turner, R.C., Kamundi, D.A. & Manyama, P.A. (2009). *Red list of South African plants 2009*. Pretoria: South African National Biodiversity Institute.

Reed, D.N. (2007). Serengeti micromamammals and their implications for Olduvai paleoenvironments. **In**: Bobé, R., Alemseged, Z. & Behrensmeyer, A.K. (2007). *Hominin environments in the East African Pliocene: an assessment of the faunal evidence*. New York: Springer. pp. 217-256.

Reynard, J.P., Badenhorst, S. & Henshilwood, C.S. (2014). Inferring animal size from the unidentified long bones from the Middle Stone Age layers at Blombos Cave, South Africa. *Annals of the Ditsong National Museum of Natural History* **4**: 9-25.

Reynard, J.P. (2011). *The unidentified long bone fragments from the Middle Stone Age Still Bay layers at Blombos Cave, southern Cape, South Africa*. Unpublished MSc dissertation. Johannesburg: University of the Witwatersrand.

Richards, D. A. & Dorale, J. A. (2003).Uranium-series chronology and environmental applications of speleothems. *Reviews in Mineralogy and Geochemistry* **52**: 407-460.

Rightmire, G. P. & Deacon, H. J. (1991). Comparative studies of Late Pleistocene human remains from Klasies River Mouth, South Africa. *Journal of Human Evolution* **20**: 131-156.

Roberts, P. (2013).*Stable carbon and oxygen isotope analysis of ostrich eggshell (OES) samples from LSA and MSA levels at Blombos Cave, Klipdrift Shelter and Klipdrift Cave (South Africa).* Unpublished MSc Dissertation. Oxford: Oxford University.

Romanek, C. S., Grossman, E. L., & Morse, J. W. (1992). Carbon isotopic fractionation in synthetic aragonite and calcite: effects of temperature and precipitation rate. *Geochimica et Cosmochimica Acta* **56**: 419-430.

Rosholt, J. N., Shields, W. R. & Garner, E. L. (1963). Isotopic fractionation of uranium in sandstone. *Science* **139**: 224-226.

Ryano, K.P. (2014). *The Later Stone Age in the southern Cape, South Africa, during the terminal Pleistocene/early Holocene with a focus on Klipdrift Cave*. Unpublished PhD thesis. Johannesburg: University of the Witwatersrand.

Sachs, J. P. & Anderson, R. F. (2003). Fidelity of alkenone paleotemperatures in southern Cape Basin sediment drifts. *Paleoceanography* **18**. DOI: 10.1029/2002PA000862

Scholz, D., Mühlinghaus, C. & Mangini, A. (2009).Modelling $\delta^{13}C$ and $\delta^{18}O$ in the solution layer on stalagmite surfaces. *Geochimica et Cosmochimica Acta* **73**:2592-2602.

Scholz, D., & Hoffmann, D. L. (2011). StalAge–an algorithm designed for construction of speleothem age models. *Quaternary Geochronology* **6**: 369-382.

Scholtz, A. (1986). *Palynological and palaeobotanical studies in the southern Cape*. Unpublished Masters dissertation. Stellenbosch: University of Stellenbosch. Available from http://hdl.handle.net/10019.1/3071 [Accessed May 07, 2015]

Schwarcz, H. P. & Rink, W. J. (1999). ESR dating of the Die Kelders Cave 1 site, South Africa. *Journal of Human Evolution* **38***:* 121-128.

Schwarcz, H. P. & Latham, A. G. (1989). Dirty calcites 1. Uranium-series dating of contaminated calcite using leachates alone. *Chemical Geology* **80**: 35-43.

Schweitzer, F.R. (1970). A preliminary report of excavations of a cave at Die Kelders. *South African Archaeological Bulletin* **25**: 136-138.

Scott, L., & Lee-Thorp, J. A. (2004).Holocene climatic trends and rhythms in southern Africa. **In**: *Past Climate Variability through Europe and Africa.* Netherlands: Springer. pp. 69-91.

Scott, L. (1999). Vegetation history and climate in the Savanna biome South Africa since 190,000 ka: a comparison of pollen data from the Tswaing Crater (the Pretoria Saltpan) and Wonderkrater. *Quaternary International* **57**: 215-223.

Shen, C.C., Edwards, R.L., Cheng, H., Dorale, J.A., Thomas, R.B., Moran, S.B., Weinstein, S.E. & Edmonds, H.N. (2000). Uranium and thorium isotopic and concentration measurements by magnetic sector inductively coupled plasma mass spectrometry. *Chemical Geology* **185**: 165-178.

Shen, C. C., Li, K. S., Sieh, K., Natawidjaja, D., Cheng, H., Wang, X., Edwards, R.L., Lam, D.D., Hsieh, Y.T., Fan, T.Y., Meltzner, A.J., Taylor, F.W., Quinn, T.M., Chang, H.W. & Kilbourne, K. H. (2008). Variation of initial $^{230}Th/^{232}Th$ and limits of high precision U–Th dating of shallow-water corals. *Geochimica et Cosmochimica Acta* **72**: 4201-4223.

Shipley, L.A. (1999). Grazers and browsers: how digestive morphology affects diet selection. *Grazing Behaviour of Livestock & Wildlife* **70**: 20-27.

Siddall, M., Rohling, E. J., Thompson, W. G. & Waelbroeck, C. (2008). Marine isotope stage 3 sea level fluctuations: data synthesis and new outlook. *Reviews of Geophysics* **46**: 1-29.

Singer, R. & Wymer, J. (1982).*The Middle Stone Age at Klasies River Mouth in South Africa.* Chicago: Chicago University Press.

Skinner, J.D. & Chimimba, C.T. (2005).*The mammals of the southern African sub-region*. Cambridge: Cambridge University Press. pp.41-50.

Smart, P.L. & Frances, P.D. (1991).Uranium series dating. **In**: Smart, P.L & Frances, P.D. (eds) *Quaternary dating methods – a user's guide* (Technical Guide No. 4). London: Quaternary Research Association. pp 45-83.

Spötl, C. & Mattey, D. (2006). Stable isotope microsampling of speleothems for palaeoenvironmental studies: a comparison of microdrill, micromill and laser ablation techniques. *Chemical Geology* **235**: 48-58.

Spötl, C., Mangini, A. & Richards, D. A. (2006).Chronology and paleoenvironment of Marine Isotope Stage 3 from two high-elevation speleothems, Austrian Alps. *Quaternary Science Reviews* **25**: 1127-1136.

Stokes, S., Thomas, D.S. & Washington, R. (1997). Multiple episodes of aridity in southern Africa since the last interglacial period. *Nature* **388**: 154-158.

Stuut, J. B. W., Prins, M. A., Schneider, R. R., Weltje, G. J., Jansen, J. F. & Postma, G. (2002). A 300-kyr record of aridity and wind strength in southwestern Africa: inferences from grain-size distributions of sediments on Walvis Ridge, SE Atlantic. *Marine Geology* **180**: 221-233.

Sundqvist, H. S., Baker, A. & Holmgren, K. (2005). Luminescence variations in fast-growing stalagmites from Uppsala, Sweden. *Geografiska Annaler: Series A, Physical Geography* **87**: 539-548.

Talma, A. S. & Netterberg, F. (1983). Stable isotope abundances in calcretes. *Geological Society London: Special Publications* **11**: 221-233.

Talma, A.S. & Vogel, J.C. (1992). Late Quaternary palaeotemperatures derived from a speleothem from Cango Caves, Cape Province, South Africa. *Quaternary Research* **37**: 203-213.

Tankard, A.J., Jackson, M.P.A., Eriksson, K.A., Hobday, D.K., Hunter, D.R. & Minter, W.E.L. (2012).*Crustal evolution of southern Africa: 3.8 billion years of Earth history.* New York: Springer-Verlag.

Tarutani, T., Clayton, R. N. & Mayeda, T. K. (1969).The effect of polymorphism and magnesium substitution on oxygen isotope fractionation between calcium carbonate and water. *Geochimica et Cosmochimica Acta* **33**: 987-996.

Thackeray, J. F. (2009). Chronology, climate and technological innovation associated with the Howieson's Poort and Still Bay industries in South Africa. *South African Journal of Science* **105**: 90-90.

Thackeray, J.F. (1992). Chronology of Late Pleistocene deposits associated with *Homo sapiens* at Klasies River Mouth, South Africa. *Palaeoecology of Africa and the Surrounding Islands* **23**: 177-191

Thackeray, J. F. (1990). Temperature indices from late Quaternary sequences in South Africa: comparisons with the Vostok core. *South African Geographical Journal* **72**: 47-49.

Thackeray, J.F. & Avery, D.M. (1990). A comparison between temperature indices for Late Pleistocene sequences at Klasies River and Border Cave, South Africa. *Palaeoecology of Africa* **21**: 311-315.

Thackeray, J. F. (1988). Molluscan fauna from Klasies River, South Africa. *South African Archaeological Bulletin* **43**: 27-32.

Thackeray, J. F. (1987). Late Quaternary environmental changes inferred from small mammalian fauna, southern Africa. *Climatic Change* **10:** 285-305.

ThermoFinnigan.(2002). Kiel carbonate device operating manual (Ident.No. 111 3791). Bremen: ThermoFinnigan. *Thermo Scientific Element 2 & Element XR* Available from: http://www.thermoscientific.com/ecomm/servlet/productscatalog_11152__87279_-1_4 [Accessed 26 April 2013]

Thomas, R. (2001). Spectroscopy tutorial: a beginner's guide to ICP-MS Part I. *Spectroscopy***16:** 38-42.

Thomas, D. S. & Burrough, S. L. (2012). Interpreting geoproxies of late Quaternary climate change in African drylands: implications for understanding environmental change and early human behaviour. *Quaternary International* **253**: 5-17.

Thompson, J. C. & Henshilwood, C. S. (2014a).Tortoise taphonomy and tortoise butchery patterns at Blombos Cave, South Africa. *Journal of Archaeological Science* **41**: 214-229.

Thompson, J. C. & Henshilwood, C. S. (2014b). Nutritional values of tortoises relative to ungulates from the Middle Stone Age levels at Blombos Cave, South Africa: implications for foraging and social behaviour. *Journal of Human Evolution* **67**: 33-47.

Thompson, J. C. & Henshilwood, C. S. (2011). Taphonomic analysis of the Middle Stone Age larger mammal faunal assemblage from Blombos Cave, southern Cape, South Africa. *Journal of Human Evolution* **60**: 746-767.

Thompson, E., Williams, H. M. & Minichillo, T. (2010). Middle and Late Pleistocene Middle Stone Age lithic technology from Pinnacle Point 13B (Mossel Bay, Western Cape Province, South Africa). *Journal of Human Evolution* **59**: 358-377.

Thwaites, R. N. & Cowling, R. M. (1988). Soil-vegetation relationships on the Agulhas plain, South Africa. *Catena* **15**: 333-345.

Tremaine, D. M., Froelich, P. N. & Wang, Y. (2011). Speleothem calcite farmed *insitu*: Modern calibration of $\delta^{18}O$ and $\delta^{13}C$ palaeoclimate proxies in a continuously-monitored natural cave system. *Geochimica et Cosmochimica Acta* **75**: 4929-4950.

Tribolo, C., Mercier, N., Douville, E., Joron, J.L., Reyss, J.L., Rufer, D., Cantin, N., Lefrais, Y., Miller, C.E., Porraz, G., Parkington, J., Rigaud, J.P. &Texier, P.J. (2013). OSL and TL dating of the Middle Stone Age

sequence at Diepkloof Rock Shelter (South Africa): a clarification. *Journal of Archaeological Science* **40**: 3401-3411.

Tribolo, C., Mercier, N. &Valladas, H. (2005). Chronology of the Howieson'sPoort and Still Bay techno-complexes: assessment and new data from luminescence. **In**: Backwell, L. & d'Errico, F. (eds) *From tools to symbols: from early hominids to modern humans.* Johannesburg: University of the Witwatersrand Press. pp. 493-511.

Tribolo, C. (2003). *Apport des methodes de la luminescence à la chronologie des techno-facies du Middle Stone Age associés aux premiershommesmodernes du Sud de l'Afrique*. Unpublished PhD Thesis. Bordeaux: University of Bordeaux [Abstract]. Available from http://www.theses.fr/2003BOR12725 [Accessed May 06, 2015].

Turney, C.M. & Bird, M.I. (2002).Determining the timing and pattern of human colonisation in Australia: proposals for radiocarbon dating 'early' sequences. *Australian Archaeology* **54**: 1-4.

Tyson, P.D. & Preston-Whyte, R.A. (2000). *The weather and climate of southern Africa*. Cape Town: Oxford University Press.

Tyson, P.D. (1986). *Climatic change and variability in southern Africa*. Cape Town: Oxford University Press.

van Andel, T. H. (1989). Late Quaternary sea-level changes and archaeology. *Antiquity* **63**: 733-745.

van Campo, E., Duplessy, J.C., Prell, W.L., Barratt, N. & Sabatier, R. (1990). Comparison of terrestrial and marine temperature estimates for the past 135 kyr off southeast Africa: a test for GCM simulations of palaeoclimate. *Nature* **348**: 209-212.

Van Meerbeeck, C. J., Renssen, H. & Roche, D. M. (2009). How did Marine Isotope Stage 3 and Last Glacial Maximum climates differ?–perspectives from equilibrium simulations. *Climate of the Past* **5**: 33-51.

van Pletzen, L. (2000). *The large mammal fauna from Klasies River* . Unpublished PhD Thesis. Stellenbosch: Stellenbosch University.

Villa, P., Soriano, S., Teyssandier, N. & Wurz, S. (2010). The Howiesons Poort and MSA III at Klasies River main site, cave 1A. *Journal of Archaeological Science* **37**: 630-655.

Vogel, J.C. 2001. Radiometric dates for the Middle Stone Age in South Africa. **In**: Tobias, P.V., Raath, M.A., Maggi-Cecchi, J. & Doyle, G.A. (eds) *Humanity from African naissance to coming millennia*. Florence: Florence University Press. pp. 261-268.

Volman, T.P. (1984). Early prehistory of southern Africa. **In**: Klein, R.G. (ed.) Southern African prehistory and palaeoenvironments. Rotterdam: AA Balkema. pp. 169-220.

Vosloo, D. &Vosloo, A. (2010). Response of cold-acclimated, farmed South African abalone (*Haliotismidae*) to short-term and long-term changes in temperature. *Journal of Thermal Biology* **35**: 317-323.

Wadley, L. (2015). The marvellous millennia: the Middle Stone Age of southern Africa. *Azania: Archaeological Research in Africa* **50**: 155-226.

Wadley, L. (2013). Recognizing complex cognition through innovative technology in Stone Age and Palaeolithic sites. *Cambridge Archaeological Journal* **23**: 163–183.

Wadley, L., Hodgkiss, T. & Grant, M. (2009).Implications for complex cognition from the hafting tools with compound adhesives in the Middle Stone Age, South Africa. *Proceedings of the National Academy of Sciences* **106**: 9590-9594.

Wadley, L. & Jacobs, Z. (2006).Sibudu Cave: background to the excavations, stratigraphy and dating. *Southern African Humanities* **18**: 1-26.

Wadley, L. (1991). Rose Cottage Cave: background and a preliminary report on the recent excavations. *South African Archaeological Bulletin* **46**: 125-130.

Walker, M. (2005).*Quaternary dating methods.* John Wiley & Sons: England.

White, W.B. (2007). Cave sediments and palaeoclimate. *Journal of Cave and Karst Studies* **69**: 76-93.

White, W.B. (2004). Palaeoclimate records from speleothems in limestone caves. **In:** Sasowsky, I.D. & Mylroie, J. (eds) *Studies of cave sediments: physical and chemical records of palaeoclimate*. New York: Kluwer Academic. pp. 135-175.

Whitehead, N.E., Ditchburn, R.G., Williams, P.W. & McCabe, W.J. (1999).^{231}Pa and ^{230}Th contamination at zero age: a possible limitation on the U/Th series dating of speleothem material. *Chemical Geology* **156**: 359-366.

Wigley, T.M.L & Brown, M.C. (1976).*The physics of caves*. **In**: Ford, T.D. &Cullingford, C.H.D. (eds). *The science of speleology*. London: Academic Press. pp. 329-358.

Willis, C. K., Cowling, R. M. & Lombard, A. T. (1996).Patterns of endemism in the limestone flora of South African lowland fynbos. *Biodiversity & Conservation* **5**: 55-73.

Wurz, S. (2013). Technological trends in the Middle Stone Age of South Africa between MIS 7 and MIS 3. *Current Anthropology* **54**: S305-S319.

Wurz, S. (2002).Variability in the Middle Stone Age lithic sequence, 115,000–60,000 years ago at Klasies River, South Africa. *Journal of Archaeological Science* **29**: 1001-1015.

Wurz, S. J. D. (2000). *The Middle Stone Age at Klasies River, South Africa.* Unpublished PhD Thesis. Stellenbosch: Stellenbosch University.

Wurz, S. (1999). The Howiesons Poort backed artefacts from Klasies River: an argument for symbolic behaviour. *South African Archaeological Bulletin***54**: 38-50.

Zheng, Y. F. (1999). Oxygen isotope fractionation in carbonate and sulfate minerals. *Geochemical Journal-Japan* **33**:109-126.

Zhou, H., Zhao, J., Qing, W., Feng, Y. & Tang, J. (2011). Speleothem-derived Asian summer monsoon variations in Central China, 54–46 ka. *Journal of Quaternary Science* **26**: 781-790.

Ziegler, M., Simon, M. H., Hall, I. R., Barker, S., Stringer, C. & Zahn, R. (2013). Development of Middle Stone Age innovation linked to rapid climate change. *Nature Communications* **4**: 1905.

Appendix – RESULTS FROM THE BL2 STALAGMITE

A1.1 BL2 Sample

Uranium concentration and activity ratios

Fifteen U-Th ages were obtained for the BL2 stalagmite and the data are summarised in Table A1.1. Values are given for the uranium concentration and each of the activity ratios of uranium ($^{234}U/^{238}U$, $(^{234}U/^{238}U)_{initial}$) and thorium ($^{230}Th/^{232}Th$) and includes the isotopes of $^{230}Th/^{234}U$. Changes in the latter ratio form the basis for the dating method used in this study. The stratigraphic position of each of the subsamples is denoted either by T (top), M (middle) or B (base). Errors are 1σ and ages are reported as ka (thousand years).

Variations in the ^{238}U concentration of the BL2 stalagmite are not unlike those observed for the BL1 sample. However, in the BL2 sample there is a wider degree of heterogeneity as the uranium concentration values peak and dip along the vertical length of the stalagmite. In BL2, the ^{238}U concentrations vary between 0.71 ppm and 0.17 ppm with an average of 0.41 ppm. The highest concentration is observed in the depositional layer at 7.5mm from the top with a value of 0.71 ppm. This layer has a corresponding U-Th age estimate of 137 ± 2.2 ka. The ^{238}U content decreases incrementally along the subsampled layers at 17, 38 and 73 mm from the top. These layers date respectively to 136 ± 5.8 ka, 123 ± 6.5 ka and 129 ± 9.6 ka.

The ^{238}U concentration increases again to 0.45 ppm in the layer at 140 mm which is dated to 145 ± 1.8 ka. The ^{238}U concentration dips slightly to 0.24 ppm in the layer at 152.5 mm followed by an increase to 0.36 ppm in the layer at 242 mm. The layer at 152.5 mm is dated to 155 ± 3.8 ka and the layer located farther below it at 242mm dates to 118 ± 2.6 ka. Uranium concentrations are fairly consistent in the layers at 275 mm and 309 mm

with corresponding values of 0.69 ppm and 0.62 ppm. These layers date respectively to 150 ± 3.6 ka and 130 ± 1.9 ka. The ^{238}U values decrease again in the layers located closer towards the base of the sample. Concentrations of 0.40 ppm, 0.46 ppm and 0.39 ppm were recorded for the basal layers at 351 mm, 375 mm and 380 mm, respectively. These layers date respectively to 113 ± 1.9 ka, 119 ± 7.1 ka and 116 ± 1.4 ka. In the layers between 407 mm and 440 mm the uranium concentrations are 0.37 ppm and 0.31 ppm which is comparatively lower than the concentration value for the overlying layer at 380 mm. The stratigraphic layers at 407 mm and 440 mm date respectively to 117 ± 1.5 ka and 112 ± 2.8 ka. The ^{238}U concentration for the layer at 466 mm is 0.54 ppm and falls within the range of values observed for the layers at 351 mm and 309 mm. The layer at 466 mm dates to 126 ± 2.2 ka. Overall for the BL2 stalagmite, the ^{238}U content varies throughout the sample with no clear trends in uranium concentration from the top to the base of BL2.

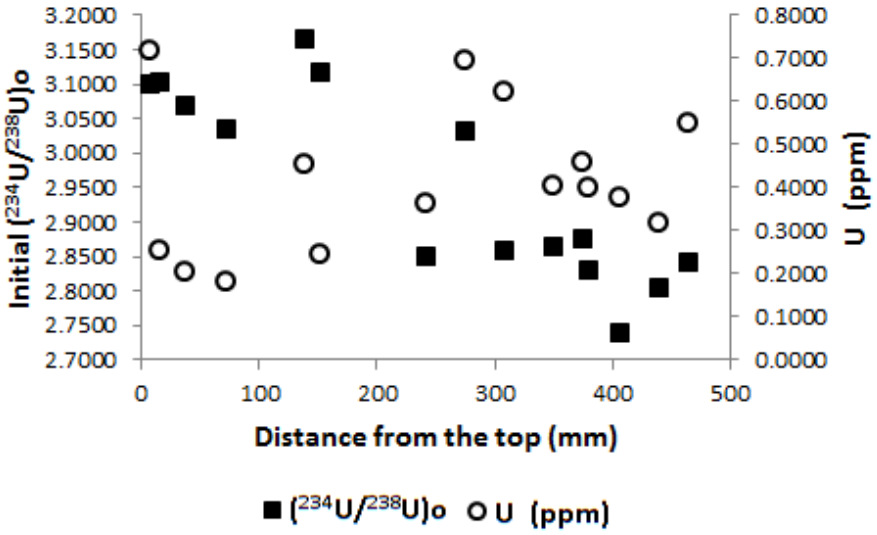

Fig. A1.1 Changes in the initial ($^{234}U/^{238}U$) activity ratio and uranium concentration (in ppm) along the length of BL2

In contrast to the highly variable values obtained for the uranium concentrations the corresponding $^{238}U/^{234}U$ activity ratio values are fairly

consistent with activity ratio values ranging between 2.24 and 2.46 and average values of 2.35. There is however some variation in these values moving from the top towards the base of BL2. Relatively higher $^{238}U/^{234}U$ activity ratio values tend to occur in layers closer to the top whereas fairly lower values are found in layers at the base. Overall, the $^{238}U/^{234}U$ activity ratio values exhibit a generally increasing trend from the base to the top of BL2. This trend of comparatively higher values moving towards the top of the sample is also reflected in the initial $(^{238}U/^{234}U)_0$ ratio values. The initial $(^{238}U/^{234}U)_0$ activity ratio values are somewhat higher than those recorded for the $^{238}U/^{234}U$ ratio and range between 2.73 and 3.16 with a mean of 2.95.

Uranium leaching effects, as determined by comparing both initial and measured $^{234}U/^{238}U$ activity ratios, do not seem responsible for the current inversion in BL2. As an alternative the effects of thorium contamination are considered instead.

Thorium activity ratios

The $^{230}Th/^{234}U$ activity ratio relates to the proportion of radiogenic thorium to uranium and forms the basis for the age determinations in this study. For BL2 the $^{230}Th/^{234}U$ activity ratio values are fairly homogeneous, particularly closer towards the base of the sample at *c.* 341 mm to 466 mm from the top. Notable exceptions with non-homogeneous ratio values occur primarily in the middle at 309 mm, 275 mm, 152.5 and 140 mm as well as at the top of the sample at 17 mm and at 7.5 mm from the top. Overall, the $^{230}Th/^{234}U$ activity ratio values range between 0.69 and 0.84 with an average of 0.75. With regards to the corresponding age determinations, this particular stalagmite sample has a number of stratigraphic inversions. Relatively older ages tend to occur from the middle to the top whereas younger ages occur at the base of BL2 (Table A1.1). These stratigraphic inversions are located in those regions of the stalagmite where fairly higher $^{230}Th/^{234}U$ activity ratio values were

observed. That is, in the middle and top growth layers mentioned previously. The middle growth layers at 309 mm, 275 mm and 152.5 mm date respectively to 135 ± 1.9 ka, 150 ± 3.5 ka, 155 ± 3.7 ka and 145 ± 1.8 ka. The layers at the top at 17 mm and 7.5 mm date respectively to 136 ± 5.8 ka and 137 ± 2.2 ka. The reasons for the stratigraphic inversions are evaluated further by considering the possible effects of thorium contamination.

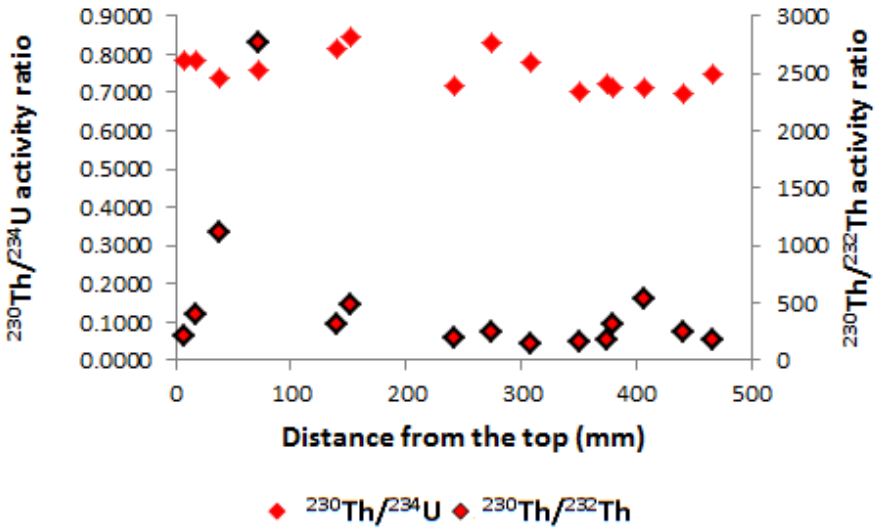

Fig. A1.2 Changes in the $^{230}Th/^{234}U$ and $^{230}Th/^{232}Th$ activity ratios along the vertical length of BL2

The $^{230}Th/^{232}Th$ activity ratio is conventionally used to evaluate the contribution of detrital thorium. This along with the influence of uranium leaching can produce spurious age determinations not unlike those observed in the BL2 sample. In BL2 the thorium activity ratio values are between 144 and 2763 with an average of 497.7. All of the BL2 subsamples had $^{230}Th/^{232}Th$ ratios exceeding the minimum of 50 which is the baseline value used to apply corrections for initial Th in this particular study (see Chapter 3 section 3.4.3 for details). Of the fifteen subsamples from BL2, seven of these exhibit $^{230}Th/^{232}Th$ ratio values that collectively

exceed the standard baseline of 300 which is typically used to correct U-Th ages measured by ICPMS (see Chapter 3). The remaining eight ages while all well above 50 do not meet the standard ICPMS minimum of 300. These particular samples occur at 275 mm from the top and extend along the vertical length of BL2 towards the base at 466 mm. For BL2 the $^{230}Th/^{232}Th$ activity ratios values closer towards the top of the sample are much higher than those found at the top of the sample. This coincides with the chronostratigraphic problem of decreasing age towards the base in the sample. Underestimating the actual contribution of outside thorium (*ie.,* initial thorium in the sample not due to radiogenic decay) is an inherent risk when limiting corrections for initial Th to those ratios below 50. In the case of BL2, the upside down stratigraphy suggests that the effects of allogenic thorium contamination may be one of the variables responsible for the stratigraphic inversion identified in BL2. In other words, the age determinations produced for this sample could be compromised by a significant contribution of allogenic thorium. Furthermore, on the day prior to the analytical run of some of the BL2 samples (*i.e.,* 967, 968, 969, 970 & 971) a sample with very high thorium concentrations was analysed previously and it is possible that the instrumentation was affected. This instrument memory effect may have been transferred onto the BL2 samples. Thus the stratigraphic problem in BL2 may be due to a combination of factors such as analytical error and extraneous contamination by allogenic thorium which collectively affected the age determinations based on the $^{230}Th/^{234}U$ ratio.

Overall for BL2, the geochemical data indicates that the integrity of the uranium and thorium systems for the stalagmite may have been compromised either through contamination by detrital thorium, by analytical problems or a combination of these. Based on this, the precise uranium-series age estimates that were generated for BL2 may not accurately reflect the true growth history of the sample. Another possibility is that the BL2 sample may have formed quite rapidly which is inferred

from the closely banded laminations identified along the vertical length of the sample and its uncharacteristic shape. If BL2 does indeed represent a fast growing stalagmite then it is also likely that it could have formed anywhere between a few hundred or a several thousand years. In other words, it is difficult at this stage to establish when BL2 was formed. Therefore because of the inherent problems in establishing a sound chronology for this sample no age models are presented and further interpretation of this particular sample is not possible at this stage.

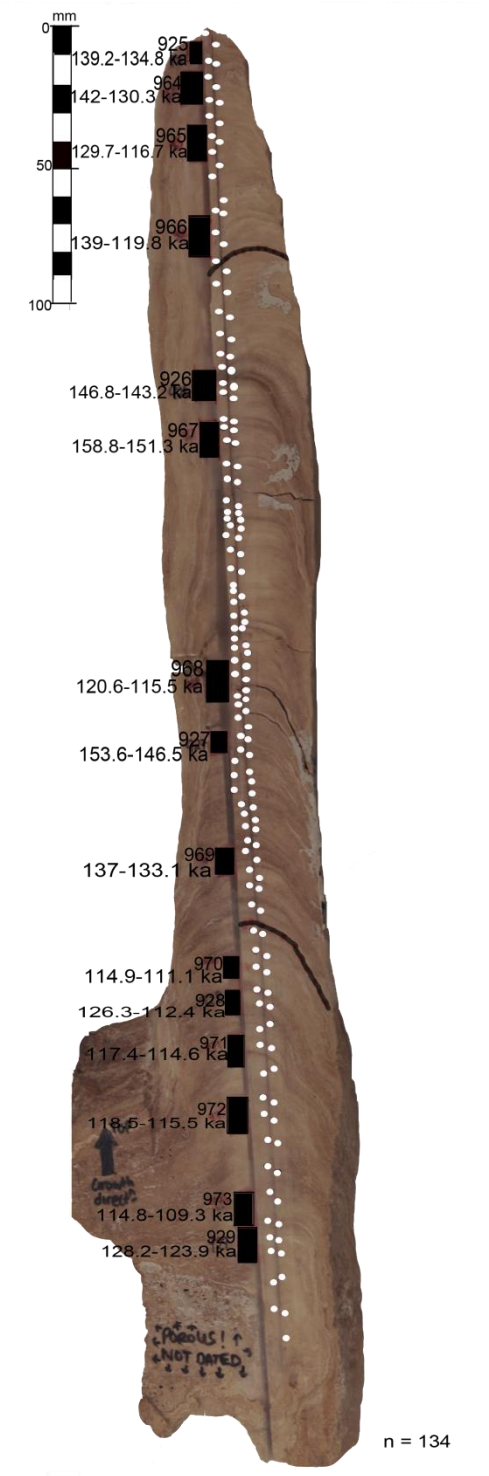

Fig A1.3 Stratigraphic position of each of the uranium series age determinations obtained for the BL2 sample from Bloukrantz Cave. The associated U-Th lab journal numbers are also shown. Uranium-series dated intervals are presented in *ka.* Individual isotope subsamples taken along the vertical length of the sample are shown as black dots (●). White dots represent those isotope points that were either lost, too small for measurement or compromised by analytical problems. The Hendy test traverses are represented by solid dark lines (-).

Table A1.1 Results from ICPMS U-Th analyses of the BL2 stalagmite from Bloukrantz Cave

J. No.	Level	Centre position (mm)	mm interval	Sample (g)	Spike (g)	^{238}U (ppm)	$^{230}Th/^{234}U$		σ	$^{234}U/^{238}U$		σ	$^{230}Th/^{232}Th$		σ	$(^{234}U/^{238}U)_0$		σ	kyr		+σ		-σ
925	T	7.5	0-15	0.2265	0.0513	0.7132	0.7863	±	0.0071	2.4265	±	0.010	204	±	15	3.0986	±	0.013	137	+	2.2	-	2.2
964	T	17	11-23	0.5160	0.0995	0.2508	0.7860	±	0.0188	2.4297	±	0.030	406	±	9.9	3.1026	±	0.039	136	+	6.0	-	5.7
965	T	38	30-46	0.5375	0.1007	0.2001	0.7394	±	0.0231	2.4592	±	0.045	1107	±	28.9	3.0664	±	0.056	123	+	6.7	-	6.3
966	M	73	65-81	0.5528	0.1020	0.1785	0.7592	±	0.0330	2.4123	±	0.048	2763	±	108	3.0325	±	0.060	129	+	10	-	9.2
926	M	140	135-145	0.5951	0.0528	0.4510	0.8145	±	0.0054	2.4352	±	0.009	313	±	35	3.1634	±	0.011	145	+	1.8	-	1.8
967	M	152.5	145-160	0.4851	0.0995	0.2436	0.8439	±	0.0104	2.3606	±	0.020	493	±	5.8	3.1164	±	0.026	155	+	3.8	-	3.7
968	M	242	235-249	0.5779	0.1000	0.3630	0.7182	±	0.0093	2.3250	±	0.020	187	±	11.5	2.8499	±	0.025	118	+	2.6	-	2.5
927	M	275	270-280	0.3638	0.0520	0.6938	0.8284	±	0.0099	2.3263	±	0.017	249	±	61	3.0299	±	0.023	150	+	3.6	-	3.5
969	M	309	303-315	0.5773	0.1039	0.6196	0.7783	±	0.0062	2.2681	±	0.015	144	±	18.0	2.8585	±	0.019	135	+	2.0	-	1.9
970	B	351	343-359	0.4421	0.1034	0.4031	0.7006	±	0.0073	2.3519	±	0.016	154	±	4.0	2.8628	±	0.020	113	+	1.9	-	1.9
928	B	375	370-380	0.1354	0.0518	0.4574	0.7219	±	0.0263	2.3383	±	0.032	179	±	8.7	2.8732	±	0.039	119	+	7.3	-	6.9
971	B	380	373-387	0.5447	0.1037	0.3971	0.7131	±	0.0052	2.3146	±	0.010	318	±	5.1	2.8287	±	0.013	116	+	1.4	-	1.4
972	B	407	400-414	0.5871	0.1016	0.3752	0.7119	±	0.0055	2.2486	±	0.008	538	±	6.2	2.7370	±	0.010	117	+	1.5	-	1.5
973	B	440	443-447	0.6962	0.1033	0.3137	0.6957	±	0.0106	2.3182	±	0.020	239	±	7.5	2.8048	±	0.025	112	+	2.8	-	2.7
929	B	466	460-472	0.5960	0.5020	0.5487	0.7482	±	0.0073	2.2865	±	0.020	171	±	81	2.8390	±	0.025	126	+	2.2	-	2.1